In-situ Characterisation of Positive Photoresist Development During Automated Wafer Processing

Thesis submitted by

Stewart A. Robertson

for the degree of

Doctor of Philosophy

Edinburgh Microfabrication Facility,

Department of Electrical Engineering,

University of Edinburgh,

Scotland.

October 1994

Abstract

The place of optical lithography within integrated circuit manufacture is discussed, and the key nature of its role identified. All aspects of lithographic processing are reviewed, highlighting the long list of process conditions which influence the final results. The manner in which lithographic processes are evaluated and characterised is also reviewed, illustrating the large amount of work required to compare different processes. Computer simulation of lithography is reviewed as a quick and cheap way of investigating the effect of key processing parameters on process results. Such simulations are only useful, in this respect, if they exhibit the same trends as genuine processes and are quantitatively accurate.

Experimental results reveal discrepancies between modern track-based development techniques and the immersion processes generally used to generate the input parameters for simulation of the development.

A novel polychromatic Development Rate Monitor (DRM) is introduced capable of measuring resist dissolution rates in-situ on manufacturing equipment. Results from this equipment demonstrate significant differences between immersion and track development.

The detailed output from the DRM system coupled with a new analysis technique allow accurate estimation of post exposure bake diffusion lengths and have led to the derivation of a new model describing surface induction effects during development.

Having accurately characterised continuous spray and static puddle development processes, a new 'interrupted development' simulation technique is introduced to simulate the spray/puddle processes commonly employed in manufacturing facilities. Excellent correlation is demonstrated between these simulations and experimental results.

Declaration

I declare that this thesis has been completed by myself and that all the work included in this thesis is entirely my own except where otherwise indicated.

Stewart A. Robertson

Acknowledgements

I would like to thank my supervisor, Dr. J.T.M.Stevenson for all the assistance, encouragement and proof reading he has provided over the duration of this project. Thanks is also due Dr. R.J.Holwill for the assistance in obtaining sponsorship and equipment in the early stages of the work.

I have received invaluable help from the EMF staff over the years and would like to particularly thank A.Gundlach, J.Gow, C.McGuigen, A.Welch, D.Black, I.Rutherford, D.Hope, A.O'Hara, A.Ross, A.Walton and A.Ruthven

My fellow PhD students have been a good source of both help and welcome distraction. R. Smith, G.Gaston and G.Allan provided useful advice with regard to computing problems and document preparation. G. Davis provided expert assistance on the KLA5015 CPM. N.Porfiris, A.Chester, R.Hannah and I.Binnie also provided many ideas, over coffee.

Financial assistance was recieved from SERC and OCG Microelectronic Materials. Thanks must go to all the staff of OCG Europe, particularly I.Daraktchiev, S. Bellini and M.Thirsk (now with Nikon Precision Gmbh) for their assistance and advice.

Further thanks is due to the staff of the OCG Research and Development Centre, East Providence, Rhode Island where I spent 3 months in 1992, including B.Beauchemin, A.Blekeney, D.Brzozowy, C.Ebersole, J.Ferri, K.Honda, R.Leonard, S.Slater, P.Spragg and M.Toukhy. I am especially indebted to S.Hansen, for the guidance and help he provided, and to R.J. Hurditch and family who 'put up' my wife and I during our stay in the US.

I appreciate the consideration and support shown by my current employers Shipley Europe Ltd whilst completing the written section of this work.

Finally, and most importantly, I would like to thank my wife for her support and tolerance during the preparation of this thesis.

List of Publications

Portions of the work presented in Chapters 5, 6 and 7 have been published prior to the completion of this thesis in the following papers:

- S.A.Robertson, J.T.M.Stevenson, R.J.Holwill, M.Thirsk, I.S.Daraktchiev and S.G.Hansen. "Photoresist dissolution rates: A comparison of puddle, spray and immersion processes" In *Integrated Circuit Metrology, Inspection and Process Control V*, pages 232 - 244. SPIE Volume 1464, 1991.

- S.A.Robertson, J.T.M.Stevenson, R.J.Holwill, S.G.Hansen, C.E.Ebersole, M.Thirsk and I.S.Daraktchiev "The modelling of post exposure bake and surface inhibition effects in positive photoresist using absolute thickness data" In *Advances in Resist Technology and Processing IX*, pages 540 - 552. SPIE Volume 1672, 1992.

- S.A.Robertson, J.T.M.Stevenson, R.J.Holwill, S.G.Hansen, R.J.Hurditch, M.Thirsk and I.S.Daraktchiev "The simulation of spray/puddle resist development" In *Advances in Resist Technology and Processing X*, pages 178 - 185. SPIE Volume 1925, 1993.

Table of Contents

Chapter 1

Introduction

1.1 Introduction

The use of Integrated Circuits (ICs) is now so widespread that there is hardly a single electrical item, either domestic or commercial, which does not rely on at least one. As with any mass produced product, selling prices are continually falling, therefore manufacturers must always strive to reduce their manufacturing costs and develop new higher value products.

Lithography is one of the chief process steps in IC manufacture and is the patterning process which ultimately determines the function, and value, of the finished product. It is also the lithography process which limits the total area available for a single chip and the minimum size of features within that area.

1.2 The Role of Lithography in the IC Fabrication Sequence

All semiconductor devices (MOS, bipolar etc.) are multilayer structures and are formed sequentially from the bottom upward. Each process layer is deposited and then patterned or selectively implanted using the process flow detailed in Figure 1–1.[1] Typically between 7 (simple nMOS) and 18 (advanced BIMOS) iterations of the central loop are required.

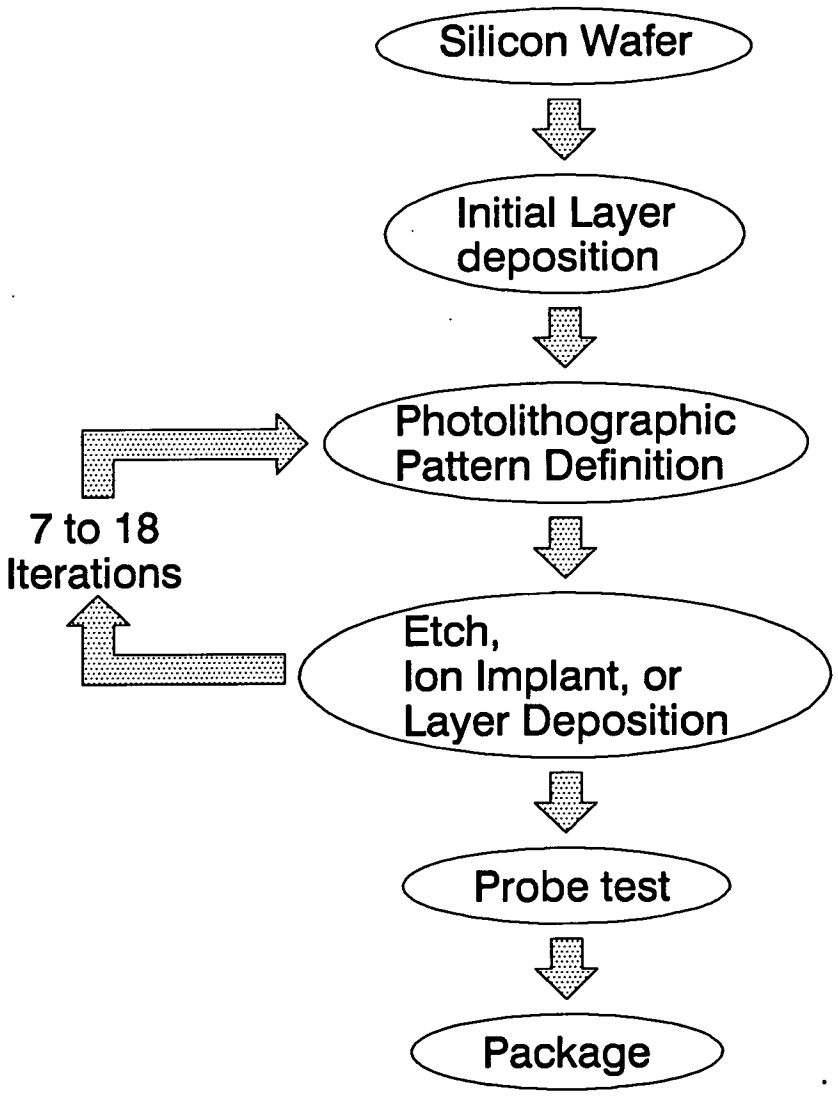

Figure 1–1: *The IC fabrication sequence.*

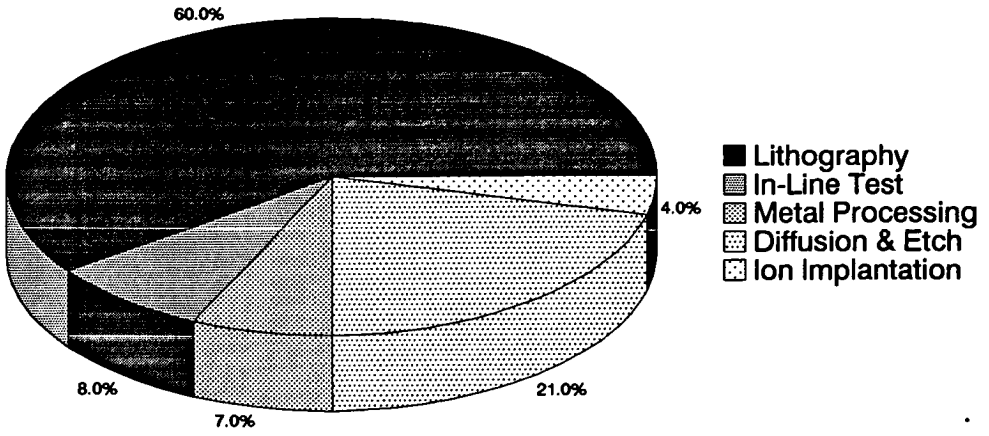

Figure 1–2: *Manufacturing cycle time by process step for megabit technologies.*

From Figure 1–1 it is clear that lithography is the most frequently called upon step in any IC fabrication process. An analysis of wafer processing times for megabit technologies[2] showed that over 50% of the total manufacturing cycle time was due to lithography steps, as illustrated in Figure 1–2.

1.3 Technology Trends

It can be clearly seen, from the discussion so far, that lithography is a very important part of IC manufacture, as it determines the device function and it is generally a bottle neck in the production cycle. Attempts to improve IC complexity and reduce manufacturing costs have led to many industry-wide technology trends. These trends, and the reasoning behind them, are now reviewed.

1.3.1 Minimum Feature Size and Tolerances

Since the first ICs were produced in 1959, there has been an ongoing push towards smaller and smaller feature sizes. There are two main drivers for this change.

Firstly, the device switching speed is primarily determined by transistor size; thus smaller geometries produce faster IC chips[3] which can be sold at a premium.

Secondly, reducing feature size allows circuit density to be increased; die areas are decreased correspondingly, allowing more ICs to be produced per wafer.

These advantages can be quantified for a MOS type IC by considering a minimum feature size shrink of a factor 's'. The following conditions are realised:[3]

- Device delay time decreases by $\frac{1}{s}$
- Packing density increases by s^2

Whilst scaling feature size offers the manufacturer economic advantages in terms of capacity and product value, technical penalties are incurred. Correct circuit performance requires that features are reproduced at, or close to, their nominal sizes. Deviation from this size results in non-functioning or unreliable devices. Generally, feature sizes must be within $\pm 10\%$ of their nominal size. This means that as minimum feature sizes scale, the acceptable deviation reduces dramatically in absolute terms, e.g., for a 2.00μm nominal feature deviations of $\pm 0.20\mu$m are acceptable, but this reduces to $\pm 0.05\mu$m for a 0.50μm nominal feature. Moreover, as feature sizes shrink below 0.80μm device considerations are reducing deviation tolerances even further, often down to $\pm 5\%$.[4,5]

The minimum Critical Dimension (CD) feature sizes used in the industry have historically been driven by DRAM technology. Whilst it is true that some logic (microprocessor) geometries are currently at the leading edge of lithography processing, these features generally occur on a single mask layer (polysilicon gate definition) and involve isolated lines. Since dynamic memory manufacture has a much higher number of critical layers and considerably tighter line spacing requirements, it can still be considered the 'lithography driver'. Figure 1–3 illustrates current and future minimum CD trends for three DRAM generations, as determined by Dataquest.[6] This figure clearly exhibits the points discussed above: each successive technology is introduced at a smaller feature size, allowing a higher intrinsic product value (increased speed and complexity) and undergoes dimensional shrinks as the process matures, increasing the number of die per wafer.

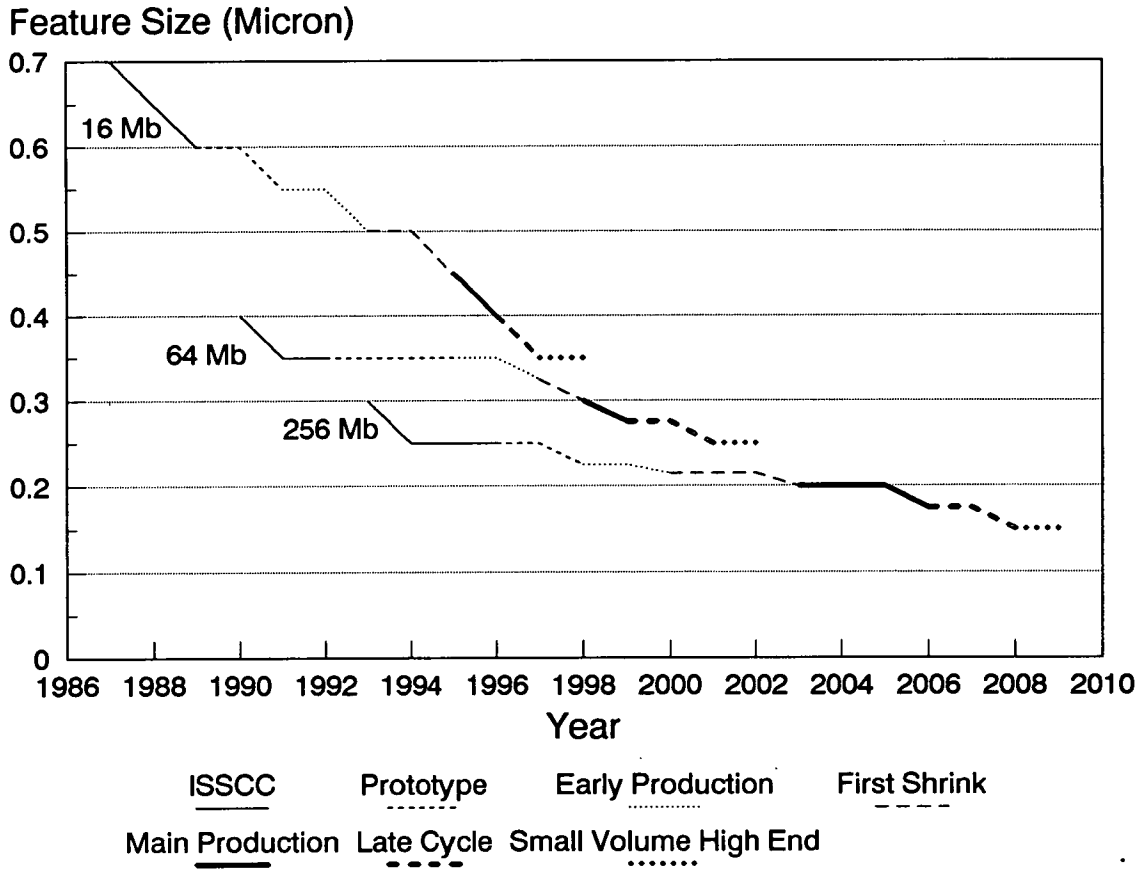

Figure 1–3: *DRAM minimum feature geometries and introduction times.*

1.3.2 Layer-to-Layer Registration

ICs are multilayer structures which will only function correctly if the layers are correctly aligned with each other. A device specific registration, or overlay, budget will detail the allowable spatial deviation between a given layer and the initial layer. In general, this budget is one third to one quarter of the minimum feature size. Consequently, overlay budgets are becoming more and more stringent.

1.3.3 Chip Size

Although smaller geometries allow chip areas to be reduced, there is a tendency to produce larger chips using smaller minimum geometries. This allows greater and greater levels of integration which once again increases product value. Figure 1–4 illustrates actual and predicted silicon area requirements for 3 generations of DRAM devices, as predicted by Dataquest.[6] It can be seen that each new technology requires a greater silicon area than the last, but that area reduces as the technology matures and geometries shrink.

1.3.4 Wafer Diameter

Increasing wafer diameter produces enormous economic benefits; the area of silicon available increases by the square of the diameter whilst fabrication costs rise in an approximately linear fashion.[7] Wafer sizes initially started at 2" and 3" but now 100mm (4") and 150mm (6") prevail. Many new production facilities are employing 200mm (8") wafers.

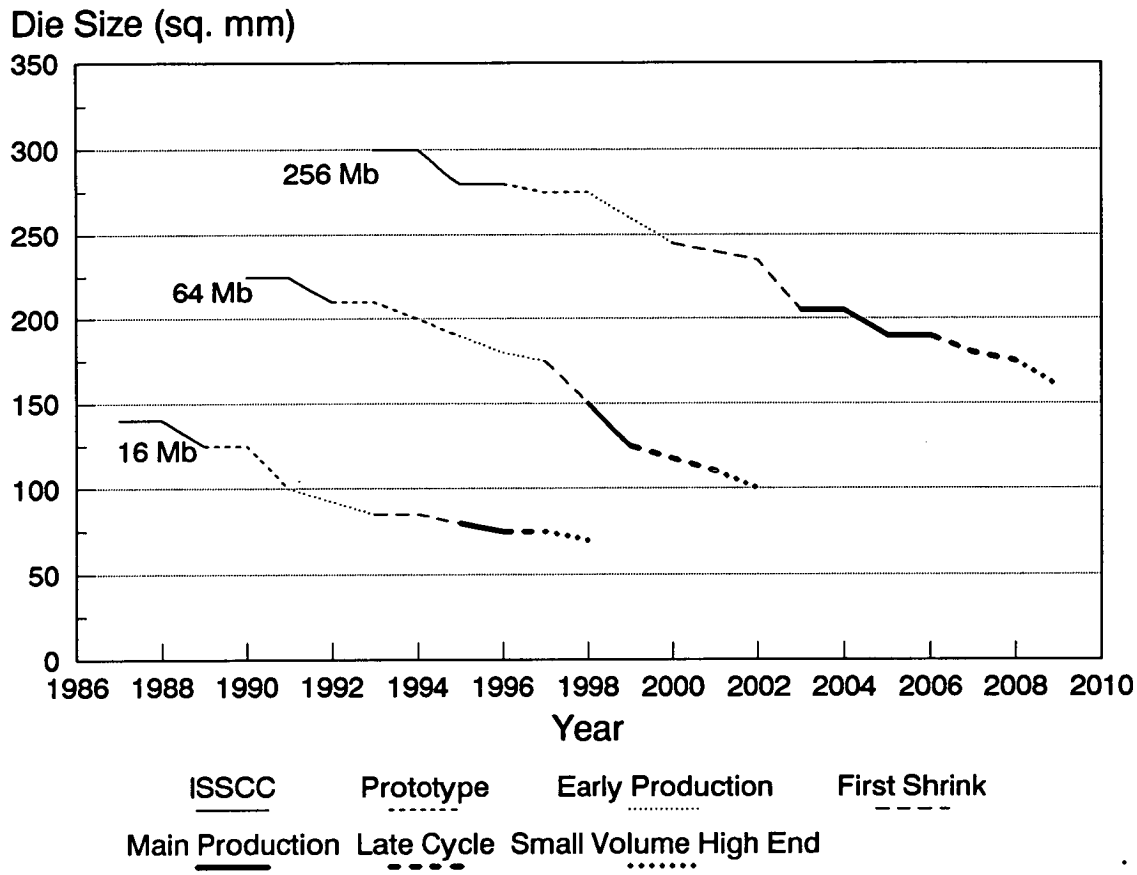

Figure 1–4: *DRAM Die areas and introduction times.*

1.4 Exposure Tool Equipment Advances

Lithography processing is dominated by optical exposure techniques. Ten years ago, even the strongest proponents of optical lithography believed it would be limited to dimensions of around 1.0μm,[6] however today features of 0.5μm are manufactured routinely and research facilities are operating in the 0.25 to 0.30μm region.

Billions of dollars have been spent on high resolution non-optical exposure technologies, e.g. direct write e-beam and x-ray lithography. However, the continued evolution of optical lithography, through improved equipment and mask technology, has delayed the introduction of these techniques, perhaps indefinitely. Although the non-optical techniques generally offer higher resolution, they have yet to become viable and economical alternatives to optical lithography.[8]

1.4.1 Optical Lithography Limitations

Consideration of exposure tool optics in Chapter 2, Section 2.8.2.3 shall show that the theoretical resolution of a monochromatic optical exposure system is proportional to the exposure wavelength, λ and inversely proportional to the numerical aperture (NA) of the system such that

$$\text{Resolution} = \frac{k_1 \lambda}{NA} \tag{1.1}$$

where k_1 is a proportionality constant. The theoretical minimum value for k_1 is 0.5 (the Rayleigh limit) but is usually taken to be 0.6 for laboratory work and 0.8 for production manufacturing.

Equation 1.1, known as the Rayleigh resolution criterion shows that the minimum resolvable feature can be improved by reducing the exposure wavelength and/or increasing the system numerical aperture. However, the system's resolving capabilities cannot be viewed in isolation; its tolerance to topography steps

and imperfections in wafer flatness must also be considered. A second Rayleigh criterion, also examined in Chapter 2, Section 2.8.2.3, describes an optical system's depth of focus (DOF), i.e., the size of the region around optimum focus where C.D.s are reproduced within tolerance limits. The DOF is proportional to wavelength and inversely proportional to the square of the numerical aperture:

$$\mathrm{DOF} = \pm\frac{k_2\lambda}{2\mathrm{NA}^2} \tag{1.2}$$

where k_2 is a process constant. Inspection of Equation 1.2 reveals that both options for enhancing resolution have negative impacts on DOF.

Sections 1.4.2 to 1.4.4 describe how exposure tools have adapted to improve resolution and some of the new techniques that have been developed to overcome the Rayleigh limitations.

1.4.2 Mercury Lamp-based Optical Exposure Tools

The mercury arc lamp is a good source of the UV and near-UV light required to expose the photoresist types discussed in Chapter 2 , Section 2.2. In this wavelength range three strong discrete spectral lines are observed. They are at 436nm, 405nm and 365nm and are often designated g-line, h-line and i-line, respectively.

Although broadband exposure to the mercury spectrum would result in photoresist exposure, the refractive optics utilised in most industry standard, high resolution steppers may only be optimised for operation at a single wavelength. Therefore, the mercury spectrum is typically limited to a single emission line by a filter system.

Early stepper systems utilised g-line illumination with relatively low NA values (around 0.3) and had small exposure fields (10mm by 10mm). As lens design and materials improved numerical aperture values increased, as did field sizes, resulting in advanced machines such as the Nikon body 8 stepper which has a numerical aperture of 0.54 and an exposure field of approximately 20mm by 20mm. The

production capabilities of these advanced g-line machines appears to be limited to approximately 0.5μm.

Resolution has also been improved by reducing exposure wavelengths. Although brief attempts at producing h-line steppers were made,[9] the majority of manufacturers went straight to i-line. Again, the exposure systems started with low NA values and restricted field sizes. However, lens technology rapidly progressed with current 'state of the art' equipment employing numerical apertures of up to 0.6 and field sizes in excess of 20mm by 20mm. High NA i-line steppers seem to be capable of delivering production processes operating in the 0.40 to 0.45 μm range.

Recently, all the major stepper manufacturers have demonstrated off-axis, or annular, illumination systems which enhance resolution and DOF beyond the Rayleigh limits, by eliminating the zero order illumination.[10] Although this technique offers improved resolution, design restrictions are placed on pattern layouts and throughput is decreased (as the exposure energy at the wafer is reduced).[6] This is thought to extend the operational resolution of an i-line system by around 0.05μm and can be applied to any optical exposure system.

1.4.3 Mask Technology

Resolution and DOF enhancements can also be realised using Phase-Shift Masks (PSMs). These mask schemes utilise areas with different phase properties to maximise the image contrast at the edge of small mask features. Many different schemes have been proposed and demonstrated,[11–15] however each imposes a set of constraints on the possible device layout. Again, the resolution improvement is gained at a cost; phase-shift masks are extremely difficult and expensive to manufacture and repair.

This technique is estimated to add 0.05μm to the resolution capabilities of an advanced i-line sytem, and like off-axis illumination can be applied to any optical exposure technque.

When used in conjunction with annular illumination, PSM technology should allow 0.30 and 0.35μm technologies to be manufactured using standard i-line processing. Many Japanese companies incuding NEC, Toshiba, Hitachi, Mitsubishi, Oki and Sharp have indicated that this is their preferred option for these geometries.[16]

1.4.4 Excimer Laser-based Optical Exposure Tools

Resolution can be enhanced further by reducing the exposing wavelength beyond i-line. Systems operating at 248nm and 193nm are being used in pilot line facilities. These new wavelengths known respectively as Deep UV (DUV) and Vacuum UV (VUV) take the Rayleigh Criteria further than i-line but introduce new processing problems.

At these short wavelengths refractive optical systems exhibit high chromatic aberrations, so the illumination source must have a narrow spectral bandwidth.[6] This band-narrowed illumination can be obtained from an excimer laser (KrF for DUV[8] and ArF for VUV[17]). Excimer lasers are however much more expensive than mercury arc lamps, are less reliable and are costlier to maintain.[6]

Conventional resists absorb greatly at these short wavelengths and novel chemically amplified or catalysed resists must be used. As the industry is always reluctant to move away from production-proven processes, the change to a new resist technology is being delayed for as long as possible.[8]

DUV systems should be able to take maufacturing processes below 0.30μm[8] whilst VUV should theoretically be able to reach 0.25μm with conventional masks.[17]

Off-axis illumination and PSM technology can be used to increase the resolution capability, once again.

Several Japanese companies, including Fujitsu, Matsushita and Sony, have indicated that excimer-based stepper systems are their preferred exposure tools for 0.35 and 0.30μm geometry processing.[16] It remains to be seen whether these com-

panies, or those choosing i-line processes have the most cost-effective strategies for 64Mb and 256Mb DRAM mass production.

1.5 Cost of Ownership

The increased technical requirements on stepper lenses (increased NA and field size, reduced cross-field errors), focusing systems, stage accuracy and alignment system is increasing equipment costs at an alarming rate. If the additional costs of excimer laser, off-axis illumination systems and PSMs are also required then total costs may be doubling per stepper generation. Recently, rapid changes in materials and equipment mean that each new product has tended to last for only one generation of device type.[8] This short cycle time, high outlay scenario results in a high cost of ownership for exposure equipment, so the amount of time that the equipment spends in production must be maximised to recoup the initial investment.

More significantly, the relatively small vendors developing photoresists and anti-reflective coatings for use with these 'state-of-the-art' exposure tools cannot justify the cost of ownership of such a tool for material testing under any circumstances.

1.6 Lithography Simulation

Lithography simulation allows the effects of process changes to be examined quickly, and relatively cheaply, without using valuable equipment time.

If resist characterisation and the lithography models are sufficiently accurate resist vendors can screen the performance of new resist candidates on the most modern exposure equipment without, in the first instance, requiring access to an actual stepper.[18] This screening technique relies on the fact that modern resist chemistries do not 'transcend' the current simulation models.[19] Recent results[20]

suggest that simulation is not yet sufficiently accurate for such formulation screenings.

1.7 Aim of Project

Resist characterisation for simulation work typically takes place in an immersion Development Rate Monitor (DRM) whilst advanced manufacturing processes occur on automated track systems. It is known that different lithographic results are produced by these different development techniques. The first aim of this project is therefore to derive simulation parameters for simplified manufacturing type development processes and examine how these differ from the immersion case.

Having derived parameters for simplistic track-based processes, it is then necessary to confirm that such parameters actually model track processes more accurately than immersion parameters. Ideally, accurate modelling parameters will allow easy identification of modelling weaknesses.

Finally, having fully characterised the simplified track development processes, these results can be combined to simulate a more realistic spray/puddle type development process, of the type often used in actual manufacture.

1.8 Thesis Structure

Chapter 1: Introduction. This chapter introduces the role of lithography within semiconductor manufacture and discusses the technological trends in the industry. The cost implications of these trends are identified. Lithography simulation is introduced as a low cost method of testing processes, if sufficient accuracy can be achieved.

Chapter 2: Optical Lithography. This chapter gives a comprehensive review of current near-UV optical lithography processing practices, including all the

commonly used exposure tool designs. Resist and developer chemistries are also explored in some depth.

Chapter 3: Process Characterisation. This chapter describes how the performance of a given lithographic process is assessed in quantifiable terms. Some easily measured "rule-of-thumb" process indicators which can be used as predictors of process performance are also introduced and their utility discussed.

Chapter 4: Lithography Modelling. This chapter reviews currently accepted modelling theories and outlines the reasoning behind them. The available lithography packages are introduced and some of their commonly acknowledged inadequacies are discussed.

Chapter 5: Determination of Resist Thickness During Development. The data required to characterise resist dissolution for simulation work is gathered by a Development Rate Monitor (DRM). This chapter reviews various DRM techniques and describes the two-most common commercially available tools. A novel TDRM (Track Development Rate monitor) developed during this project is introduced.

Chapter 6: Development Rate Parameter Extraction and Model Refinement. This chapter describes how DRM output is used to derive dissolution rate parameters suitable for simulation of resist development. A parameter verification process is introduced which identifies some weaknesses in the conventional lithography models. Model refinements are proposed to address these issues and the practical problems of implementing these changes are discussed. Full process characterisation for two resists under three different development processes are presented.

Chapter 7: Modelling Production Development Processes. This chapter examines the modelling accuracy of the processes characterised in Chapter 6. It then goes on to use these parameters to model a more realistic process, which might be found in an IC manufacturing facility.

Chapter 8: Conclusions and Further Work. This chapter summarises the thesis and examines its outcome with regard to its original aims. Areas of further investigation are identified and more recent work by others, based on this research, is discussed.

Chapter 2

Optical Lithography

2.1 Introduction

This chapter gives an overview of current optical lithography practices. A full review of lithographic materials and the processes utilising them, shows how both resist/developer chemistries and processing nuances strongly influence the results obtained.

2.2 Photoresist Materials

Photoresists are the key to optical lithography. These light-sensitive chemicals are used to coat the substrate surface from where they are selectively removed by optical illumination (usually in the UV or near-UV range) followed by a liquid development process.

While the chemistries of different resist systems are extremely varied, all resists can be placed in one of two categories; negative tone or positive tone. If UV exposed areas remain after development, the resist is termed negative; conversely, the resist is termed positive when exposed areas are removed.

All resists consist of four main components:[21,22]

- **A film-forming resin:** This makes up the bulk of the final film and largely determines its physical properties, such as adhesion, thermal stability and resistance to implant/etch.

- **A sensitiser or photoinitiator:** This component, also known as PhotoActive Compound (PAC), alters the film's solubility in developer solution, when exposed to radiation of a suitable wavelength.

- **A solvent system:** This keeps the solid resist components (sensitiser and resin) in a liquid form suitable for film deposition by spin-casting.

- **Additives:** These substances are incorporated to improve the performance of the resist and include dyes, levelling agents, antioxidants and adhesion promoters.

Negative resists are generally used for low resolution applications whilst nearly all high resolution work (under 2μm geometries) is performed using diazo-type positive resists. A few very high resolution i-line and DUV resists, for sub-0.4μm lithography, are negative tone (e.g., Shipley SNR248).

Mack[23] has shown that, for most IC applications, a positive resist is preferable to a negative resist, especially at contact hole definition. This originates from exposure tool optics which produce a better contrast image when a positive (light field) mask is employed. This being said, it should be noted that isolated features are reproduced better by a negative resist.

2.2.1 Polyisoprene Based Negative Resists

The majority of negative resists are based on a resin formed from natural or synthetic polyisoprene rubbers. The solid rubber is made up of very long chains of a basic repeating unit, illustrated in Figure 2–1(a).[24] Each of these chains has an extremely high molecular weight (exceeding 1,000,000) and is practically insoluble in any solvent. The solid rubber is ground up, physically breaking many of the chains, and placed in a solution of organic solvent (often xylene or mixtures of aliphatic and aryl hydrocarbons[25]). An acid catalyst is added to the solution and the polyisoprene chains (Figure 2–1(b)) undergo a cyclisation process. The resulting cyclised polyisoprene (Figure 2–1(c)) is tougher and more chemically

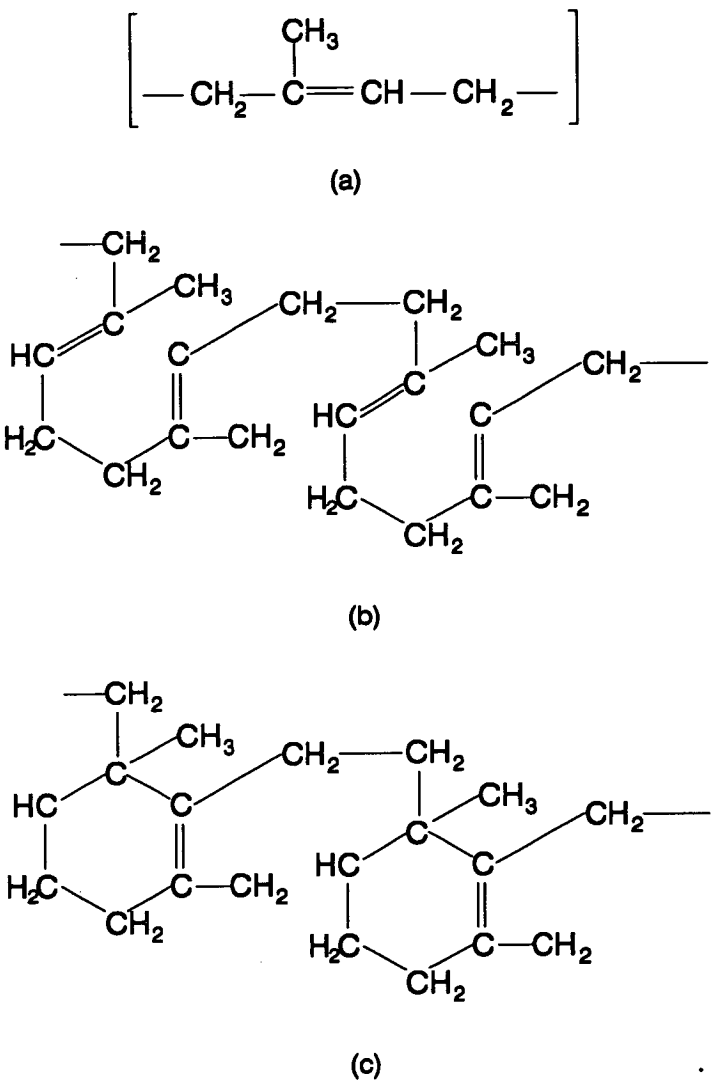

Figure 2–1: *(a) The basic polyisoprene repeating unit. (b) Polyisoprene chain in folded configuration. (c) Cyclised polyisoprene*

resistant than the original rubber. This material has a lower molecular weight (<250,000) which renders it soluble in organic solvent and therefore suitable for spin-cast deposition.

Although the rubber crosslinks to some degree when exposed to radiation of 300nm or less, a photoinitiator is required to extend photosensitivity upto 450nm.[21] 4-4'-diazidostilbene (Figure 2–2) is a typical photoinitiator. During illumination, N_2 is lost from both ends of the photoinitiator creating a free radical. The ends react with alkene sites in the polyisoprene chains, often linking two chains

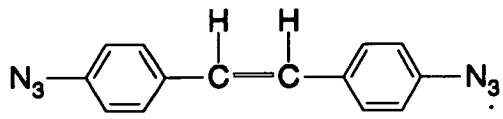

Figure 2–2: *The photoinitiator 4-4'-diazidostilbene.*

together. When enough photoinitiator molecules are present, enormous molecules can be formed by crosslinking polymerisation. Practically, this requires 1-3% of the dried film weight to consist of photoinitiator. The photoinitiator can be tuned to particular wavelengths by altering the structure between the benzene rings.[25]

Since the large molecules formed during polymerisation are insoluble in organic solvents, development can be implemented using a casting solvent. The solvent dissolves the unexposed regions, leaving only those areas which have been crosslinked.

Unfortunately, this process has one major resolution limiting feature; the polymerised regions swell when saturated with solvent. Although they retract on drying, this phenomenon limits the physical size of a space which can be reproduced. If two adjacent features swell sufficiently to touch, strings of resist remain bridging the gap when the resist recedes. This 'webbing', or 'stringing', limits negative resist to applications requiring geometries of 2μm or greater.

2.2.2 DUV Chemically Amplified Negative Resists

Conventional diazo-type positive resists (Section 2.2.3) are not suited to DUV (248nm) applications because the novolak resin absorbs excessively at this wavelength. The commercial resists that have been developed to operate at this wavelength are generally negative acting and utilise a combination of crosslinking and chemical amplification.

The materials consist of base-soluble polyvinylphenolic (PVP) resins and contain a thermally assisted, acid activated crosslinking agent (such as melamine), in addition to a photoacid generator (PAG). During exposure the PAG produces a

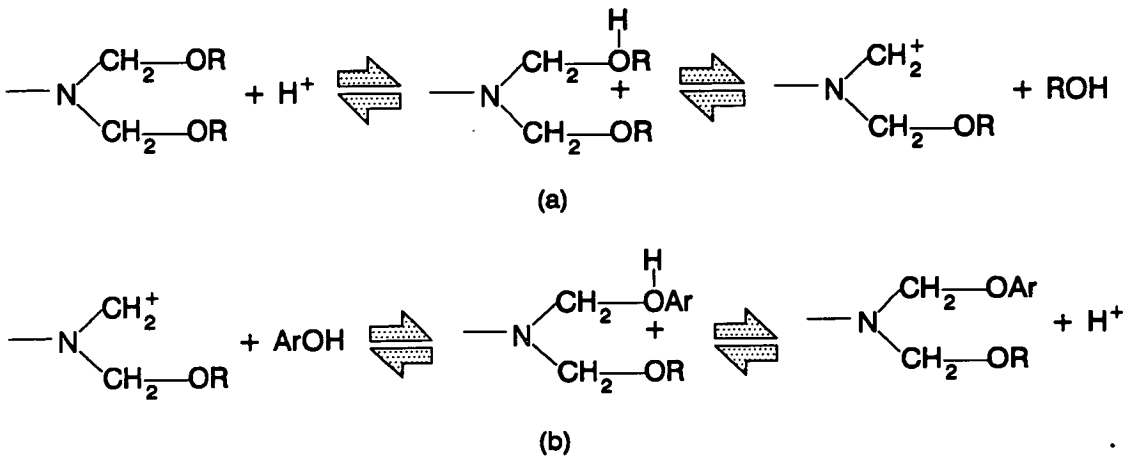

Figure 2–3: *(a) The acid reacts with the melamine to form an alcohol molecule and a carbonium ion. (b) This ion reacts with the resin by alkylation of the oxygen or carbon on its aromatic ring producing in the process another* H^+ *ion.*

small quantity of acid, which causes, under thermal assistance, melamine crosslinking of the PVP resin.[26] Although the chemistry of the reaction is uncertain, the mechanism proposed for SNR248 shall be discussed.

The small quantity of acid produced by the PAG after photoexcitation leaves a concentration of H^+ ions within the resist. Figure 2–3 illustrates the chemically amplified crosslinking mechanism that occurs during PEB, as proposed by Thackeray.[27]

During the bake, an H^+ ion can cause melamine to release an alcohol molecule leaving a reactive carbonium ion. This will react with any appropriate electrophilic species, in this case from the resin, by alkylation of the oxygen or carbon on the aromatic ring. This not only forms a crosslink, but also a further H^+ ion.

Since the crosslink reaction produces the ion necessary for a further similar reaction, the process is termed chemically amplified. The cascading nature of the reaction means that low levels of initial acid are required. Consequently exposure doses can be kept very low, typically in the 1 - 20mJ/cm^2 range.[28]

The crosslinked molecules are insoluble in the developer, which in this case is an alkaline solution.

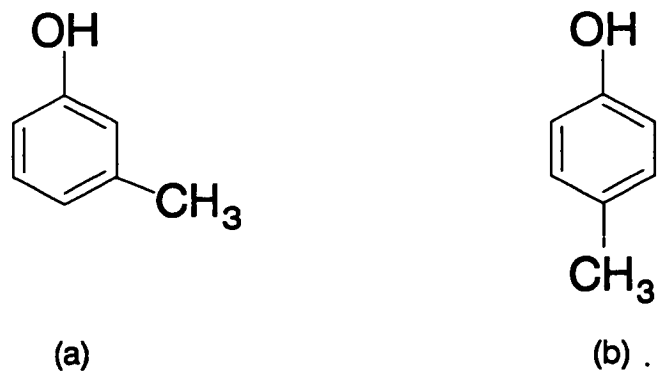

(a) (b) .

Figure 2–4: *(a) meta[m]-cresol monomer. (b) Para[p]-cresol monomer.*

2.2.3 Diazonaphthaquinone/Novolak Positive Resists

This resist type is the 'workhorse' of high resolution g and i-line lithography and is the only kind considered during this study. Consequently, unless otherwise stated all following instances of the words resist and photoresist, refer to novolak-based diazo-type positive resist.

2.2.3.1 Resin

These resists are based upon cresol-formaldehyde novolak resins. The novolak polymers are typically synthesised by reacting formaldehyde with cresol monomers in the presence of a catalyst, often oxalic acid. Typically m- and p-cresol monomers, illustrated in Figure 2–4, are used, although others can be utilised.[29]

Figure 2–5 shows the condensation reaction used in the formation of the resin polymer.[30] The chain length, n, is typically between 3 and 10.

The molecular weight and chemical structure of the resulting novolak influence the thermal stability and the lithographic performance of the finished resist. It has been well documented[29,31] how thermal flow properties improve with increasing molecular weight. Unfortunately, solubility decreases as the molecule size increases and gradually lithographic performance deteriorates.

Other studies[29,32–37] have shown that the higher the level of ortho-ortho bonding between the monomers (i.e., methyl bridges are formed on either side of the

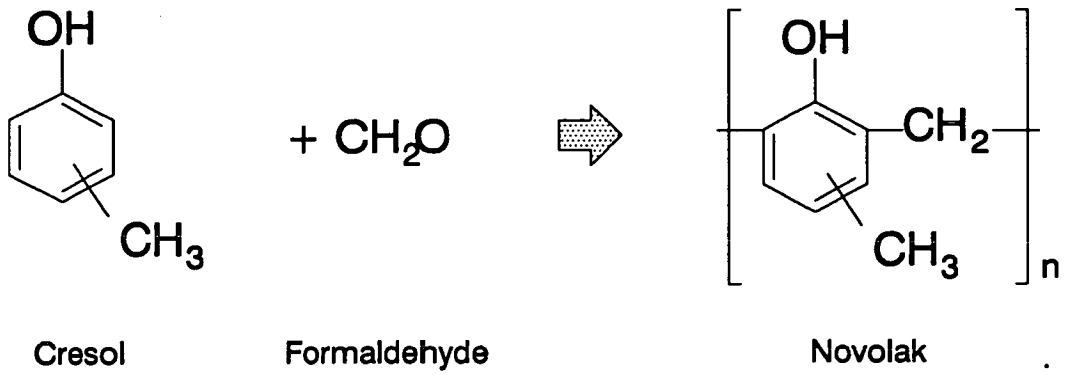

Figure 2–5: *The novolak polymerisation process.*

hydroxyl group), the better the resist's lithographic performance. The level of such bonding in the novolak is controlled by the p-cresol content, which also improves the resin's thermal properties.[38] However, p-cresol is relatively insoluble in developer and polymerises slowly. M-cresol is therefore added to increase the resist's solubility[31] and to decrease the polymerisation reaction time (it is eight times more reactive than p-cresol).[29]

The chain length and chemical composition of the novolak is controlled by varying the monomer feed ratios, the amount of formaldehyde present and the catalysing material. Figure 2–6 illustrates a novolak with good lithographic properties (entirely ortho-ortho bonded).

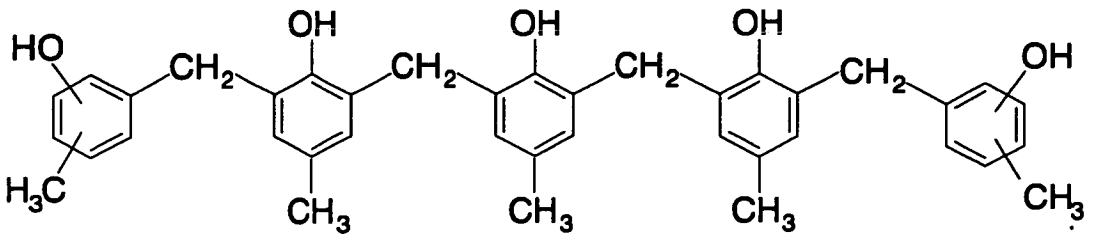

Figure 2–6: *A hybrid pentamer novolak.*

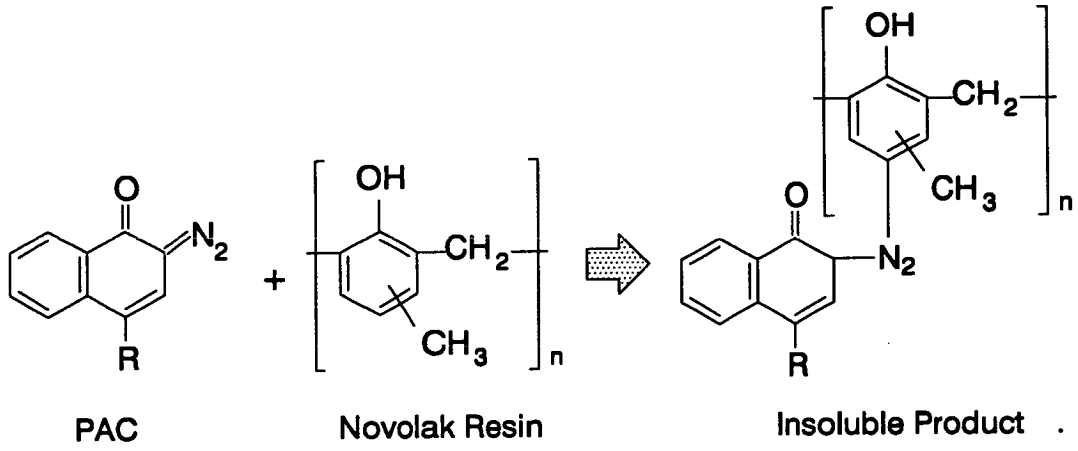

Figure 2–7: *The interaction of PAC and novolak.*

2.2.3.2 Photoactive Compound

Novolak resin is moderately soluble in alkaline developer (typical dissolution rates are between 100 and 400 Å/s) and is insensitive to illumination. A photoactive compound, or PAC, is added to the resin, typically 25-50% by total solids weight, to inhibit dissolution. The PAC, also known as sensitizer or inhibitor, is usually a 2,1 diazonaphthaquinone (DNQ) based material. Figure 2–7 illustrates how the PAC is thought to interact with the novolak.[30] The resulting structure has a solubility around 10 -100 times less than the original resin.

On exposure to UV radiation in the 300-500 nm wavelength range, the PAC undergoes a chemical reaction. In the presence of water, nitrogen is evolved and the PAC is converted via a intermediate ketene into a indenecarboxylic acid. When no water is available the intermediate ketene reacts with the hydroxyl group of the novolak resin to form an ester compound. While this product is highly insoluble in developer, the reaction is reversible and the subsequent introduction of water after exposure results in the formation of the indenecarboxylic acid. Figure 2–8 illustrates the reaction paths.[39]

The indenecarboxylic acid, or photoproduct, is highly soluble in developer and has been shown[39,40] to enhance the dissolution rate of the exposed resist above that of the resin alone.

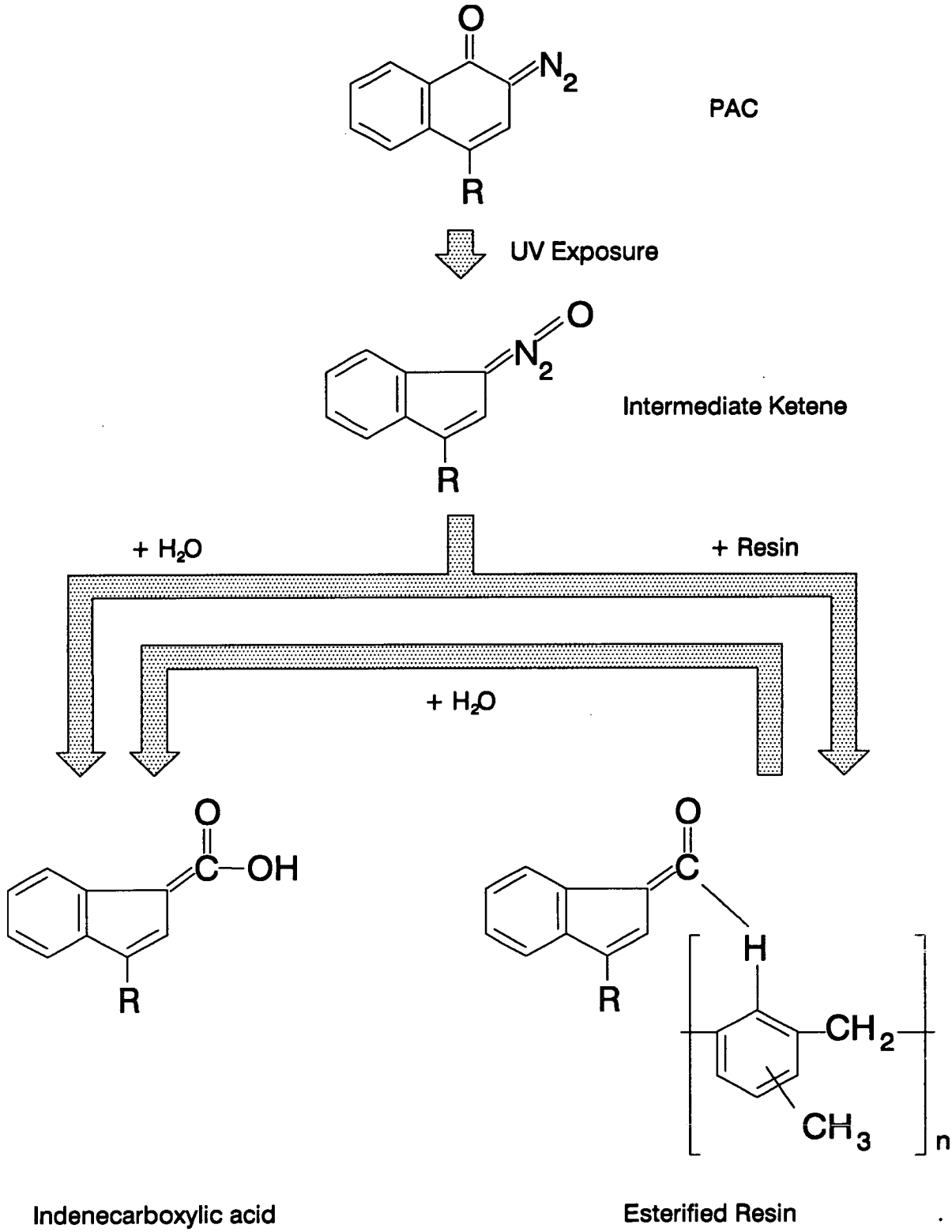

Figure 2–8: *The possible reaction paths of a DNQ after UV exposure.*

The region of the PAC molecule labelled R in Figures 2–7 and 2–8 is known as the backbone, or ballast group, and is often connected to multiple DNQ groups. When more than one DNQ is connected to the backbone, as is the case with most commercial resists, the PAC is described as being polyfunctional.[41]

The PAC has little influence on the resist's thermal properties altering them by a maximum of 5 - 10°C. Again extensive work[42–45] has been carried out on the optimum chemical composition for PACs. These studies indicate a polyfunctional PAC built on a hydrophobic backbone should maximise lithographic performance. This performance improves as DNQ numbers increase, provided that each DNQ group is not in close proximity to another. Lithographic performance is also enhanced when the backbone structure is transparent at the exposing wavelength.

Differences in the number of DNQs per PAC molecule, their position on the backbone and the backbone's structure affect the degree of dissolution inhibition/enhancement exhibited by the unexposed/exposed areas of the resist, though it should be noted that alteration of the PAC structure influences inhibition more significantly than enhancement.

2.2.3.3 Solvent

The solvent is present purely for the purpose of film deposition. Diglyme and ethylene glycol monoethyl ether (EGME) have traditionally been used as casting solvents. However recent concern over the possible adverse effects of these solvents on the female reproductive system has led to resists utilising 'safer' solvent systems, based on materials such as propylene glycol monomethyl ether acetate (PGMEA) and ethyl lactate.

2.3 A Generic Photolithographic Process

Section 2.2.3.2, discussed how resist photoactive compound is sensitive to radiation in the 300 - 500nm wavelength range. To prevent undesired exposure by the low end of the visible spectrum, it is normal for all lithographic processing to be performed under yellow lighting.

A typical positive resist lithographic process is graphically illustrated in Figure 2–9.[46] The substrate is given a dehydration bake and primed with HMDS (Hexamethyl Disilazane). This removes molecular water from the surface and should ensure the adhesion of the resist film.[22]

Liquid photoresist is dispensed at the wafer centre and high speed rotation is used to spread the resist out into a thin, uniform, dry film, typically 0.6 - 3.5 microns thick.

Directly after film deposition, a softbake or prebake is applied, rendering the coating stable at ambient temperatures. The elevated softbake temperature drives off a large percentage of the film's residual solvent.

A transmission mask is used to selectively choose the areas of resist for removal. A variety of illumination tools are commercially used to transfer the mask pattern onto the substrate and are reviewed in Section 2.8.

After exposure, a Post-Exposure Bake (PEB) may be applied. This optional process improves the adhesion and thermal stability of the final image and can also enhance the profile of the resulting features.

The resist is now developed, by the introduction of an aqueous base developer. This may be achieved by submerging the substrate in a bath of developer or by spraying developer on to the surface of a horizontal wafer. The variety of techniques available are discussed in Sections 2.10.4 and 2.10.5.

Following development, the wafer receives a high temperature hardbake which gives the pattern additional resistance to subsequent etch and implantation processes.

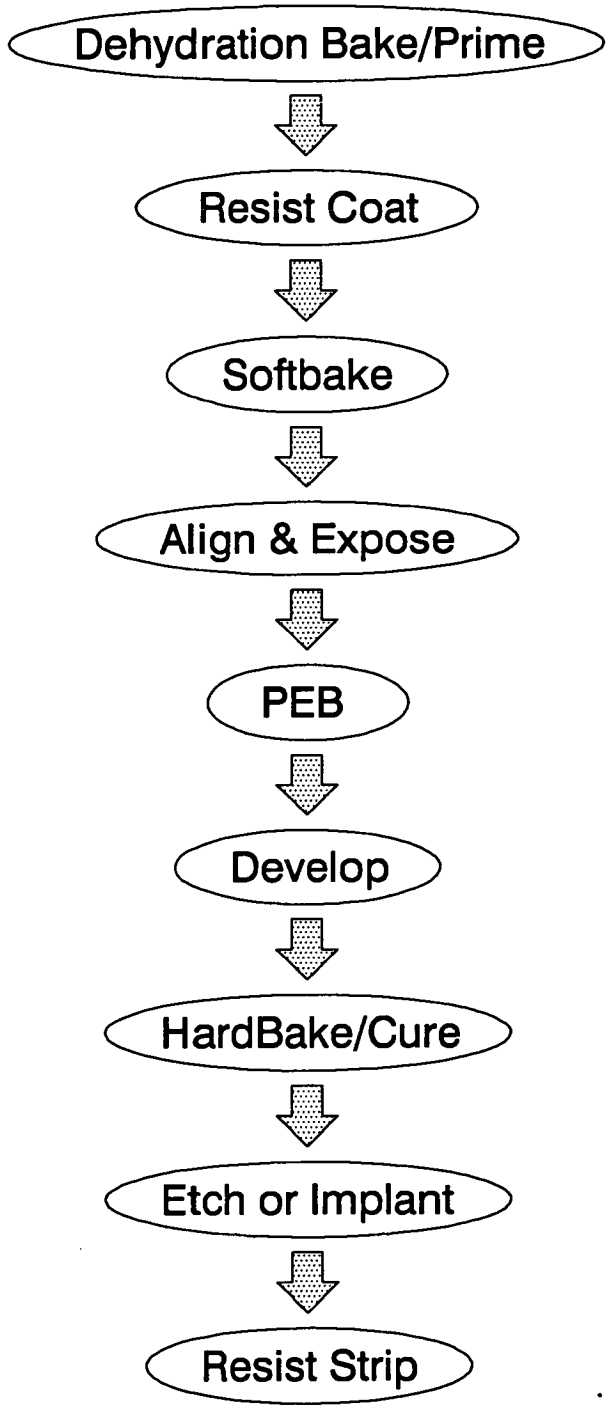

Figure 2–9: *Process flow diagram for a generic lithography process*

Finally, following the manufacturing process step, the remaining resist must be stripped away before further processing can take place. This is usually achieved by using an oxygen plasma or a strongly oxidising mineral acid.

Figure 2–10 illustrates the lithographic step involved in the etching of 'windows' in a silicon dioxide layer on a silicon substrate.[47]

2.4 Wafer Tracks and Lithographic Cluster Systems

Although lithographic process operations used to be performed on separate pieces of stand-alone equipment, the Eighties saw this practice replaced by automated wafer tracks. More recently, the introduction of lithographic cluster tools has given even higher levels of process integration in advanced fabrication facilities.

Stand-alone equipment tends to utilise batch processing, except for spin coating and exposure which are serial by nature, to maximise throughput. This contrasts with the integrated equipment approach where each wafer is processed individually at every sub-process and is automatically sent from one to the next under computer control. This automated approach gives a substantial increase in the final functional device yield when compared to batch processing. The improvement stems from three factors.

- The wafers receive less exposure to human operators,[48] thus decreasing the number of defects caused by operator contamination (particulates and alkaline metals).

- increased automation decreases the potential for 'human error' within the processing (missed process sub-step etc.) and therefore the level of reworks.[49]

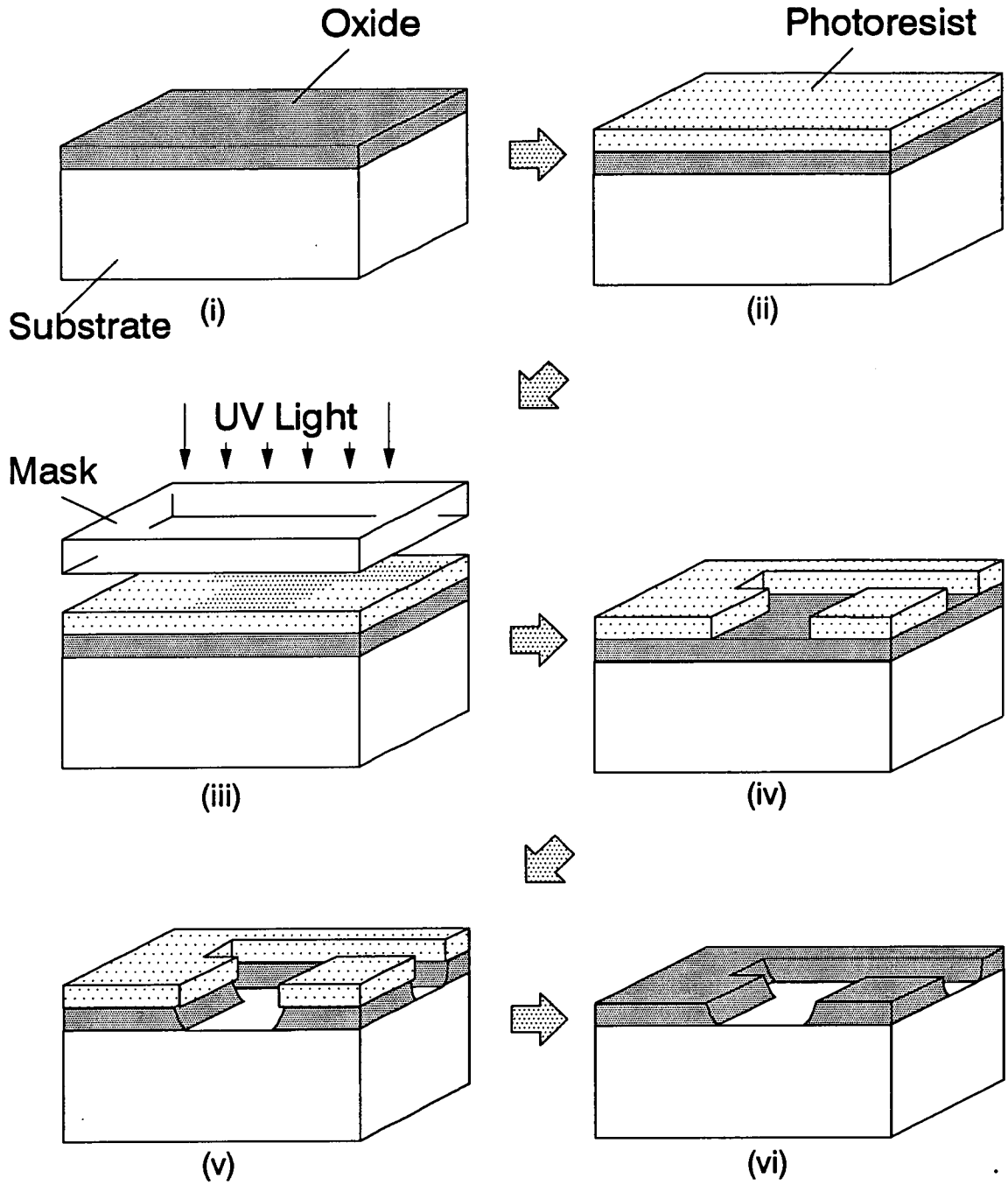

Figure 2–10: *ThelLithographic step involved in the etching of 'windows' in a silicon dioxide layer. (i) An oxide layer is grown on a silicon substrate. (ii) Photoresist is applied to the surface. (iii) The resist is exposed using either a patterned mask or reticle. (iv) The selected regions are developed away in aqueous developer. (v) The oxide is etched using HF or a plasma. (vi) The remaining resist is stripped off.*

- The computerised control of the wafer 'flow' allows tight control of the wafer-to-wafer interprocess wait time, which has been shown to have a significant effect on Critical Dimension (CD) control.[50,51]

2.4.1 Track Systems

Tracks consist of multiple modules linked by a linear transfer mechanism. Each of these modules, or stations, performs an individual process function such as prime, develop or bake.

Wafers are moved from one module to the next in a serial fashion using an air track or o-ring band transfer mechanism. Recent track systems, such as the SVG 88 series, utilise pick-and-place robot arms for transport between stations which reduce front-side particulate levels by almost two orders of magnitude.[52]

Tracks are arranged in either a 'coat' or 'develop' configuration, each consisting of two or three modules. The 'coat' track performs all pre-exposure processing whilst the 'develop' track does post-exposure processing. Often both types of track are found within a single housing, though it is equally possible to find multiple identical tracks in one frame. The number of modules on a given track is variable since some functions are optional (PEB and Hardbake) whilst others (dehydration bake/prime and hardbake) are still performed in off-line batch systems, for reasons that are discussed in Sections 2.5.3 and 2.11.1.

Track systems do not include an exposure tool, but can be interfaced to one to form a lithocell. Figure 2–11 illustrates a track and a stepper in a lithocell configuration. In this situation, the track system is dedicated to one particular stepper.

The linear nature of a track process means that the overall throughput is set by the slowest process function, very often development.

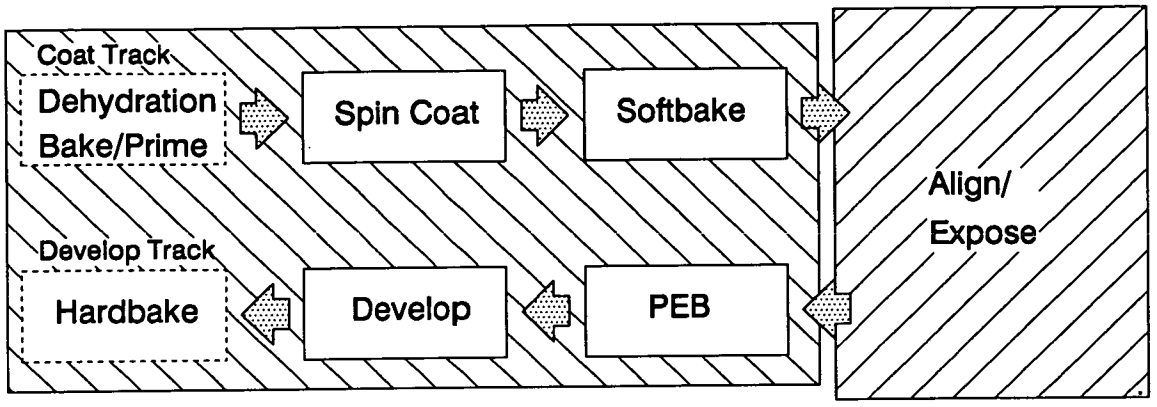

Figure 2–11: *A track system and stepper in a lithocell configuration. The arrows indicate the wafer flow. The functions within dashed boxes are those which are commonly performed off-line.*

2.4.2 Lithographic Cluster Systems

Lithographic cluster systems, such as POLARIS, SVG90 Series and TEL MkV - MKVIII, are essentially 'random-access' tracks, developed to maximise stepper utilisation. The stepper is the most costly piece of equipment in the lithography process; Cost of Ownership issues dictate that its maximum throughput should determine that of the complete process.

Figure 2–12 illustrates a typical POLARIS cluster tool layout. A central pick-and-place arm, responsible for all wafer transfers is surrounded by a stepper and all the process modules. The pick-and-place arm allows station to station transfers to be made in a random access fashion. A wafer need not wait at a module until the preceeding wafer has finished at the next station. Instead, it is moved to another station with equivalent function. Modules of each type are added until all the sub-processes have a capacity which equals or exceeds that of the stepper.[48]

This approach allows greater optimisation of individual process steps as time constraints can be relaxed to some degree. Clifford[48] describes the cluster tool configuration utilised by Texas Instruments in Dallas: 2 HMDS prime modules, 1

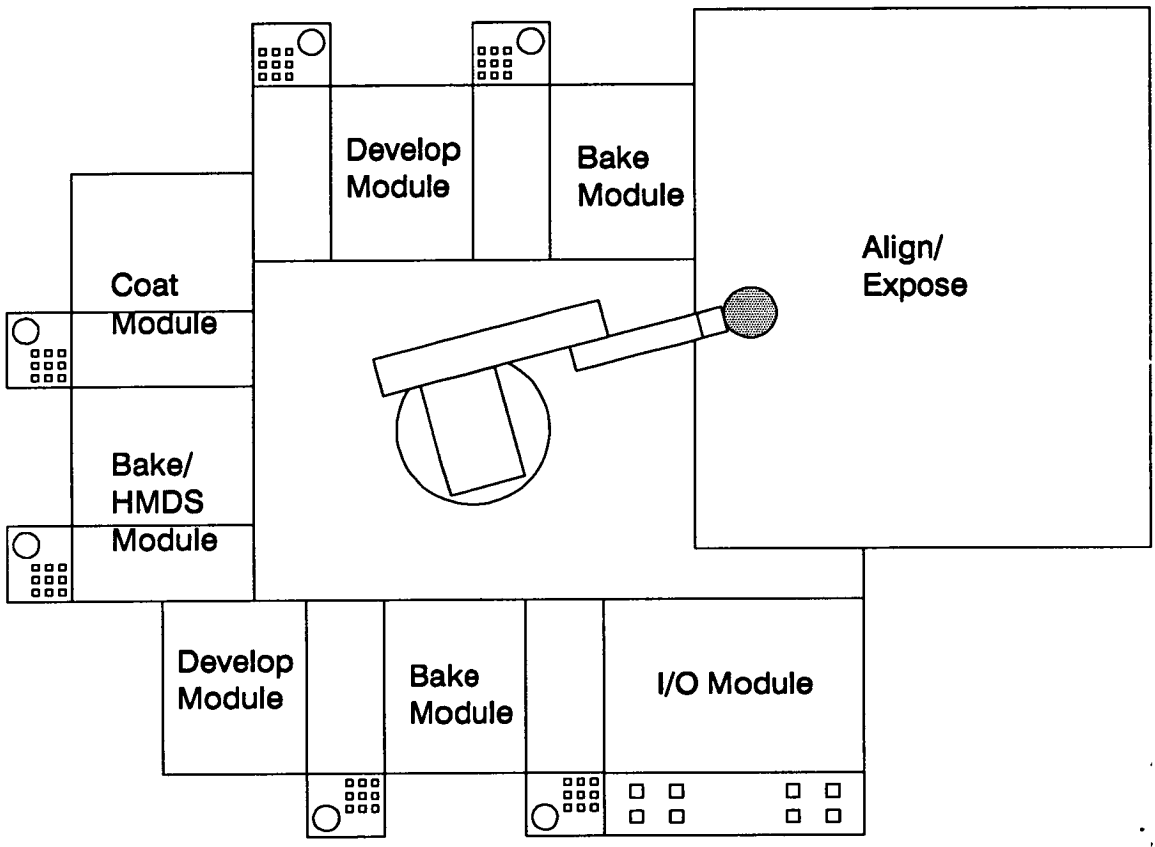

Figure 2–12: *A typical cluster tool configuration.*

coater, 1 softbake hotplate, 1 stepper, 1 PEB hotplate, 3 develop modules and 1 hardbake hotplate.

The use of complex scheduling software allows the wafer-to-wafer interprocess delays to be controlled much more tightly than on a conventional track, where the queueing time for the first few wafers differs from that of those subsequently processed. Clifford[48] describes how the use of cluster tools improved functional device yield by 4.3% over a previous track based system, through both improved CD control and an eightfold particulate reduction.

The following sections examine the individual process steps, reviewing both their purpose and their implementation in a modular system.

2.5 Adhesion Promotion

In lithography water is a serious contaminant. It reacts on the wafer surface to form a barrier between the substrate and the resist coating, as illustrated in Figure 2–13.[53]

In extreme cases this can cause the resist to 'lift' off the wafer during development, or etch, but more often leads to excessive etch undercut which impacts CD control.[54] The problem is size dependant, affecting smaller geometries first;[55] water removal is of particular importance in sub and deep submicron processes.

The water is normally removed by a dehydration bake. A chemical adhesion prime is then appied to the surface to prevent a subsequent re-hydrolysation of the surface.

2.5.1 Dehydration Bake

The dehydration bake is simply a high temperature bake ($> 100\,^{\circ}C$) that dissociates or 'boils off' the moisture from the wafer surface. Even after complete water removal, the substrate is still hydrophylic and can quickly reabsorb am-

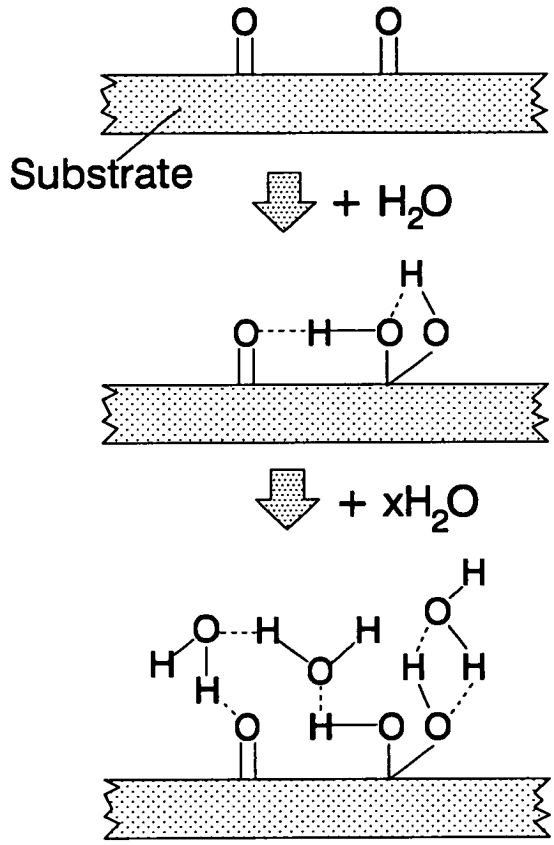

Figure 2–13: *Hydrolysation of a substrate surface.*

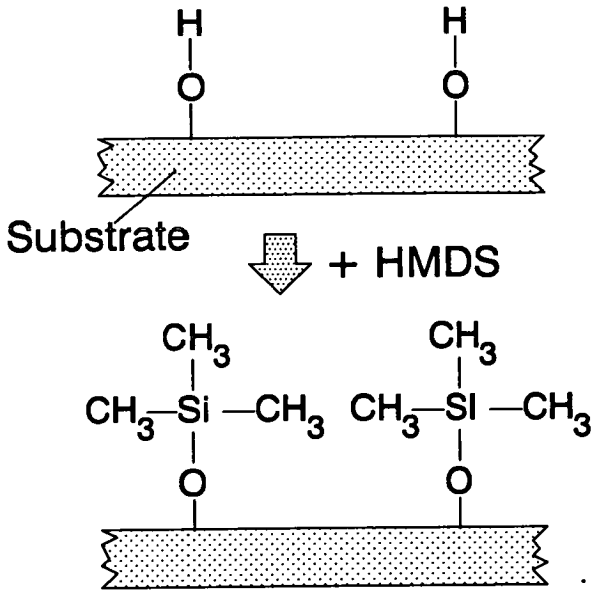

Figure 2–14: *Removal of hydrophylic surface hydoxyl groups by HMDS.*

bient moisture from the atmosphere, if not chemically treated with an adhesion promoter.[56]

2.5.2 Adhesion Prime

There are several chemicals available for adhesion promotion TCPS (trichlorophenylsilane), BSA (bistrimethylsilylacetimide), Monazoline C, Trichlorobenzene, Xylene and HMDS (Hexamethyldisilazane).[55] However, those containing chlorine are unsatisfactory since they cause aluminium corrosion. Of the remaining substances HMDS has become the industry 'workhorse' because the working lifetime of a primed wafer is days rather than hours.

Figure 2–14 shows the HMDS priming reaction, where hydrophilic hydroxyl groups on the wafer surface are replaced by hydrophobic trimethylsiloxyl groups.

The hydrophobic surface layer remains stable over long periods of time, when kept in a low humidity environment. Macbeth[57] demonstrated that adhesion enhancement did not deteriorate significantly over a six day period and elsewhere[58] lifetimes of up to 2 weeks have been reported.

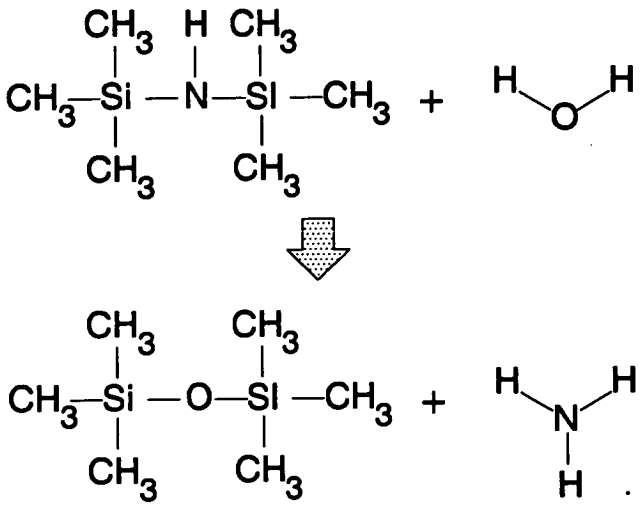

Figure 2–15: *The chemical removal of water by HMDS.*

In addition to priming the wafer surface, HMDS chemically removes any residual water left after the dehydration bake, by the reaction shown in Figure 2–15.[53,57]

The priming layer prevents undercut and 'lifting' because the hydrophobic bed of $-CH_3$ groups prevents developer from penetrating along the resist/substrate interface, whilst the hydrophylic hydroxyl groups on an unprimed surface actively encourage this kind of liquid penetration.[59]

It should be noted that although this process is known as adhesion promotion, the mechanical adhesion (in the sense of peel, pull etc) of a treated surface is far lower than that of a superdry surface, since hydroxyl bonding is much stronger.[59]

2.5.3 Dehydration Bake and HMDS Prime Application

Modular dehydration bake/prime systems usually utilise a conduction hotplate which bakes each wafer for 30-60 seconds. The bake may utilise reduced pressure, which enhances the process by substantially lowering the boiling point of water. Low pressure bakes tend to use temperatures under 150°C, while temperatures in excess of 200°C are more typical in atmospheric systems.

HMDS priming typically occurs in the same module, commonly while the wafer remains on the hotplate. HMDS vapour (formed by bubbling nitrogen through

HMDS liquid) is flooded into a chamber surrounding the wafer, again usually under reduced pressure, for a further 30 - 60 seconds. The wafer is then moved onto a chill plate for several seconds to return it to ambient temperature.

As previously mentioned, batch priming is used extensively in manufacturing facilities. Up to 200 wafers are placed in a vacuum convection oven and baked at 150°C for around 20 minutes. Then low pressure HMDS vapour is introduced to the oven for 5 - 10 minutes.

Experimental evidence[56,57] shows that both techniques are considerably better than the original technique of priming with liquid HMDS followed by a spin dry and yield equally good adhesion characteristics when equivalent pressure is used during prime,[55,56,60] with lower pressures giving the best results.

Arguably, in-line processing is preferable because of the reduced handling and improved rework times.[56] However, the fast purge speeds required for a 1 minute track prime result in high particle counts within the priming chamber and robotic handling arms on modern batch systems go some way to equalising the cleanliness issues.[61]

The choice of in-line versus batch priming should therefore be decided depending on the criteria of a particular production facility, considering particulate levels, number of wafers and photo rework rates.

2.6 Resist Coating

Photoresist is applied to substrates by spin-casting. It is the radial symmetry associated with this technique that dictates the essentially circular shape of silicon wafers. Wafer flats and notches, are present solely for alignment and identification purposes.

2.6.1 The Coating Process

Coating takes place within a spinbowl under a forced exhaust, which removes toxic solvents from the cleanroom atmosphere. In the centre of the spinbowl is a vacuum chuck. A wafer is placed on the chuck by the transfer system and is held under vacuum. Liquid photoresist is applied to the surface of the wafer. A short, low speed spin (around 1000 rpm) is used to spread the resist over the entire wafer surface. The application may be made either in a static or dynamic mode. During static dispense, the wafer is stationary whilst the resist is applied; the spread cycle commences only after the dispense is completed. In the dynamic case, the wafer is rotating at the spread speed when the resist is dispensed. In both instances the spread cycle duration is between 2 and 5 seconds.

The wafer is accelerated to a higher final spin speed (2000 - 7000 rpm) to spin off the excess resist. The duration of this spin is usually 15 - 40 seconds. During this time a thin uniform coating of resist is formed on the substrate surface.

During spin-off two things occur: firstly a rough, thick and uneven edge-bead is formed at the wafer periphery and secondly small resist droplets 'splash-back' on to the underside of the wafer. The edge-bead is extremely brittle and generates particulate even when touched gently, whilst the resist droplets can cause pre-alignment and focus problems on exposure tools.

An Edge-Bead Removal (EBR) process is therefore incorporated at this time to remove these problem sources. This involves application of a solvent to the underside (and sometimes top-side) of the rotating substrate. A final spin dries

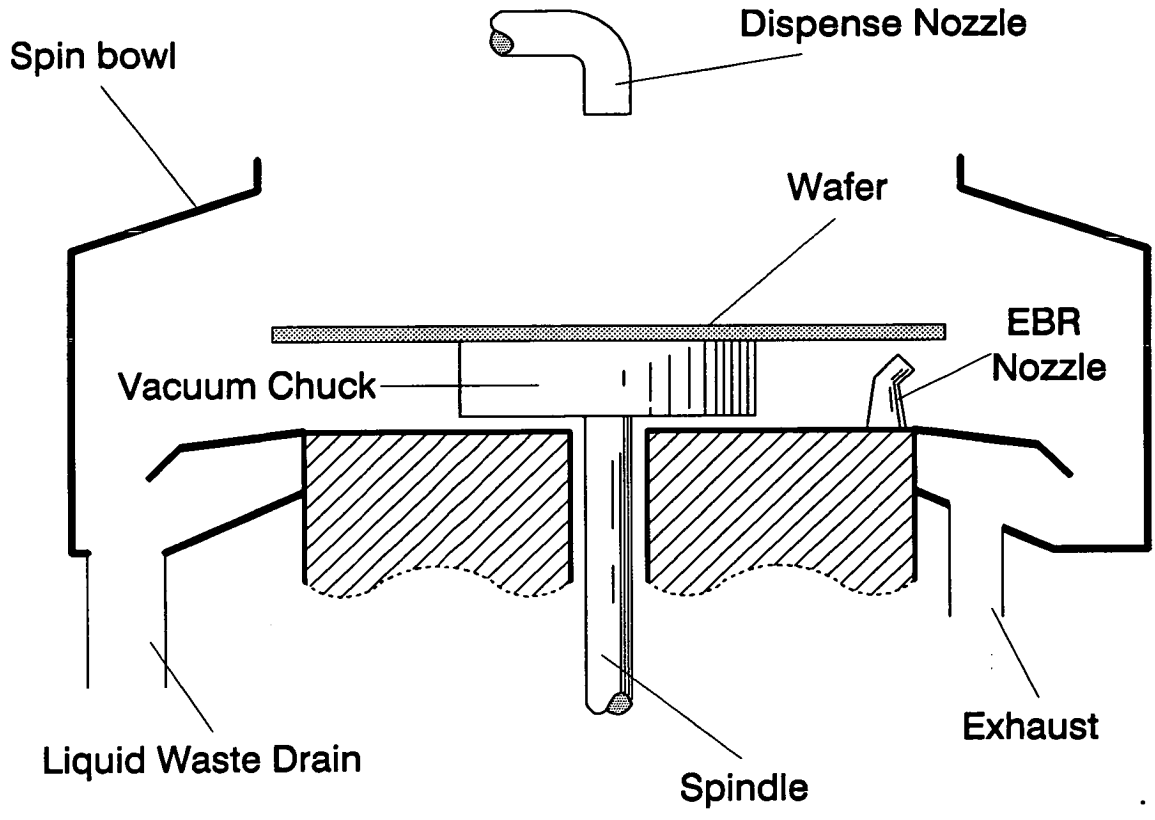

Figure 2–16: *Schematic diagram of a photoresist coater unit.*

off any residual solvent, then the wafer is returned to the handling system. Figure 2–16 shows a typical coater configuration.

2.6.2 Spin Casting Physics

The spin casting process can be broken down into 4 stages, illustrated on Figure 2–17: Deposition, spin-up, spin-off and evaporation of solvent.[62] There is an element of cross-over in the first three stages whilst the fourth occurs throughout the entire duration. There follows a short description of each stage.

Deposition: Excess resist is delivered to the substrate so that the centre of the wafer is covered, or wetted.

Spin-up: The entire wafer surface is wetted with excess resist. Rotation is used to make the deposited material flow radially under centrifugal force. A low, constant angular velocity provides the best conditions for spin-up. During a dynamic dispense, this process occurs simultaneously with deposition.

Spin-off: Excess resist is removed from the surface. Again the liquid flows radially under centrifugal force (but at higher speed). When it reaches the wafer edge the resist 'spins-off' breaking up into small droplets. A film of near uniform thickness is formed. This film continues to thin until either it becomes a solid (excessive solvent evaporation) or the wafer dewets (no resist left on the substrate). The process can overlap with the spin-up stage under certain conditions.

Solvent evaporation: This is the process of polymer concentration within the resist. The rate of solvent evaporation is controlled by the partial pressures of the solvent within the resist and the surrounding air, and by the convective and diffusive transport of the solvent vapor at the resist/air interface. Evaporation is on going throughout the coating process but becomes the dominating thinning mechanism after approximately 30 seconds of spin-off.[63]

It is desirable to control not only the mean thickness of the coating, but additionally its cross-wafer uniformity and wafer-to-wafer reproducibility. Many factors affect these three properties including resist viscosity, dispense volume, dispense rate, exhaust rate, spread speed, spread time, final spin acceleration, final spin speed and final spin duration. The two following Sections (2.6.3 and 2.6.4) review the influence of these factors on mean thickness, uniformity and repeatability.

2.6.3 Film Thickness

The mean thickness of a resist coating is primarily a function of the liquid resist viscosity and of the spin-off speed and duration,[64] though dispense volume,[64,65] spin-up speed[64] and the final spin acceleration[66] have all been shown to have

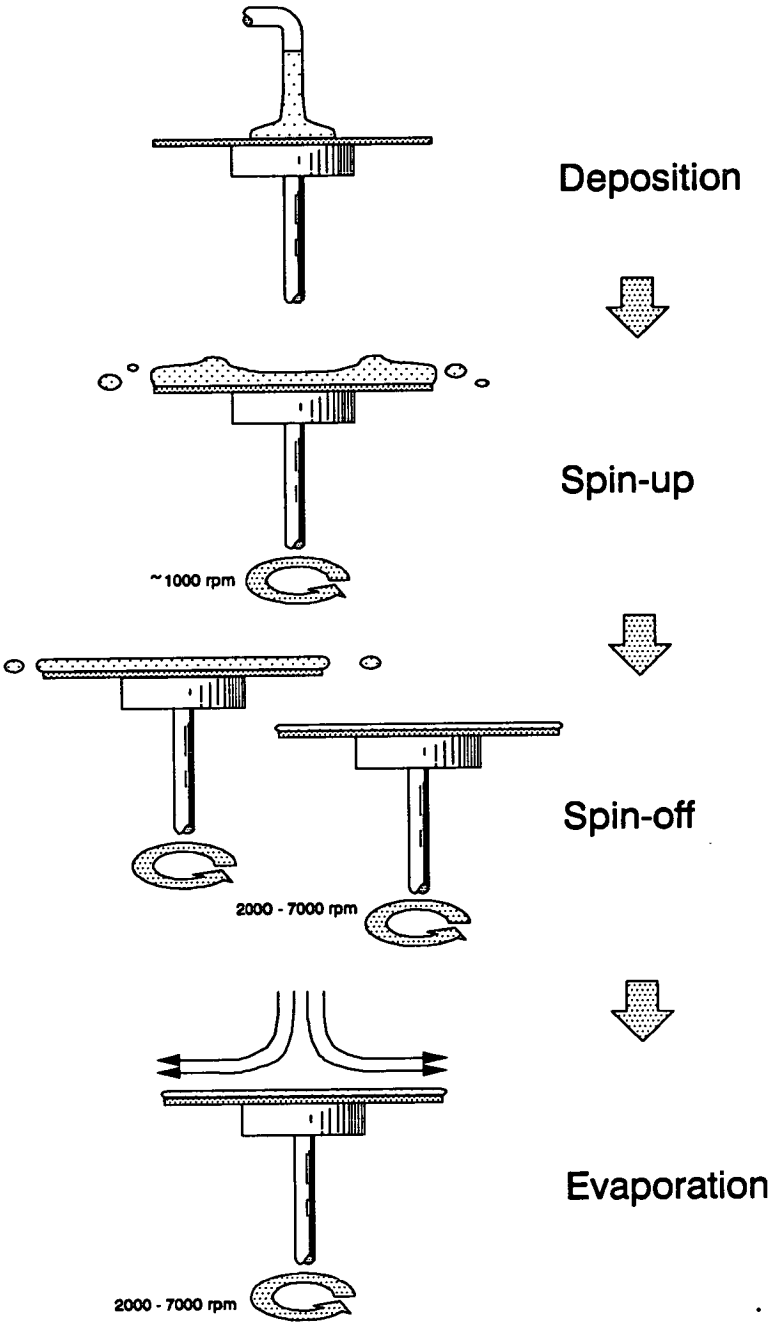

Figure 2–17: *The 4 stages of a spin-casting process.*

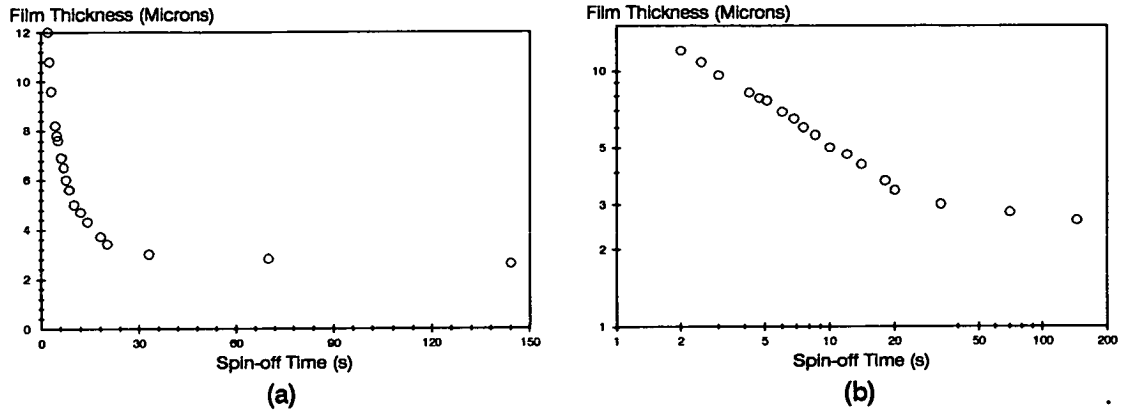

Figure 2–18: *Film thickness versus time during final spin (4100 rpm) for Shipley Microposit 1400-31 (a) on a linear scale and (b) on a log/log scale.*

second order effects. It is also commonly acknowledged[66–68] that exhaust rate has negligible effect on the average thickness.

Peurrung *et al.*[63] used in-situ interferometry to monitor the thickness of Shipley Microposit 1400-31 during coating. Figure 2–18[63] shows the results of this experiment. After approximately 30 seconds the rate of thinning decreases markedly and is particularly noticeable on the log/log data plot (Figure 2–18(b)). This is thought to be the point at which evaporation replaces physical flow as the dominant thinning mechanism.

Figure 2–19 illustrates how resist thickness varies with final spin speed when the spin time is kept constant. The data shows how OCG HiPR6512 and HiPR6517 thickness changes with spin speed when a 30 second final spin is used. The HiPR 6512 data was experimentally measured in the EMF and the HiPR 6517 data was taken from the manufacturer's literature.[69] Practical spin speeds range from around 2000 rpm to 7000 rpm. Below this range, too little resist is spun-off, leading to dewetting of the wafer periphery. Prolonged spinning at higher speeds results in the formation of stress fractures in the resist coating.[70] The final spin speeds used for large diameter wafers (200mm) are restricted to less than 3500 rpm, for mechanical reasons relating to the substrate mass.

Resist viscosity plays a significant role in the average coating thickness, with

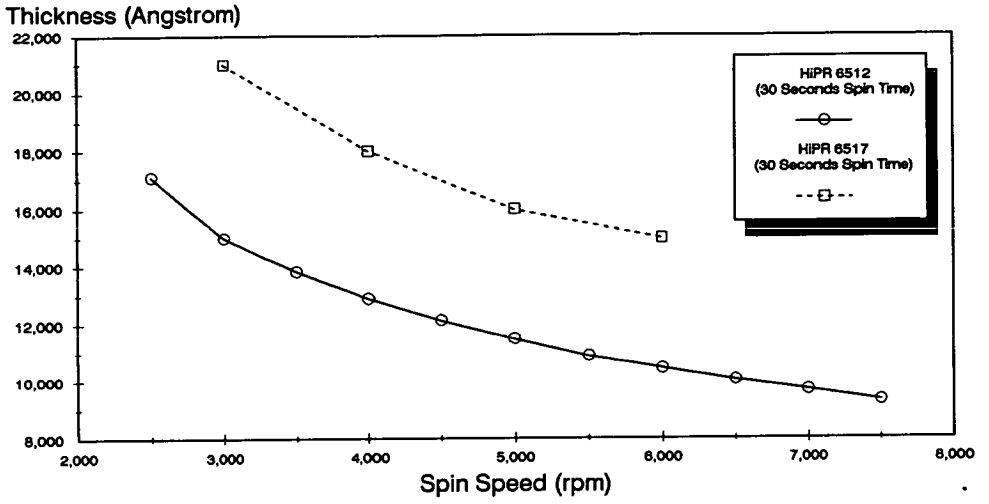

Figure 2–19: *Film thickness versus spin speed for a 30 second spin for HiPR 6512 and HiPR 6517 Resists.*

more viscous materials yielding thicker films. Since spin speed limitations restrict the range of thicknesses that can be produced by a single viscosity, resist vendors tend to produce a family of viscosities for each resist formulation so that the desired thickness can be realised. The viscosity is altered by varying the solids content (ie the PAC and novolak:solvent ratio). This is demonstrated in Figure 2–19, where HiPR 6517 is a higher solids content version of the standard HiPR 6512.

2.6.4 Thickness Uniformity and Repeatability

Resist thickness at the time of exposure plays an important role in determining the dimensions of developed features (discussed in Section 2.8.4.1). It is therefore important that cross wafer uniformity and wafer-to-wafer repeatability should be as good as possible.

Temperature and humidity have a strong influence on both values as accelerated drying causes large thickness differences between the wafer centre and the edge, resulting in a characteristic bowl shape.[71] Therefore day-to-day temperature and humidity control play a large part in the long term repeatability and uniformity

of a coating process. Advanced coating modules now have environmental control chambers which, because of their small volume, can maintain tighter specifications than a cleanroom.

Although dynamic dispense is often recommended by most resist manufacturers, theoretical predictions[64] and experimental evidence[72] indicate that static dispense produces equal, if not better, uniformity and repeatability. However, static dispense appears to be more susceptible to random coating defects[73] (Section 2.6.5).

Uniformity and repeatability improve with increased dispense volumes,[66] however the increased chemical costs must be considered. Love[71] demonstrated how increasing the dispense rate during dynamic dispense improves uniformity with no added expense.

Uniformity is best when low spread speeds are used (< 1000 rpm), however very low speeds (< 700rpm) lead to dewetting of the wafer periphery.[74] Similar results are observed when the spread cycle is made too long.

Both uniformity and repeatability are affected by the acceleration used to reach the final spin speed. Low accelerations give poor cross-wafer results. Moderate accelerations yield good uniformity, though the mean thickness is sensitive to minor acceleration fluctuations. High acceleration is preferable, providing a process which is stable in terms of repeatability and uniformity.[66,74]

Final spin time has the largest effect on both repeatability and uniformity, with short times providing the worst results. After the spin time exceeds 30 seconds, the improvements induced by additional increments become less noticeable.[74] This suggests that a process which ends while spin-off is still occurring produces a more variable coating than one which has entered the evaporative regime. The final spin speed also affects uniformity, with better films being produced at the lower speeds.[74]

The final factor affecting uniformity and repeatability is spinbowl exhaust. Uniformity and repeatability are optimum with zero exhaust,[66–68] however this condition does not remove the toxic solvents and so is unacceptable. Repeatability

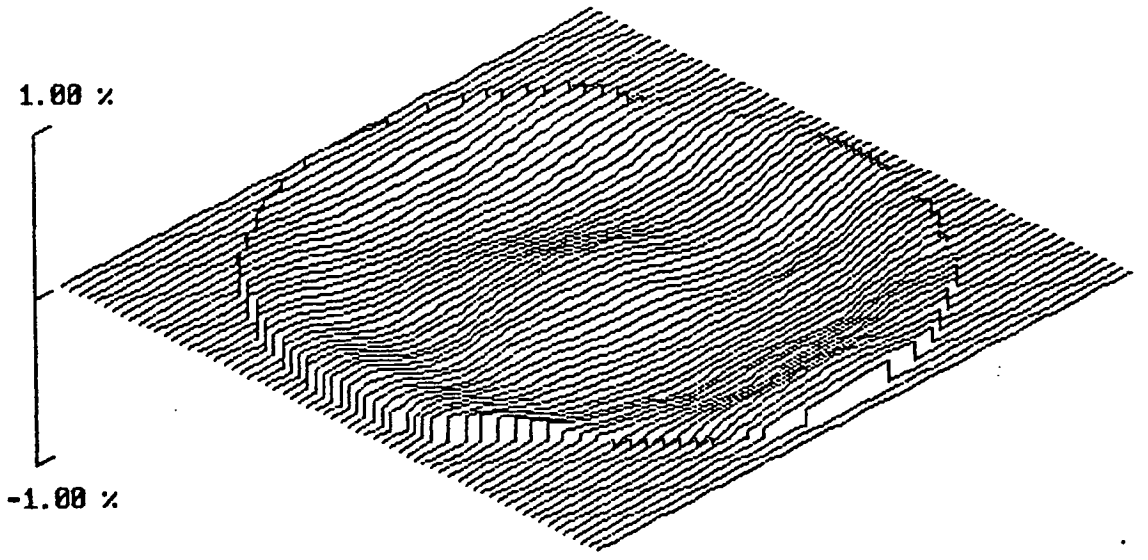

Figure 2–20: *A typical cross-wafer uniformity profile.*

decreases as the exhaust rate is increased but uniformity returns to a second minimum value at somewhere between 10 and 16 SCFM. Although the uniformity at this point is worse than that at zero extract, the cross-wafer variations are 50% less than those observed at non-optimum exhaust rates.[67,68] The precise optimum exhaust level depends on resist type and the air flow over the wafer surface which is determined by the wafer diameter and the spinbowl design.

Figure 2–20 shows typical cross-wafer thickness variations, with the film thickening towards the edge, as produced by a Prometrix Lithomap considering 49 measurement sites.[68]

2.6.5 Coating defects

Coating defects (i.e., regions where the resist thickness varies significantly from the wafer average) can occur for a variety of reasons. The most common types of defect are striations and 'comet tails'. Striations are radial streaks that result from flow within the resist due to vertical temperature gradients which are caused by evaporative cooling at the resist surface.[75] The addition of Surface Levelling

Agent (SLA) to a resist substantially reduces the amount of conductive flow within the forming film and therefore the number of striations that occur.[75]

'Comet tails' are thickness defects caused by particulates, either within the resist or on the wafer surface. The particle causes turbulence in the normal radial flow during spin-off and forms the 'head' of the comet. The 'tail' extends from the particle radially towards the wafer edge. The frequency of this kind of defect is closely linked with particulate control.

Air bubbles within the liquid resist can represent a serious defect source, particularly in more viscous materials. Bubbles trapped within the deposited resist form tiny pinholes in the final coating.[76] They are more prevalent in manually dispensed situations and can be reduced by using an automatic dispense system with wide bore tubing for resist transport.

2.6.6 Edge Bead Removal (EBR)

An extremely thick region of resist (2 or 3 times the mean value) is formed at the periphery of the wafer, due to surface tension effects. This lip of resist, known as the edge bead, is easily broken off by casual contact with tweezers or other handling equipment.

In addition to the edge bead, some of the droplets formed during spin-off stay attached to the wafer edge in an extruded form (see Figure 2–21).[77] These brittle extrusions can be knocked off by even the most gentle contact. Some of the droplets are deposited on the underside of the wafer near the edge and can cause handling problems on steppers[78] and projection aligners.[79]

Edge Bead Removal (EBR) is used to eliminate the three spin-coating problems mentioned above. Two forms of EBR are used; backside and frontside, though the latter is always used in conjunction with the former.

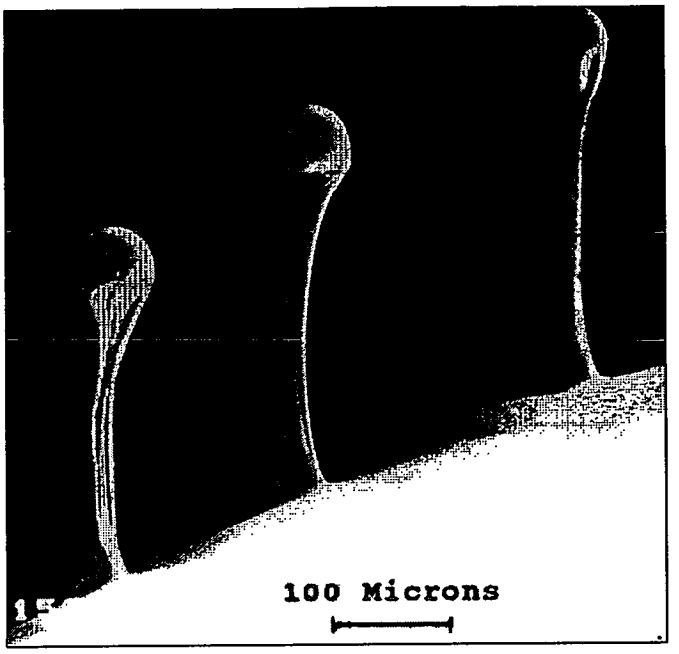

Figure 2–21: *SEM photo of extruded resist at a wafer edge.*

2.6.6.1 Backside EBR

During a backside EBR process, solvent (commonly PGMEA, n-butyl acetate or ethyl lactate) is supplied from a nozzle to the backside of the substrate. Centrifugal force moves the liquid radially outward. The solvent dissolves any resist it contacts on the wafer underside or edge, before spinning off as droplets (Figure 2–22)(a)).[80]

Increasing the solvent supply rate or decreasing the rotation speed allows the liquid to transfer to the front of the wafer and remove the edge bead (Figure 2–22(b)). A short high speed spin dries the substrate after solvent application.

As the amount of resist removed from the wafer topside during a backside EBR process is very sensitive to minor changes in solvent flow rate and wafer centring, the outer edge of the remaining resist often has a ragged appearance.

2.6.6.2 Frontside EBR

Topside EBR is applied after a backside EBR process as depicted in Figure 2–22(a). A fine stream of solvent is applied to the wafer surface, approximately 1-2

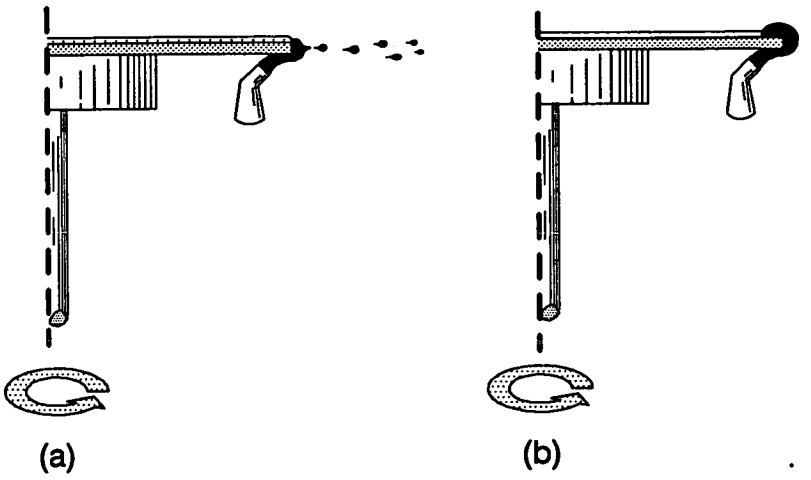

Figure 2–22: *(a) Removal of extruded resist by backside EBR. (b) Removal of the actual edge bead by backside EBR.*

mm from the wafer edge using a mobile dispense arm. The solvent is dispensed for a few seconds whilst the substrate is rotated at relatively high speed (2000 - 3000 rpm). The wafer is then spun dry. The resulting EBR ring is much 'cleaner', i.e. better defined, than that produced by a backside process and has greater repeatability.

2.7 Softbake

2.7.1 Motivation for Softbake

After film deposition, the photoresist coating has a high residual solvent content. This makes the film tacky and somewhat unstable since evaporation is still occuring. As solvent is lost the tackiness decreases and the film thins and densifies. The coating takes several hours to become stable at room temperature.[81]

A softbake accelerates the evaporation/densification process and can stabilise the film thickness in under a minute. The level of densification increases with both temperature and time. Paniez *et al.*[81] have shown how thickness corresponds to log time in a linear manner for all temperatures. Data collected in the EMF using

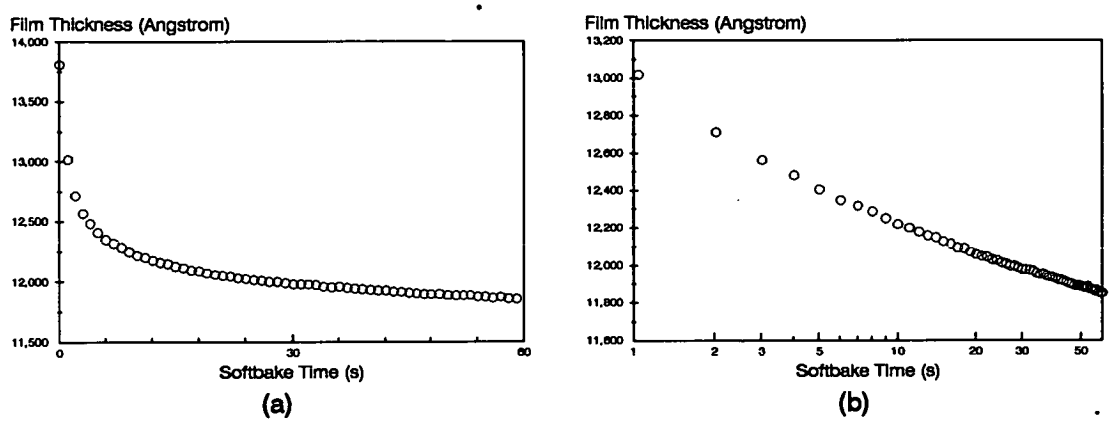

Figure 2–23: *Thickness changes in HiPR 6512 during a 60 second, 90°C softbake (a) on a linear scale. (b) on a log time scale.*

the real time thickness monitoring equipment described in Chapter 4, verified this result (illustrated in Figure 2–23).

The softbake relieves much of the internal stress within the film (introduced by spin-casting) and consequently improves the resist's adhesion qualities.[59]

The final benefit provided by the softbake is increased thermal stability of the developed features. Higher bake temperatures provide the greatest improvements.

2.7.2 Softbake Application

The softbake is typically applied to each wafer individually on a contact, or proximity hotplate, although it can be applied batchwise in a convection oven. In the latter case, the batch of wafers is baked for between 30 minutes and 1 hour at a temperature around 100°C.

Modular systems utilise hotplates where each wafer is baked individually for a period of between 30 and 90 seconds. A hotplate consists of a large piece of metal with a high thermal inertia. It contains a heater unit and a thermocouple which are used to hold the metal plate at a preset temperature, usually to better than ±2°C.

During a contact bake the wafer is held, under vacuum, against the hotplate. The large thermal inertia of the plate prevents excessive cooling when the 'cold' wafer contacts it; this is a particular problem with large (150mm and 200mm) wafers. Contact bakes are typically 30 seconds to 1 minute in duration.

It has become common to use proximity baking, where the wafer is held very close to, but not touching the hotplate. This prevents hotplate temperature fluctuations when using large wafers and reduces frontside particulate levels.[82] The absence of direct thermal conduction imposes a slight time penalty on this approach and bake times are typically 75 - 90 seconds.

Subsequent to hotplate baking the wafer is returned to ambient temperature by several seconds of contact with a water-cooled chill plate.

2.7.3 PAC Degradation During Softbake

PAC is not only photosensitive but also thermosensitive. When exposed to elevated temperatures, ($> 70°C$) it begins to thermally decompose into non-photosensitive products.[83] This destruction of the PAC results in a decrease in photospeed and therefore a decrease in throughput. It is generally accepted that at temperatures of between 110 and 130 °C significant PAC breakdown occurs (20-30%). Once this point is reached, each further 10°C increment destroys approximately 50% of the remaining inhibitor.

2.7.4 Softbake/PEB Combination

Thermal stability can be improved without sacrificing photospeed when a two stage bake is administered. A low temperature softbake ($< 100°C$) is applied to stabilise the film before exposure. Following exposure, a second Post Exposure Bake (PEB) at a higher temperature, is performed. This enhances the film's thermal and adhesion characteristics. At this point PAC degradation has less impact on throughput as the indene carboxylic acid has already been formed.

When a single stage bake procedure is used, i.e. no PEB, softbake temperatures are generally slightly higher (110 - 115°C) to maximise adhesion and thermal stability.[84]

2.8 Resist Exposure

Several exposure techniques are available, and the best choice for a given application depends on three main technical and economic criteria.

These are:[21]

Resolution: The system must be capable of resolving the finest detail, or Critical Dimension (CD), on the mask. This CD is determined by the product design and must be reproduced over the entire wafer with a certain dimensional tolerance, also specified by the product design (typically ±10%).

Registration: All functioning devices require several lithography stages, each with a separate mask pattern. Each layer, other than the first, must be aligned to the prior patterning. The misalignment that can be tolerated is generally one third to one fifth of the smallest feature.

Yield: This is the percentage of good die (i.e. devices working within specifications) produced. Production costs are determined by total throughput, hence economic success is directly related to yield. Yield is reduced by misalignment, bad CD control, coating defects and errors in the processing sequence.

2.8.1 Shadow Techniques

This is the simplest form of exposure and entails flood exposing a resist-covered wafer through a mask. The mask, usually made of quartz, is transparent at U-V wavelengths. Opaque regions are defined in chromium which attenuates the exposing radiation by a factor of around 100, depending on thickness.

2.8.1.1 Contact Printing

The wafer and mask are held around 50 microns apart while alignment is performed. The wafer is viewed through windows in the mask using a split-field microscope.[46] The wafer is moved until two diametrically opposite alignment targets, placed during the initial lithographic stage, are centred in alignment windows in the mask pattern. After alignment is complete, the mask is brought into contact with the wafer. The resist is exposed using a collimated light beam from a mercury arc lamp with suitable condenser optics. Hard contact printing is limited only by diffraction at the mask edge and so transfers the mask pattern with almost 100% accuracy.[85] No other imaging technique offers a higher resolution capability. However, this ultimate capability is seldom achieved, as debris between the mask and wafer and surface flatness variations result in finite gaps between the mask and substrate. Where gaps occur, Fresnel diffraction results, causing a significant loss of linewidth control.

Although capable of submicron geometries, the problems associated with producing a wafer scale 1:1 mask at such feature sizes and alignment considerations make such processing impractical.

The most serious implication of contact printing is defect damage.[21,85] Debris between the mask and wafer tends to either damage, or adhere to, the mask. The defects and damage are not only printed onto the current wafer but are also reproduced on all subsequent prints. The accumulation of damage and particles results in continually falling yield. Practically, a mask must be cleaned after 10, or so, exposures and replaced with reasonable frequency.

2.8.1.2 Proximity Printing

Proximity printing is identical to contact printing, except that a constant, finite gap is maintained between the mask and wafer during exposure.[21,85] The resulting improvement in defect control increases the period between cleans to around 4 hours and significantly increases the mask lifetime. However, these benefits are

gained at the expense of resolution and linewidth control. The minimum dimension, CD_{min}, which can be reliably produced is[46]

$$CD_{min} = \sqrt{s\lambda} \tag{2.1}$$

where s is the mask/wafer separation and λ is the exposing wavelength. In a practical system where $\lambda = 365$nm and s = 15 μm, the printing resolution is limited to around 2.4 μm.

Wafer and mask flatness tolerances dictate a separation of at least 5 μm. However, small working distances lead to poor cross-wafer linewidth uniformity and a working distance of 15 μm or more is required to produce reliable cross-wafer results.

2.8.2 Projection Systems: Image Formation

A system of lenses can be used to project the image of a mask onto a wafer surface. The resulting image has a resolution far superior to that obtained by proximity printing, whilst defect problems are further reduced. The resolution and quality of the image formed are highly dependent on the characteristics of both the optics and the illumination source.

Before the various types of projection exposure equipment are introduced, the system characteristics which limit the performance of a general projection system will be reviewed.

2.8.2.1 Numerical Aperture (NA)

A lens has a finite size, therefore only those rays which leave an object in a certain solid angle can pass through it and be imaged. Every optical system has some aperture that limits the rays which can be imaged, whether it is a physical hole or simply a lens edge.[86] The Numerical Aperture (NA) is related to the collecting ability of the optical system and is given by

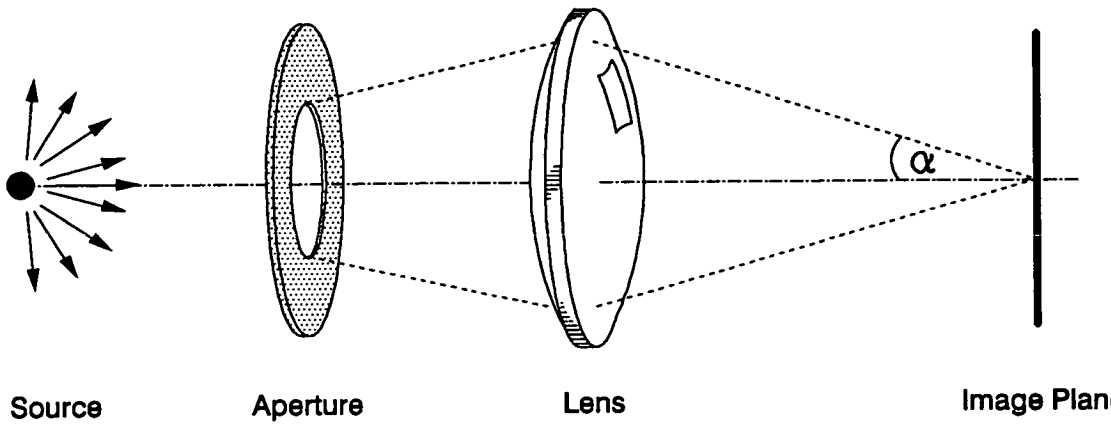

Figure 2–24: *NA equals nsinα. The NA illustrated is for the lens/aperture system. The NA for the lens by itself would be larger with the lens edge restricting the light collection.*

$$\mathrm{NA} = n\sin\alpha \tag{2.2}$$

where n is the refractive index of the transmission medium on the image side of the lens (usually air) and α is the angle subtended at the image by the outermost ray from the exit pupil of the system (See Figure 2–24).

2.8.2.2 Partial Coherence (σ)

Monochromatic light waves have identical frequency but may differ in phase. Partial coherence is a measure of the correlation between the optical disturbances produced by different points in an extended light source.[87]

Lasers are a source of totally coherent light, where all the light has identical phase. Most other sources produce incoherent light; the phase of their light is completely random. Incoherent sources can be used to produce coherent illumination within an optical system.[86] This is possible because all the light radiating from a given point within the source is coherent; it can only radiate at one intensity at any given time. Coherence can therefore be obtained by illuminating the object

with light from a small region of the source. The smaller the region the higher the degree of coherency.

In general, condenser optics are used to direct light from the source on to the object (mask) which is then imaged by the objective optics.

The degree of coherence, or the partial coherence, σ, in such a system is defined as[86]

$$\sigma = \frac{r_s}{r_o} \tag{2.3}$$

where r_s is the radius of the image of the source at the objective and r_o is the radius of the objective. σ can also be evaluated by taking the ratio of the numerical apertures of the condenser and the objective.[21]

$$\sigma = \frac{NA_{condenser}}{NA_{objective}} \tag{2.4}$$

Coherent and incoherent illumination have σ values of 0 and ∞, respectively. Most projection exposure tools operate with partial coherences in the range $0.5 < \sigma < 0.8$.

2.8.2.3 Modulation Transfer Function (MTF)

The Modulation Transfer Function (MTF) is used to measure how accurately an optical system transfers an image, with respect to contrast and sharpness. Ideally the object to be imaged should have a sinusoidally varying intensity, however this is impractical in a lithographic situation.[21] Instead a periodic grating of equally sized lines and spaces is substituted, where the spatial frequency is x.

$$\text{Spatial Frequency} = \frac{1}{\text{Line Pitch}} \tag{2.5}$$

The modulation or contrast, M, of an image of given spatial fequency is defined as[86]

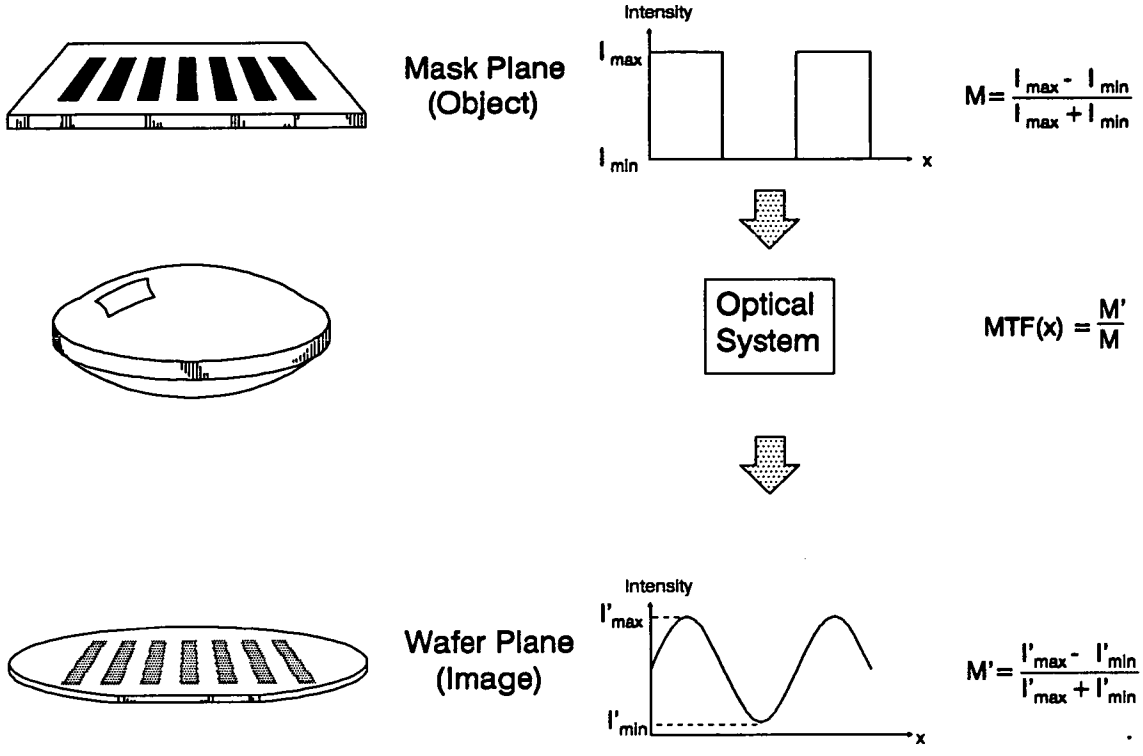

Figure 2–25: *The MTF is calculated by dividing the contrast of the image intensity profile with that of the object intensity profile.*

$$M = \frac{I_{max} - I_{min}}{I_{max} + I_{min}} \tag{2.6}$$

where I_{max} is the maximum intensity at the centre of a clear region and I_{min} is the intensity at the centre of an opaque area. The MTF is the ratio of the modulation in the image plane, M' to that in the object plane, M, and is always less than, or equal to, one. Figure 2–25 illustrates how the MTF of an optical system is calculated.

The MTF is a function of both the spatial frequency, x, and the system NA. Figure 2–26(a) illustrates how MTF varies with spatial frequency for various ideal lenses of different NA under incoherent illumination.[88]

If the spatial frequency is normalised by $\frac{NA}{\lambda}$ then the various lines of Figure

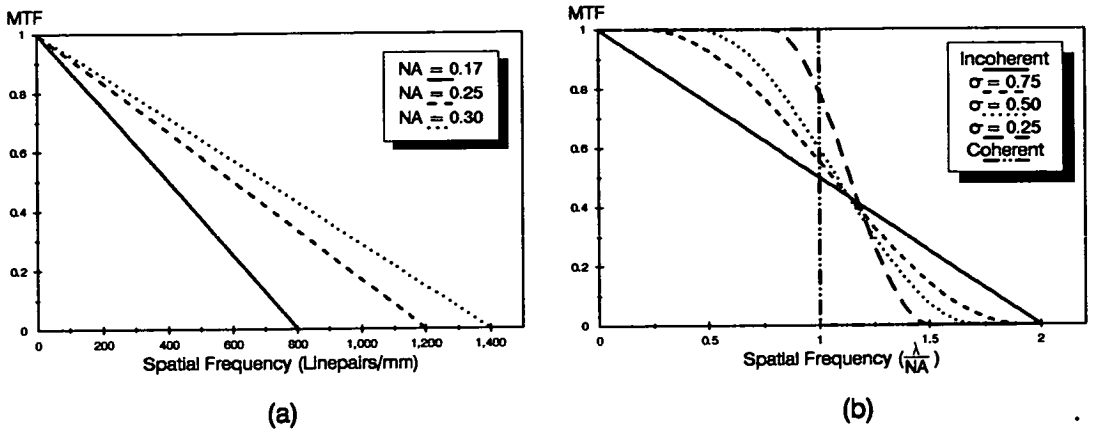

Figure 2–26: *(a) MTF variation with spatial frequency for several different NA ideal lenses under incoherent illumination (λ = 400nm). (b) MTF variation with spatial frequency under several different partial coherencies (spatial frequency normalised by $\frac{\lambda}{NA}$).*

2–26(a) lie on top of each other, decreasing linearly from 1 to intersect the x axis at 2, as shown in Figure 2–26(b).[88]

This same figure shows the effect of partial coherence on MTF. The second limiting case, coherent illumination, produces a unity step function which cuts-off to zero at a spatial frequency of $\frac{\lambda}{NA}$. The use of partially coherent over incoherent illumination enhances the contrast of images with a lower spatial frequency and decreases the contrast of those with higher frequency.

The Rayleigh criterion defines the minimum resolvable feature in the projected image as:

$$d_{min} = \frac{k_1 \lambda}{NA} \tag{2.7}$$

From Figure 2–26(b) it can be seen that k_1 has a minimum value of 0.5 when an ideal lens is used in incoherent illumination. In practice, this value cannot be realised because all lenses have some imperfections and the illumination will have some coherence.

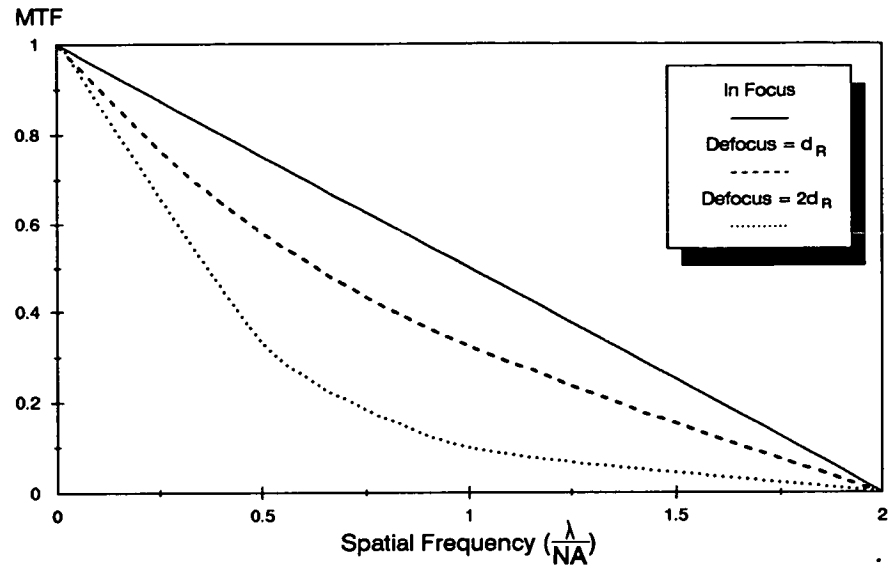

Figure 2–27: *MTF degradation due to defocus under incoherent illumination*

The MTF magnitude is also altered by focus changes. As the image is moved away from the plane of ideal focus the MTF and hence the image contrast decreases. The Rayleigh depth, d_R, is a convenient measure of defocus, and is given by the expression:

$$d_R = \frac{\lambda}{2NA^2} \tag{2.8}$$

At a distance d_R from the ideal focal plane, perceptible MTF degradation is observed and at $2d_R$ defocus the usable spatial frequency decreases by around two thirds (see Figure 2–27).[86]

This leads to the second of the Rayleigh criteria which defines the depth of focus (DOF) of a projected image as:

$$DOF = \pm \frac{\lambda}{2NA^2} \tag{2.9}$$

Inspection of the first Rayleigh criterion (Equation 2.7) shows that it is desirable to increase NA and shorten the exposing wavelength, so that resolution can be enhanced. However, the DOF expression (Equation 2.9) indicates that this

will decrease depth-of-focus. Since a reasonable DOF is required to compensate for flatness imperfections, topography and the finite thickness of the resist layer, a compromise is required between resolution and DOF. It should be remembered that Equations 2.7 and 2.9 refer only to the image intensity and that various other effects involved in the transfer of the image to the resist mean that the minimum printable feature size and its depth of focus are in practice different from the values predicted by Equations 2.7 and 2.9.

It is therefore customary to describe the resolution of a given resist/developer process using Equation 2.7 and to include the finite contrast required by the resist into the k_1 factor.

Similarly, the second Rayleigh Criteria (Equation 2.9) is usually modified to:

$$\mathrm{DOF} = \pm \frac{k_2 \lambda}{2\mathrm{NA}^2} \tag{2.10}$$

where k_2 is a term that depends on feature size and resist contrast requirements.

Resist processes are often described in terms of the k values they can realise. Obviously, small (less than 0.7) k_1 and large (over 1) k_2 values are best.

2.8.3 Projection Systems: Implementation

It is difficult, and extremely expensive, to produce an optical system capable of achieving high resolution over a complete wafer, especially as fabrication trends move towards larger wafers and smaller critical dimensions. Consequently, a reduced image field is used, where the required resolution and cross-field distortion limits can be met at reasonable cost.[21] This field is then used to expose the entire wafer either with a mechanical scan or by a step-and-repeat procedure. Figure 2–28 illustrates the 3 main projection exposure techniques, 1:1 wafer scan, reduction step-and-repeat and 1:1 step-and-repeat.[85]

In each case, the mask is divorced from the wafer and hence is protected from particulate contamination . The effects of defects can be further reduced by fitting

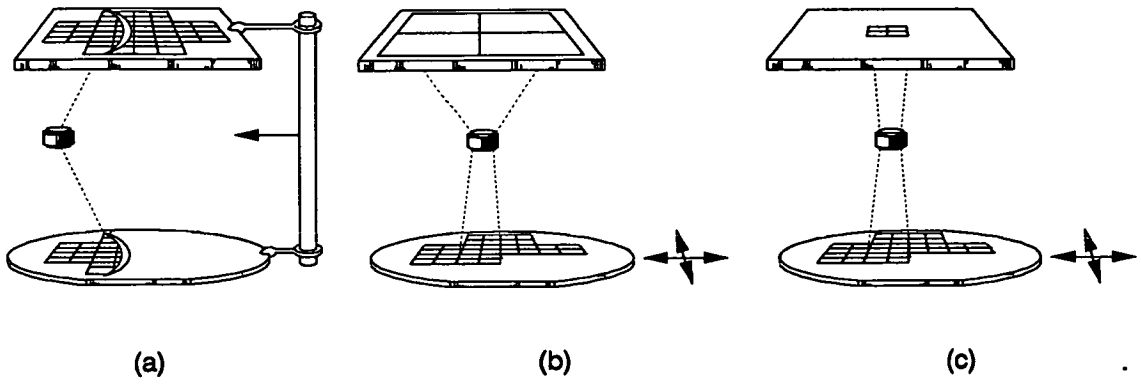

Figure 2–28: *Schematic representations of the 3 main projection exposure techniques. (a) 1:1 Projection scan. (b) M:1 Reduction step-and-repeat. (c) 1:1 Step-and-repeat.*

the mask with a pellicle.[21,86] This thin transparent film holds particles a few millimetres from the mask surface, rendering them out of focus in the image plane and significantly reducing the number of printed defects.

2.8.3.1 Scanning Projection Systems

This type of equipment is typified by the Perkin Elmer 'Micralign 340' series.[21,46,85] A series of spherical mirrors is used to produce a 1:1 image of the mask pattern on

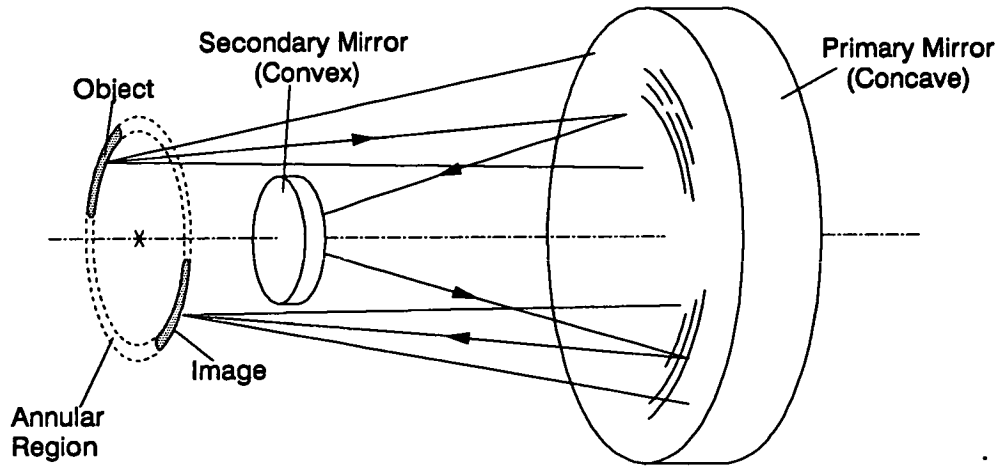

Figure 2–29: *The reflective optics of the Perkin Elmer 'Micralign' series*

the wafer, in the manner shown in Figure 2–29. The optics design gives optimum performance over an annular field about 1mm wide, within which all aberrations are negligible. Folding mirrors are used to move the object and image planes to locations convenient for mask and wafer placement.

The mask is illuminated by a mercury lamp and condenser system with the illumination field restricted by a 'banana' shaped slit to the annular region.

The mask and wafer are both scanned past the optical system so that the entire wafer surface can be exposed. The mechanical scan system has uniform velocity and is vibration free to ensure uniform exposure.

The use of reflective optics eliminates chromatic aberrations and, in principle, allows the entire mercury spectrum to be used for exposure. Thus, the maximum possible incident exposure energy is used and exposure times are minimised.

The 'Micralign 340' systems have an NA of 0.16, and have a usable resolution of around 2μm with a $\pm 8\mu$m DOF.

2.8.3.2 Reduction Step-and-Repeat Systems (Steppers)

Whole-wafer projection systems have been superseded by step-and-repeat equipment, also known as steppers, for very high resolution applications. A mask pattern is imaged on the wafer surface with a reduction ratio of 5x or 10x. The image field is usually 20 mm square or less. An XY stage is used to step the wafer under the optics and the mask image is repeated at a pitch fractionally greater than the field size, over the entire wafer. Exposure occurs once the stage has come to rest at a site. Figure 2–28(b) schematically illustrates this technique.

The use of reduction optics has several advantages.[21]

- The effect of mask defects is reduced by the demagnification factor.
- Dimension and placement control is maximised. Each is improved over that of the mask-making equipment by the magnification factor.
- Focus and alignment corrections can be made at each site.

These advantages are gained at the expense of throughput. The practice of serially positioning the stage and then exposing each site is inherently slower than all other exposure techniques. Typically, a stepper may align and expose 45 wafers per hour whilst a scan system may manage 75 and a proximity system 100.[46]

The Numerical Aperture of Projection optics has steadily increased over the last decade, as part of the drive towards smaller geometries. Initial NA values of between 0.3 and 0.35 have been superseded by values of 0.45 to 0.57.

The effort to produce higher resolution has also reduced exposing wavelengths. Ten years ago, production steppers almost exclusively utilised g-line (435.8nm) illumination but now i-line (365nm) is begining to dominate. Experimental systems have moved to even shorter wavelengths, DUV (248nm) and VUV(194nm). However, these latter systems use laser illumination sources and require special resists, such as the type discussed in Section 2.2.2.

Even basic 0.3 NA g-line steppers are capable of 1μm resolutions,whilst the most advanced conventional (i-line) machines can reach resolutions of around 0.5μm.[89–92] The shorter wavelength machines can produce 0.35μm geometries[91,93] as can the high NA i-line machines when phase shift[15,93,94] and/or oblique illumination[10,95–97] techniques are employed.

The DOF of processes running at these resolutions is typically 1.4μm or better.

2.8.3.3 1:1 Steppers

Various 1:1 steppers based on reflecting optics are produced by Ultratech, and are capable of producing 1.0μm geometries.[21,46] The optics' lack of chromatic aberration allows polychromatic illumination, which again allows maximum exposure power.

While there are difficulties in producing 1:1 masks at such small geometries, it should be remembered that only 1 perfect die need be produced.

The tool is approximately half the price of a reduction stepper and can easily be adapted to cope with 150mm and 200mm wafers, unlike a wafer scan system.

2.8.3.4 Step-and-Scan Projection Systems

As the semiconductor industry moves towards DUV technology, a new type of exposure tool has been presented by equipment vendors, most notably SVG-Lithography[98] and Nikon.[99] This new exposure technique, known as step-and-scan, is a cross between conventional reduction stepping and projection scanning.

Typically, a 4x reticle is scanned onto the wafer through a slit using a 'sweet spot' in a conventional stepper lens, where magnification and distortion errors are low. A step-and-repeat process is used to replicate the complete reticle image field over the entire wafer.

This approach maintains the benefits gained from using reduction optics but allows field sizes to be enlarged without substantial increases in lens size or complexity. Capital costs can therefore be kept down.

Although initial results using DUV step-and-scan appear promising, it is too early to say whether they will be generally accepted within the industry.

2.8.4 Image Transfer

The image that has been discussed thus far has been purely optical in nature. This optical, or aerial, image produces a three dimensional latent image within the resist, and it is this which determines the size and profile of the developed resist features (see Chapter 3, Section 3.2.2).

The term, latent image, refers to the distribution of PAC/indenecarboxylic acid within the exposed resist which is proportional to the total exposing energy delivered to each point. The solubility of the resist in developer is, in turn, proportional to the exposure dose.

The precise exposing intensity at any point in the resist depends not only on the exposure details, but also on absorption within the resist and substrate reflection effects.

2.8.4.1 Reflectivity Effects: Standing Waves

The refractive index mismatch at the air/resist interface causes the partial reflection of incident light. Reflection also occurs at the resist/substrate interface unless a substrate of matched refractive index has been chosen. When an unmatched substrate, such as silicon, is used thin film effects produce strong standing waves in the resist.

If the simple case of the monochromatic exposure of a resist film on a bare substrate is examined, some insight into standing waves can be gained.

Consider a thin film of thickness, D, on a thick substrate in an ambient environment. Let the complex indices of refraction for the three materials be $\mathbf{n_2}$, $\mathbf{n_3}$ and $\mathbf{n_1}$,respectively, when the complex index of refraction is defined as

$$\mathbf{n_i} = \mathrm{n_i} \pm iK_\mathrm{i} \tag{2.11}$$

$\mathrm{n_i}$ is the real part of the index and K_i is the absorption, or extinction coefficient.

The reflection coefficient, ρ_{ij}, and transmission coefficient, τ_{ij}, affecting a beam travelling from medium i to medium j are given by:

$$\rho_{\mathrm{ij}} = \frac{\mathbf{n_i} - \mathbf{n_j}}{\mathbf{n_i} + \mathbf{n_j}} \tag{2.12}$$

$$\tau_{\mathrm{ij}} = \frac{2\mathbf{n_i}}{\mathbf{n_i} + \mathbf{n_j}} \tag{2.13}$$

and the internal transmittance of the film, τ_D, is

$$\tau_\mathrm{D} = \mathrm{e}^{-\mathrm{ik_2 D}} \tag{2.14}$$

where $\mathrm{k_2}$ is the propagation constant in the film, given that

$$k_i = \frac{2\pi n_i}{\lambda} \tag{2.15}$$

and, that λ is the vacuum wavelength of the incident light.

If an incident plane wave with electric field, E_I, arrives at the ambient/film interface with normal incidence then the electric field, E_0, of the wave which propagates into the film is expressed as

$$E_0(x) = E_I \tau_{12} e^{-ik_2 x} \tag{2.16}$$

This wave is then reflected by the substrate at x = D, giving rise to a new wave:

$$E_1(x) = \rho_{23} E_0(D) e^{ik_2(x-D)} = E_I \rho_{23} \tau_{12} \tau_D^2 e^{ik_2 x} \tag{2.17}$$

Similarly this wave is in turn partially reflected at the film/ambient interface to produce E_2:

$$E_2(x) = E_I \rho_{21} \rho_{23} \tau_{12} \tau_D^2 e^{-ik_2 x} \tag{2.18}$$

and so on

$$E_3(x) = E_I \rho_{21} \rho_{23}^2 \tau_{12} \tau_D^4 e^{ik_2 x} \tag{2.19}$$

$$E_4(x) = E_I \rho_{21}^2 \rho_{23}^2 \tau_{12} \tau_D^4 e^{-ik_2 x} \tag{2.20}$$

etc.

The total electric field within the thin film, $E_T(x)$, is given by the superposition of all E_i:

$$E_T(x) = E_I \tau_{12} \left[e^{-ik_2 x} + \rho_{23} \tau_D^2 e^{ik_2 x} \right] S \tag{2.21}$$

where

$$S = 1 + \rho_{21}\rho_{23}\tau_D^2 \left(1 + \rho_{21}\rho_{23}\tau_D^2 \left(1 + \rho_{21}\rho_{23}\tau_D^2 \left(1 + \ldots . \right. \right. \right. \tag{2.22}$$

The summation of this geometric series is given by

$$S = \frac{1}{1 - \rho_{21}\rho_{23}\tau_D^2} = \frac{1}{1 + \rho_{12}\rho_{23}\tau_D^2} \tag{2.23}$$

Thus allowing Equation 2.21 is be rewritten as

$$E_T(x) = E_I \tau_{12} \frac{e^{-ik_2 x} + \rho_{23}\tau_D^2 e^{ik_2 x}}{1 + \rho_{12}\rho_{23}\tau_D^2} \tag{2.24}$$

The exact expression for the light intensity can be obtained by multiplying E_T by its conjugate E_T^*. However, if it is assumed that the film is only weakly absorbing, the imaginary parts of ρ_{12} and τ_{12} can be neglected and it can be shown[100,101] that the intensity can be calculated from

$$I(x) = I_0 \tau_{12}^2 e^{-\alpha x} \frac{1 + g(D - x) + |\rho_{23}|^2 e^{-2\alpha(D-x)}}{1 + \rho_{12} g(D) + \rho_{12}^2 |\rho_{23}|^2 e^{-2\alpha D}} \tag{2.25}$$

where

$$g(\Delta) = 2e^{-\alpha\Delta} \left[re\{\rho_{23}\} \cos\left(\frac{4\pi n_2 \Delta}{\lambda}\right) + im\{\rho_{23}\} \sin\left(\frac{4\pi n_2 \Delta}{\lambda}\right) \right] \tag{2.26}$$

and α is the absorption coefficient of medium 2.

$$\alpha = \frac{4\pi k_2}{\lambda} \tag{2.27}$$

Interpretation of these Equations is helped by removing the constant term C, such that

$$C = \frac{I_0 \tau_{12}^2}{1 + \rho_{12} g(D) + \rho_{12}^2 |\rho_{23}|^2 e^{-2\alpha D}} \tag{2.28}$$

Equation 2.25 becomes

$$I(x) = Ce^{-\alpha x}\left[1 + g(D - x) + |\rho_{23}|^2 e^{-2\alpha(D-x)}\right] \tag{2.29}$$

Absorption of the incoming light by the film is accounted for by the term $e^{-\alpha x}$, whilst $|\rho_{23}|^2 e^{-2\alpha(D-x)}$ deals with the absorption of the relected light.

The interference effects are described by the remaining g(D-x) term

$$g(D - x) = 2e^{-\alpha(D-x)}\left[re\{\rho_{23}\}\cos\left(\frac{4\pi n_2(D - x)}{\lambda}\right) + im\{\rho_{23}\}\sin\left(\frac{4\pi n_2(D - x)}{\lambda}\right)\right] \tag{2.30}$$

Thus it it is clear that the intensity within the film varies in sinusoidal manner with period $\frac{\lambda}{2n_2}$ and that a minimum intensity will occur at the film-substrate interface (x = D) when there is a reflecting substrate ($\rho_{23} < 1$). This minimum will be zero if the substrate is a perfect reflector ($\rho_{23} = -1$).

Evidence of the standing wave effect is generally visible on developed features where periodic 'nibbles' are visible on the resist sidewalls (see examples in Chapter 3, Figure 3–1). Although this phenomenon occurs when broadband exposure is utilised, inteference between the different exposing wavelengths acts to smooth out the feature profile. The effect is only a serious problem in monochromatic systems, i.e. i-line and g-line steppers.

These same thin film interference effects lead to changes in the amount of incident energy coupled into the resist (and consequently the amount reflected).

When an intensity node (minimum) occurs at the film surface, constructive interference between the incident and outgoing waves is highest and the system

reflectivity is maximised therefore the fraction of light coupled into the resist is a minimum.[102] As the standing wave period is $\frac{\lambda}{2n}$, this criterion is met at resist thicknesses of $(2N) \times \frac{\lambda}{4n}$ where N is integer.[103]

The fraction of incident energy coupled into the film is maximised and reflectivity is minimised when an intesity antinode (maximum) occurs at the resist surface. This criterion is met by resist thicknesses of $(2N + 1) \times \frac{\lambda}{4n}$.

Between these two extreme values the reflectivity and energy incoupling levels vary in a sinusiodal manner.

The case described above is true when the resist film is placed directly upon a reflecting substrate such as silicon, polysilicon or metal. The situation is slightly more complicated if the resist film is deposited on a reflecting substrate (silicon) which has one or several 'semi-transparent' films deposited on top of it. Semi-transparent films commonly occuring in semi-conductor fabrication are silicon oxide and silicon nitride.

The thin film interference effects are further complicated by the partial reflections and transmissons occurring at the additional interfaces. Now the intensity nodes occuring at the resist/substrate interface in the case described above, occur at the bottom of the transparent film next to the reflecting substrate. The separation between such nodes is still $\frac{\lambda}{2n}$ but the refractive index, n, must be altered to account for any media change as they recede from the initial node.

Maximum incoupling still occurs when an intensity antinode is at the resist surface, however the resist thickness at which this occurs is dependent on the number of films beneath the resist, their thickness and their refractive indices.

The incoupling to a resist film on a film stack remains a sinusiodal function and the stack merely introduces a phase change.

It should be noted that as wavelengths decrease from g-line to i-line to DUV, standing wave problems become greater as the reflectivity of silicon and other semiconductor materials increases significantly, as shown in Table 2–1.[102]

	Wavelength (nm)	Reflectivity of Silicon
G-Line	436	42%
I-Line	365	59%
DUV	248	68%

Table 2–1: *The Reflectivity of Silicon at various exposing wavelengths.*

2.8.4.2 Image-Resist Interactions

The ideal aerial image produced by the exposure tool exists in a single, infinitely thin plane whilst the resist coating has a thickness of between 1 and 2μm. Thus at all but one depth, in the film, exposure is occurring with a defocused, rather than optimal image. However, this is acceptable when the resist film is less than the DOF of the image.

Light absorption by the resist also changes the optical image intensity. Even during a uniform, unpatterned exposure, the exposing intensity decreases with depth from the resist surface.

Although absorption due to the novolak resin and the residual solvent remains constant during exposure, the level of absorption due to the PAC changes during exposure. The bulk of PAC absorption is due to the the photo-reaction which creates the indenecarboxylic acid, therefore as PAC is converted the level of attenuation associated with it decreases.

Figure 2–30 compares the absorption at different wavelengths of an unexposed and completely exposed sample of Shipley S1813 photoresist.[104] It can be clearly seen that the level of absorption alters greatly with exposure.

The level of illumination at a given point is therefore determined by the depth of resist above it, and the level of converted inhibitor within that thickness.

When this complication is added to the standing wave effects, described in Section 2.8.4.1, it can be seen that the optical intensity of exposing light at a

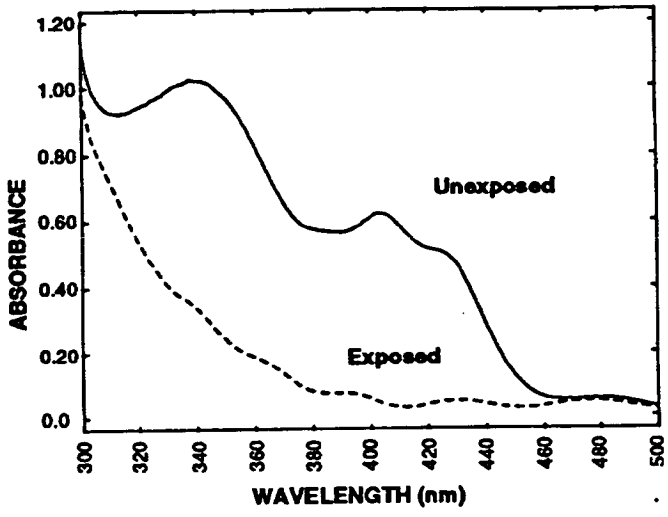

Figure 2–30: *The absorbance spectrum for Shipley Microposit S1813 Photoresist.*

given point depends not only on the incident energy but also on its position above the reflecting substrate, the resist thickness, any intermediate semi-transparent layers, and the resist's exposure history.

2.9 Post Exposure Bake (PEB)

Following exposure, the substrate may optionally receive a post exposure bake; if the bake is not implemented then the wafer proceeds directly to development.

2.9.1 Motivation for PEB

There are two motivations for PEB, the first is increased thermal stability as discussed in Section 2.7.4. The second function of the PEB is removal and/or reduction of standing wave remnants on the developed feature profiles. Examples of features produced with and without PEB can be found in Chapter 3, Section 3.2.2.

Experimental work[105] has shown that the smoothing effect is accomplished by thermally assisted diffusion of the PAC and indenecarboxylic acid within the film.

The amount of diffusion is dependant on the bake temperature, bake time, novolak composition, PAC type and the level of solvent within the film (which is related to the softbake conditions). Very little diffusion will occur if the PAC molecule or resin molecules are too large or if too much solvent has been driven from the film.

It is interesting to note that, given identical softbake conditions, the introduction of a moderate temperature (< 120°C) PEB improves the photospeed of a resist exposed under g-line, i-line and broadband conditions.[106] The reason for this is connected to latent image diffusion and is explored more fully in Chapter 6, Section 6.6.4.

2.9.2 Implementation of PEB

The PEB is exclusively performed using a contact, or proximity, hotplate as described in Section 2.7.2. Typically, the duration of a contact bake is 30 to 60 seconds whilst 60 to 90 seconds is more appropriate for a proximity bake. Temperatures vary from around 105°C to 120°C.

2.10 Development

2.10.1 Developers

Developers for diazonaphthaquinone/novolak photoresists are aqueous, alkaline solutions and can be divided into two main catagories: Metal Ion Bearing (MIB) and Metal Ion Free (MIF).

The 'strength' of both types of developer is measured in terms of the alkaline normality. Higher normality developers generally give faster processes but decrease performance in terms of unexposed resist loss, sidewall angle and CD control (see Chapter 3, Section 3.2.2).

Although it was common some years ago for developer to be supplied as concentrate which was diluted with de-ionized water to form the product 'as used', the

supply of prediluted developer is now common. Prediluted developers from resist vendors offer the high level of batch-to-batch normality and surfactant level control necessary for submicron manufacturing. It is difficult to match this accuracy when diluting concentrates at the point of use. There is currently a movement in the industry for large fabrication facilities to have their own developer plants, which continuously make developer from concentrates and de-ionized water.[107] However, the degree of normality control which such a continuous dilution system can offer is open to question.

2.10.1.1 Metal Ion Bearing (MIB) Developers

MIB developers are based upon alkali metal hydroxides, such as sodium and potassium hydroxide. These materials are generally used for immersion development of large feature geometries in processes where ionic contamination of the substrate will not affect the performance of the final devices.

The high mobility of alkali metal ions can potentially cause contamination of the substrate surfaces they contact. In the case of MOS devices, this could lead to serious detrimental effects on device performance and yield. This has caused a movement away from MIB developer towards Metal Ion Free (MIF) developers.

2.10.1.2 Metal Ion Free (MIF) Developers

MIF developers are usually based on organic bases such as N-(2-Hydroxyethyl)-N,N,N-Trimethyl Ammonium Hydroxide (THAH, or Choline), or more commonly Tetramethyl Ammonium Hydroxide (TMAH).

These materials not only reduce the possibility of substrate contaminaton but also have been demonstrated to behave much better in track-based processing modes.[108] In view of the near universal predominance of TMAH based developers, this is the only type of material which will be considered in this study.

2.10.2 Surfactants

The term surfactant, derived from 'surface-active agent', is applied to a material that can dramatically alter the energetics of interfaces or surfaces when present in very small quantities.[109]

A wide variety of different types, usually of a proprietary nature, are used in developer formulation to achieve the following:

- Buffer the solution for immersion development.
- Improve surface wetting during spray application.
- Prevent foaming during spray application.
- Prevent puddle 'pull-back' during puddle processing.

2.10.3 Development Kinetics

As lithography progresses into the sub-0.5μm regime, the influence of development becomes of great importance. Many kinetic properties have been identified, as a function of basic parameters (temperature, resist loading etc.) and the developer chemistry, although the basic chemical reactions have still not been identified. The following Sections 2.10.3.1 through 2.10.3.4 discuss those areas which have been positively identified and documented.

2.10.3.1 The Chemistry of Development

The precise mechanisms for photoresist development are unknown, though it is certainly a multistage process.[110] Despite the uncertainty of the precise reaction, several features of development have been identified.

Firstly, the aggressiveness of the development is only partially determined by the alkaline normality (i.e. amount of OH^-); the size of the unsolvated cation (TMA^+, Na^+ etc.) also plays a significant role. Dissolution rates decrease as

the cation size increases.[111] This has been attributed to either the influence of the ionic size on diffusion rate or electrostatic interactions between the developer cations and those in the resin.

Two other phenomena have been identified which appear to facilitate dissolution; one is the formation of ion pairs between the developer cation and the phenolate monoanion units in the resin, and the second is the formation of strongly polarized hydrogen bonds between the oxygen on the phenolate monoanion and the proton on the indenecarboxylic acid.[110]

2.10.3.2 Influence of Temperature

Intuition and conventional chemistry theory dictate that chemical reaction rate increases with increasing temperature because the chemical surroundings provide more energy to drive the reaction over the activation energy barrier. Thus development rates should increase with temperature.

In the case of choline[112] and MIB developer[113] this is the case. However, it is well documented that for TMAH developer, activity decreases with increased temperature.[110,112,114,115] In the case of an 0.26N TMAH developer a decrease in E_0 photospeed of around $1.2 mJcm^{-2}$ is observed for each one degree increase in developer temperature.[114] No firm explanation of this behaviour has been identified but it has been proposed[110] that it results from the weak ion pair formed between the TMA^+ cation and the resin phenolate anion, since the stability of this pair is lessened as temperature increases.

2.10.3.3 Influence of Air

When developer is exposed to air, carbon dioxide is absorbed, neutralising some of the alkalinity of the solution. Obviously this lowering of normality slows down photoresist development. Experimental work[113] indicates that this effect typically reduces development action by around 38% over a 24 hour period, though it is dependant on the developer volume and the surface area exposed to the atmosphere.

Such neutralisation is only a significant problem during immersion development (see Section 2.10.4), where quantities of developer remain in an open bath for long periods (often between 8 and 24 hours, i.e. 1 to 3 shifts).

Track processing is relatively immune to this phenomenon as 'fresh' developer is applied to each wafer. This developer is maintained under an inert (usually nitrogen) blanket. Likewise, a nitrogen blanket is used by vendors during developer manufacture and packaging to maintain the product integrity and specifications.[116]

2.10.3.4 Influence of Dissolved Resist loading

It is known that the loading of dissolved novolak resin within a developer solution affects the dissolution activity of that developer. Activity decreases markedly as the loading increases to 250mg/ltr, but stabilises over the ranges 250 to 450mg/ltr, after which activity starts to decrease again, but more gradually.[113]

Again, this problem is more prevalent in the immersion situation where a bath of developer is utilised over one, or more shifts. If it is considered that one 100mm wafer coated with 1.3μm of resist contains around 10mg of positive resist then a batch of 24 wafers exposed with a 50% brightfield pattern will add 120mg of novolak to a bath.

In a localised form, this phenomenon can also affect track-based high resolution processes. If one considers the bottom of a sub-micron contact hole in a thick (2μm) resist coating during a static puddle process, the localised novolak loading could be very high indeed. This could produce a CD bias between these small features and large exposed areas where dissolved novolak can be transported away more easily into the bulk of the puddle.

2.10.4 Immersion (Batch) Development

Immersion development is a simple and cheap form of development. A relatively large quantity of developer is kept in a bath. Wafers, generally a batch at a time,

are submerged in the bath for a predetermined period of time, typically 1 minute; the wafers are removed and fully rinsed in deionised water.

The bath is continually used until either a set time has elapsed or a certain number of batches have been processed.

Despite the loading and carbon dioxide absorption effects discussed above, some precautions are taken to maximise the repeatability of development. Baths are generally temperature controlled by a heat exchanger and the developer is circulated around the bath to ensure uniform temperature control.

In stagnant, or non-agitated, development removal of resist is diffusion limited. The introduction of agitation allows physical removal of dissolution products and can increase development rates. The sensitivity to agitation can be appreciated by considering the doubling to tripling of development rates reported by Zee *et al.* when comparing agitated development to stagnant immersion.[117]

The repeatability of intra-batch development is further affected by the currents and eddies caused by the wafers and wafer jig interacting with the agitated developer movement. In an attempt to reduce this systematic effect, the wafer jig is also agitated. Unless this is applied using an automated system, this process adds an operator dependent variable to the process as the degree of movement will vary from one technician to the next.

The repeatability of immersion development, both batch-to-batch and intra-batch, is inadaquate for demanding submicron geometries and has been replaced in the main, by more controllable track processing.

The process parameters which affect immersion development rates are agitation levels, the level of novolak loading in the developer and the ambient exposure time.

2.10.5 Track/Cluster Development

An automated developer station is very similar to a coater unit. A vacuum chuck, on which a single wafer is held horizontally, is mounted in the centre of a circular spinbowl. This bowl is has both a drain and exhaust system. The drain allows the

removal of developer and rinse water, whilst the exhaust prevents aerosol liquid particles, formed during rinse and spin dry procedures, from 'splashing back' onto the substrate surface.

Developer and deionised water are supplied from above from either fixed nozzles mounted on a diametric bar or from a mobile arm which can be positioned above the wafer. The various ways of dispensing from these positions will be discussed in the following subsections.

2.10.5.1 Continuous Spray Development

The first option for track development is continuous spray development. The substrate is rotated at between 100 and 300 rpm and developer is sprayed onto the substrate surface. The centrifugal force removes excess developer from the wafer surface ensuring a stable volume of liquid on the wafer surface.

This continues for between 15 and 40 seconds when the developer supply is shut off and the wafer is rinsed. The rinse utilises dionised water which is either sprayed or streamed onto the wafer surface. Following the rinse, the wafer is spun dry using high speed rotation.

The developer spray is typically formed by a fan type nozzle, where developer is supplied under pressure and forced through a restricted aperture which forms a fan-shape curtain of droplets. Nozzles are available which produce 80° and 110° fan angles.

As development rate is sensitive to agitation, operating parameters must be selected carefully. The first form of agitation comes from the physical impact of the developer on the wafer surface and is controlled by the developer nozzle pressure (flow rate). Chemical cost considerations dictate that this flow rate should be as low as possible, though the rate must be such that the fan is stable and completely open.

Nozzle positioning and fan angle is wafer size dependant and should be chosen so that all parts of the substrate are under spray for an equal time during each

revolution. Non uniform spray coverage results in relative under-development in areas which receive less, or no direct spray, and over-development in areas which see permanent spray(normally the wafer centre). Figure 2–31 illustrates processes which exhibit both poor and ideal develop uniformity.

Spin speed also influences develop uniformity, yet it must be high enough to transport away excess developer preventing it from 'running' over the wafer edge and onto the backside of the substrate. However, since centripetal force accelerates the liquid out across the wafer, care must be taken to control the speed of the liquid at the edge. If it becomes too great then the increasing agitation (due to increasing flow) results in a gradient in developer activity across the substrate.

Continuous spray development typically lasts between 15 and 40 seconds, and is costly in terms of photochemical, but offers higher development rates than other techniques. It tends to be utilised where either developer cost is low or on layers where the physical impact of the developer significantly improves the process, e.g. it aids clearing contact holes in thick resist.

The process parameters which affect continuous spray development rate are developer flow rate and application spin speed.

Many developers foam up when used in a spray mode, therefore developers intended for track processing often include surfactants which reduce this effect.

2.10.5.2 Puddle Development

Puddle development is the second, more common option available for track processing. It is a preferred technique since it offers improved reproducibility and speed over immersion development, whilst having much lower chemical costs than continuous spray.

A puddle of developer is formed on the wafer surface, typically using a short spray process of 4 to 6 seconds. A low spin speed of around 100rpm is used during developer application, so that a puddle of reasonable depth is formed. The puddle is allowed to sit on the wafer surface for a time of between 15 and 90 seconds.

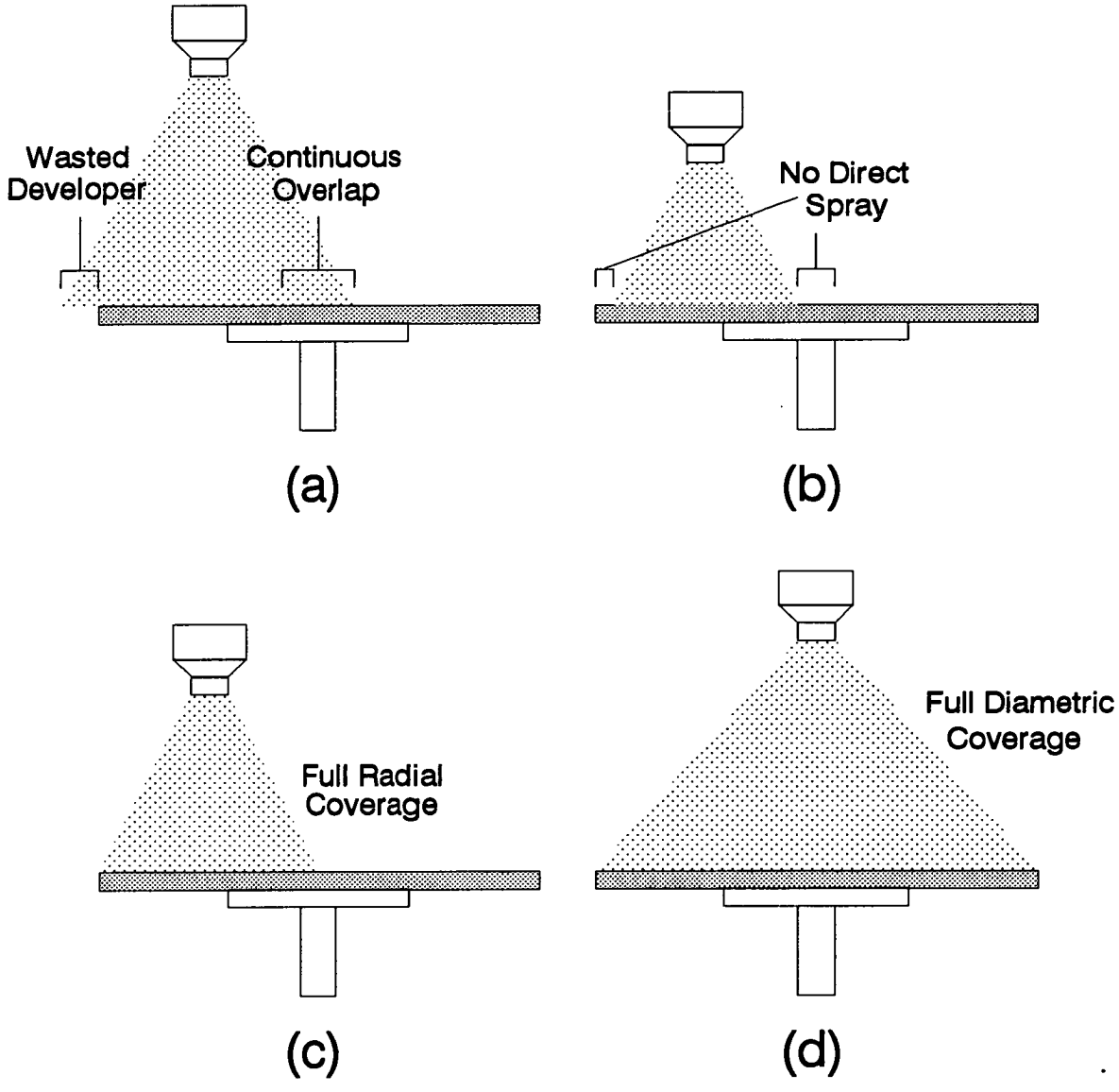

Figure 2–31: *Some example spray develop processes which exhibiting good and poor cross-wafer develop uniformity (a) Radial spray configuration where centre is overdeveloped and developer is wasted at wafer edge. (b) Radial spray configuration where wafer centre and periphery are underdeveloped. (c) Ideal radial development. (d) Ideal diametric development*

The wafer is usually kept stationary, but may be spun at low speed (e.g. 20 rpm) to produce slight agitation. After the full puddle time has elapsed, the wafer is rinsed and dried, as with continuous spray development.

Puddle processing development rates are a little lower than those obtained using continuous spray techniques,[118–121] but are faster and more repeatable than immersion rates.[118,119]

At the expense of additional developer quantities, multiple puddle processes can be implemented. A double or even triple puddle process can increase process speed by replacing loaded developer with fresh material. At the end of the designated puddle period, a short (less than 1 second) spin of moderate speed (500 - 1000 rpm) is used to clear the wafer surface of the used developer. Fresh developer is applied during this spin to prevent drying of the resist. Whilst the developer supply remains on, the spin speed is reduced to allow the formation of a new puddle. This process is repeated for as many puddles as required.

Fan spray is not the only technique used for puddle formation, low impact dispense systems and developer stream are also used.

Stream processes are relatively simple: puddle formation is achieved by letting developer 'stream' from a small tube over the substrate centre for several seconds. Rotation is used to transport the developer evenly over the entire wafer surface.

A variety of low impact dispense systems, such as ultrasonic nozzles[122,123] and TEL's E^2 dispense system, are available. In general, these low impact dispenses offer reduced developer usage rates and improved develop uniformity. A slight photospeed penalty is incurred using such a system as the physical impact normally present during spray application is missing.

Many developers, including pure TMAH solutions, have some wetting problems when used in a puddle mode. The short spray period during puddle formation often has difficulty in ensuring the entire surface is covered. This can be overcome by the inclusion of a wetting surfactant or by prewetting the wafer[124] with deionised water prior to developer application. If this second technique is utilised, excess

developer must be used to ensure all the water initially on the wafer is replaced and there is no random localised dilution.

The second wetting problem associated with puddle development is 'pullback'. As development proceeds the puddle pulls back from the substrate edge leaving dewetted areas. Perera *et al.*[125] demonstrated that pullback is a function of percentage area of exposed pattern. They attribute the effect to changes in the puddle surface tension as the level of resist photoproduct increases. Pullback can be overcome by the addition of surfactant or by building up deep puddles, using very low spin speeds.

The process parameters affecting puddle process dissolution rates are application method, number of puddle refreshes and agitation (spin speed) during the puddle.

2.11 Hardbake

Following development a hardbake may be applied. This improves the resist's adhesion for the case of wet etch processes and improves the resist's resistance to particularly aggressive dry etches and implants.

For many processes a hardbake is not required. The hardbake temperature should be chosen carefully; it should be high enough to toughen the surface of the resist but low enough so that the resist does not pass its glass transition temperature and start to flow. Typically, temperatures are between 100°C and 140 °C but is resist dependant.

Hardbake alone does not always provide enough toughening for some very aggressive processes, such as metal etch and high energy implants. In these cases a Deep Ultraviolet (DUV) cure is applied to increase the strength of the resist. This practice is briefly discussed in Section 2.11.2.

2.11.1 Hardbake Application

Hardbake may occur either on a track hotplate (as previously described) or in a convection oven. Again process times are between 30 and 90 seconds for a track-based process or around half an hour in the case of an oven bake.

2.11.2 DUV Curing

DUV curing is a single wafer operation utilising dedicated equipment, typically a 'FUSION' microlite system. The resist receives a ramped bake from around 100°C to over 200°C. During this bake the resist is exposed to DUV illumination (wavelength 280nm - 350nm). The illumination causes crosslinking of the outer novolak resin. This hard outer 'casing' prevents the resist from flowing during the latter parts of the bake.[126]

2.12 Resist Stripping

After the patterned resist has performed its masking function, it must be removed so that further processing can occur. Generally, the resist can be removed by a wet process, i.e. submerging the wafers in a chemical solution. However, after particularly harsh processing, such as medium/high dose implants or fluorine/chlorine based dry etches, a carbonized skin is formed.[127] Wet stripping alone is unable to remove such resist coatings and dry stripping must be used. A wet strip is often included after dry stripping to remove any remaining residues.

Wet stripping is preferable on layers which are sensitive to ionic contamination, such as gate oxide, as dry etch processes can cause radiation damage and drive any surface contaminants into the substrate.

2.12.1 Wet Stripping

A wide variety of wet strip chemicals are in common use: the following list details some and discusses their use.[128]

Fuming Nitric Acid: This is an effective stripper of all organic materials. A 5 to 10 minute room temperature dip will remove a moderately processed resist film leaving no residues. It also has a pot-life of several weeks. Many production facilities consider this solution too dangerous for routine resist stripping.

Caro's Acid: This solution is a mixture of concentrated sulphuric acid and highly concentrated (85 - 90%) hydrogen peroxide. The mixture is used at room temperature. Normally processed resist can be completely stripped in 10 minutes.

Piranha solution: This is the name given to Caro's acid when used at elevated temperature. The strip is more aggressive but pot-life is reduced.

Sulphuric Acid/Nitric Acid mix: Elevated temperature (100 o C) must be employed to make this mixture effective. It may only be used on certain process layers as both metal and oxide layers are attacked by the solution.

Acetone: This is a room-temperature stripper with a very active solvent action. However it is very volatile and flammable. If any degree of cross-linking has occurred within the resist, residues are left on the substrate.

2.12.2 Dry Stripping

A wide variety of dry strip options are available including barrel strippers, parallel plate strippers, downstream RF plasma etchers, downstream microwave etchers, Electron Cyclotron Resonance (ECR) etchers, surface wave plasma ashers and UV/ozone reactor strippers.[128]

Each offers particular advantages and disadvantages in terms of strip rate, strip selectivity, radiation damage, ion damage and remaining residues. The particular technique employed must be tailored to the aggressiveness of the preceeding process step and the sensitivity of the device layer to the various types of damage.

2.13 EMF Lithographic Chemicals and Equipment

Having outlined the principles of conventional optical lithography and standard photoresist processing, this section details the chemicals, equipment and processes utilised in the EMF and during this work in particular.

2.13.1 OCG HiPR6512 and HPR204 Photoresists

The resists primarily studied during this work were HPR204 and HiPR6512, manufactured by OCG Microelectronic Materials.

HPR204 is a broadband/g-line resist based on a proprietary novolak/PAC combination in EGMEA solvent introduced in 1977.[129]

HiPR6512 is an advanced g-line resist which is also suitable for i-line and broadband applications, introduced in 1988. Again it is based on a proprietary novolak/PAC combination utilising a cosolvent system of ethyl lactate and ethyl 3-ethoxy propionate, both of which are considered 'safe' solvents.

All resist stripping was achieved using a 10 minute immersion in fuming nitric acid followed by a 3 cycle dump rinse in deionised water and 7 minute spin dry.

2.13.2 OCG HPRD428 MIF Developer

The EMF developer, and the only developer studied on depth during this work, was HPRD428, manufactured by OCG Microelectronic materials. This is a 0.245

Resist Type	HPR204	HiPR6512
Prime	In-line HMDS	In-line HMDS
Coating Thickness	$1.18 \pm 0.005\mu m$	$1.18 \pm 0.005\mu m$
Softbake	100°C/60s Contact	90°C/60s Contact
PEB	110°C/60s Contact	120°C/60s Contact
Hardbake	None	None

Table 2–2: *EMF Resist processing conditions.*

normal TMAH based developer containing proprietary surfactants which render it suitable for track and immersion processing.

2.13.3 SVG 86 Series Track

The track equipment utilised during this work was an SVG 86 Series track. The track is fitted to handle 75mm wafers, the size used in the EMF.

The coat track consists of an in-line HMDS module with chill plate, a coat module and softbake hotplate with chill unit. Resists are dispensed dynamically at the wafer centre from a mobile dispense arm.

The develop track consists of a PEB hotplate with chill plate, a developer module, and a hardbake hotplate. The developer application is by means of a radially mounted 80° fan nozzle.

Table 2–2 details the process conditions used for all following work unless otherwise specified.

2.13.3.1 EMF Dehydration Bake/HMDS Prime Process

The prime procedure consists of a 10 second reduced pressure dehydration bake at 100°C followed by a 30 second reduced pressure HMDS prime.

2.13.3.2 EMF Resist Coat Program

The coat process utilises a dynamic dispense at 2000 rpm. This spread continues for 2 seconds and is followed by a 30 second spin at approximately 4900rpm.

2.13.4 EATON Optimetrix 8010 and 8605 Steppers

The steppers utilised for this work were manufactured by the Optimetrix division of Eaton. The Optimetrix 8010 is a 10x g-line stepper with a numerical aperture of 0.32 and a partial coherence of 0.55. The Optimetrix 8605 is a 5x g-line stepper with identical NA and partial coherence.

The 10x machine has a 10mm square field size and a 350 Watt lamp power supply, whilst the 5x machine has a 14.5mm square field and a 750 Watt power supply. The higher lamp intensity of the 8605 model reduces exposure times to almost one third of those of the 8010 machine.

2.14 Summary

This chapter has reviewed the chemistry of lithographic materials, the manner in which they are processed and the equipment utilised. The large number of factors which influence the final pattern definition have been highlighted. Particular attention has been paid to the complexities of substrate reflections during exposure and the nuances of development processes.

Chapter 3

Process Characterisation

3.1 Introduction

Chapter 2 described the materals and techniques used to produce lithographic patterns and detailed the process parameters which influence the developed features. This chapter reviews how process performance is assessed. Absolute quantifiable values must be available, so that a given process can be compared to alternative processes and against device layer requirements.

Many of these quantifiable values are difficult and tedious to measure, so more easily measured "rule-of-thumb" process indicators are often used as predictors of process performance. The most commonly used of these indicators are described and their utility discussed.

3.2 Feature Evaluation

3.2.1 Critical Dimension (CD)

The basic function of all lithographic processes is to reproduce the mask pattern in resist on the substrate with all the features at their correct nominal size.

The size of the actual resist feature produced (whether it be a line, a space, an island or a window) is known as its Critical Dimension (CD). Ideally this CD should be identical to the nominal mask size (or n times smaller in the case of an nx reduction stepper).

The amount by which CD can deviate from its nominal value is determined by the final device specifications. In general, a MOS type process can withstand a deviation of ±10%.

Unlike the mask patterns, resist features are three dimensional. The focus, absorption and reflection effects, discussed in Chapter 2, result in a structure whose width varies with height (from the substrate). It is therefore important that dimensional measurements are made in a consistent and meaningful manner. To this end, it is generally accepted that the CD of a feature is its base width, i.e. size at the resist/substrate interface.

CD variations are caused by over-exposure, under-exposure, resist thickness (hence optical coupling) variations, substrate reflectivity variations and changes in focus offset. In production, substrate topography, film stack thickness variations, nonconformal resist coverage and stepper illumination and lens distortions introduce an element of each effect.

3.2.2 Profile

3.2.2.1 Factors Affecting Profile

An ideal resist feature has perfectly vertical sidewalls and is equal in height to the original film. In reality a large number of effects combine to produce features which vary in width with height and which may have experienced significant resist loss in nominally unexposed areas. The following list details some of the causes of non-ideal behaviour and the effect they have on profile.

Standing Waves: The standing wave effects, described in Chapter 2, Section 2.8.4.1, can result in periodic width variations with distance from the substrate. This can be reduced and/or eliminated by using a PEB (as descibed in Chapter 2, Section 2.9.1). Figure 3–1 is a SEM photograph clearly illustrating standing wave remnants on the developed resist feature.

Focus Offset: As the aerial image moves out of the ideal imaging plane the contrast between the bright and dark regions within the resist alters. More light

is coupled into the nominally unexposed areas and less into the nominally exposed areas,[130] see Figure 3–2. This alters the degree of PAC conversion during exposure and hence development rates. The resulting image is degraded altering the CD and decreasing the profile sidewall angle (i.e. features contrast). Figures 3–3 and 3–4 respectively show resist features at optimal and less than optimal focus settings.[131]

Absorption: This unavoidable phenomenon reduces the level of exposing illumination as it propagates deeper into the film. The resulting exposure gradient gives rise to average development rates which decrease with distance from the film surface. Resist linewidths therefore tend to decrease with height from the substrate surface while space dimensions tend to increase.

Development: As development is a surface-rate limited etch process, a feature top is exposed to the developing action for a longer period than the base.[130] Again, this results in linewidths which decrease with distance from the substrate and space widths which increase. This phenomenon causes extremely sloped profiles when the developer is very aggressive ($>$ 0.28 Normal) and the develop time is short (15 to 30 seconds). Figure 3–5 illustrates the results of a short, aggressive development process.[132]

Exposure Tool Parameters: Mack[133] has shown that the optical contrast at a feature edge increases with numerical aperture. This leads to improved resolution capabilities and more vertical sidewalls. Mack[133] also shows that for a fixed NA similar improvements are observed in resolution and sidewall angle as the exposing wavelength is reduced.

Surface Induction: A thin skin is produced on a resist coating during softbake and PEB. This skin causes a retardation of the initial development action, i.e. the resist surface is harder to remove. If this induction is suitably high, then a ridge, lip or 'cap' may be formed at the top of the fully developed feature. The degree of induction has been shown to be dependent on bake conditions[134] (higher temperatures yield more extreme inhibition), resist formulations and developer chemistry (surfactants can enhance the effect but

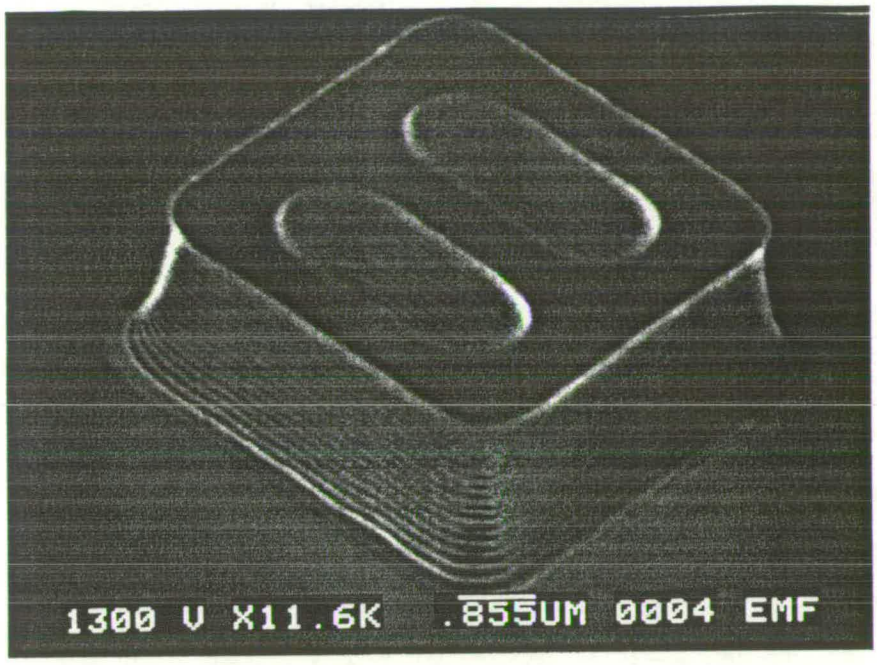

Figure 3–1: *SEM photograph of a standing wave remnants on a developed feature.*

increasing normality reduces it). Figure 3–6 illustrates a resist profile exhibiting a surface induction 'cap'. The mechanism for surface induction is unknown but various explanations are explored in Chapter 4, Section 4.6.3.1.

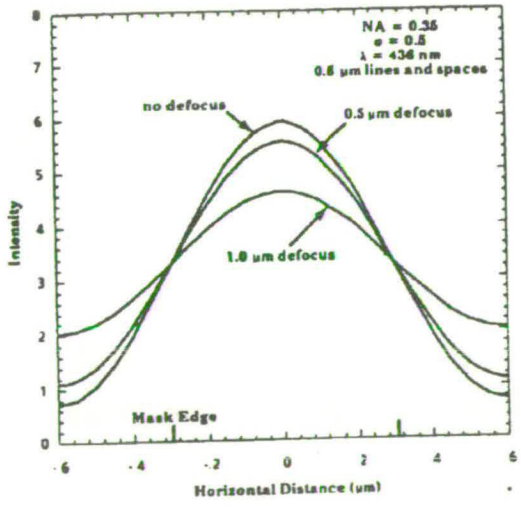

Figure 3–2: *The effect of defocus on aerial image, as Predicted by PROLITH*

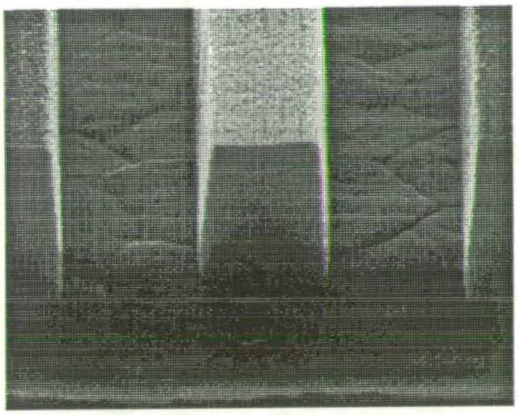

Figure 3–3: *A 1.4μm Shipley SPR-2FX 1.8JM resist feature profile at near optimal focus.*

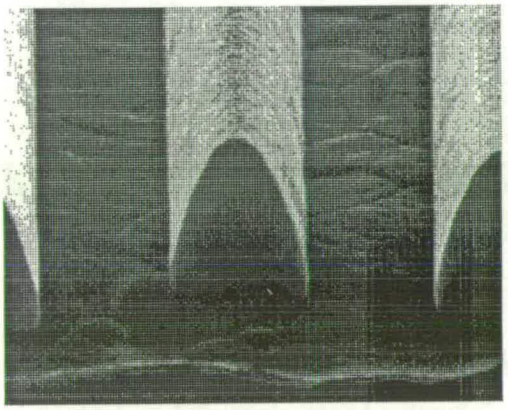

Figure 3–4: *A 1.4μm Shipley SPR-2FX 1.8JM resist feature profile at +1.5μm defocus.*

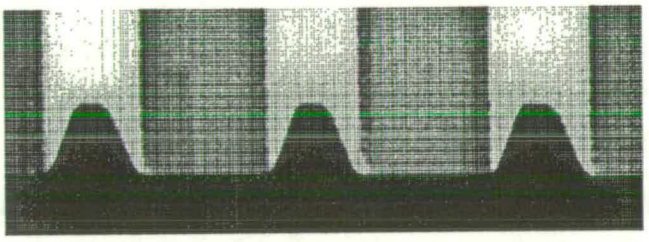

Figure 3–5: *Short duration, high normality (0.29N) development results in sloping profile sidewalls.*

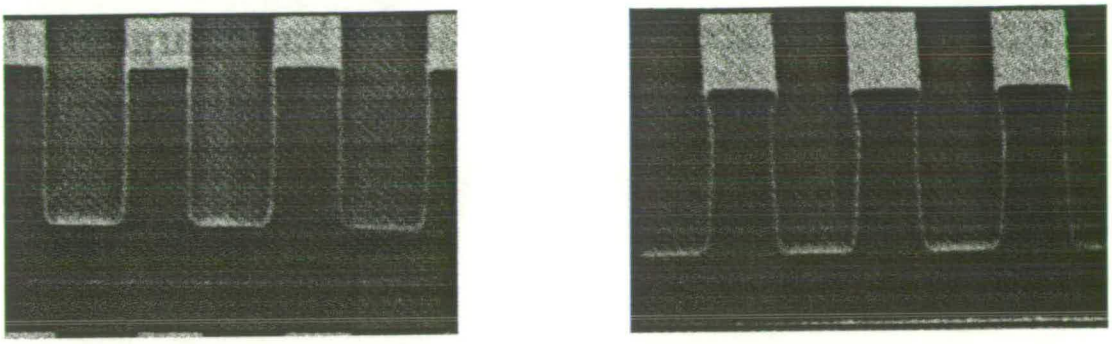

Figure 3–6: *In the left SEM image, the resist profiles are vertical showing no evidence of surface induction. In the right SEM image, an overhang is apparent at the top of the feature profiles. This phenomena is often referred to as a surface induction 'cap'.*

3.2.2.2 Sidewall Angle

Profile considerations, in addition to CD specifications, define a features' usefulness. Aggressive processing during ion implantation and dry etch steps erodes exposed resist surfaces at a finite rate. This causes alterations in the CD of a non-ideal feature.

If a feature has vertical sidewalls, the resist erosion merely thins the resist layer; however when the sidewalls are sloped the CD decreases during the erosion process. This results in a corresponding change in the area of substrate protected. Figure 3–7 illustrates how for a fixed rate of resist removal, the CD change is dependant on the sidewall slope.

Sidewall angle is defined as the angle between the substrate surface and the best fit line to the feature edge, ignoring standing wave cusps and any 'cap'. Typically, an angle in excess of 80° is required for adequate CD transfer during an aggressive dry etch process.

In the deep sub-micron regime some profiles can no longer be classified by sidewall angle, because the edge slope is not basically linear. An experienced engineer must evaluate each profile to decide whether it is acceptable. However, for all the work presented in this study the sidewall angle criteria will be sufficient.

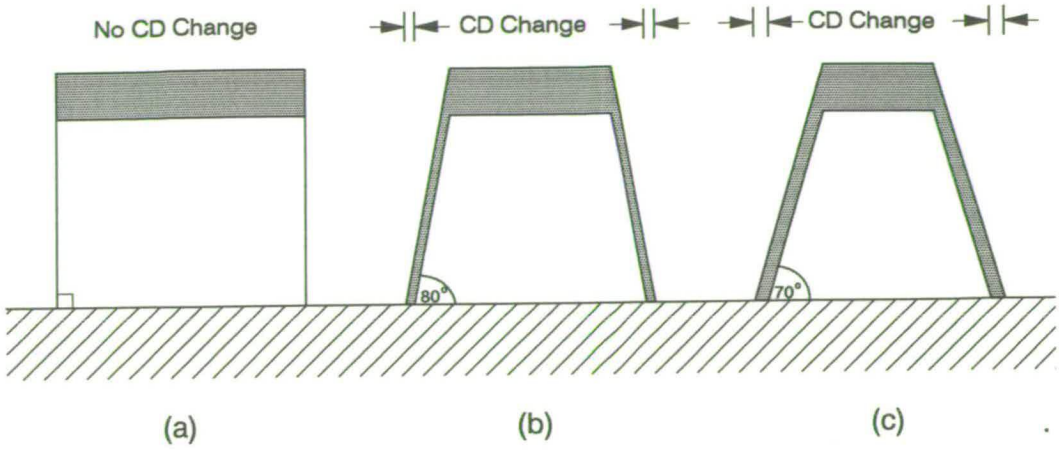

Figure 3–7: *Effects of aggressive processing on resist features. Shaded area is resist removed during processing. (a) The CD of an ideal feature is left unaltered. (b) A slight CD decrease is observed for a feature with slightly sloping walls. (c) A large, and unacceptable change in CD is observed in the case of a feature with relatively severe sloping.*

3.2.2.3 Unexposed Resist Loss

The second profile criteria is the resist loss in nominally unexposed areas. Ideally, the full pre-development thickness should remain in the centre of resist features. However, a low selectivity development process, or excessive image defocus can cause unacceptable loss of resist. Typically the loss of up 10% of the total resist thickness is considered tolerable.

3.2.3 Measurement of CD and Profile

CD and profile measurement is a challenge, especially as the dimensions of advanced process geometries approach the wavelength of visible light. Two factors govern the reliability of CD measurements, accuracy and repeatability. The first factor describes how the measurement result compares to an absolute, i.e. 'accurate', standard and the second how the measurement varies with time, e.g., on a day-to-day basis. For process set-up and evaluation purposes, it is desirable to have accurate, and repeatable, results.[103] However, in a manufacturing

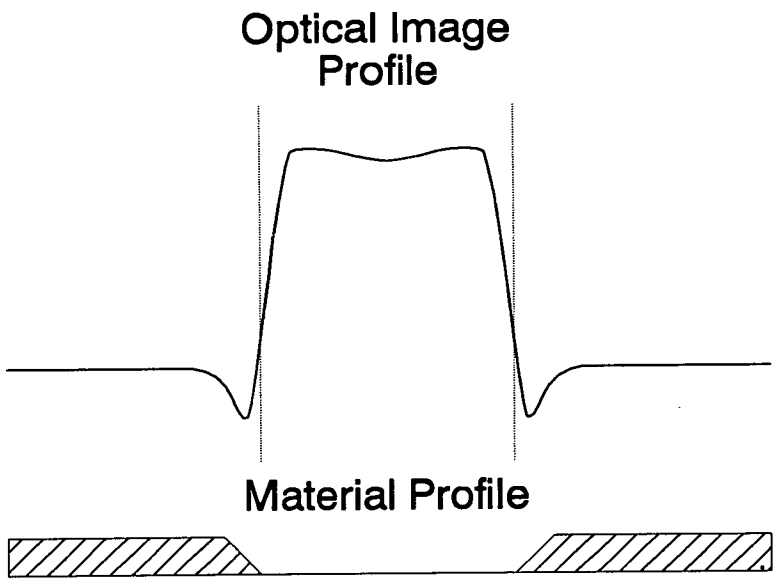

Figure 3–8: *This diagram illustrates the relationship between the profile of a physical feature and the image profile produced by optical video scan equipment. Sloping sidewalls on the feature result in dark regions in the optical image profile, whilst the focus setting and finite objective NA, produce slopes with finite gradient on either side of these dark areas. These combined factors necessitate the use of thresholding techniques (coupled with auto-focus and auto-illumination techniques).*

environment where a high yielding process has been established, ensuring the repeatability of measurements is paramount in controlling the process. Accuracy is far less important in this case.

3.2.3.1 Optical Video Scan Techniques

This technique is appropriate for CD and overlay measurement. The feature to be measured is examined topdown through a microscope objective by a video camera. An optical image profile is then extracted for that image, see Figure 3–8.[135]

If the optical image profile is examined it can be seen that the object edge is sloped and not abrupt, this is due to the limited NA of the objective, the slope of the feature profile, the difference in focus between feature top and bottom,

imperfections in the inspection optics and video detection system. A threshold technique is usually employed to determine the line edge location, i.e. the edge is defined as where the image intensity falls to a given percentage of its maximum value.[136]

The feature linewidth can now be calculated if the ratio of video pixel to actual size at the substrate is known for the given lens magnification.

Typically, the threshold value which yields the best repeatability will be chosen and the pixel width size will be calibrated so that measurements reflect those determined by SEM measurements.

Such CD measurements are very sensitive to focus setting and illumination levels. Correspondingly, the repeatablity of a manually focused and illuminated system is inferior to that of an automated system, and is operator dependant, to some degree. The CD values are also sensitive to feature sidewall angles as sloped edges scatter the incident light, increasing the width of the sloped region of the optical intensity profile. The resulting movement of the threshold positions does not necessarily reflect a change in feature basewidth.

Modern video scan equipment such as the EMF's Bio Rad Quaestor CD07A critical dimension measurement system,[137] feature high magnification objectives with advanced auto-illumination and autofocus software. Pattern recognition allows fully automated wafer measurements which are reliable on feature sizes down to about 0.7μm.[46]

3.2.3.2 Coherence Probe Metrology

Coherence Probe Metrology (CPM) is an optical measurement technique based on a white light Linnik interferometer. Figure 3–9 illustrates the basic system layout.[138] Incoherent light is split into two wave fronts by the interferometer. One passes through a microscope objective and is returned to the interferometer via a reference mirror. The other is directed through a second identical objective at the sample. If light is reflected by a feature surface perpendicular to the beam at a distance equal to that of the reference mirror an interference signal is generated

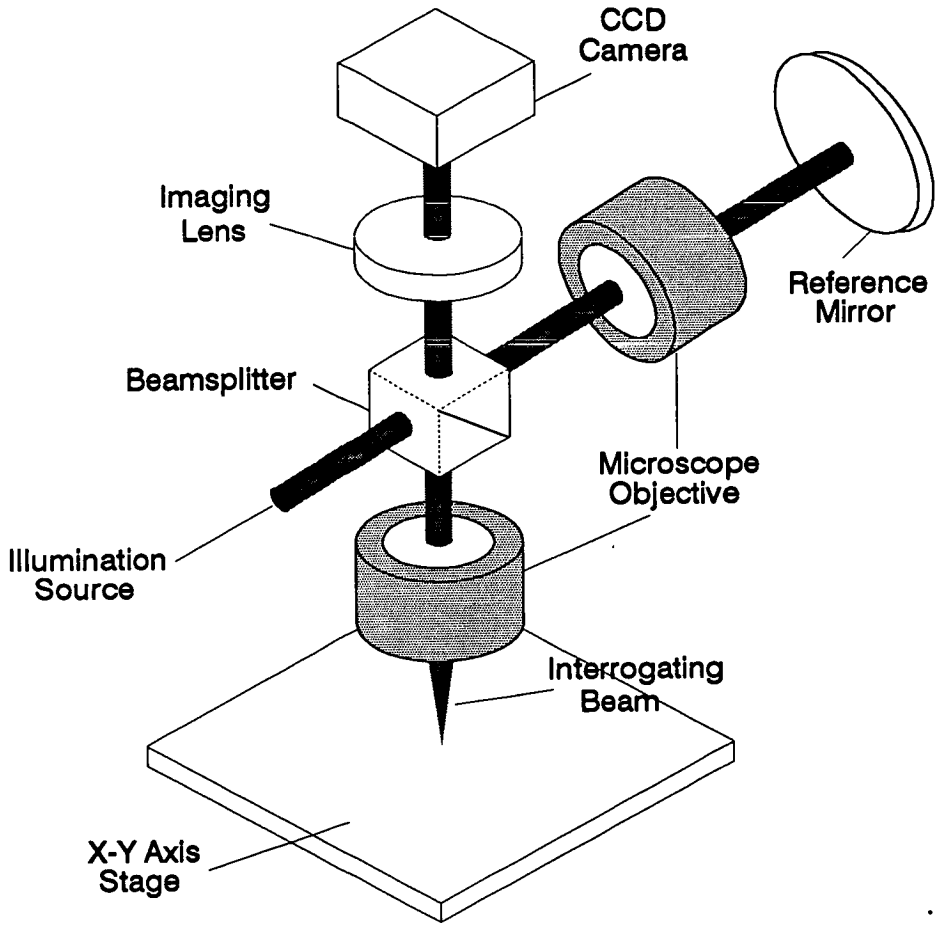

Figure 3–9: *Schematic diagram of a coherence probe metrology system.*

at the camera. Interference only occurs when the optical paths are nearly equal, i.e., when the surface is within a narrow zone, known as the coherence region.

By scanning the sample through z, the direction parallel to the interrogating beam, horizontal features separated in z (i.e., feature top and base) can be measured independently. Figure 3–10 illustrates the typical output. Proprietary image processing techniques are used to determine top and bottom widths and provide feature height information.[139,140]

This system is typified by the EMF's KLA 5015 CPM system. The ability to measure CD, unexposed resist loss and estimate sidewall angle, coupled with automatic pattern rocognition, makes this piece of equipment ideal for the examination of focus-exposure matrices (see Section 3.3.6).

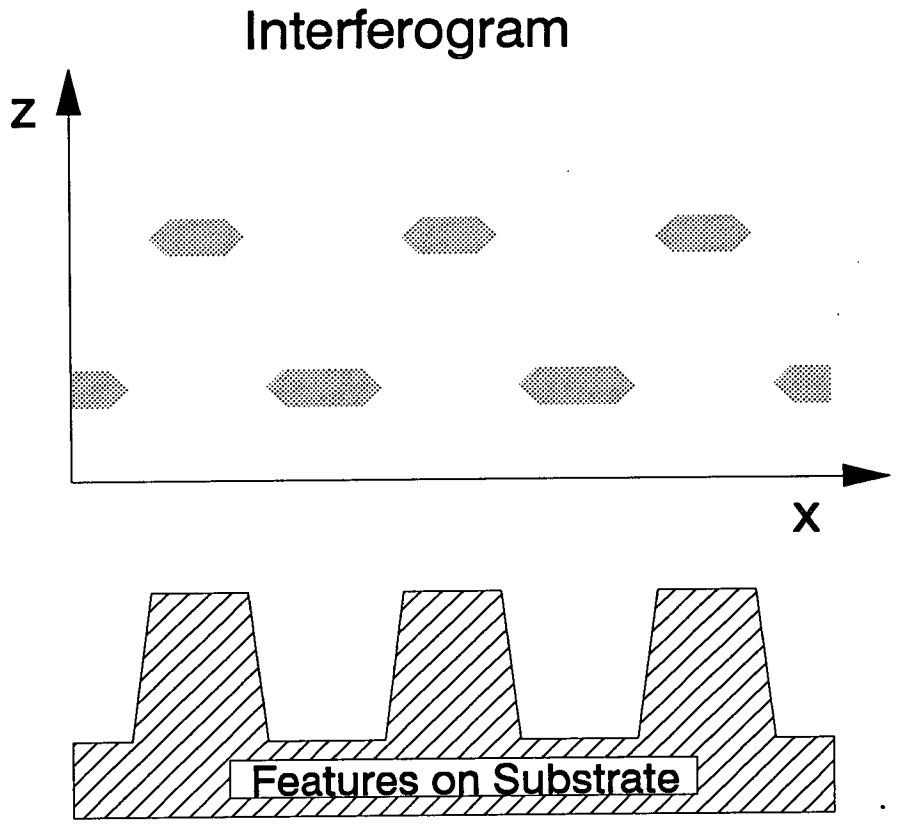

Figure 3–10: *This figure shows the relationship between a physical resist line/space pattern and the interferogram produced by a CPM system observing that pattern. The inteferogram represents a two dimensional plane equating to the feature cross-section. Dark areas are indicate regions where interference occurs, i.e. flat surfaces parallel to the substrate surface, such as the top of the resist and the bottom of the spaces.*

Again, CD measurement reliability is limited to features larger than about 0.7μm, by optical constraints.[46]

3.2.3.3 Scanning Electron Microscope

Scanning Electron Beam Microscopes (SEMs) offer very high resolution inspection, typically 20nm. This is significantly better than any optical inspection system. SEMs also offer a high depth of focus which is not limited by optical considerations i.e. Rayleigh criteria[141,142] . However, high accelerating voltages can damage substrate materials, so low voltage ($<$ 1.5kV) SEM equipment must be utilised for in-line inspection purposes.

During SEM operation an electron beam is raster scanned across the surface under observation, which is situated in an evacuated chamber. As the beam hits the surface, secondary and backscattered electrons are produced. The number and direction of such electrons is dependent on the topography and geometry of the scanned surface. The reflected electrons are detected and translated into a video image.

CD measurements are generally made in a topdown fashion; the linewidth is calculated from the video image in a similar manner to that used for optical video scan systems. Pixel calibration is set by measuring the pitch of a known period structure, usually attached to the wafer stage. A variety of low voltage linewidth SEMs are now avaiable for in-line metrology for 0.5μm technologies and below.

Profile characterisation and extremely accurate CD measurements are made by cleaving a wafer perpendicular to the features of interest and viewing the wafer edge on. Accurate CD measurements at the base of features can be made when they are arranged on a known pitch: cursors are used to compare the width of the feature at the substrate interface with that pitch. Figures 3–3 to 3–6 are examples of SEM profiles.

The EMF has a Cambridge S100 High Voltage SEM and a Bio Rad DL3006 Low Voltage inspection SEM.

3.3 Process Characteristics

3.3.1 Dose-to-Clear (E_0)

Photospeed is a key process characteristic. Also known as dose-to-clear or E_0, photospeed is the minimum exposure dose required to just clear a large open area of resist in the given development period.

E_0 varies with thickness, and exhibits a bulk dependence and a periodic 'swing' effect.

As resist thickness increases, so does the average exposure dose required to remove the film. This results from the extra mass of film which must be removed during the fixed time develop stage, hence it is called the bulk effect.

Chapter 2, Section 2.8.4.1 described how the fraction of incident energy coupled into the film varies in a periodic manner. In a given thickness range, neglecting the small bulk effect, an equal amount of PAC must be converted to remove the film in a given time. To achieve this an equal amount of incident energy must be coupled into the film. Incident energy therefore must vary in a sinusoidal manner to meet this requirement.

From Section 2.8.4.1, for a reflective substrate, maximum incoupling and therefore minimum E_0 values occur at resist thicknesses which are odd multiples of $\frac{\lambda}{4n}$. Minimum incoupling and maximum E_0 values occur at thicknesses which are even multiples of $\frac{\lambda}{4n}$.

Figure 3–11 illustrates experimental measurements of E_0 variations with thickness for a resist under typical processing conditions.

It has been proposed that the thickness dependence of E_0 can be described by the equation

$$E_0(t) = at + b\cos(ct)\sin(ct) \tag{3.1}$$

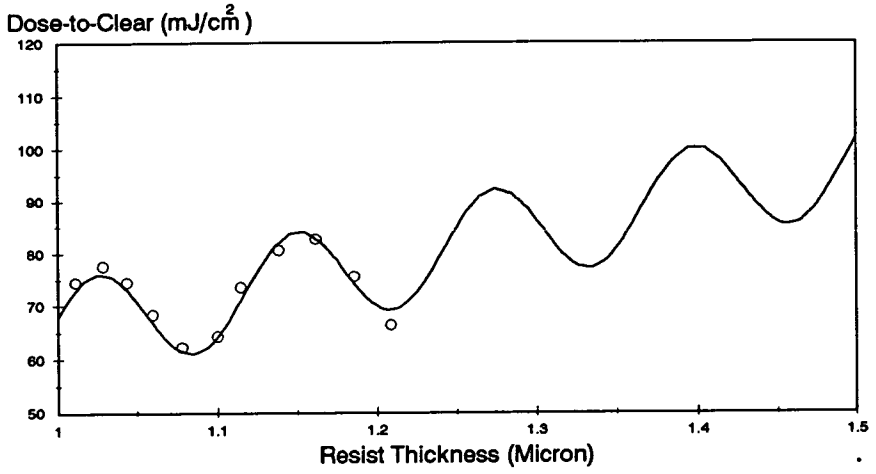

Figure 3–11: *Swing curve for HiPR6512 developed in HPRD428 with standard EMF process conditions. Development is 60 seconds of continuous spray. Solid line is best fit of equation 3.1.*

where t is the film thickness, a is the constant describing the bulk behaviour and b and c describe the swing effect. Such a fit is shown in Figure 3–11.

Photospeed can be measured with relative ease. A bare wafer is covered with resist and exposed with a series of open frame exposures. The exposure dose used for the first exposure is chosen to be well below E_0 and is incremented by a set amount for each subsequent exposure. The increment value should be chosen to ensure that the final dose is in excess of the dose-to-clear.

Most steppers have an exposure run option which will produce a serpentine pattern of such exposures (as illustrated in Figure 3–12). A similar effect can be achieved on shadow or scanning projection equipment, by using a mask which has square regions of differing, but known, transmission.

After development, a visual inspection of the wafer with the naked eye allows the first exposed region totally free of resist to be identified. The energy dose used for this exposure is taken to be E_0. The uncertainty in the determined value is $\pm$ half the exposure increment. This experiment is particularly useful since it can also be used to determine the process indicator gamma (see Section 3.4.1.3).

Monitoring the photospeed of an established process is a good technique for

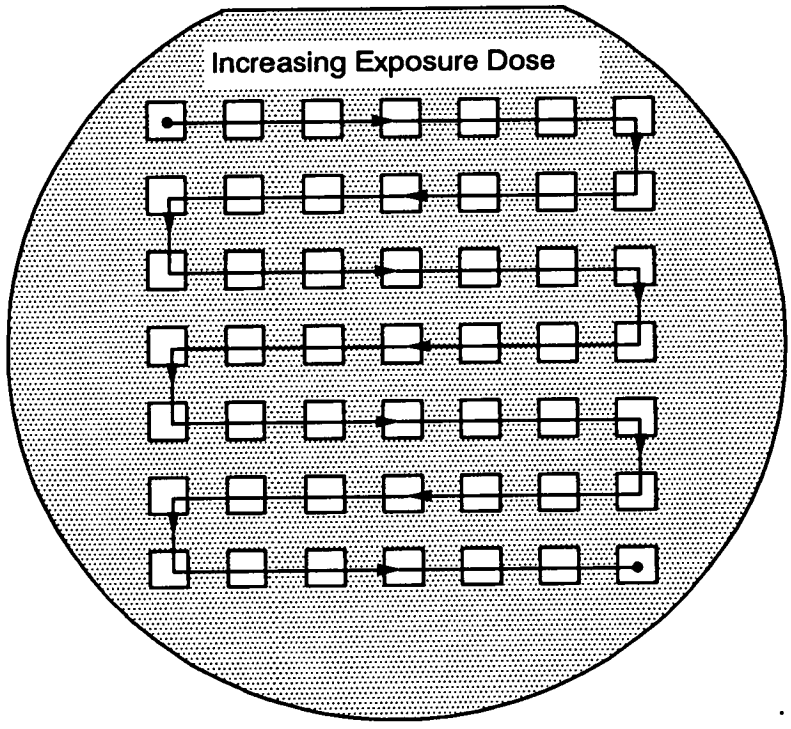

Figure 3–12: *A typical stepper-produced serpentine exposure run. The exposure dose used at each site is incremented by a fixed amount at each site with the user specifying the dose at the initial (top left) corner.*

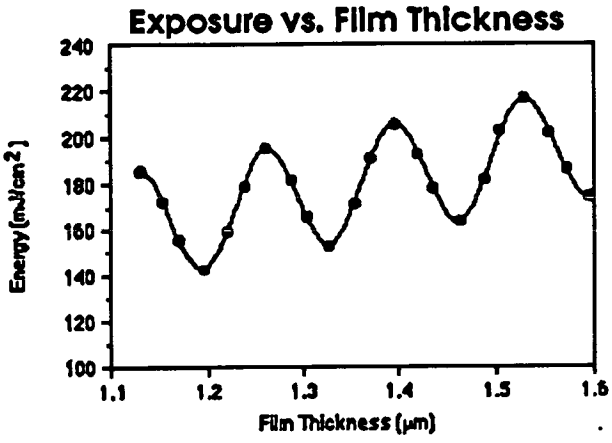

Figure 3–13: $E_{1:1}$ *as a function of film thickness for a 1 μm feature in HiPR6512 resist developed in HDRD437. Softbake: 100° for 60 sec. Exposure: Canon 0.43NA g-line. PEB: None. Development: 3/40 second spray/puddle process.*

detecting process drift, as the test is sensitive to deviations in the coating, baking, exposing and development steps.

3.3.2 Dose-to-Size ($E_{1:1}$)

$E_{1:1}$, the dose-to-size is the exposure dose required to reproduce the mask dimension exactly in resist. The value of $E_{1:1}$ varies with feature size. At large geometries the change is negligible, but as dimensions approach the resolution limit it rapidly increases. This effect is illustrated in Section 3–17 when exposure latitude is discussed.

$E_{1:1}$, like E_0, is thickness dependent and also exhibits bulk and swing behaviour. The swing period and phase are identical to that of E_0. Figure 3–13[69] illustrates the dependence of $E_{1:1}$ on film thickness.

$E_{1:1}$ can be difficult to measure. The mask feature of interest must be printed many times using different exposure doses. Then the printed features must be measured optically, or preferably by SEM in cross-section, until the feature of nominal mask size is found. This is a time consuming and tedious process.

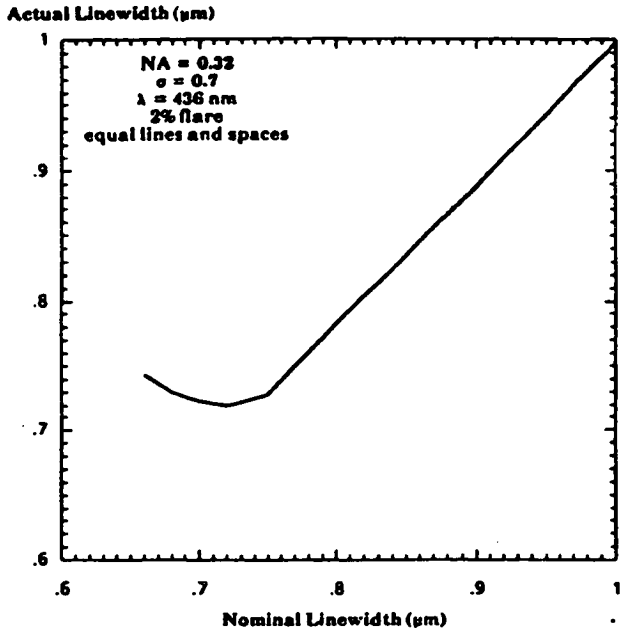

Figure 3–14: *A masking linearity plot.*

Dose-to-size is an important value for semiconductor production as it determines the total throughput of the exposure tool.

3.3.3 Mask Linearity

Mask linearity is a measure of mask dimension reproducibility. It consists of a plot of printed CD versus mask dimension for a given exposure dose. The dose chosen should be the $E_{1:1}$ for a feature significantly larger than the resolution limit.

The resulting plot can be used to identify CD_{min}, the smallest feature which can be printed without overexposing. Thus CD_{min} is the smallest mask dimension size which is reproduced within its CD tolerance limits whilst faithfully reproducing larger features. Figure 3–14[143] llustrates a linearity plot; in this case CD_{min} is about 0.74μm.

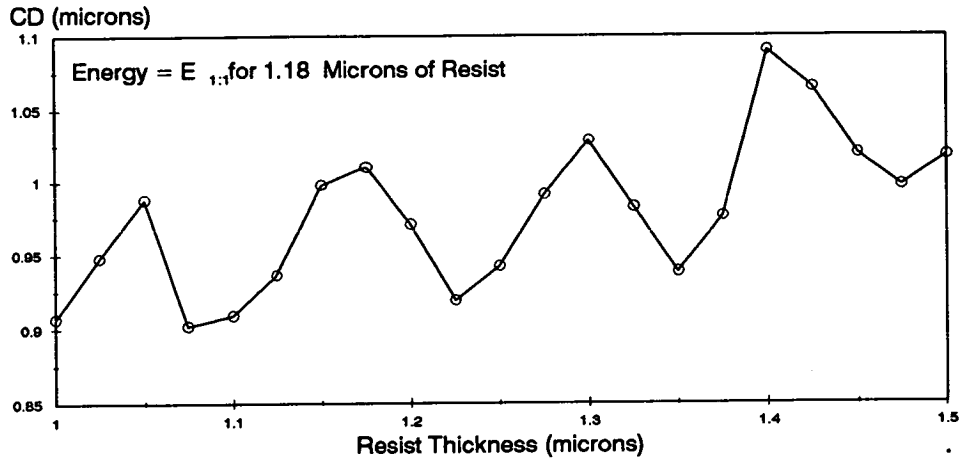

Figure 3–15: *Experimental CD swing with resist thickness for HiPR6512 resist. Softbake 60 seconds at 90°. Exposure 0.32 NA g-line. PEB 60 seconds at 120°. Development 60 seconds continuous spray in HPRD428.*

3.3.4 Exposure Latitude

Section 3.3.2 described how $E_{1:1}$ varies with resist thickness. Conversely, CD changes with resist thickness when the exposing energy dose is constant (see Figure 3–15).

Whilst, in a production environment fixed exposure doses are used for each process level, there are always finite cross-wafer and wafer-to-wafer thickness variation. Further thickness changes are introduced when topography is considered. Obviously, the changes in energy coupling caused by such variations gives rise to CD variations in features which are of identical size on the mask.

The response of a feature to changes in incoupling can be gauged by measuring its sensitivity to exposure dose. This is a useful test, as CD versus exposure dose can be measured quickly utilising a single test wafer.

Exposure latitude is the range of energy over which a given feature is reproduced on the substrate within its CD specifications. It can be expressed as either an absolute value or a percentage of $E_{1:1}$. Figure 3–16 illustrates a 1.4μm process where a $\pm$10% CD specification gives a 64% exposure latitude.

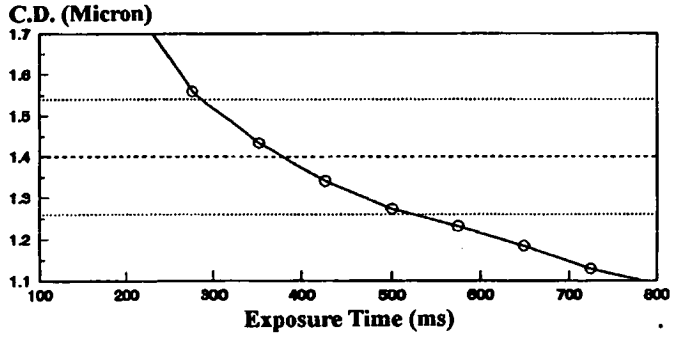

Figure 3–16: *The g-line Exposure Latitude plot for a 1.4μm SPR-2FX 1.8JM resist feature on Aluminium/Silicon.*

The latitude is sensitive to feature size, and decreases with geometry. This phenomenon is shown in Figure 3–17, which also illustrates the way in which dose-to-size rises as features approach the resolution limit.

Exposure latitude is traditionally measured at best focus, but can be calculated for any level of stated defocus.

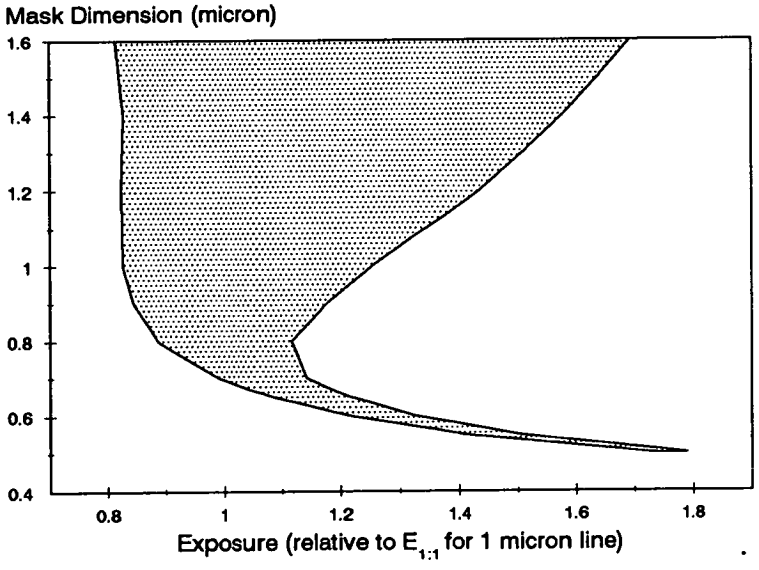

Figure 3–17: *Upper and lower exposure latitude limits as a function of nominal mask size. Shaded region represents exposure values which produce a feature that is in specification.*

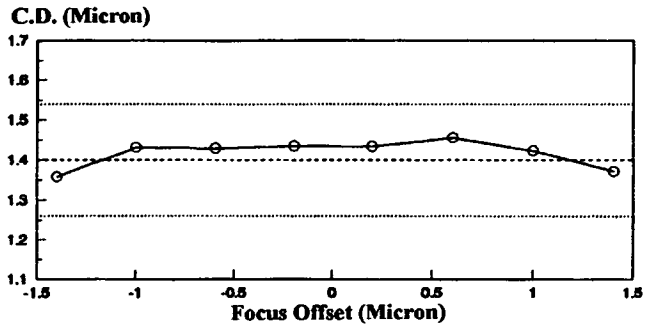

Figure 3–18: *The Focus Latitude for a 1.4μm SPR-2FX 1.8JM resist feature on Aluminium/Silicon exceeds 2.8μm when using a 0.54NA g-line Nikon stepper.*

Whilst a process with a large exposure latitude is preferable, its value should be scaled by the $E_{1:1}$ swing magnitude when comparing different resist systems. This gives a fair representation of the utility of each process in the presence of thickness fluctuations.

3.3.5 Focus Latitude

Substrate topography yields a resist coating which has elements at a variety of heights. Consequently, some regions of resist will be in perfect focus whilst others are in varying states of defocus. The CD and profile sensitivity to defocus is therefore another important characterising parameter.

Focus latitude, also known as Depth Of Focus (DOF), is defined as the defocus range over which a feature is produced within given CD and sidewall specifications. Figure 3–18 illustrates a typical focus latitude plot.

Focus Latitude should be assessed at the optimum exposure energy (i.e. $E_{1:1}$ for best focus) but, again, can be measured for any stated energy value.

Obviously, a large DOF is preferable, but as long as it is greater than the largest topography step plus the day-to-day stepper focus variation budget, a satisfactory production process can be implemented.

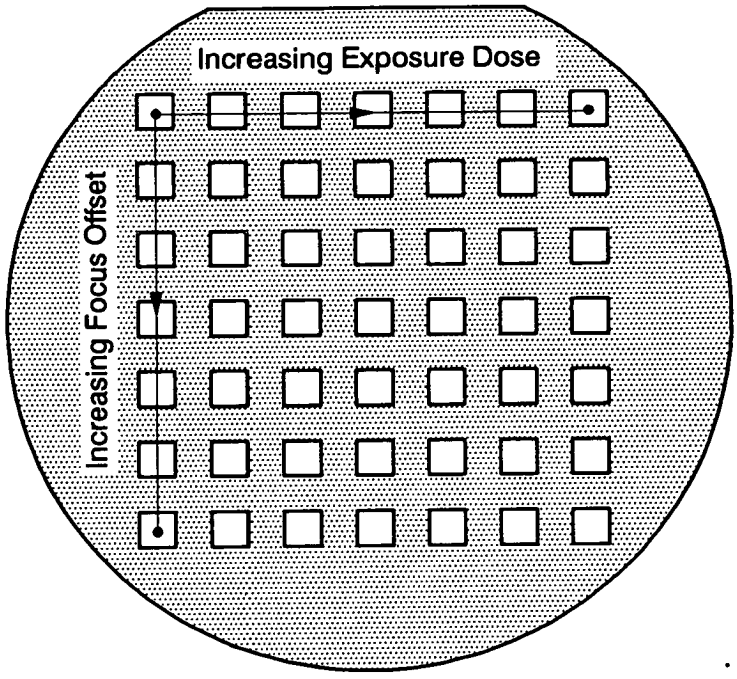

Figure 3–19: *The focus-exposure matrix exposure scheme.*

3.3.6 Process Latitude

Whilst focus and exposure latitude are valuable process parameters, they only reflect process sensitivity at particular operating points, usually optimum ones. A measure which indicates how the process behaves at all focus and exposure values gives more insight into total process utility.

Such information can be gathered from a single wafer using a focus-exposure matrix. Most steppers have a standard program for generating such matrices. The mask pattern of interest is stepped over a whole wafer and exposure and focus is adjusted at each site. Each column in the matrix is exposed at equal energy, with a constant energy increment between consecutive columns. Similarly, each row utilises the same focus offset with a constant focus increment between each row. This exposure scheme is illustrated in Figure 3–19. The centre of the matrix should be targeted on $E_{1:1}$ for the features of interest and utilise nominally best focus for the exposing tool.

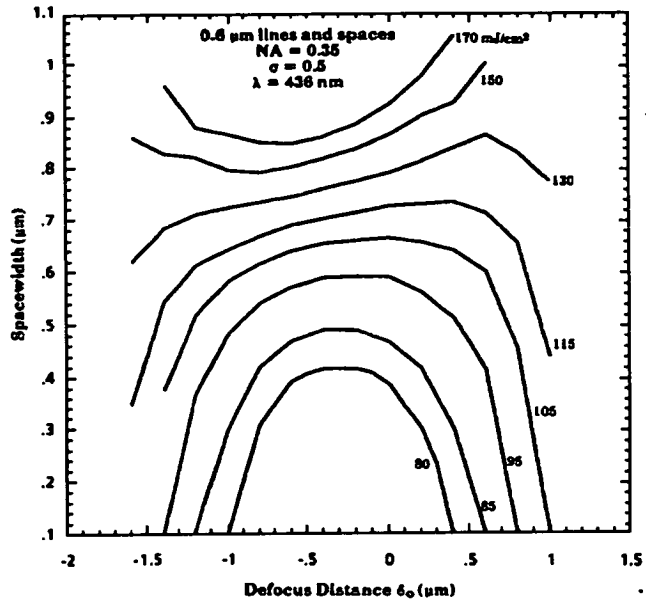

Figure 3–20: *A typical Bossung plot representation of focus-exposure matrix information.*

3.3.6.1 Bossung Plots

The Bossung plot, often called a 'smiley' or 'spider' plot, is the way in which CD process latitude information has been traditionally presented. CD is plotted against defocus and points of constant exposure are connected. Figure 3–20 shows a typical Bossung plot.

Figure 3–20 clearly illustrates that focus latitude is exposure dose dependent. The exposure dose which demonstrates the least change in CD with defocus is known the isofocal exposure energy.[144] The difference between the nominal CD and the CD produced using this energy is called the isofocal bias. Ideally this bias should be zero.

Best, or optimum, focus can also be determined from the Bossung plot. It is the defocus value at which the CD spread over all the exposures used is at a minimum.

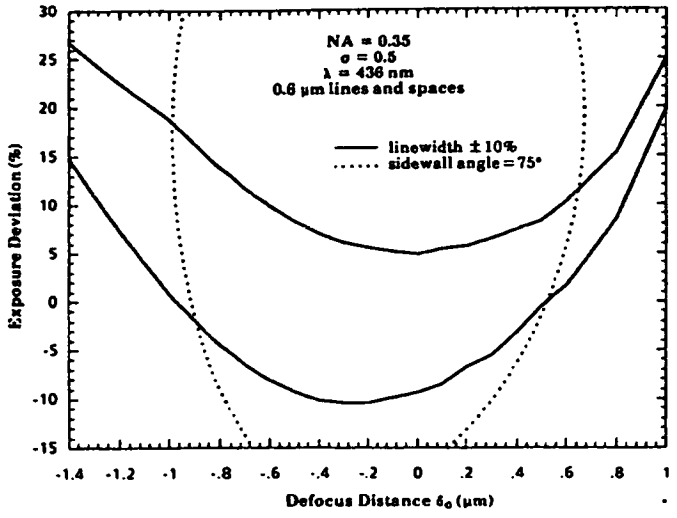

Figure 3–21: *A typical process window specified by CD and sidewall constraints.*

3.3.6.2 Process Windows

Whilst considerable information can be gained from a Bossung plot, no profile information is represented. The **process** window is a way of presenting CD and profile information on a single plot.

The plot axes are defined as exposure (or exposure latitude) and defocus. Lines of constant CD, sidewall angle and filmloss are placed on this map.[145] The contour values chosen for the plot are usually the process limit specifications (i.e. ± 10% CD, 80° sidewall and 10% filmloss). The process window is the area which meets all the process specifications. Figure 3–21 illustrates the process window formed from the CD and sidewall angle contours for a typical process.

Process windows for different resist/developer systems and varying process conditions can be compared by normalising exposure energies to $E_{1:1}$ and overlaying.[145] The process window with the largest area has the highest utility.

Process windows which bend up (as in the case of Figure 3–21) or down indicate that the isofocal bias is not zero.[23] If the bias is zero or is within 10% of the nominal CD then both linewidth and sidewall angle contours will bow outwards increasing the usable process space.

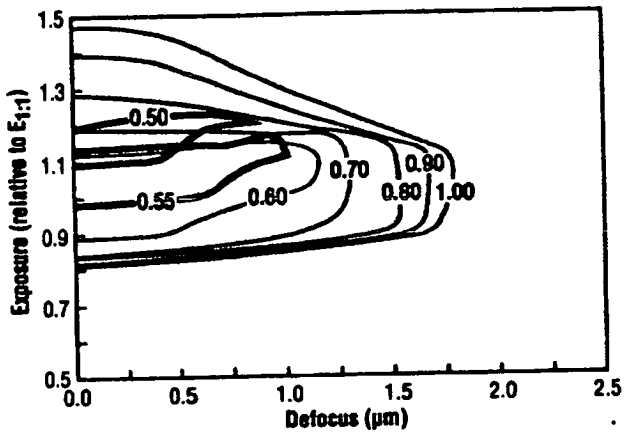

Figure 3–22: *Stacked process windows for different geometry periodic 1:1 line/space features.*

The process window shrinks with feature size. The smallest resolvable feature is the one whose process window still has a finite area. Hansen[145] has shown how stacking the process windows for various CDs (Figure 3–22) can yield a considerable amount of information about a process. It can be clearly seen that the exposure energy required to produce small features rises and CD_{min}, the limit of mask linearity, is given by the smallest feature whose process window overlaps a finite region of all larger features process windows.

3.4 Process Indicators

Although a full evaluation of a process window even for multiple feature sizes can be made from a single wafer, making all the necessary measurements can be a time consuming process. Evaluation of a full focus-exposure matrix using a totally automated optical inspection system (such as the KLA 5015) may take several hours per feature size, whilst inspection by SEM takes many times longer.

It is therefore common for lithographic engineers to use more simply determined process indicators to predict the performance of a process. Although care should be taken when using these values to compare processes using different resist

and developer chemistries, they can be of considerable use when optimising the processing conditions of a particular resist/developer system.

The following sections examine the three most useful and commonly used indicators, outlining how they are measured and which of the process characterising values they correlate to.

3.4.1 Contrast (γ)

The most commonly used process indicator is contrast. This is an adaptation of the Hurter and Driffield plot that was used to characterise photographic processes.

Contrast, or gamma (γ), is defined as the slope of the plot of normalised thickness remaining versus the logarithm of the exposure dose, at the point where the thickness goes to zero.[146] This is given by the expression

$$\gamma = -\frac{1}{log\left(\frac{E_0}{E_1}\right)} \tag{3.2}$$

where E_0 is the dose-to-clear and E_1 is the threshold energy at which resist dissolution would commence if the curve were linear.

However, experience shows that this is not a practical way of measuring gamma as the onset of dissolution is gradual and often a small foot occurs in the curve just before zero thickness.

Gamma is more commonly calculated by the least squares fit to the curve in a defined 'near-linear' range of thickness remaining. The standard ASTM procedure[147] uses 10% to 70% of the softbake thickness, but other ranges are often used. Figure 3–23 illustrates a Hurter-Driffield plot and both the classical (γ_0) and the ASTM (γ_{ASTM}) definitions of gamma

A high contrast process is one which has a rapid change in film loss (dissolution rate) as a function of exposure in the exposure range closely below E_0

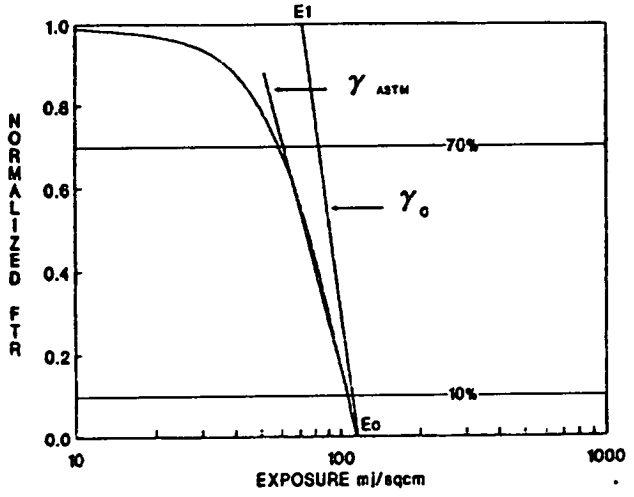

Figure 3–23: *The two alternative gamma definitions.*

3.4.1.1 The Utility of Contrast

It is a generally believed "rule of thumb" that a higher gamma corresponds to a steeper side wall angle and a better resolution. The results of many studies have indeed shown that there is a degree of correlation between higher gamma values and improved sidewall angle,[148–150] exposure latitude,[149–152] defocus latitude[150] and CD_{min}.[153]

However, several of these studies[148–150] point out that the relationships show a high degree of scatter and hence large differences in gamma are required to positively conclude one process is better than another.

It has also been demonstrated[146,150,154] that the relative performance of resists exhibiting a strong optical absorbance (i.e., a dyed resist) is underestimated by gamma and that in the presence of strong surface induction a high gamma value need not infer a steep sidewall angle.[148]

Most importantly, gamma has a strong thickness dependence. This should be expected as its definition is closely related to both the thickness at exposure and the exposing dose and hence is altered by the degree of energy coupling. Both a bulk and swing effect have been noted during experimental and theoretical work[146,155,156] and is illustrated in Figure 3–24.[146]

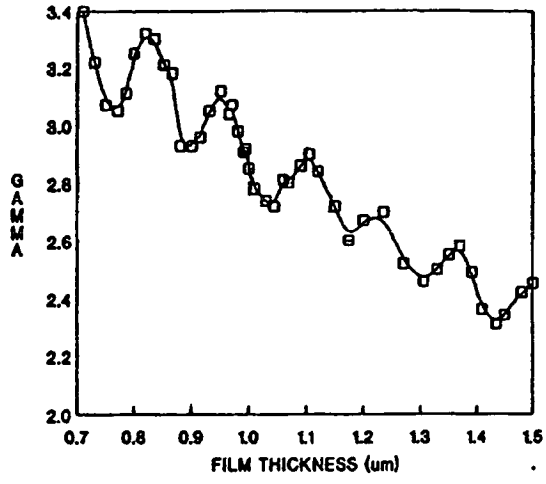

Figure 3–24: *The variation of constrast with thickness exhibits both a swing and bulk effect.*

Again the swing period is $\frac{\lambda}{2n}$. Its phase, however, in relation to the E_0 swing curve, is determined by processing factors (Exposure and PEB conditions etc.) and by the amount of surface induction.

Spragg *et al.*[146] have shown that exposure latitude is virtually insensitive to thickness variations, therefore correlations of gamma and exposure latitude should be made with care.

Caution must be exercised when using gamma to compare the use of processes that utilise different chemistries, especially if there are differences in optical absorption and surface induction. However, gamma can be used with a greater degree of confidence when comparing the same resist/developer combination under varying process conditions (bake conditions, development technique, development time etc.) if the film thickness, and hence optical coupling, is kept constant.

3.4.1.2 The Effect of Processing on Contrast

Investigations into the effects of process conditions on gamma have shown that development technique has a major influence; spray processes produce the highest gamma values, puddle processes intermediate values and immersion processes the

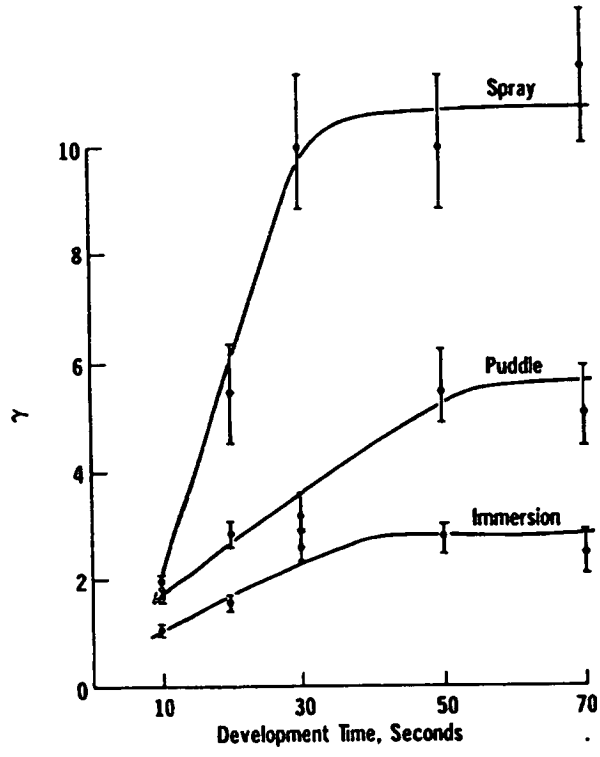

Figure 3–25: *For a given resist/developer combination, development technique and time strongly influence the resulting contrast value.*

lowest.[157] Increasing development time also raises the gamma value[157,158] though the value eventually saturates. Both phenomena are illustrated in fig 3–25.

Gamma has been shown to increase as the PEB is made more aggressive (either increased time or temperature) and as the developer is made less aggressive (i.e., normality is lowered). In both cases threshold (E_0) and sizing energies ($E_{1:1}$)are increased.[157]

3.4.1.3 Measurement of Contrast

Gamma can be easily determined from the dose-to-clear experiment described in Section 3.3.1, if the initial exposure dose is made suitably low (i.e., negligible resist loss occurs).

The remaining resist thickness is measured at each exposure site and normalised to the pre-exposure thickness. The values obtained are plotted against

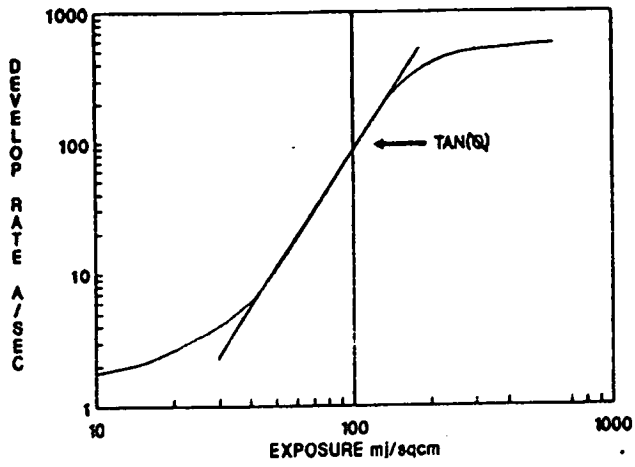

Figure 3–26: *Tan ϕ is defined as the gradient of a log dissolution rate versus log exposure plot in the region of maximum steepness.*

the relevant exposure dose. The measurement criteria described in Section 3.4.1 are then applied. Experiments have shown[157] that at least five points are required for a reliable line fit which yields a repeatable gamma value.

Several automated measurement systems, such as the Prometrix Lithomap[159] and the Site Services PACscan 1000[160] can determine contrast automatically, given an appropriately exposed and developed wafer.

3.4.2 Theoretical Contrast (Tanϕ)

Theoretical contrast, also known as tanϕ to avoid confusion with gamma, is an alternative measure of contrast.

Tanϕ is defined as the slope of the plot of **dissolution rate** versus **exposure dose** in the region of maximum steepness, when both axes use logarithmic scales,[146] as illustrated in Figure 3–26.[146]

Mack[156] has shown that tanϕ and γ become equal for the hypothetical case of a non-absorbing resist on a non-reflecting substrate.

Spragg *et al.*[146] have demonstrated that the value of tanϕ is essentially independent of film thickness. Changes in incoupling result in parallel curves, offset in the exposure axis but with identical gradient.

This work and another study[150] have shown that tanϕ is a superior predictor of exposure latitude, when compared to gamma, and that the relationship holds even in the presence of surface induction and changes in optical absorbance. It is also a better predictor of CD_{min} and sidewall angle though these results are skewed by changes in optical absorbance.

Although tanϕ offers higher utility than gamma, it is considerably harder to measure. Dissolution rates must be derived from Development Rate Monitor (DRM) experiments, as described in Chapter 5, over a wide range of exposure energies. Even this procedure is impossible when complex spray/puddle processes are utilised.

3.4.3 Exposure Margin (EM)

Exposure Margin (EM), proposed by Hansen *et al.*,[161] is defined as the ratio of $E_{1:1}$, the exposure dose required to reproduce the mask dimension with zero bias, and E_0, the dose-to-clear, i.e.

$$EM = \frac{E_{1:1}}{E_0} \tag{3.3}$$

Both the initial study[161] and further work[150] have shown that exposure margin is an almost perfect indicator for CD-related latitudes such as CD_{min} and exposure latitude even in the presence of strong surface induction and optical absorption. It has also been found to correlate well with process latitude if optical absorption remains constant.

Again, although exposure margin offers a higher utility than gamma, it is harder to measure. Both E_0 and $E_{1:1}$ must be found, this latter value involves a great many optical or SEM linewidth measurements and should be verified by a SEM profile measurement.

3.5 Summary

This chapter has reviewed how the utility of a resist process is defined and measured. Some commonly used process indicators have been introduced and their relevance to actual process characteristics and latitudes have been described.

The discussion of how process latitudes and the more significant process indicators are experimentally determined details the large amount of measurements required to characterise a single process. As latitudes change with process conditions (softbake temperature, develop time, mask bias, single puddle versus double puddle etc.) the vast amount of work required to even optimise a process using a given resist/developer combination can be appreciated.

Chapter 4

Lithography Modelling

4.1 Introduction

This chapter reviews currently accepted modelling theories and outlines the reasoning behind them. It goes on to discuss some of the inadequacies in the models and finally reviews the available simulation software, focusing particularly on those programs used during this study.

4.2 The Dill Model

All current lithography modelling is based on the pioneering work of Dill *et al.*[162–165] Although more complex development models have replaced the equation originally proposed by Dill, modern simulation packages utilise the techniques and principles laid down by Dill and his co-workers in 1975. They proposed that the lithography process could be modelled in two completely separate stages, exposure and development. The two stages are linked by the manner in which inhibitor is distributed throughout the film.

During exposure the resist is chemically modified; inhibitor is destroyed as it absorbs light of an appropriate wavelength. This effect is highly localised around the point where the photon is absorbed. The rate of inhibitor breakdown can be calculated if the exposing intensity is modelled for each point in the resist.

As discussed in Chapter 2, Section 2.2.3.2, the solubility of the resist is highly dependant on the level of inhibitor after exposure. Development can therefore be

considered as a surface-rate limited etching process which removes photoresist at a rate related to the amount of remaining inhibitor.

4.3 Exposure modelling

The main premise of Dill's work is that a resist film is a multicomponent, homogeneous, solid material consisting of resin, inhibitor and residual casting solvent. Its behaviour during exposure and development can be described by solely considering the amount of inhibitor remaining at each point in the film.

Although indenecarboxylic acid, which aids dissolution, is formed within the resist during exposure, its concentration is proportional to the amount of PAC converted and can be inferred from the level of remaining inhibitor.

The inhibitor distribution within the resist is mapped using a relative inhibitor term, M(x,y,z;t), which represents the normalised amount of unconverted PAC at point x,y,z after time, t, of exposure. This map of inhibitor concentration is often called the latent image as it is the differential solubility of this 'image' which leads to the feature profile after development.

Since the inhibitor distribution in the unexposed film is considered to be homogeneous, M(x,y,z;0) is set to unity for all x,y and z values.

During exposure, the rate of inhibitor destruction at a given point is directly related to the illumination intensity at that point. This value must be calculated for each point in the map of inhibitor concentration.

4.3.1 Calculation of Exposing Intensity

For low to moderate numerical aperture values, the exposing intensity at any point in the resist may be calculated by dividing it into two separate expressions. At position (x, y, z) in the resist, where x and y define the substrate plane and z is the axis perpendicular to that plane, the exposing intensity at that point at time, t, may be written as:

$$I(x, y, z; t) = I_{incident}(x, y)I_{sw}(z; t) \tag{4.1}$$

In this expression, $I_{incident}(x, y)$ is the incident image intensity, or aerial image, dependant upon the illumination, imaging system and mask pattern. $I_{sw}(x; t)$ is the standing wave intensity which depends upon the exposing wavelength, the complex refractive index variations within the resist and the substrate material. The following Sections, 4.3.1.1 to 4.3.1.4, examine the generation of these expressions for monochromatic illumination. However, polychromatic (broadband) exposure may also be simulated by forming the latent image for one wavelength and modifying it further by exposure to the next wavelength. This procedure is repeated until all the desired exposing wavelengths have been considered.[166] Care must be taken to measure the precise ratio of power in the different wavelengths, as they will not all be equal.

4.3.1.1 Simulation of Aerial Images: Incoherent Illumination

In the case of incoherent illumination, the aerial image produced by a diffraction limited optical system can be calculated using the system's Modulation Transfer Function (MTF), see Chapter 2, Section2.8.2.3, and for the perfect focus case is given by:[165,167]

$$MTF(\nu) = \frac{2}{\pi}[\cos^{-1}(\nu_r) - \nu_r(1 - \nu_r^2)] \tag{4.2}$$

where ν_r is is the relative spatial frequency of the object such that

$$\nu_r = \frac{\nu}{\nu_0} \tag{4.3}$$

ν is the spatial frequency of the mask pattern and ν_0 is the lens cut-off frequency, given by

$$\nu_0 = \frac{2NA}{\lambda} \tag{4.4}$$

If a focus shift of distance d is included then Equation 4.2 becomes[167]

$$\mathrm{MTF}(\nu, \mathrm{z}) = \frac{4}{\pi}\int_{\nu_r}^{1}\sqrt{1-\nu'^2}\cos[2\pi\nu_r(\nu'-\nu_r)\Delta(\mathrm{z})]\mathrm{dv}' \tag{4.5}$$

where $\Delta(\mathrm{z})$ is a normalised defocus length, measured in Rayleigh units and the defocus length, defined by Levinson and Arnold[168,169] as

$$\Delta(\mathrm{z}) = 2\frac{\mathrm{NA}^2}{\lambda}\left[\left|\delta_0 + \frac{\mathrm{z}}{\mathrm{n}_2}\right| + |\mathrm{d_{ab}}|\right] \tag{4.6}$$

where n_2 is the refractive index of the resist, δ_0 is the distance between the plane of focus and the resist surface. By convention, δ_0 is considered negative when the focal plane is below the resist surface whilst z adopts a positive value. Aberrations in the optics, such as internal reflections and surface imperfections, can be modelled by the variable $\mathrm{d_{ab}}$ which introduces a fixed level of defocus. This last parameter is often called lens flare.

4.3.1.2 Simulation of Aerial Images: Coherent Illumination

When coherent light is illuminating the mask pattern, use of the MTF is no longer sufficient and a more rigorous approach must be utilised.

The first step in calculating a coherently produced aerial image is determination of the diffraction pattern produced by the incident light on the mask. This can be achieved by using Fraunhofer scalar diffraction theory[170] where the electric and magnetic field components of the exposing radiation can be considered separately.

If the x, y plane is taken to be the reticle surface then the electric field transmittance of the mask pattern can be defined as $m(x, y)$. For a simple chrome type mask $m(x, y)$ takes the value 1 under the glass and 0 under the chrome. If the x', y' plane is the diffraction plane, i.e., entrance pupil of the objective lens, then for the case of monochromatic illumination the electic field intensity in that plane is given by:[170]

$$E(x', y') = \int_{-\infty}^{\infty} m(x, y) e^{-2\pi i(f_x x + f_y y)} dxdy \tag{4.7}$$

if the distance between the objective entrance pupil and the mask is z then f_x and f_y the spatial frequencies of the diffraction pattern are given by:

$$f_x = \frac{x'}{z\lambda} \tag{4.8}$$

and

$$f_y = \frac{y'}{z\lambda} \tag{4.9}$$

Inspection of Equation 4.7 reveals it to be a Fourier transform. Thus the electric field pattern entering the objective is the Fourier transform of the mask pattern. The electric field pattern at the objective entrance pupil is therefore given by:

$$M(f_x, f_y) = F\{m(x, y)\} \tag{4.10}$$

where F represents the Fourier Transform and the spatial frequencies are simply scaled co-ordinates in the x', y' plane.

Generally, the diffraction pattern extends infinitely in the x', y' plane, whilst the objective lens is of a finite size, defined by it's NA. The lens cannot therefore collect all the light within the diffraction pattern.

An ideal imaging lens is defined as one which produces the inverse Fourier Transform of the diffraction pattern.[171] This could only be achieved if the lens has infinite size and so is not possible. In reality the image quality is limited by the diffracted light which is not caught by the lens. Such an optical system is described as being diffraction limited.

The aerial image can be fully described if an aperture, or pupil, function is introduced. This function indicates what portions of the diffraction pattern is captured by the lens; it is one inside the aperture and zero outwith:

$$P(f_x, f_y) = \begin{cases} 1, & \sqrt{f_x^2 + f_y^2} < \frac{NA}{\lambda} \\ 0, & \sqrt{f_x^2 + f_y^2} > \frac{NA}{\lambda} \end{cases} \tag{4.11}$$

The electric field at the image plane (i.e. at the wafer) is given by the expression:[171]

$$E(x, y) = F^{-1}\{F\{m(x, y)\} P(f_x, f_y)\} \tag{4.12}$$

The aerial image, i.e. optical intensity distribution in the image plane, is obtained by taking the square of the magnitude of the electric field.

Again, the algorithm can be corrected for defocus by using $\Delta(z)$ as defined in Equation 4.6.[167] Aerial image formation in this fashion is discussed at length by Mack in a series of articles.[170–173]

4.3.1.3 Simulation of Aerial Images: Partially Coherent Illumination

Most exposure tools utilise an illumination source which is partially coherent, as discussed in Chapter 2, Section 2.8.2.2. The extended-source method allows a partially coherent source to be considered as a set of coherent point sources. A coherent image is calculated for each point independantly and the resulting image intensities are combined according to[167]

$$I_a(x, y, z) = \frac{4}{\pi NA_c^2} \int_0^{NA_c} \sqrt{NA_c^2 - u^2} I'_a(x, z, u)\, du \tag{4.13}$$

where NA_c is the numerical aperture of the condenser and $I'_a(x, y, z)$ is the intensity distribution produced by a coherent point-source wave with an angle of incidence $\sin^{-1} u$.[167]

4.3.1.4 Simulation of Standing Waves and Resist Absorption

The exposing intensity at a given depth in the resist can be calculated using the standing wave Equation 2.29, derived in Chapter 2, Section 2.8.4.1. The effect of any underlying layers must also be included using a similar expression.

As mentioned in Chapter2, Section 2.8.4.1, the $e^{-\alpha x}$ term in the equation accounts for absorption within the resist film. This term is in accordance with the Lambert Law of absorption:[174,175]

$$\frac{dI}{dz} = -\alpha I \tag{4.14}$$

where I is the intensity of light travelling in direction z through a medium with an absorption coefficient of α. This coefficient is, of course, wavelength dependent. In a homogeneous medium, such as completely unexposed or completely exposed resist, α is constant, so Equation 4.14 may be integrated to[175]

$$I(z) = I_o e^{-\alpha z} \tag{4.15}$$

where I_0 is the light intensity at z=0. If the medium is inhomogeneous, as in the case of partially exposed resist, the integral becomes:[175]

$$I(z) = I_o e^{-[\int_0^z \alpha(z')dz']} \tag{4.16}$$

Dill defined 3 parameters, A,B and C, now known as the Dill parameters, which describe how photoresist absorption varies with exposure.[162,163] A and B are measurable parameters (see Section 4.3.4) which respectively describe the bleachable and unbleachable portions of the resist absorption and are wavelength dependant, such that:

$$\alpha = AM(z,t) + B \tag{4.17}$$

where M(z,t) is the relative inhibitor term for depth z at time t. M(z,t) becomes zero when complete exposure has occurred and has an initial, unexposed, value of unity, i.e. M(z,0) = 1.

The rate of inhibitor destruction and hence reduction in absorbance is dependant on the local optical intensity I(z,t), the local inhibitor concentration and the third Dill parameter C, in the following manner:

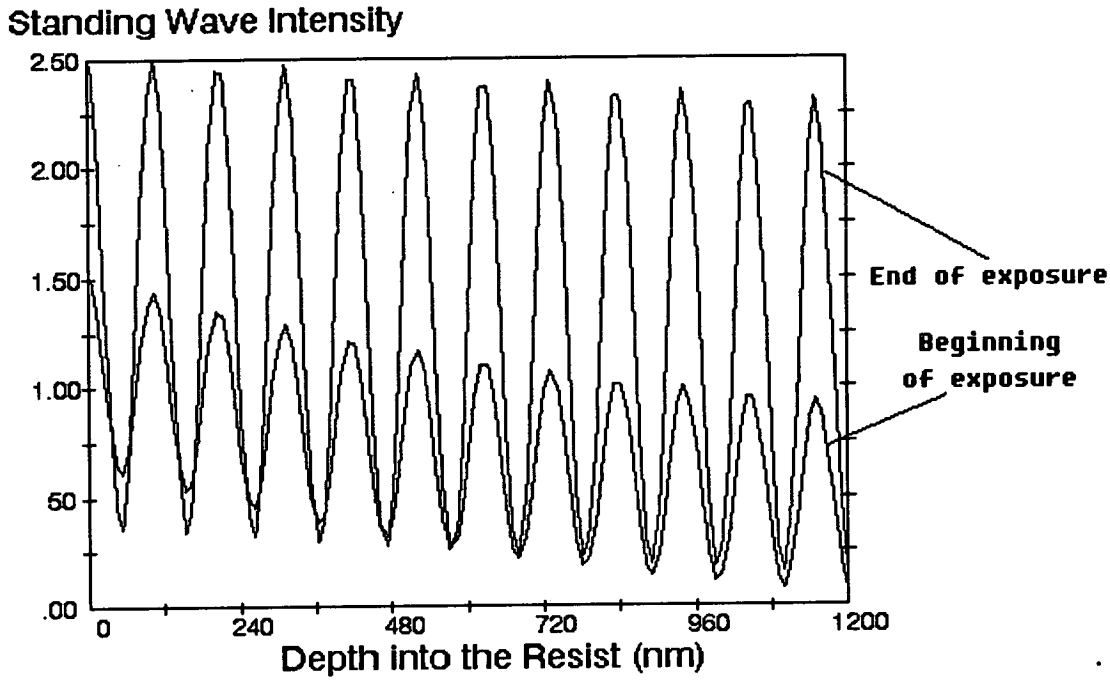

Figure 4–1: *A PROLITH/2 simulation of the change in standing wave intensity due to a* $115\,mJcm^{-2}$ *365nm exposure in a typical i-line resist.*

$$\frac{dM}{dt} = -I(z,t)M(z,t)C \tag{4.18}$$

C is a measurable (see Section 4.3.4) optical sensitivity term, which is once again wavelength dependent.

Using the Dill ABC parameters to describe absorption in the standing wave equation the exposing intensity at time, t, can be calculated. The expression must be continually recalculated using small time increments, as the absorption of the material is continually altering.

In reality, the equation is solved for small increments of exposing energy as resist exposure exhibits reciprocity between exposure time and source intensity, i.e. results are determined by the product of source power and exposure time.

Figure 4–1 illustrates the change in standing wave intensity between the beginning and end of exposure for a typical $1.2\mu m$ resist film.

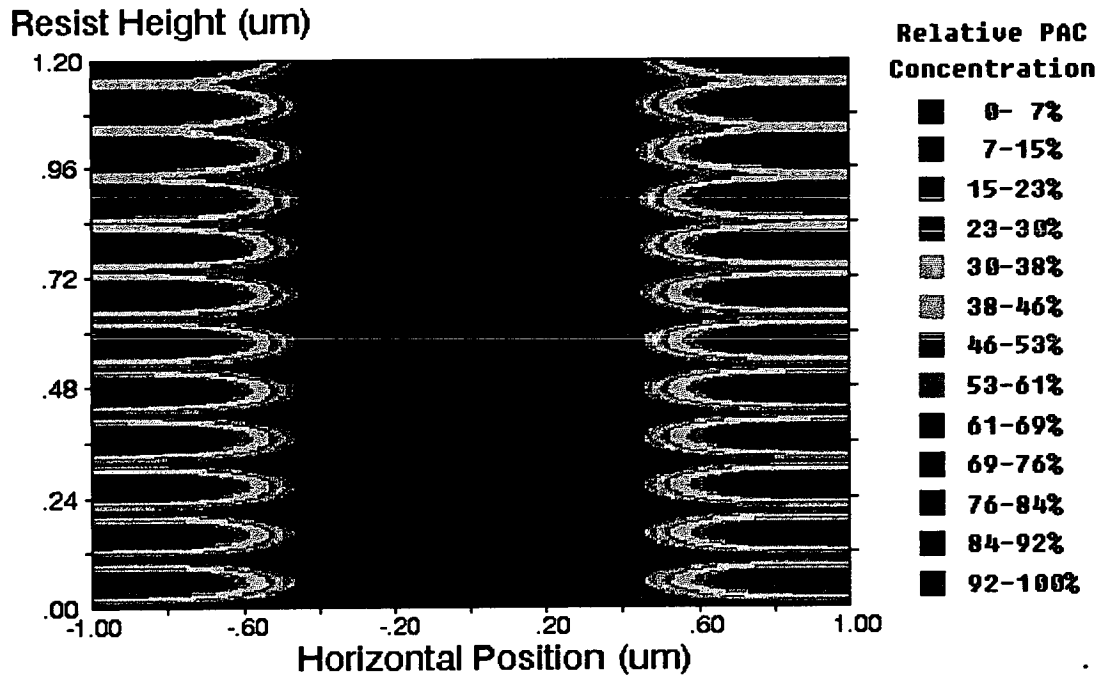

Figure 4–2: *A PROLITH/2 generated latent image.*

4.3.2 Latent Image Formation

The full latent image is formed by calculating the aerial image and standing wave intensity for each point in the film in an iterative fashion for small energy increments until the desired total of incident energy has been deposited. Obviously, the choice of the energy step size will influence the accuracy of the answer. The aerial image need only be calculated once as it is time independent.

Figure 4–2 illustrates a latent image produced by PROLITH/2 under the same conditions described for Figure 4–1. The exposure tool has a NA and partial coherence of 0.5. The feature is a one dimensional line profile of 1μm width on a 2μm pitch. In such simulations the line is considered to be infinitely long.

4.3.3 Simulation of Very High NA Exposure Tools

The separation of the aerial image and standing wave intensity made in Equation 4.1 is an approximation. Yeung[176] has modelled latent image formation rigorously

using electromagnetic diffraction theory and demonstrated that the results of the approximation are very close to those of the rigorous treatment, even for relatively high NA values.[177] Significant errors only start to occur when NA values exceed 0.6.[178] At this point rigorous intensity calculations must be made, introducing a calculation time penalty of several orders of magnitude.

4.3.4 Measurement of the Dill ABC Parameters

The Dill parameters are wavelength dependant, but can be measured with relative ease. A matched transparent substrate, of known absorption, is coated with a resist film of a given thickness. The absoprtion of this substrate/film combination, as a function of wavelength, is then measured using a low power spectrophotometer. The absorbance of the unexposed resist, $\alpha_{\text{unexposed}}(\lambda)$, is calculated by dividing the additional absorbance of the resist by the coating thickness.

All the inhibitor within the film is then destroyed by prolonged flood exposure with an illumination source of suitable wavelength. The measurement procedure is then repeated to yield the absorbance of completely exposed resist, $\alpha_{\text{exposed}}(\lambda)$. Figure 2–30, in Chapter 2, illustrates α_{exposed} and $\alpha_{\text{unexposed}}$ as a function of wavelength for Shipley S1813 resist.

From the definition of A and B, given in Section 4.3.1.4, B is the unbleachable component of the resist absorbance, i.e.

$$\mathrm{B}(\lambda) = \alpha_{\text{exposed}}(\lambda) \tag{4.19}$$

and A is the bleachable component of the resists absorbance, therefore:

$$\mathrm{A}(\lambda) = \alpha_{\text{unexposed}}(\lambda) - \alpha_{\text{exposed}}(\lambda) \tag{4.20}$$

The measurement of C is more complex but allows A and B to be calculated simultanously. Again a resist coating of thickness, d, is placed on a matched

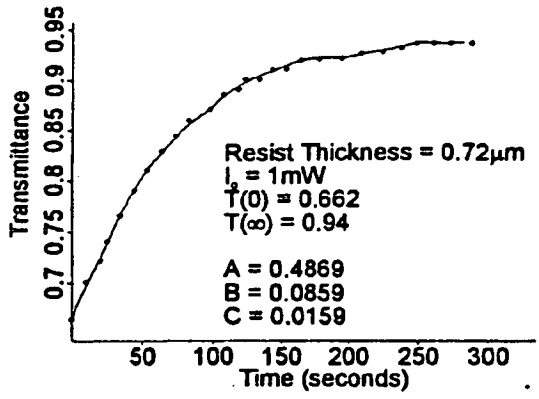

Figure 4–3: *Plot of i-line transmission for JSR PFR IX 500 EL resist with time during exposure.*

transparent substrate. The known transmittance of the substrate can be subtracted from the transmittance of the resist/substrate combination to yield that of the film alone.

The total transmittance at a single wavelength is measured by a spectrophotometer whilst the film is irradiated with light of that wavelength.[179] A plot of transmittance versus time, as illustrated in Figure 4–3,[180] can be used to determine the 3 parameters using the following expressions derived by Dill[163]

$$A = \frac{1}{d}\ln\left[\frac{T(\infty)}{T(0)}\right] \tag{4.21}$$

$$B = -\frac{1}{d}\ln T(\infty) \tag{4.22}$$

$$C = \frac{A + B}{AI_0 t(0)\{1 - T(0)\}}\frac{dT(0)}{dt} \tag{4.23}$$

where T(0) is the transmittance of the resist at the start of exposure, T(∞) is the transmittance of fully exposed resist and I_0 is the intensity of the exposing illumination. This experiment assumes that the exposing intensity remains constant throughout.

Resist	A μm^{-1}	B μm^{-1}	C cm^2mJ^{-1}
HiPR 6512	0.61	0.065	0.013
HPR 204	0.65	0.010	0.012

Table 4–1: *Experimentally determined g-line Dill parameters for OCG resists.*

It should be noted that C must be calculated explicitly for every wavelength of interest.

Table 4–1 details the g-line (436nm) Dill parameters for OCG HiPR6512 and HPR204 photoresist as determined by S.G.Hansen[181] (OCG Research and Development, Providence, Rhode Island). These values are used extensively in the simulation work described in Chapters 6 and 7.

4.4 Softbake Modelling

Mack[83] has proposed a model which modifies the Dill ABC parameters to reflect the level of thermal PAC degradation seen under varying softbake conditions. However, as he notes, a quantity of indenecarboxylic acid can be formed during this degradation which modifies the film's dissolution properties. Additionally, extensive work by Rao *etal.*[182–185] has shown that the dissolution rate of resist is highly dependent on the amount of residual casting solvent in the film, which is directly related to softbake temperature and time.

No model is available which reflects the changes in dissolution behaviour as a function of softbake temperature, therefore any Dill parameters and development rate parameters collected under a given set of softbake conditions are only valid for simulations assuming those same bake conditions.

4.5 Post Exposure Bake (PEB) Modelling

During the PEB, photoactive compound diffuses through the resist film according to local gradients, i.e. inhibitor moves from regions of high concentration to those where it is lower. This effect can be simulated in the Dill latent image model by applying Fick's second law of diffusion:[186]

$$\frac{\delta C_A}{\delta t} = D\frac{\delta^2 C_A}{\delta x^2} \tag{4.24}$$

where C_A is the concentration of species A, D is a diffusion constant for some temperature T and t is the time that the system is at that temperature. Mack[143] derived the following equation to describe the level of inhibitor at point (x,z) in a two dimensional simulated latent image after PEB:

$$M^*(x,z) = \frac{1}{2\pi D_l^2}\int_{-\infty}^{\infty}\int_{-\infty}^{\infty} M(x-x_0, z-z_0)e^{-\left[\frac{x_0^2+z_0^2}{2D_l^2}\right]}dx_0\,dz_0 \tag{4.25}$$

where $M^*(x,y)$ is the relative inhibitor concentration after the diffusion and D_l is the characteristic diffusion length, such that

$$D_l = \sqrt{2Dt} \tag{4.26}$$

where t is the bake time and D is the diffusion constant of the PAC in the resist at temperature T. D is the same constant as in Equation 4.24.

The characteristic diffusion length is determined by the size of Novolak and PAC molecules, the level of residual solvent within the film, the temperature of the PEB and the bake time. As the residual solvent level depends on the softbake conditions, diffusion length is not determined solely by PEB conditions. The measurement and even estimation of the characteristic diffusion length is very difficult from experimental results. Instead, it is usual to specify an arbritary

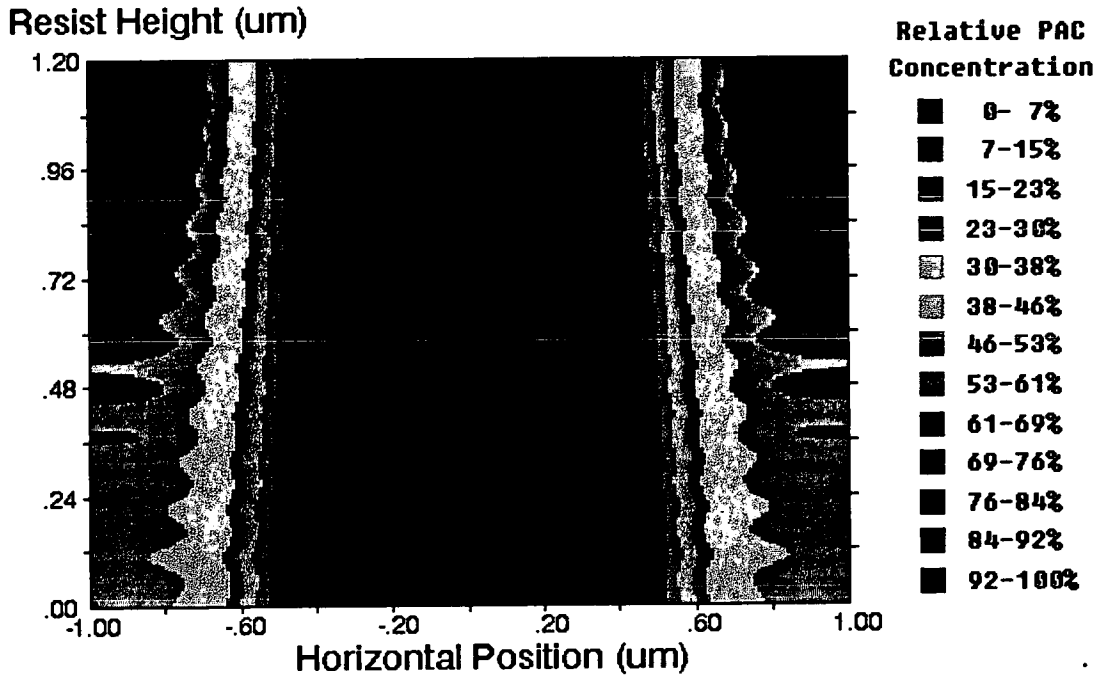

Figure 4–4: *The PROLITH/2 latent image of Figure 4-2 after a PEB diffusion*

diffusion length which suppresses the standing waves on simulated profiles to the same extent as is observed on experimental samples. In Chapter 6, Section 6.6.4 a technique is introduced for accurately estimating the diffusion length of a given process from experimental Development Rate Monitor data.

The residual solvent level within a resist film alters during PEB as the high temperature induces further densification. Again, modified dissolution behaviour results. Therefore, as was the case with softbake, simulation cannot be reliably used to characterise the process alterations resulting from changes in PEB condition. The characteristic diffusion length should be recalculated or re-estimated for each combination of softbake/PEB conditions.

Figure 4–4 shows the latent image of Figure 4–2 after receiving a PEB with a characteristic diffusion length of 40nm, as predicted by PROLITH/2.

4.6 Development Modelling

In the bulk of the resist, the rate of removal during development is dependant on the instantaneous inhibitor level at the resist/developer interface. In a simulation, the development rate is therefore a function of the relative inhibitor concentration, M, at the resist interface. The relationship between this bulk development rate, R_{bulk}, and M is given by a dissolution rate equation. Section 4.6.1 reviews the most common equations.

As discussed in Chapter 3, Section 3.2.2.1, an effect known as surface inhibition, or surface induction, retards dissolution near the original film surface. This occurs in all resists and is usually negligible, but can be significant depending upon thermal processing and the resist and developer chemistries. Surface inhibition is modelled using a multiplier function, f(z,M) which depends on z, the vertical distance from the predevelopment film surface, and M. The development rate at a given point is obtained from the expression:

$$\text{Rate}(z, M) = f(z, M) R_{bulk}(M) \tag{4.27}$$

Section 4.6.3 explores the possible surface induction mechanisms and introduces the commonly used f(z,M) functions.

As with the formation of the latent image, development calculations must be performed in an iterative manner using small time increments, as the development rate is dependant on the instantaneous M value at the interface.

Figure 4–5 shows how the resist/developer interface proceeds during a 60 second development of the latent image shown in Figure 4–4. The first three illustrations show how the feature forms during the process and the final illustration details the final fully developed resist profile. Figure 4–6 compares this profile with a similar simulation where no PEB diffusion was implemented. The points seen on the second profile are idealised. In reality, physical liquid flow during

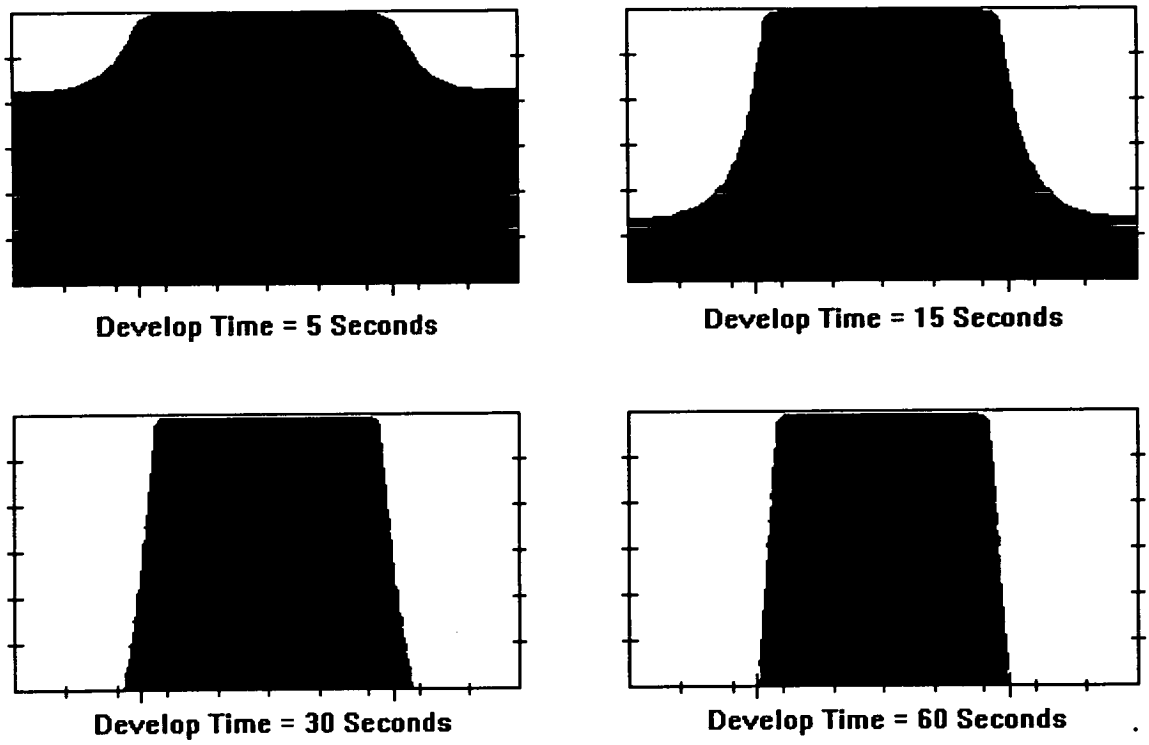

Figure 4–5: *As development proceeds the final resist profile is formed.*

development, rinse and sin dry, remove the sharp, thin points, only residual ridges will remain (see the SEM image in Figure 3–1, Chapter 3).

4.6.1 Development Rate Equations

For convenience and insight, development rate equations are usually presented graphically, as in Section 4.6.2. To accommodate the large differences between unexposed and completely bleached development rates, a logarithmic scale is employed on the y (development rate) axis. The relative inhibitor concentration, M, is plotted on the x axis using a linear scale.

4.6.1.1 The Dill Rate Equation

The original dissolution rate equation presented by Dill[163] has the form:

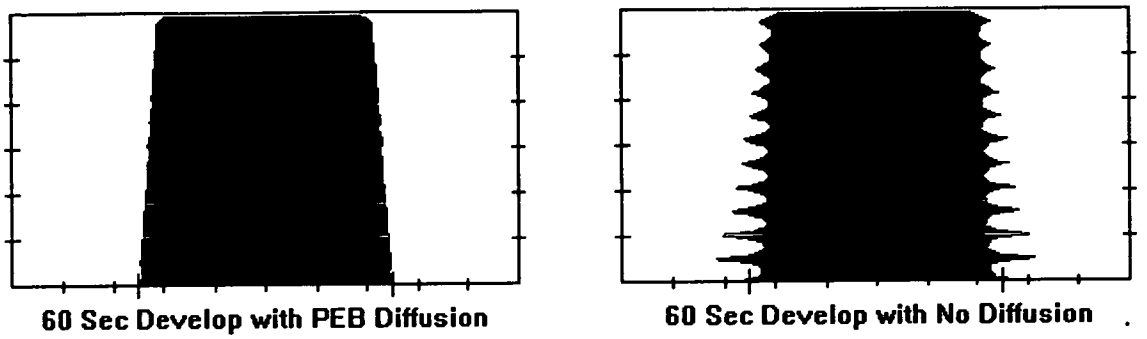

Figure 4–6: *Comparison of PROLITH/2 simulated resist profiles with and without PEB diffusion.*

$$R_{bulk}(M) = e^{E_1 + E_2 M + E_3 M^2} \tag{4.28}$$

where E_1, E_2 and E_3 are 'best fit' values of the equation to experimental data.[163] Although the three parameters have no explicit physical meaning, inspection of the equation shows that the minimum development rate ($M = 1$) is $e^{E_1+E_2+E_3}$ and that the maximum development rate ($M = 0$) is e^{E_1}. It should be noted that typically E_1 has a positive value and R_3 a negative one whilst R_2 may be either.

It was realised that this model was insufficient to describe the dissolution behaviour of many resists and a variety of superior rate equations have been presented.

4.6.1.2 The Kim Rate Equation

This equation was proposed by Kim *et al.*[187] of the University of California, Berkeley and takes the form:

$$R_{bulk}(M) = \frac{1}{\frac{1-P}{R_1} + \frac{P}{R_2}} \tag{4.29}$$

$$P = Me^{-R_s(1-M)} \tag{4.30}$$

where R_1 is the maximum develop rate, when $M = 0$, and R_2 is the minimum develop rate, when $M = 1$. R_s is a sensitivity parameter describing how the development rate varies between the two extreme values. Although the parameters are obtained by an empirical fit of the rate equation to experimental data, R_1 and R_2 do have some physical meaning.

4.6.1.3 The Modified Kim Rate Equation

Hansen[161] proposed altering the Kim rate equation to incorporate a double exponential sensitivity. The new rate equation is described by the following equations:

$$R_{bulk}(M) = \frac{1}{\frac{1-P}{R_1} + \frac{P}{R_2}} \tag{4.31}$$

$$P = M(be^{-R_s(1-M)} + (1-b)e^{-a(1-M)}) \tag{4.32}$$

where R_1 and R_2 are again the maximum and minimum development rates and R_s, a and b are the terms that describe the double exponential sensitivity. This revised equation allows greater flexibility than the original Kim equation whilst retaining the basic form.

4.6.1.4 The 4 Parameter Mack Rate Equation

Mack[188] proposed that, from kinetic considerations, the behaviour of resist dissolution could be represented by the following rate equation:

$$R_{bulk}(M) = R_{max}\frac{(a+1)(1-M)^n}{a+(1-M)^n} + R_{min} \tag{4.33}$$

where R_{max} and R_{min} are the maximum and minimum dissolution rates, n is developer selectivity (an experimentally determined constant) and a is given by the expression

$$a = \frac{n+1}{n-1}(1 - M_{TH})^n \tag{4.34}$$

where M_{TH} is the threshold relative PAC concentration (again an experimentally determined value). Given the form of the rate equation, M_{TH} is an inflection point and values of M below M_{TH} can be considered to be low development rates and those above M_{TH} can be considered to be high development rates.

Again, three of the four parameters have some physical meaning but must be determined by fitting the equation to experimental data.

4.6.1.5 The 5 Parameter Mack Rate Equation

Mack proposed a second kinetic model[189,190] relating to resist chemistry. It takes into account the inherent dissolution rate of the novolak resin, the level of inhibition provided by the PAC and the level of dissolution rate enhancement associated with the indenecarboxylic acid. This equation differs from others in that the describing parameters can be measured individually by experiment. The equation takes the form:

$$R_{bulk}(M) = R_{resin}\frac{1 + K_{enh}(1 - M)^n}{1 + K_{inh}(M)^l} \tag{4.35}$$

Where R_{resin} is the development rate of the resin alone, K_{enh} and K_{inh} are rate constants for the enhancement and inhibition mechanisms and 'n' and 'l' are the enhancement and inhibition reaction orders.

At the extremes of relative inhibitor concentration, M, the following conditions are met:

$$\text{Unexposed PAC; } M = 1,\ R_{min} = \frac{R_{resin}}{1 + K_{inh}} \tag{4.36}$$

$$\text{Fully bleached PAC; } M = 0,\ R_{max} = R_{resin}(1 + k_{enh}) \tag{4.37}$$

The development rate equation is therefore characterised by five parameters: R_{resin}, n, l and either R_{min} and R_{max} or k_{inh} and k_{enh}.

Toukhy *et al.*[190] described how the individual parameters might be measured. This work showed that, as resist chemistry is altered, the model describes the changes in dissolution qualitatively but not quantitatively. However, when the function was fitted to experimental dissolution data it yielded an excellent fit for all 23 resist chemistries examined. This suggests that the simplified assumptions that dissolution rate, enhancement, and inhibition can be treated separately and multiplicatively is reasonable, but not completely accurate.

4.6.1.6 The 9 Parameter NEC Rate Equation

Experimental data measured by researchers at NEC[191] produced dissolution rate versus M plots which had three approximately linear regions with different gradients. At low and high M values the linear gradients (on an Log(R) vs linear(M) plot) were discrete but relatively low whilst in the middle M region the slope was much steeper. As no existing model fitted the data sufficiently, the following 9 parameter empirical model was introduced:

$$R_{bulk} = \frac{1}{\frac{1}{R_1(M)} + \frac{1}{R_2(M)}} + R_3(M) \tag{4.38}$$

where

$$R_n(M) = e^{a_n M^2 + b_n M + c_n} \text{ for } n = 1, 2, 3 \tag{4.39}$$

The large number of variables in this equation make it very flexible, but also make the empirical fit much harder. Unless appropriate starting values are used no converging solution will be found.

4.6.2 Selection of Appropriate Development Rate Equation

Two criteria decide the most appropriate development rate equation for a given set of experimentally determined points, these are:

- Which models can describe the data accurately?
- Which models are supported by the simulation package being utilised?

Table 4–2 shows the best fit parameters, to a set of experimental data points, for each of the development rate equations. This typical experimental data is for Shipley SPRT4180M photoresist in a generic 0.237N TMAH developer and was generated on a Perkin-Elmer Development Rate Monitor.

The best fit was determined using the program DRM5, described in Chapter 6, Section 6.4.1. The table values include χ^2, a fit parameter, which indicates the quality of the equation fit to the experimental data. The closer χ^2 is to 1 the better the fit. Figure 4–7 illustrates each of these fits graphically, in comparison with the actual data points.

In general, increasing the number of model parameters improves the quality of the fit. However, a large number of parameters makes finding 'best fit' values more difficult and greatly increases the computation time required to perform a simulation, as tens of thousands of calculations are performed.

It should be noted that the nine parameter equation is so flexible that it can appear to be discontinuous. Although this may produce a good fit to experimental measurements, the validity of simulations based on such a fit must be considered.

The use of a five parameter model appeared to represent the best compromise between fit quality to an arbritary data set and computational efficiency. Although the Mack model appears to be the more meaningful of the two 5 parameter models, it was not published until this work was well advanced, therefore all the work discussed in the following chapters uses the modified Kim model.

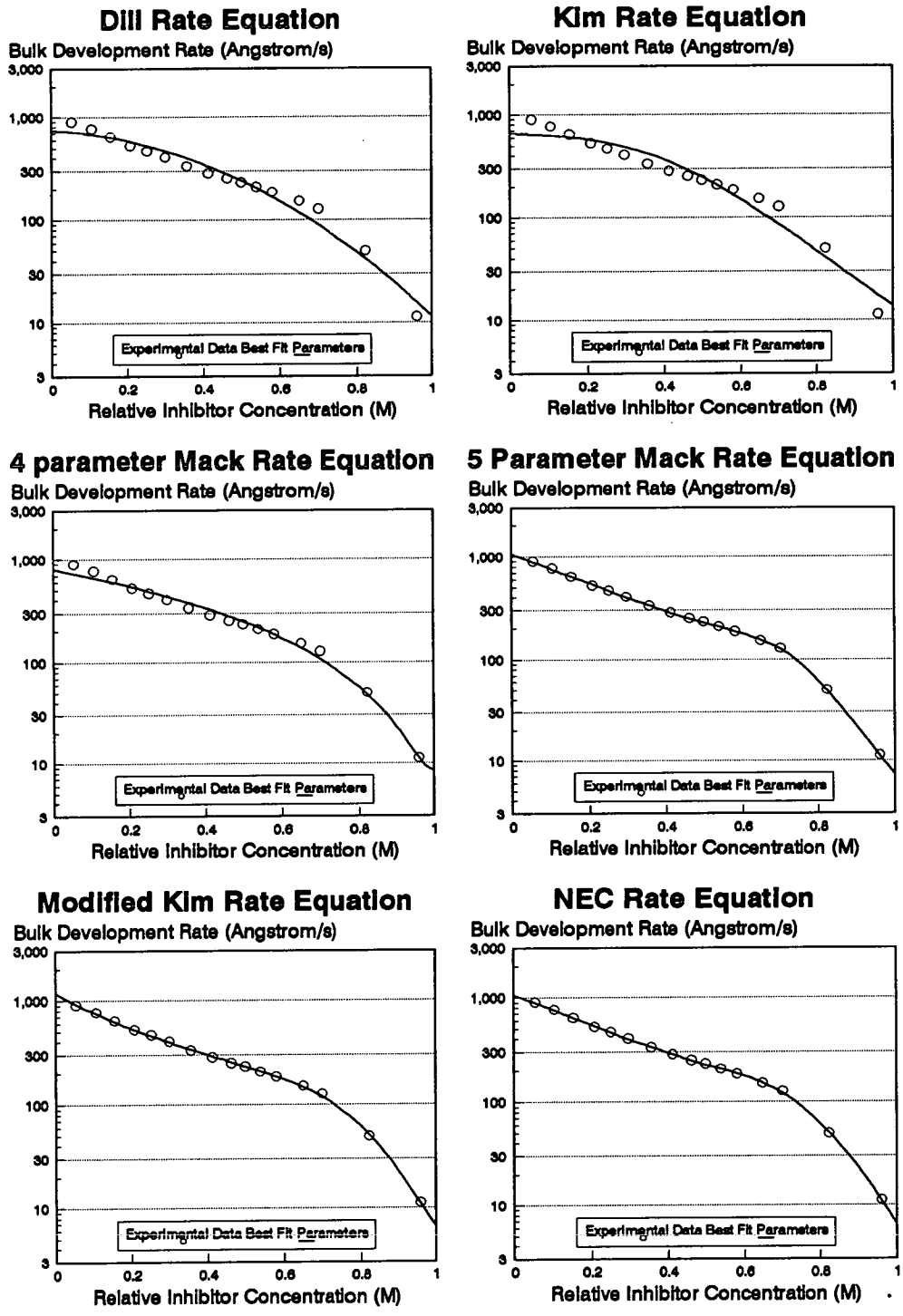

Figure 4–7: *A comparison of the 'best fit' of each of the six development rate equations.*

Dill Rate Equation Parameters

E_1	E_2	E_3	χ^2
6.609	-0.3563	-3.797	0.9380

Kim Rate Equation Parameters

R_1 (Å/s)	R_2 (Å/s)	R_s	χ^2
657.1	13.83	5.303	0.8863

Original Mack Rate Equation Parameters

R_{max} (Å/s)	R_{min} (Å/s)	n	M_{TH}	χ^2
801.2	8.529	1.734	-5868	0.9655

Second Mack Rate Equation Parameters

R_{max} (Å/s)	R_{min} (Å/s)	R_{resin} (Å/s)	n	l	χ^2
1066	7.346	159.3	3.697	11.40	0.9996

Modified Kim Rate Equation Parameters

R_1 (Å/s)	R_2 (Å/s)	R_s	a	b	χ^2
1188	6.680	13.22	0.9531	0.9276	0.9985

NEC Rate Equation Parameters

n	a_n	b_n	c_n	χ^2
1	-23.92	1.772	9.062	0.9997
2	-1.629	-3.336	7.090	
3	-15.05	7.090	1.077	

Table 4–2: *Best Fit parameters for each development rate equation to typical experimental data.* χ^2 *is measure of the accuracy of the fit, with a value of 1 predicting all experimetal points exactly.*

4.6.3 Surface Inhibition

4.6.3.1 Mechanism of Surface Inhibition

Two mechanisms have been proposed for the surface inhibition discussed in Section 4.6.[31]

The first theory relies on the fact that the level of residual solvent is somewhat lower near the film surface. As discussed previously, Rao[182–185] has shown that dissolution rate is highly dependent on residual solvent content. NMR test results have shown that the PAC:solvent ratio increases exponentially near the film surface but is constant in the bulk of the film.[192] This indicates that either PAC collects near the film surface or, more likely, that the residual solvent content lowers. The exponential form of this decay matches well with the surface induction models proposed by Kim and Mack (see Section 4.6.3.2) which are based on development rate measurement data.

A second theory involves the reaction between Novolak and PAC in the absence of water, as discussed in Chapter 2, Section 2.2.3.2. The reasoning suggests that the water content in the resist surface is reduced during softbake and exposure results in the formation of esterified resin. The subsequent introduction of water, in the form of developer, converts this product into indenecarboxylic acid, as illustrated in Figure 2–8, and development proceeds as normal. However in this case, the development is rate limited by the rehydrolysation rate of the esterified resin, not the development reaction rate.

4.6.3.2 Modelling Surface Inhibition

Kim[187] presented the multiplicative surface induction procedure described in equation 6.2. Based on experimetal results, he proposed that the induction multiplier, f(z,M), should take the form,

$$f(z,M) = 1 - (1 - f(0,M))e^{-\frac{z}{R_L}} \tag{4.40}$$

where z is the vertical depth into the resist from the predevelopment surface, R_L is the characteristic induction depth and f(0,M) is a function describing the ratio of the development rate at the surface to that in the bulk as a function of M.

The depth parameter, R_L, can be thought of as a measure of the thickness of the surface 'skin' which is dependant on the resist and its thermal processing whilst the function, f(0,M) is also strongly dependant on development details such as developer type, normality and temperature. Kim[187] showed that in some cases, f(0,M) can be modelled adequately by a simple linear function of M

$$f(0,M) = R_5 - (R_5 - R_6)M \tag{4.41}$$

where R_5 is the ratio of surface rate to bulk rate at M = 0 and R_6 is the ratio at M = 1. However, for other resist/developer systems this was not sufficient and a more complex discontinuous piecewise linear function had to be introduced.

Mack[188] introduced a near identical multiplier function, but utilised a constant, r_0, instead of f(0,M). The value of r_0 can be calculated, assuming a first order cross-linking reaction from

$$r_0 = e^{-K(T)t} \tag{4.42}$$

where t is the bake time and K is a cross-linking constant whch is a function of temperature, T. Mack proposed that this function could be described by the Arrhenius equation

$$K(T) = A_r e^{-\frac{E_a}{RT}} \tag{4.43}$$

where A_r is the Arrhenius coefficient, E_a is the reaction activation energy and R is the universal gas constant. Mack does however, go on to state that this simple model may not sufficiently describe the complicated behaviour described in other literature.

An alternative approach to decribing R_L and f(0,M) will be introduced in Chapter 6, based on experimental results and an analysis of equation 4.40.

4.7 Simulation Packages

4.7.1 Implementation of Models

Simulator types can be split into two main categories, two dimensional and three dimensional. The majority of common simulators are two dimensional, as this simplification reduces calculation times significantly. Moreover, the additional information gleaned from three dimensional simulations is usually minimal.

Whilst the output of a 3-dimensional simulation describes the height, width and depth of the resulting features, that of a 2-dimensional one cannot do so. 2-dimensional programs allow the simulation of resist profiles formed by patterns of lines and spaces of a finite width but infinite length. The first axis on the simulation plane, x, represents the direction in which periodic mask pattern variation occurs and is parallel to the substate surface, the second axis, z, is perpendicular to the first and represents the vertical depth in the resist layer extending from the substrate to the resist surface. A third axis, y, perpendular to both x and z is implied and represents the direction in which the features are considered to be infinitely long.[119]

In all simulators, the simulation plane, or space, is divided into finite elements in a grid-like manner. Each element is assumed to be small enough that it can be treated as homogeneous. During the exposure simulation the exposing intensity and relative inhibitor concentration is calculated for each element iteratively, as described in the preceding sections, until complete exposure has occurred.

If a PEB is required, the latent image is diffused in accordance with equation 4.25, although the integration limits $\pm 3D_l$ are substituted for $\pm\infty$.

Simulation of development is implemented with either a cell removal technique[193] or by the use of a 'string' algorithm. As all the simulators used during this study

employ string methods, this technique will be investigated more fully. It should be noted that the implementation of a string algorithm in a three-dimensional simulator is possible but extremely complex.[194,195]

When a string technique is utilised, the dissolution front is approximated by a finite number of points, or nodes, joined by straight line segments.[167] During each development iteration, the nodes of the dissolution front propagate into the film. The amount and direction of displacement is calculated individually for each node by considering the time increment and the local development rate. Advanced algorithms insert additional nodes when line segments exceeding a predetemined length.

Figure 4–8 is a graphical representation of the simulation process showing the various program inputs and outputs.

4.7.2 SAMPLE

SAMPLE (Simulation And Modelling of Profiles for Lithography and Etching) is a 2-dimensional simulator developed by the semiconductor research group at the University of California, Berkeley. The program code has been produced by a large number of contributors under the direction of Professors W.G.Oldham and A.R.Neureuther. The version of the program used in the work described in the following chapters is SAMPLE v1.7a.[196]

SAMPLE has two well documented[167] limitations. Firstly, it models positive and negative defocus symmetrically. The defocus expression $\Delta(z)$ defined in equation 4.6 is replaced by the expression

$$\Delta(z) = 2\frac{NA^2}{\lambda}|\delta_0| \tag{4.44}$$

where δ_0 is the defocus distance. Comparison of the two equations shows that answers are identical for positive defocus, when no image flare is considered, but that the results are significantly different in the case of negative defocus.

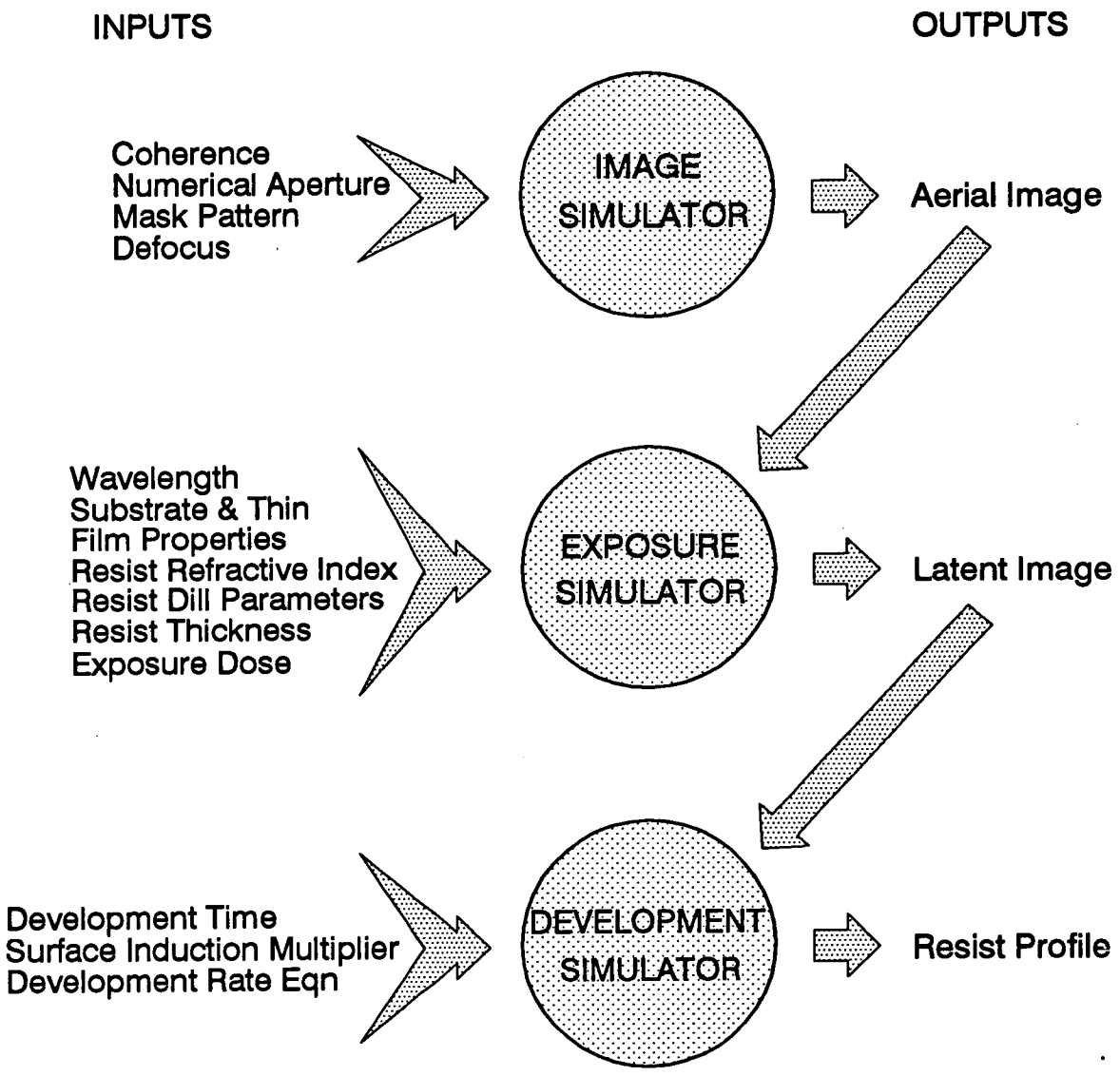

Figure 4–8: *Schematic representation of a lithography simulation program.*

Secondly, SAMPLE only implements a 1-dimensional PEB diffusion (in the z direction).

Despite these model limitations, SAMPLE has one major advantage over the other available lithography simulation programs, in that its Fortran source code is freely available and may be modified to incorporate and test new models. The version used during this study was supplied by S.G.Hansen (OCG Research and Development, Providence, Rhode Island) and had been modified to include the 4 parameter MACK, the modified Kim and the NEC rate equations.[197] The Dill and original Kim rate equations are coded into SAMPLE as standard. The ability to modify the source code of this program allowed the author to implement and test the surface induction model developed in Chapter 6. As the source code for this program was available, it could be implemented on any computer system where a FORTRAN compiler was available. It was run on the University of Edinburgh's Gould mainframe, CASTLE, the Department of Electrical Engineering Sun Workstation network and on stand-alone IBM compatible PC microcomputers. The results appeared to be computer system independant.

4.7.3 PROLITH/2

PROLITH/2 (Positive Resist Optical LITHography) is a second generation, commercial, 2-dimensional lithography simulation package written by C.A.Mack (FINLE Technologies, Plano, Texas).[198] It is a significantly improved version of PROLITH, a public domain program written by Mack whilst working for the US Department of Defense. Despite the excellent implementation of all modelling in this program, its usefulness is limited by the restrictive development models available. In the commercial version of PROLITH/2, dissolution parameters must be entered as the original Mack model in the form of R_{max}, R_{min}, n, and M_{TH}. As demonstrated in Section 4.6.2, this equation does not always yield a good fit to experimentally determined data. Additionally, surface induction may only be defined in terms of a characteristic induction length, R_L and a fixed surface to bulk development rate ratio, r_0.

OCG have a custom version of PROLITH/2 which allows the user to specify arbitrary development rates for up to one hundred individual M values. Linear interpolation is used to estimate development rates at intermediate points. Surface induction, however, is modelled using the standard PROLITH/2 approach. This enhanced version of the program was available to the author during a three month period of study at the OCG Research and Development Centre, Providence, Rhode Island, when work on the measurement of puddle development rate parameters using a modified Perkin-Elmer DRM, described in Chapter 5, was carried out.

PROLITH/2 is available for a variety of computer platforms including the SUN Work Station, the Apple Macintosh and the IBM compatible PC. All modelling work using PROLITH/2 during this study utilised the IBM PC implementation of either the OCG custom version or the standard version 2.20, as supplied to Shipley Europe Ltd by FINLE Technologies. Although PROLITH/2, like SAMPLE, models exposure with the aerial image/standing wave approximation, a rigorous high NA model is available for the program as an additional extra.

4.7.4 DEPICT2

DEPICT2 is a two-dimensional lithography, deposition and etch program produced by Technology Modeling Associates, Palo Alto, California. The program is part of a suite of programs for the simulation of microelectronic device performance and manufacture. The Edinburgh Microfabrication Facility is a licensed beta test site for this suite of software. This program was used for initial simulation during the study period. The program originally ran on the Departmental VAX mainframe but was later transferred to the Sun Workstation Network.

The program implements full defocus and diffusion modelling but only supports the Dill, Kim and 4 parameter Mack rate equations. Simple linear surface induction as described by equations 4.40 and 4.41 may be introduced when the Kim model is implemented.

Theoretically, any model utilising 6, or less, parameters, including surface induction, can be implemented by a user-definable development module. Practically,

it was found that security measures, intended to stop software piracy, prevented this module from functioning correctly. Additionally, the refined development models devised during this work required a minimum of 8 parameters to fully describe development behaviour when surface inhibition was included.

Again, exposure modelling normally uses the aerial image approach, though recent revisions of DEPICT2 offer rigorous calculations for high NA simulation.

4.7.5 Other Packages

A variety of other 2-dimensional simulators have been discussed in the literature such as Intel's iPHOTO[161] and Philips' SLIM[199] and SPESA[200] programs. 3-dimensional simulators include Matsushita's PEACE,[193] Berkeley's SAMPLE-3D,[194] the Fraunhöfer-Institut for Silicon Technology's SOLID[180] and Clarkson University's unnamed simulator.[195]

However, these programs are either proprietary to the named company or, with the possible exception of SOLID, are not commonly available.

4.7.6 Calculation Times

On average a high specification 486 IBM compatible PC or a SUN SPARC station will take approximately 10 to 20 Seconds to calculate the resist profile for a single set of input parameters. Calculation times increase greatly if polychromatic illumination is used or rigorous high NA calculations are made.

Thus a typical 10 by 10 focus-exposure matrix can be calculated in half an hour and a 25 point swing curve (E_0 or $E_{1:1}$) in under 9 minutes. These times are an order of magnitude quicker than the time it would take to perform these experiments and analyse the resulting profiles by SEM, or even optically.

4.8 Summary

This chapter has described the models and techniques used to simulate semiconductor lithography. Particular emphasis has been placed on the implementation of development rate equations and the requirements they should fulfil. The commonly utilised simulation programs have been introduced and their relative strengths and weaknesses discussed.

Chapter 5

Determination of Resist Thickness During Development

5.1 Introduction

If lithography is to be simulated in the manner described in Chapter 4, dissolution rate parameters must be determined for the process of interest. Although the calculation of these parameters is complicated, the fundamental information required for their derivation is accurate knowledge of how resist thickness changes with develop time at a variety of exposures. A Development Rate Monitor (DRM) is used to obtain this data. A variety of DRM techniques are available, but all produce an output of resist thickness versus time. This chapter describes the various alternative DRM options, concentrating on the two most commonly used commercially available machines and a novel TDRM (Track Development Rate Monitor) developed during this project. Chapter 6 describes how DRM output can be processed, in conjunction with knowledge of the resist's optical properties, to calculate the actual dissolution rate parameters.

5.2 Requirements for a DRM

An ideal DRM should be able to monitor any type of resist development process *in-situ* on standard production equipment without influencing that process in any way. Unfortunately, this is seldom realised.

The most commonly used DRM, the Perkin-Elmer DRM 5900, can only monitor immersion development within its own self-contained development tank. When it is remembered that advanced lithography processes (i.e. those one would want to simulate), use track-based development, it is reasonable to suppose that simulations using Perkin-Elmer derived dissolution parameters must contain some degree of error with respect to actual conditions. As noted in Section 3.4.1.2, significant differences in gamma are evident when immersion, puddle and spray processes are compared, therefore the errors could be considerable.

A novel DRM device, the TDRM, was constructed to investigate the effect of the development technique on the dissolution behaviour when all other resist processing details were kept constant. This equipment can be used to monitor most types of development *in-situ* and is described in Section 5.6.

Recently, another commercial tool, the Site Services DSM100, has become available for track-based DRM work. While results using this equipment are more pertinent to modern simulation needs, it cannot monitor immersion processes. Therefore, a direct comparison of track and immersion development is still impossible using only a single piece of commercially available equipment. Section 5.4.3 describes the construction and operation of the Site Services tool.

This chapter also reviews other DRM options and describes the measurement theory behind them.

5.3 Quartz Crystal Microbalance (QCM) Dissolution Rate Monitor

Piezoelectric quartz crystal oscillators have long been used for microgravimetric analysis. Hinsberg[40,201,202] has demonstrated how this technique can be extended to development rate measurement. Equation 5.1 details the relationship that Hinsberg[40] determined between the change in a quartz crystal's oscillation frequency and the thickness of a surface film.

$$\Delta F = -\frac{F_0^2}{\rho_q N}\rho_f T_f \tag{5.1}$$

where ΔF is the observed frequency change, F_0 is the frequency of the uncoated crystal, ρ_Q is the density of the quartz plate, N is the frequency constant of the crystal, ρ_f is the density of the applied film and T_f the thickness.

Figure 5–1 shows a schematic diagram of the QCM dissolution rate monitor.[40] The quartz crystal is coated with resist before being mounted in the flow cell and connected to an oscillation circuit. The crystal's oscillation frequency is measured by a high-speed frequency counter interfaced to an IBM PC-XT microcomputer.[202] The experiment commences when developer is introduced into the flow cell.

Figure 5–2 shows typical QCM DRM results.[40] As expected, the dissolution rate increases with exposure dose. Standing wave modulation of the dissolution rate is clearly visible, demonstrating good resolution.

Although this piece of apparatus can be simply and cheaply constructed, it has several drawbacks.

Firstly, the quartz substrate cannot be processed (i.e., coated, exposed and baked) in an identical manner to a production wafer, since silicon and quartz have different surface, optical and thermal properties.

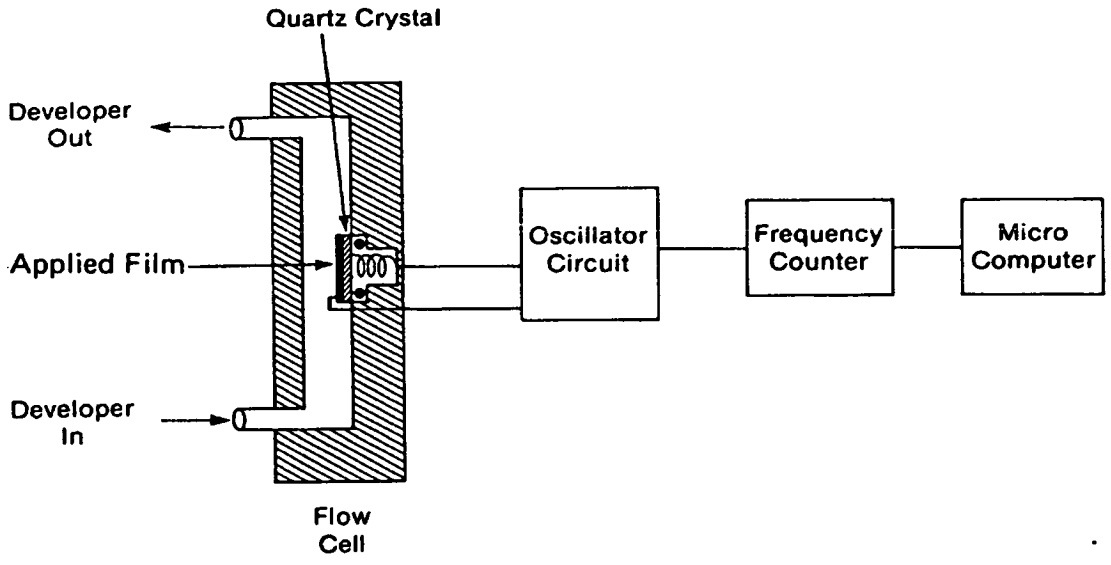

Figure 5–1: *Schematic diagram of a Quartz Crystal Microbalance (QCM) DRM.*

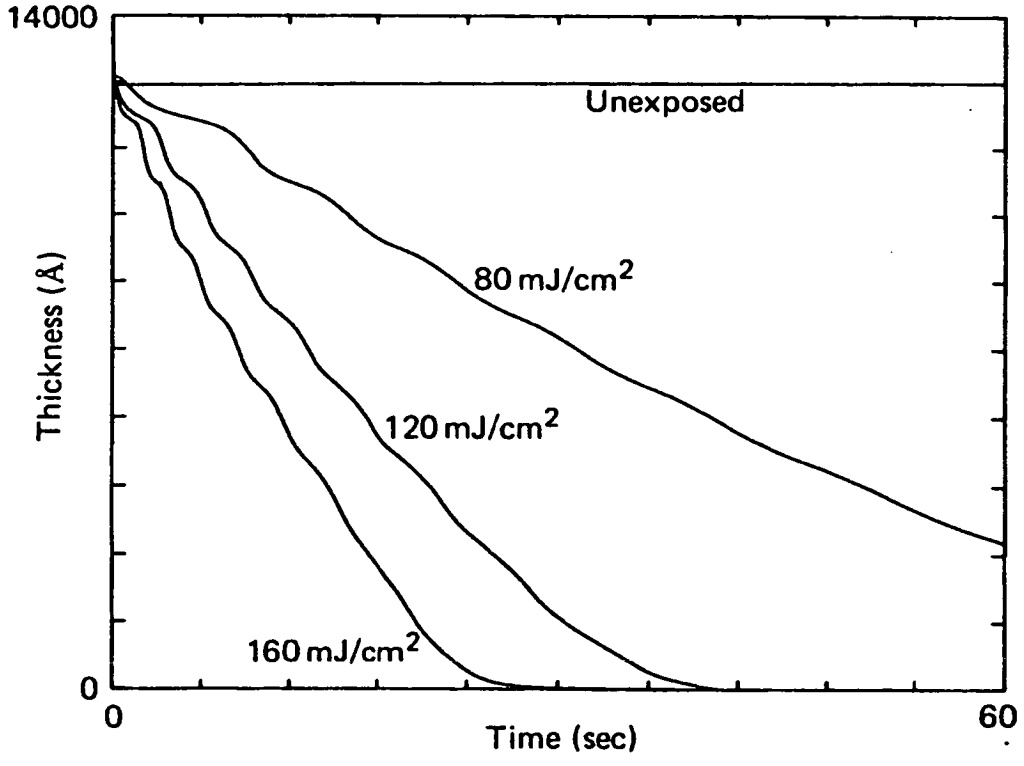

Figure 5–2: *Film thickness versus develop time for Shipley Microposit 1470 resist at various exposure levels obtained using a QCM DRM. The exposure wavelength was 346 nm and 1:2 Microposit developer/water was used.*

Secondly, the system can only function in an immersion mode. It is also debatable whether the forced substrate (crystal) oscillation alters the development dynamics.

Finally, as noted by Rao *et al.*,[183] results gathered before the flow cell is completely charged cannot be interpreted, because of excessive signal noise (a period of 10 to 20 seconds). This restricts the tool's ability to examine rapidly developing films and surface induction effects.

5.4 Monochromatic Development Rate Monitoring

5.4.1 Principles of Operation

As described in Chapter 2, Section 2.8.4.1, when monochromatic light is incident on a reflecting substrate coated by a thin transparent film, interference occurs between the light reflected from the ambient/film interface and that reflected at the substrate interface. The nature (destructive or constructive) and magnitude of this interference depends on the separation of the two interfaces and the optical characteristics of the film media. A developing resist coating on a silicon substrate is a practical example of this situation. When the resist film is placed in developer, surface material is eroded and the distance between the interfaces alters, leading to a change in the magnitude and nature of the resulting interference. As the level of light, whether or not of an exposing wavelength, coupled into the film changes so does the intensity of light reflected back towards the source at the air/resist interface.

If the reflected intensity is plotted against time a series of sinusoidally varying fringes is observed, terminating when all the resist is removed.

As the developer above the resist surface is always relatively thick ($>$ 1mm even in the case of puddle development), it is considered a 'thick film' which merely attenuates the reflected signal.

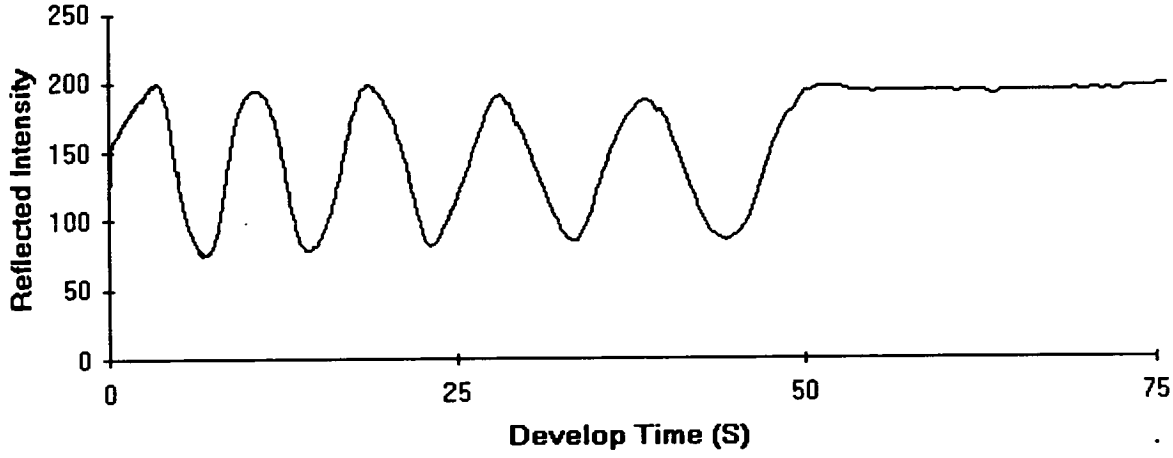

Figure 5–3: *A typical monochromatic DRM output signal for a developing resist layer on a bare silicon substrate.*

Figure 5–3 illustrates a typical reflected signal versus time plot for a developing resist layer. When a bare silicon substrate is used the reflected signal 'end-point' has a maximum value as the optical path length difference is zero. On substrates with topography the optical thickness of the film stack will determine the phase of the end-point.

Since the optical path length difference required to induce a 2π (i.e. 0) phase change in resist is $\frac{\lambda}{n}$, standing wave theory dictates that the reflected intensity fringe period will be half that distance, i.e.,

$$\text{Fringe Period} = \frac{\lambda}{2n} \tag{5.2}$$

where λ is the interrogation wavelength and n is the refractive index of the resist at that wavelength.

Since the intensity of light reflected from a thin film varies in a periodic manner, any given intensity can be mapped to a series of different thicknesses. It is therefore important that the film thickness is known for at least one point in time. The 'end-point' is most useful in this respect, since it corresponds to zero thickness and, in the case of bare silicon, is an intensity maximum. If the 'end-point' is not available,

i.e., monitoring ceased before the film cleared, then the pre-develop thickness can be used.

Once the 'end-point' has been established and the resist thickness at a given time, d(t), can be obtained by inverting the expression,

$$S(t) = C + K\cos\left[\frac{4\pi n}{\lambda}d(t)\right] \tag{5.3}$$

Where S(t) is the reflected intensity at time t, and C and K are constants based on the signal intensity, calculated from the peak and trough intensities.[203] However, it should be noted that this expression is only accurate if a near-ideal intensity versus time signal is obtained, i.e. all peak values are of similar magnitude as are trough intensities.

Unfortunately, experimental monochromatic DRM output is usually far from ideal. The magnitude of both the mean signal and the periodic swing tend to decrease, as red dissolution product 'cloud' accumulates in the developer immediately in front of the resist. The attenuation caused by this material (discussed in Section 5.6.9.1) makes continuous thickness mapping of the signal, using Equation 5.3, difficult and inaccurate.

Fortunately, a more basic approach can be used, if all the minima and maxima can be located in time. Attenuation does not alter the phase of the signal and each extrema is separated by a known thickness delta of $\frac{\lambda}{4n}$. So assuming a bare substrate, counting back from the 'end-point' the thickness corresponding to each preceding extrema is given by

$$\text{Thickness} = k\frac{\lambda}{4n} \tag{5.4}$$

where k is the extrema number (k:0 = 'end-point', k:odd = minima, k:even = maxima). Figure 5–4 illustrates this mapping.

Monochromatic interferometry is the basis of most documented experimental DRM systems[204–209] including the two most commonly used commercial systems,

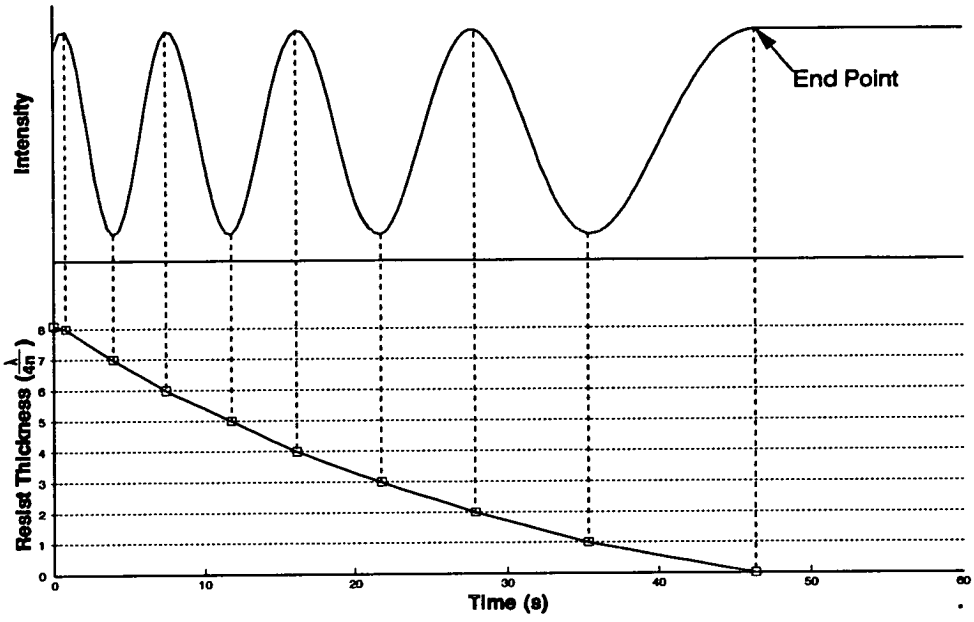

Figure 5–4: *All the intensity minima and maxima can be mapped to individual thicknesses separated by* $\frac{\lambda}{4n}$. *The Intensity end-point corresponds to zero thickness and the thickness at time zero is assumed to be that prior to development.*

the Perkin-Elmer 5900 DRM[210] and the Site Services DSM100/Lithacon 808.[211] A description of both these systems follows, though only the Perkin-Elmer equipment was utilised during this study.

5.4.2 The Perkin-Elmer DRM 5900

5.4.2.1 System Hardware

The Perkin-Elmer DRM 5900 appeared in the early 1980's and was the first commercially available development rate monitoring system. It is the most common and widely utilised DRM system.

Figure 5–5 shows the system configuration.[210] The unit is completely self contained and is designed to measure immersion development parameters. Section 5.7 describes how one has been modified to monitor a pseudo-puddle development process.

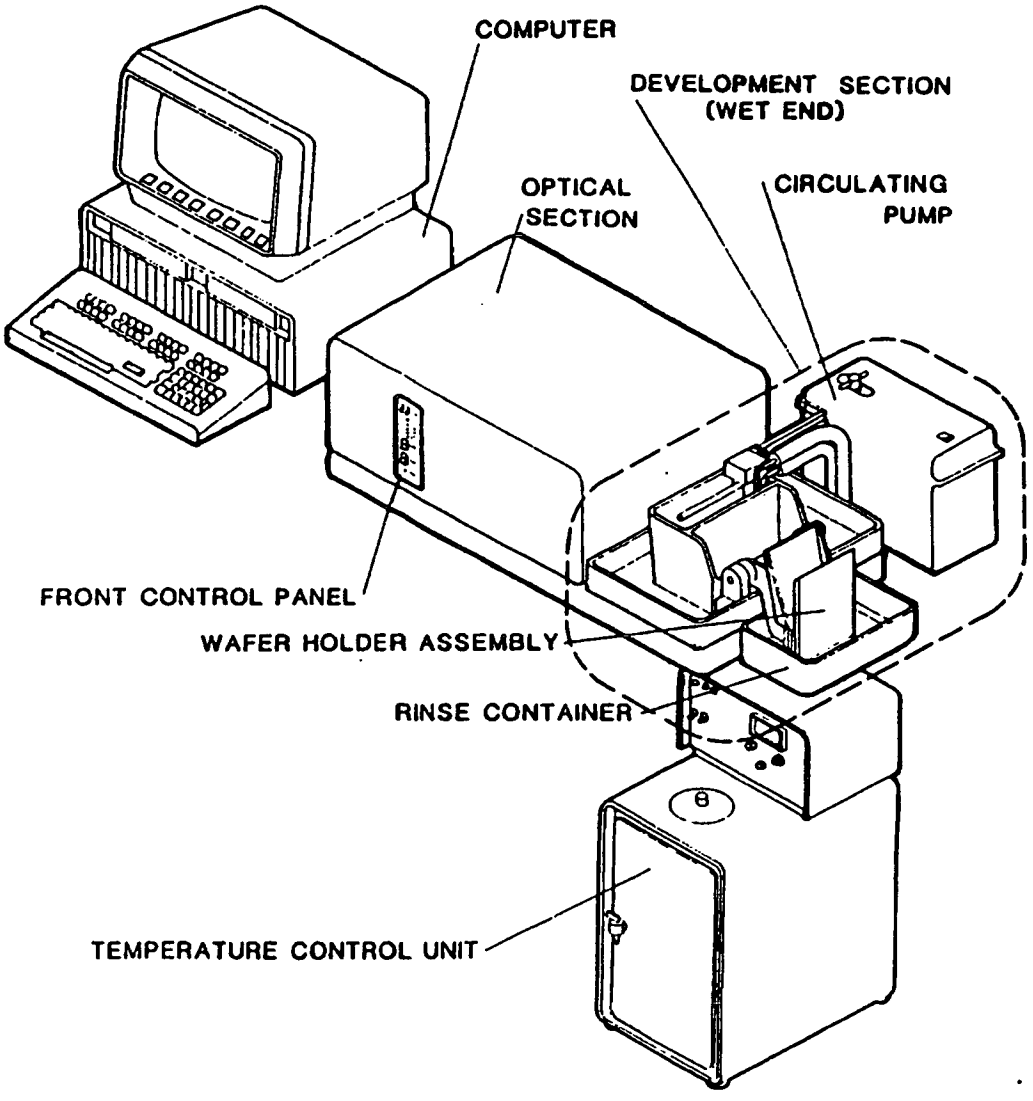

Figure 5–5: *A typical Perkin-Elmer DRM 5900 system set-up.*

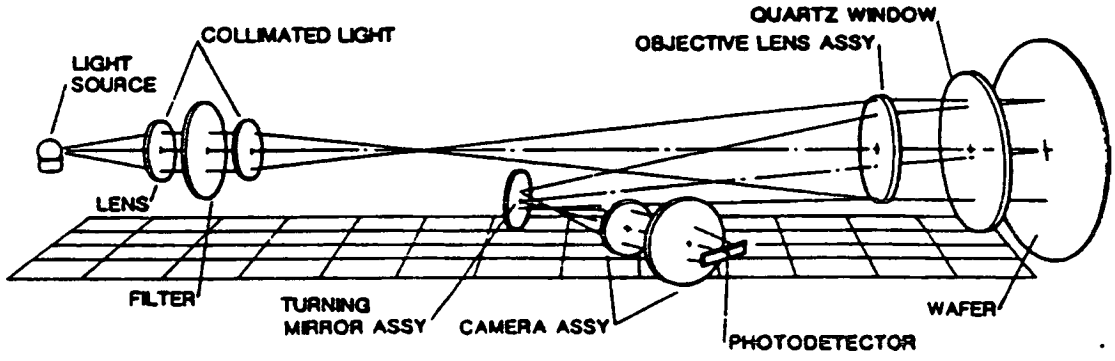

Figure 5–6: *The optical path in the PE 5900 DRM.*

The unit consists of 2 main components, a computer and the DRM itself. The computer controls the system and processes the collected data. The DRM has two distinct parts, an optical section and a development tank. The tank holds one third of a gallon of developer held at a constant temperature by a control unit with circulating pump. This pulsed pump has an outlet positioned to force developer across the wafer surface. Temperature control is accurate to $\pm 0.3°C$, but exhibits rapid 'run away' if the pump is disabled.

The wafer is placed on a pivot arm assembly which is lowered into the tank. In the lowered position the wafer is in front of a quartz window leading to the optical section of the DRM (see Figure 5–6[210]).

In the optical section, illumination is produced by a 20-watt halogen lamp fitted with a 10nm bandwidth filter centred on 632.8nm (HeNe laser wavelength). The resulting light is directed through collimating and objective assemblies onto the immersed wafer via the window.

The wafer is held at a slight downward angle so that the light reflected from the wafer passes back through the window and objective assembly on to a small turning mirror that directs the beam into the solid-state detector of the camera assembly.

The detector is a 256-element, linear photodiode array which is mapped onto the wafer with an 8x magnification. Each element corresponds to a 200 micron

square area on the wafer. The output of these detectors is digitised and sent to the computer via support electronics.

Development is assumed to start when the first non-zero reflection is detected (i.e. when the pivot arm is lowered and the wafer completes the optical path). It is important that the arm is lowered quickly, yet smoothly. Significant dissolution can occur in highly exposed regions before triggering occurs if the wafer is lowered slowly, but sudden movement can cause 'bounce' resulting in false fringes.

5.4.2.2 System Software

DRM operation is controlled via the Perkin-Elmer DREAMS software. This software allows several different exposure zones to be monitored, each having received a different, uniform blanket exposure. The photodiode sampling frequency is user defined and can be altered as the development proceeds, enabling a wide range of exposure doses to be studied simultaneously. Typically, ten to twenty samples per second are taken for the first few seconds (for rapidly developing areas). This reduces to a couple of samples per second for the next thirty seconds or so, and decreases further to a 1Hz sampling rate for the following few minutes. Finally after eight minutes or so, the sample rate is further reduced to one measurement every 5 to 15 seconds. Usually, observations are taken for between 30 minutes and one hour, depending upon resist type and developer normality.

The DREAMS software allows the user to select groups of array elements monitoring the same exposure zone to produce an averaged signal exhibiting significantly less signal noise.

Typically, 10 to 20 different exposure zones are studied. The experiments performed during this study used sixteen zones, each approximately 3mm wide (on the wafer).

The DREAMS software can transform the zone intensity versus time data into a thickness versus time profile. The algorithm uses the continuous transform method described by Equation 5.3, and is therefore liable to be misleading.

5.4.2.3 OCG Analysis Software

In all the following work, the DREAMS package was used only to collect the averaged zone intensity versus time data. The zone information was then transferred from the DRM computer onto a 486 IBM compatible PC for further analysis. The data transfer utilised a direct serial port connection. The Perkin-Elmer 'SHARE' program is run on the DRM computer. This sends the chosen zone data to the DRM printer port which is connected to the PC serial input port by a standard 25-pin RS232 cable. The data is received from the serial port and saved to hard disk using the standard communications program 'KERMIT'.

Once on the PC, the zone data is analysed using propriety software developed by S.G.Hansen[212] (OCG Microelectronic Materials). The suite of software consists of stand alone compiled BASIC programs (Power Basic, Borland International).

The first program, 'DRM1', translates the zone data into files containing x,y pairs (x=time, y=intensity). One appropriately named file is generated for each zone. The user inputs two resist thicknesses (one prior to exposure; the other prior to development, i.e., after PEB), the exposure wavelength, the resist Dill ABC parameters at that wavelength, and the exposure dose for each zone. This information is stored for use by subsequent programs. Although exposure information is not required for the initial mapping of intensity to thickness, it is required for the subsequent procedure of relating dissolution rate to converted inhibitor concentration (discussed in Chapter 6). Entry of all the data during the initial step prevents errors being made when dissolution rate analysis is performed at some later date.

The next program, 'DRM2', translates the intensity information into film thicknesses. Although substantially automated, some operator interaction is required. Each set of zone data is displayed for end-point and peak picking. End-point determination can be particularly subjective, so each set of zone data is plotted so that the user can confirm that the film cleared and thus select the end-point.

The data is then smoothed and replotted. The maxima and minima are automatically marked by a detection algorithm. The user is then asked to confirm

the extrema location and correct any errors. Often minor user modifications are required: Extrema locations may be altered and missing or extraneous peaks and troughs corrected through the use of MOVE, ADD and DELETE commands.

Once the user is satisfied that all the extrema have been correctly identified Equation 5.4 is used to calculate the thickness and time corresponding to each.

In the case of a film which has not cleared, fringe numbering is deduced by calculating the thickness of the first extrema below the initial thickness. The program alerts the user to any inconsistencies, e.g., two consecutive maxima etc.

The thickness versus time data for each zone is stored in an individual file ready for analysis by the development rate analysing programs.

5.4.3 The Site Services DSM100/Lithacon 808

The Site Services DSM100 is primarily a develop end-point control system, however the Lithacon 808 software extension module[211] allows the system to function as a track-mounted monochromatic DRM. This is the only commercial track-based DRM system. Unfortunately, it cannot be used in an immersion mode so results cannot be directly compared with those of the Perkin-Elmer system.

5.4.3.1 Principles of End-Point Detection

Before describing the auxiliary DRM operation of the DSM100, it is pertinent to examine its principal role of end-point detection.

Many studies[213–217] have shown that wafer-to-wafer CD control can be significantly improved if feedback is used to control the total develop time. The wafer is interferometrically monitored during development until the endpoint is detected. Development is then allowed to continue for a further fixed length of time or a percentage of the measured clear time, depending on the chosen control algorithm.

Both schemes produce more stable CD values than a fixed time development process and can withstand substantial thickness and/or exposure dose variations.

The situation is more complicated than the development rate case, since production wafers are covered with various film stacks. As the underlying topography thicknesses do not change during development, they introduce a fixed phase change into the endpoint. The exact phase change depends on the layer topography. In general, the system must be trained to identify the correct endpoint for each process layer. Complex algorithms[215,218] based on Fast Fourier Transforms (FFT) have been developed to detect the end-point in real time under production conditions. The use of polarized light allows monitoring to occur even under continuous spray conditions, where airborne aerosol particles and the undulating liquid surface introduce considerable signal noise.

The amplitude of the reflection fringes is determined by the percentage of exposed resist area and the speed of wafer rotation. Generally, 10% or more of the total area of resist must be exposed before the end-point can be reliably detected.

Figure 5–7[216] illustrates the improved CD control an end-point controlled development program affords over a standard fixed time development, as exposure dose is varied.

5.4.3.2 DSM100 Operation

The DSM100 consists of an optical processing head, an array of 8 detectors and a microprocessor system interfaced to a standard IBM compatible PC. A schematic representation is illustrated in Figure 5–8.[219] Within the optical head is a halogen light source. The emanating light is filtered to prevent exposure of the developing resist. A beam splitter allows the filtered light to pass through onto the developing wafer and diverts the returned light through 90° into a light guide which relays the beam to an array of photodiodes. Each of the eight photodiodes is tuned by a $\pm$10nm bandpass filter to an individual wavelength between 600nm and 900nm.[220] The microprocessor system digitises the diode signals and transmits them to the PC for either end-point or DRM applications.

In DRM mode, a uniformly blanket exposed bare silicon wafer is substituted for a production wafer during develop. The resulting data is processed by the Lithacon

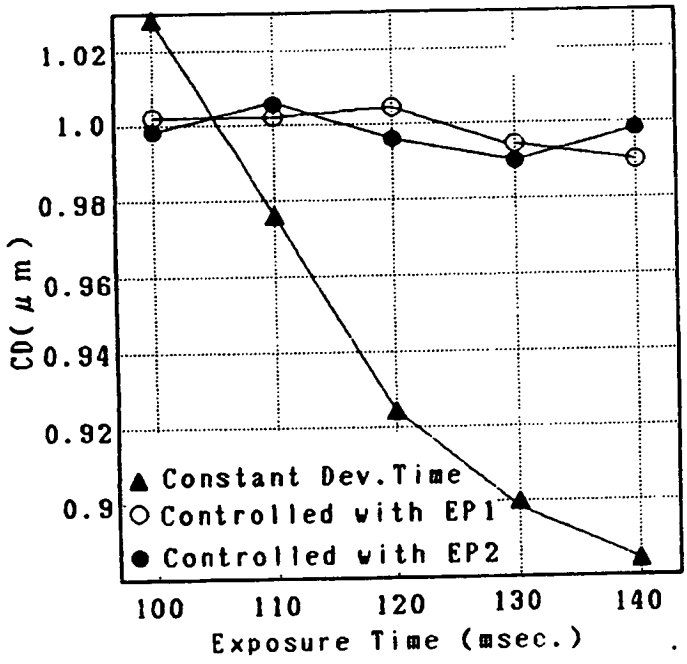

Figure 5–7: *Linewidth versus exposure dose for a fixed time develop process and two different end-point schemes.*

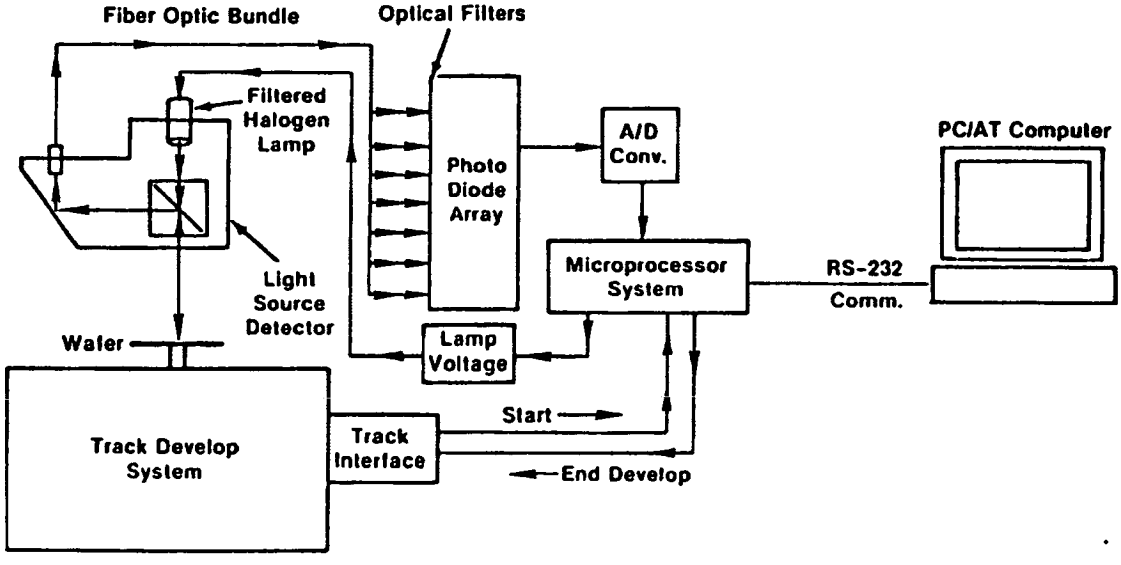

Figure 5–8: *Schematic diagram of the Site Services DSM 100.*

808 process analyser package. This software uses one of the eight monochromatic inteferrograms to generate a map of thickness versus time.

Significant signal noise arises during spray processes and the puddle formation period of puddle processes. This is due to optical scattering by aerosol developer droplets and the unstable puddle surface. The subtraction of a 'pre-recorded' background signal can compensate for this noise. The background signal is generated by monitoring an uncoated wafer in an identical develop program. Although this technique reduces noise levels considerably, Hutchinson *et al.*[121] noted that the signal is obscured until puddle stabilisation occurs. This period lasted 1 second during a continuous spray process but up to 9 seconds in the case of a spray/puddle process. This makes the study of surface induction effects, occuring during the initial development period, considerably more difficult.

To date, no published results have demonstrated that this system is capable of producing thickness versus time plots which can resolve exposure standing wave patterns. It should be noted that the Hutchinson[121] study examined DUV chemically amplified resist where such phenomena are less evident.

5.5 Polychromatic Development Rate Monitoring

A given monochromatic reflected signal intensity corresponds to a series of resist thicknesses. The use of multiple wavelengths allows this thickness ambiguity to be removed. Polychromatic DRM techniques allow a discrete absolute resist thickness to be obtained for all points in time.

5.5.1 Reflectance spectrophotometry

Most film thickness measurement tools used in the semiconductor industry utilise reflectance spectrophotometry, e.g., the Prometrix Lithomap series and the Nanometrics Nanospec series etc.

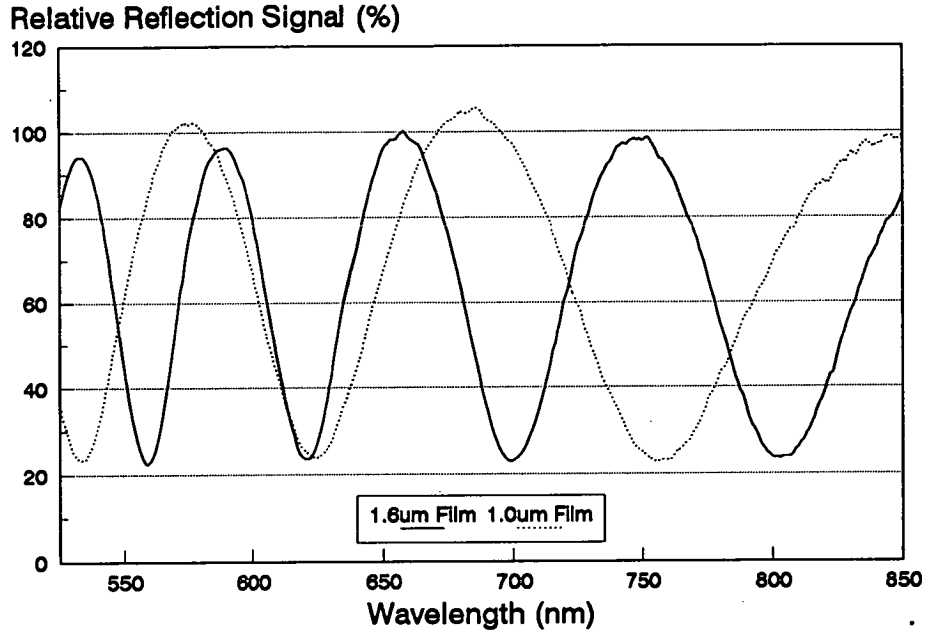

Figure 5–9: *The normalised refectance spectra for a 1.0μm and 1.6μm resist film on a bare silicon substrate over the 525nm to 850nm wavelength range.*

The technique involves directing unpolarized white light onto the transparent film at normal incidence. The intensity of reflected light is measured as a function of wavelength (typically in the range 400-800nm). The reflected spectrum is a function of the light source's spectral output, the detector linearity, the substrate's reflectance response and the thin film interference. Effects other than those induced by the film can be compensated for by normalising the reflected spectrum relative to the reflection spectrum of the uncoated substrate measured under identical conditions. The resulting 'corrected', or relative reflection, spectrum can be analysed to yield the film thickness.

Figure 5–9 illustrates the normalised reflectance spectra for two different thicknesses of resist. The thinner film has less extrema within a given wavelength window. This is generally true and with the distance (in wavelength space) between extrema increasing as the film thins. Eventually no extrema will be present within a given window.

There are several ways of measuring the thin film thickness from the relative reflectance spectrum.

The simplest technique to implement was proposed by Ananthakrishnan and Tuttle.[221] This algorithm uses the extrema wavelength positions to estimate the thickness of the film via a cosine fit. Although the technique has been used successfully in thickness studies,[103] it should be used with caution as the accuracy depends upon the number of extrema used to make the estimation. The algorithm's accuracy therefore falls off quickly as the film thickness decreases and is limited to thicknesses where at least two extrema are present.

All commercial reflectance spectrophotometers determine film thickness by comparing the observed spectrum with theoretical spectra for the given material. The theoretical spectrum which correlates most closely with the measured value is taken to be the 'actual' thickness. Generation of the theoretical spectra requires knowledge of the optical properties of the thin film material and substrate and is discussed at length in Section 5.6.5.

5.5.2 Material Optical Properties

5.5.2.1 Refractive Index and Dispersion

The optical properties of a medium are described by its refractive index (n) and extinction coefficient (k). These two constants are usually written together as a complex index of refraction:[222]

$$n = \mathrm{n} - ik \tag{5.5}$$

The real part, n, is the ratio of the speed of light in a vacuum and the speed of light in the medium, whilst the imaginary part, k, is a measure of the level of absorption within the material.

For most materials, refractive index is a function of wavelength. The way in which n varies with wavelength must be described accurately if reliable thickness

measurements are to be obtained, as it is a vital parameter in the construction of theoretical reflectance spectra.

A wide range of relationships have been used to describe the wavelength dependence, or dispersion, of refractive index.[223] However, most of the films used in the semiconductor industry exhibit *normal* dispersion where refractive index varies inversely, and monotonically, with wavelength.[224]

Cauchy proposed the following empirical formula to discribe *normal* dispersion:[225]

$$n(\lambda) - 1 = A(1 + \frac{B}{\lambda^2} + \frac{C}{\lambda^4} + \frac{D}{\lambda^6} \ldots) \tag{5.6}$$

where n is the refractive index and A, B, C etc are constants. For *normal* dispersion A and B are always positive.

For practical applications, this expression is typically rearranged and truncated to three terms, like so:

$$n(\lambda) = n_1 + \frac{n_2}{\lambda^2} + \frac{n_3}{\lambda^4} \tag{5.7}$$

where λ is the wavelength in Angstroms and n_1, n_2 and n_3 are constants known as the Cauchy co-efficients.

If the medium scatters or absorbs incident light, as polysilicon does, then the use of Cauchy extinction coefficients, k_1, k_2 and k_3 may be required. However, for most semi-transparent films such as resist, an extinction value of zero is sufficient.[224]

Dispersion within photoresist is complicated further in that the refractive index changes as the material is exposed. Figure 5–10 shows the dispersion of completely exposed and unexposed AZ1450 resist.[223] The dispersion curve for a partially exposed film will lie between these two extreme states.

The unexposed dispersion curve exhibits a discontinuity near 430nm, due to an absorption band, which is eliminated on exposure. Strictly speaking this discontinuity means that unexposed resist exhibits *abnormal* dispersion. However, in

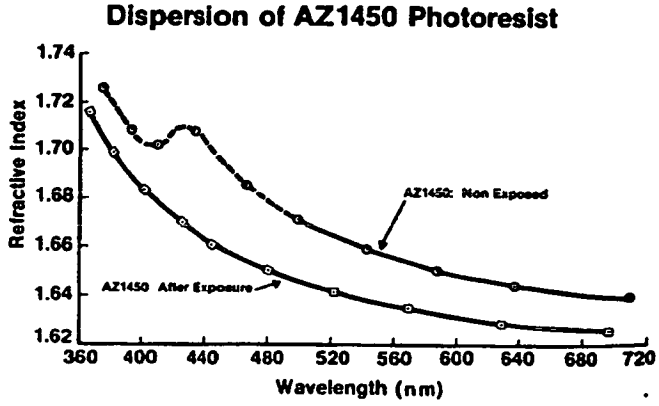

Figure 5–10: *The dispesion of AZ1450 photoresist both before and after exposure.*

the case of thin film measurement, the Cauchy equation can still be used to model dispersion as the wavelengths used to determine thickness (500 - 900nm) are in the region away from the discontinuity.

5.5.2.2 The Dispersion of HPR204 and HiPR6512 Resists

Refractive index is most reliably determined using an ellipsometer. This piece of apparatus uses a physical property of light, polarisation, to determine both the refractive index and thickness of a thin film on a reflecting substrate.[222,223] However, the parameters (detector and analyser polarization angles) used by the machine are cyclical with wavelength, hence solutions are not unique. This is not a serious problem if the approximate thickness and/or refractive index is known.

In order to generate a dispersion curve, refractive index must be measured at multiple wavelengths. Ellipsometers capable of this are expensive and not always readily available. More commonly in the semiconductor industry, reflectance spectrophotometers are used to calculate dispersion. This is possible because at minimum relative reflectance values the refractive index of a non-absorbing film (n) is related to that of its substrate (n_3) and the ambient medium (n_1) by the relationship:[226]

$$n = \sqrt{\frac{1 \pm \sqrt{R}}{1 \mp \sqrt{R}} n_3 n_1} \tag{5.8}$$

where R is the relative reflectance. This equation has a root at[226]

$$n = \sqrt{n_3 n_1} \tag{5.9}$$

At and near this condition answers are insensitive to the reflectance value and therefore are unreliable. In the case of a film on silicon in air, the root occurs at approximately 1.90. This is sufficiently far from photoresist refractive indices to be ignored.

A resist film of a thickness between 1 and 2μm will have several relative intensity minima distributed across a typical wavelength window, a range of refractive index values can be calulated for the material, if the dispersion of the air and the substrate (usually silicon) are accurately known.

Table 5–1 details the Cauchy co-efficients for bare silicon and the two photoresists used during this study, HPR204 and HiPR6512, in both an unexposed and completely bleached state.

The silicon values were calculated by fitting Equation 5.7 to published[227] elipsometer measurements made at multiple wavelengths, whilst the resist values were determined using reflectance spectrometry by Matthijs[228] of OCG Technical Service Centre, St. Niklass, Belgium, using the methodology established by Beck.[229]

5.6 A Novel Polychromatic DRM (The TDRM)

In an attempt to compare the *in-situ* development rates of production immersion and track-based processes with those derived in a Perkin-Elmer DRM, a polychromatic Track-based Development Rate Monitor (TDRM) was constructed. The use

		n_1	n_2	n_3
Silicon		3.49893	6.97652×10^6	2.86181×10^{14}
HPR204	unexposed	1.59497	1.73520×10^6	-1.6000×10^{10}
	exposed	1.60401	1.34120×10^6	-1.0000×10^{10}
HiPR6512	unexposed	1.60292	1.65070×10^6	-1.9000×10^{10}
	exposed	1.60663	1.46070×10^6	-1.6000×10^{10}

Table 5–1: *Table of Cauchy co-efficients for substrate material and photoresists used during this study.*

of polychromatic analysis techniques means that surface inhibition and residual standing wave effects can be clearly observed. The system is based on the Monolight 6800 Series Optical Spectrum Analyser utilising customised software. It can be mounted either on an SVG 86 series developer unit or in a modified wafer cassette for immersion development. The following Sections discuss the spectrum analyser hardware, the system set up, the measurement algorithm and the system software.

5.6.1 The Monolight Series 6800 Optical Spectrum Analyser

The Monolight Series 6800 Optical Spectrum Analyser (OSA) is manufactured by Monolight Instruments Ltd, Weybridge, Surrey and is based upon a scanning monochromator supported by a IBM compatible PC and a modular controller.

Figure 5–11 illustrates the components. The heart of the system is the scanning monochromator illustrated in Figure 5–12.[230] The rotating diffraction grating disperses the light incident on the input slit into its component wavelengths and sweeps them sequentially past the detector at the output slit. This converts the light intensity into an electrical signal. A simple calibration procedure utilising a HeNe (632.8nm) laser allows the relationship between encoder disc position and output wavelength to be determined.[231] The system may be optimised for any wavelength region over the range 200 to 5000 nm by a suitable choice of diffraction

grating and detector. The system in question was tuned for the 200 - 900nm range utilising a Photo Multiplier Tube (PMT) detector and a grating with a pitch of $\frac{1}{1200}$mm and a blaze of 300nm.[232]

The controller[233] acts as an interface between the computer and monchromator. It extracts the current scan data from the monochromator when requested by the host IBM PC. The controller digitises the PMT output and translates the encoder position to a wavelength value. A digitised table of intensity versus wavelength is returned to the computer. The controler is flexible and the user may specify the wavelength subset to be collected, the wavelength step size and whether the result should be the average of a number of scans.

An input signal from an external source may be sent to the controller via a BNC connection. If required the user may specify that scan collection will be triggered by a rising or falling edge on this input.

Illumination is provided by a broadband halogen source and transmitted to the wafer by a bifurcated Schotts glass light guide. The reflected light is transmitted to the input slit of the monochromator by the second arm of the lightguide.

A complete 200 to 900nm scan can be made every 95 msec, however interpretation of the output and storage of the data significantly reduces the rate at which data can be collected and stored. As a wavelength scan can only be started when the encoding disc rotates to a given position a delay of 0 - 45 msec may occur between the request for scan information and the start of data collection.

5.6.2 Experimental Equipment and Set Up

5.6.2.1 Track Configuration

Figure 5–13 schematically shows how the light is transmitted to and collected back from the wafer during track development on an SVG 86 series track. The head of the bifurcated light guide is held well above the developer spray nozzle and imaged onto a 15mm diameter spot on the wafer. The lens focuses the returned light back

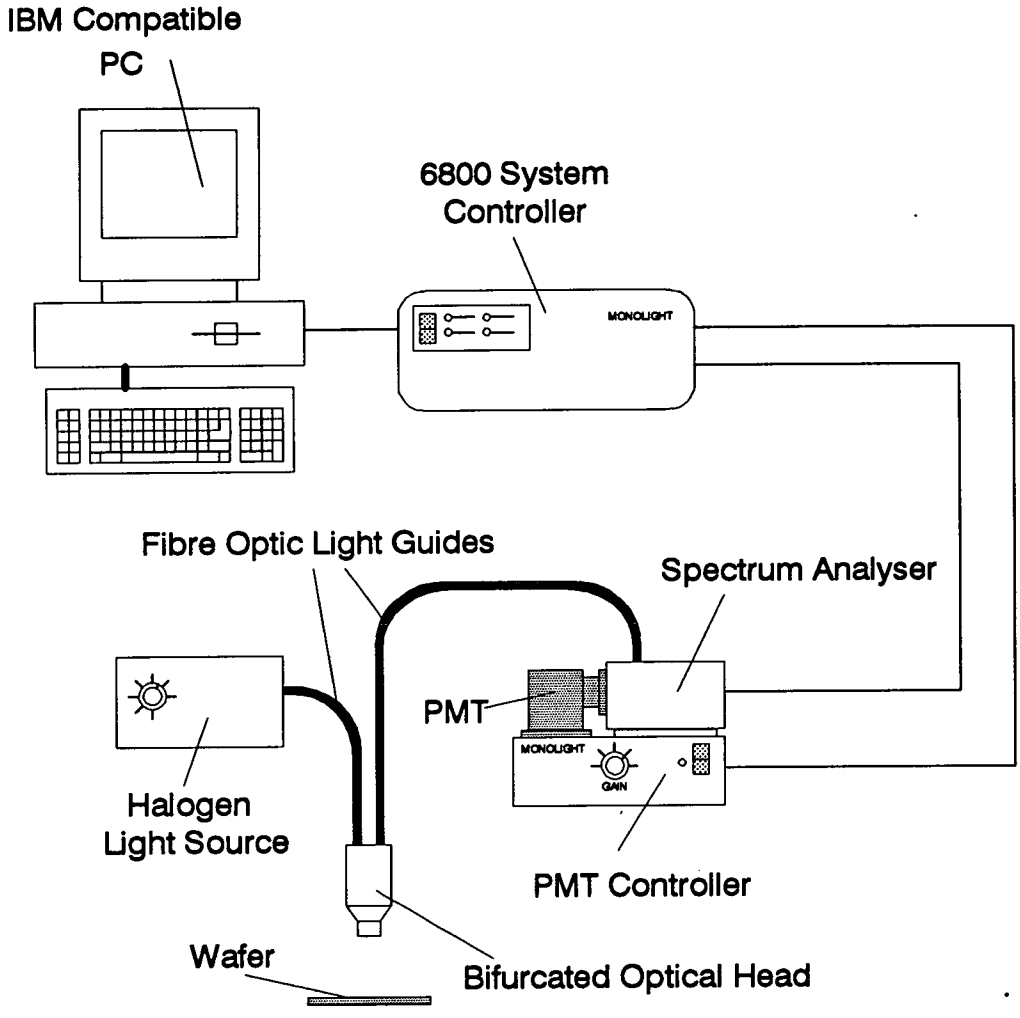

Figure 5–11: *The components and configuration of the Monolight Series 6800 Optical Spectrum Analyser.*

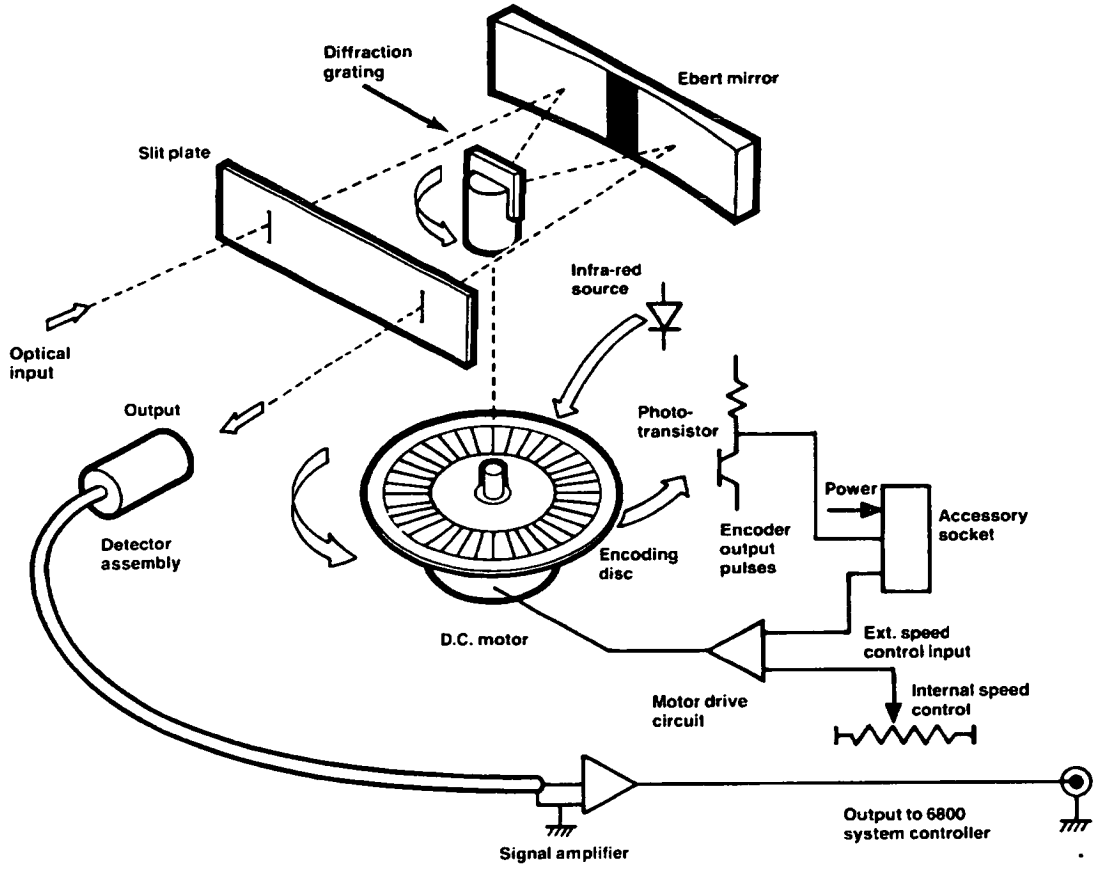

Figure 5–12: *Schematic diagram of the Monolight monochromator.*

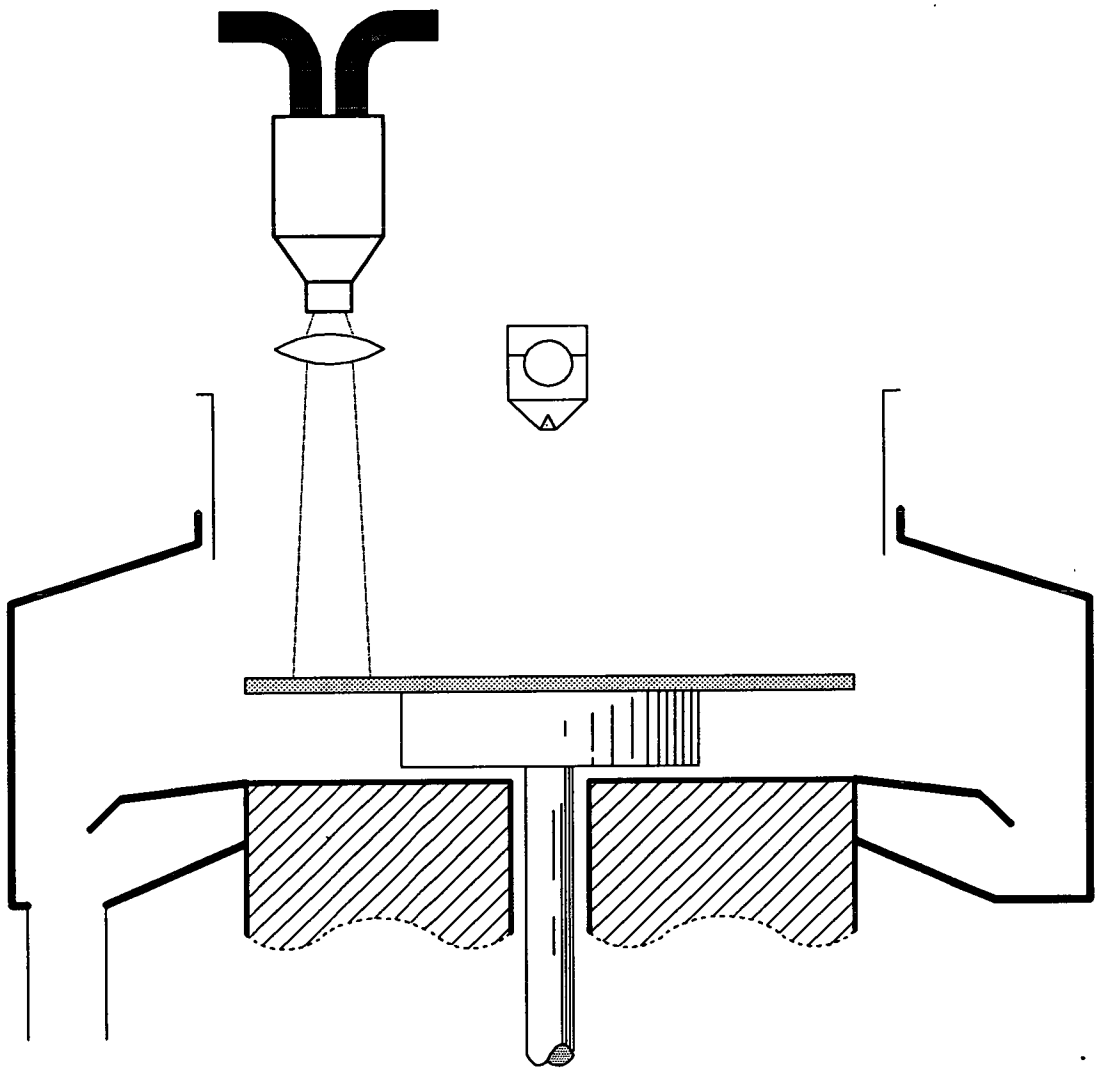

Figure 5–13: *The bifurcated light is imaged onto the wafer surface at normal incidence from above using an objective lens.*

into the bifurcated light guide. A custom bracket holding the optics is mounted on the track frame.

A microswitch is connected to the track's rising splash guard mechanism. This guard rises immediately before the development program commences. Step one of the program commences immediately after the guard locates in the up position. This signal indicates the start of development, if developer application occurs during this first program step.

As the measurement spot is near the edge of the wafer and the wafer rotates

during development, the thickness over the entire wafer must have excellent coating uniformity to minimise exposure coupling errors. Furthermore, the entire resist film must be blanket exposed with a single exposing dose. The measured spectrum is the integrated signal returned from the entire 15mm spot area,the resulting thickness measurement therefore represents the average thickness in the area. This helps reduce errors arising from local resist thickness variations.

5.6.2.2 Immersion Configuration

When the TDRM was used to monitor wafers developing in immersion mode, the optical configuration shown in Figure 5–14 was utilised. A perspex light guide is encased in a stainless steel tube. The end of the bifurcated lightguide is located flush to the perspex rod and held in place by a grub screw. Metal discs attached to the steel tube keep it centrally located in a standard twenty five wafer cassette. The tube extends from above the top of the cassette, where the bifurcated fibre optic is attached, down to wafer slot seven.

The wafer to be monitored is placed in slot five and the jig is inserted into a standard immersion develop bath. As in the track configuration, only one exposure zone may be monitored, this time in the centre of the wafer. In this case the cross-wafer uniformity of the resist coating is less critical and only the central portion of the wafer need be exposed.

5.6.2.3 Immersion Trigger Mechansm

An electronic trigger mechanism was devised to indicate when the wafer was immersed in developer. Figure 5–15 illustrates the circuit used. Two wires are attached to the side of the wafer cassette, the first parallel to slot four and the second parallel to slot five. When the cassette is submerged, the wafer and the second wire enter the developer simultaneously. The basic nature of the developer allows a small current to pass between the two submerged wires providing a base current to the transistor. This pulls the output line down from 5.1 Volts to 0 Volts. A zener diode limits the output voltage to approximately 5 Volts and a

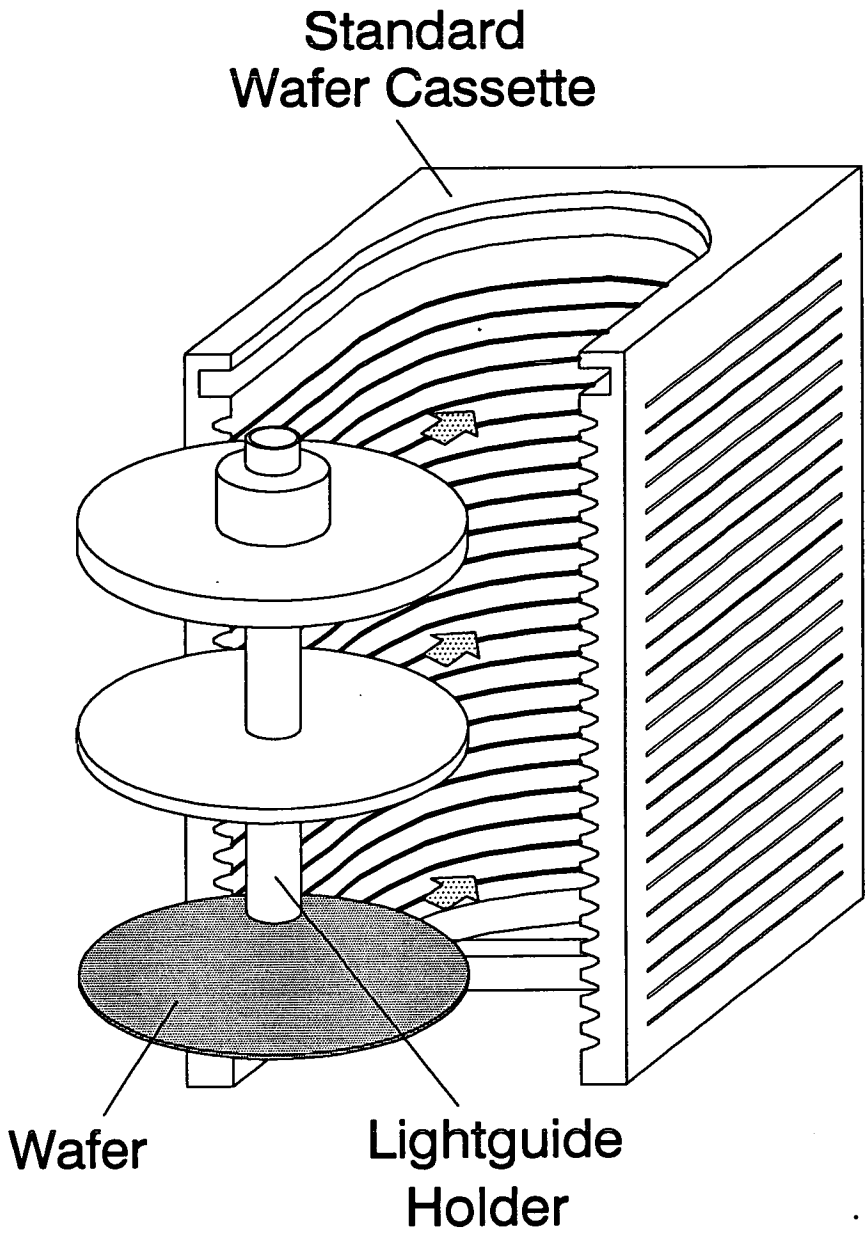

Figure 5–14: *The wafer and lightguide housing are placed in a standard wafer cassette as shown. The head of the bifurcated fibre optic cable connects in the top of the lightguide assembly.*

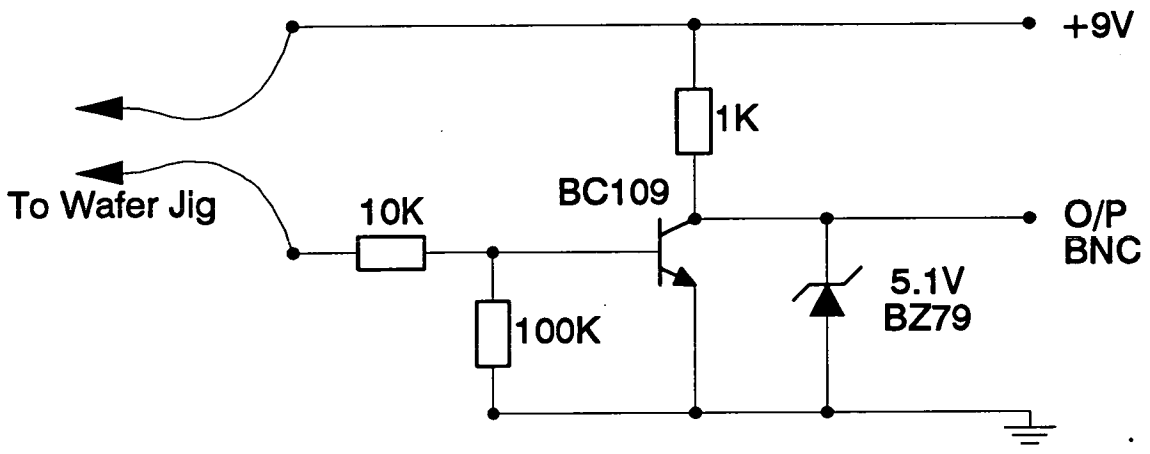

Figure 5–15: *Circuit diagram for the immersion trigger mechanism.*

10K Ohms resistor prevents the transistor from overloading if the two input wires are shorted.

5.6.3 Linearity of Reflected Spectrum

Figure 5–16 shows the detected output versus wavelength of the halogen source after reflection from a bare silcon wafer, via the bifurcated light guide. The transmission response of the Schotts light guide (Figure 5–17) restricts the low wavelength response to just below 400nm[234] whilst the PMT detector sensitivity (Figure 5–18) limits the upper wavelength response to slightly less than 900nm.[232] The signal response between these values is determined by the diffraction grating efficiency and the wavelength response of both the lamp output and the substrate reflectivity.

Wavelengths of less than 480nm will result in resist exposure, so the halogen source is filtered before transmssion to the wafer. Figure 5–19 shows the relative frequency response of the filtered illumination to that of the unfiltered signal illustrated in Figure 5–16. Clearly the signal is aproximately linear over the wavelength range 525nm to 850nm, therefore it is this range that will be utilised for the thickness calculations described below.

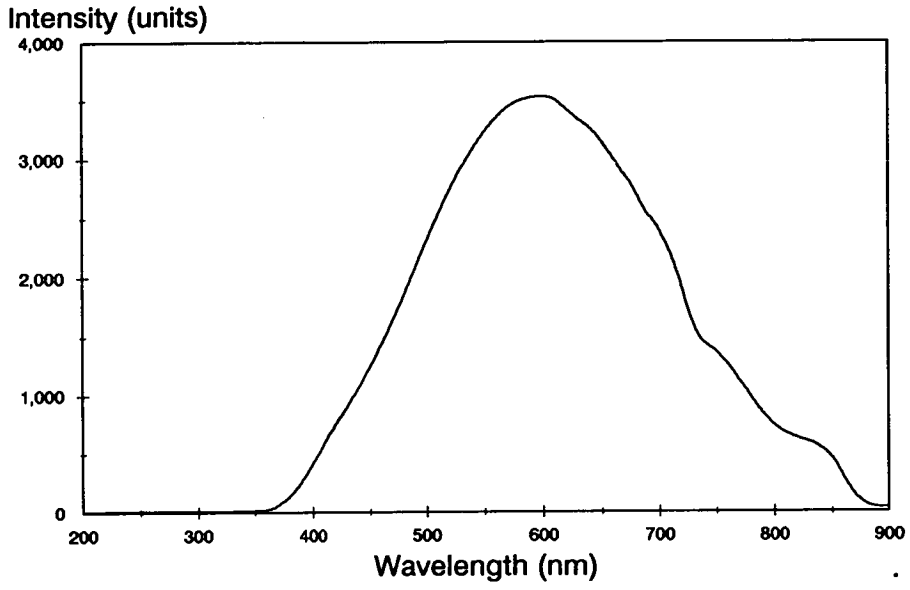

Figure 5–16: *The reflected spectral intensity of a halogen lamp from a bare silicon wafer as detected by the Monolight spectrometer.*

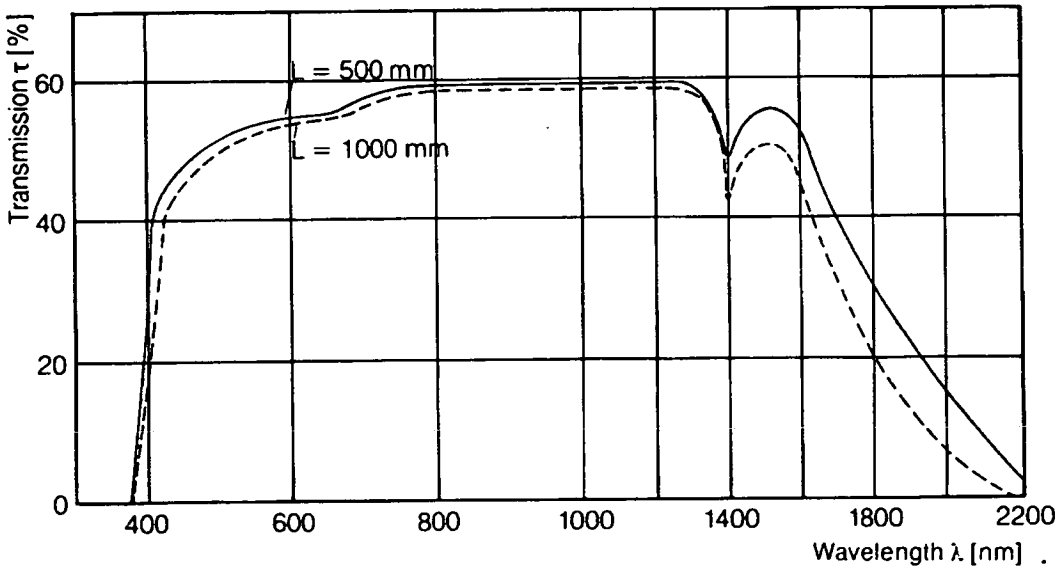

Figure 5–17: *The spectral transmission response of Schotts light guide.*

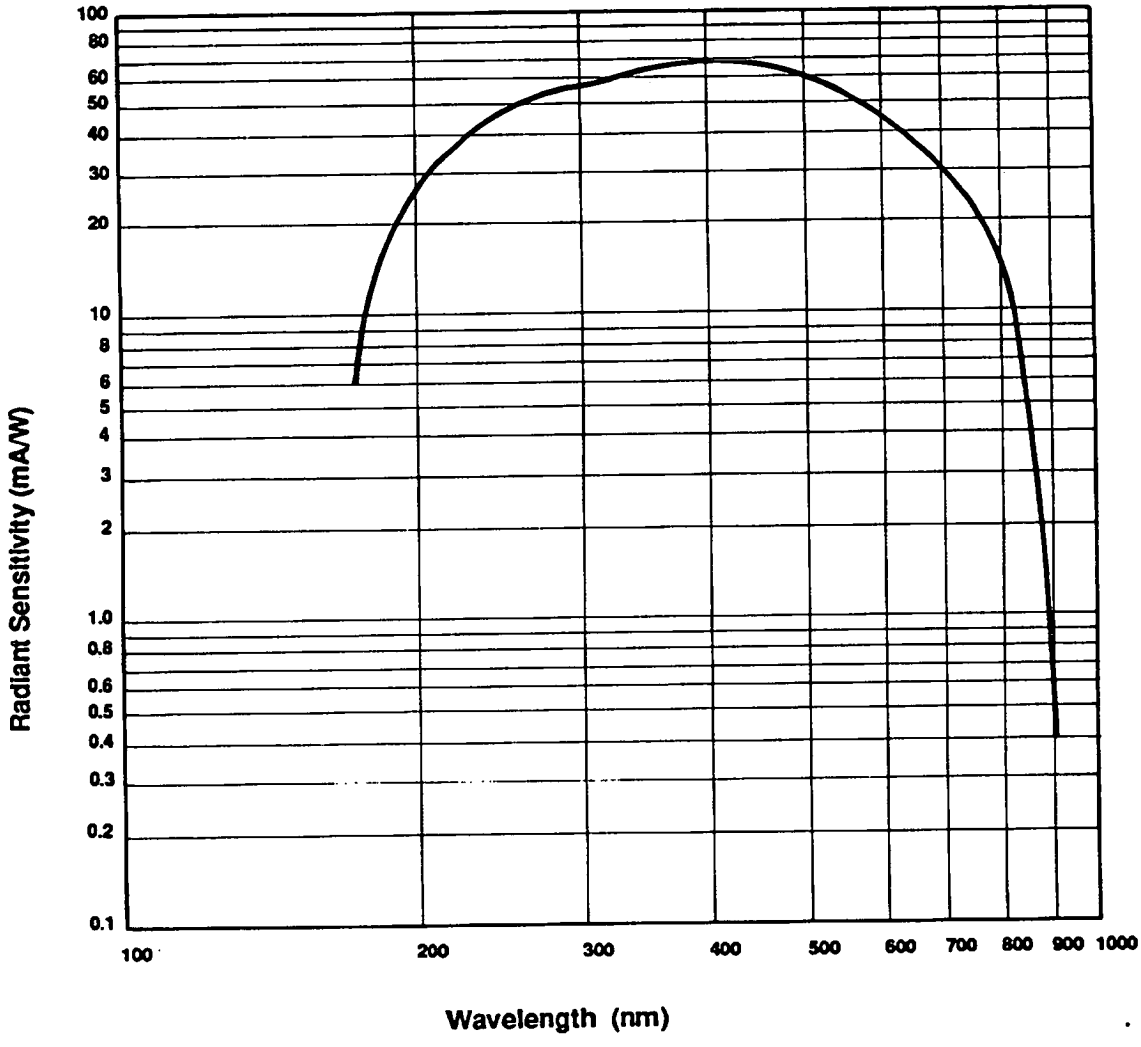

Figure 5–18: *The spectral sensitivity of the photomultiplier tube detector.*

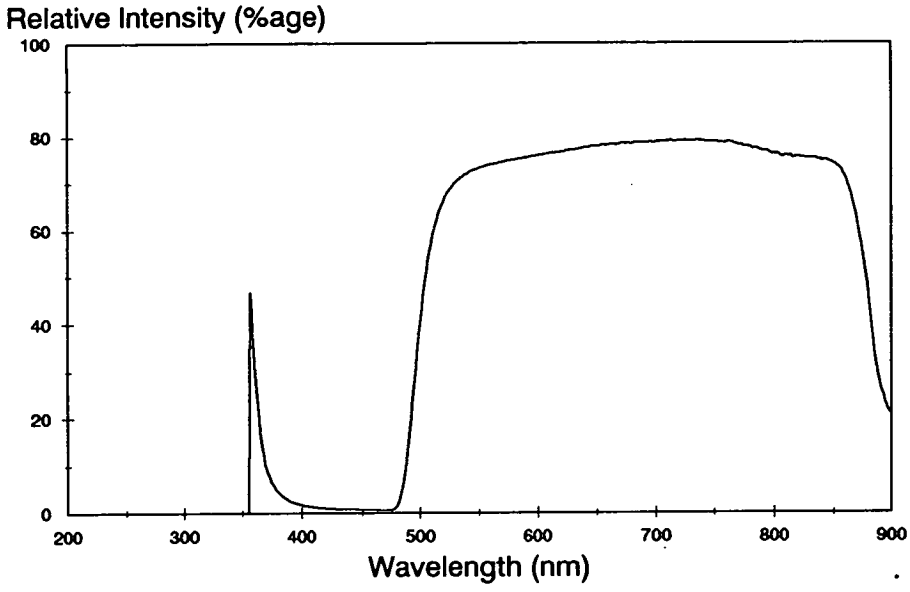

Figure 5–19: *The relative reflection spectrum of the filtered halogen source (compared to the same source with no filter).*

Although the relative intensity of illumination in the 350nm to 380nm range appears high in Figure 5–19, inspection of Figure 5–16 shows the absolute intensity of the light to be very low. Experiments showed that no unintentional exposure could be detected on wafers placed under this illumination for 15 minutes.

5.6.4 Spectral Response under Development Conditions

Figure 5–20 shows the relative intensity spectra produced by the system, in track mode, for a dry unexposed resist film and the same film with a developer puddle on the surface. The presence of the developer decreases the signal contrast but does not alter the positions of the signal extrema or introduce further intensity modulation. This means the signal from a 'wet' wafer can be used to calculate the resist thickness.

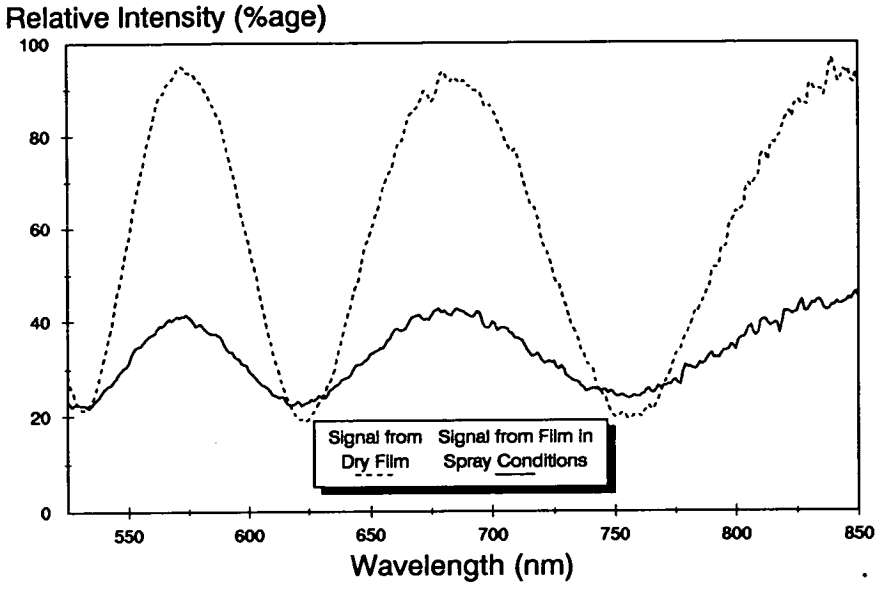

Figure 5–20: *The relative reflection spectra of a resist film on silicon and that of the same film under a puddle of developer.*

5.6.5 Film Thickness Determination Algorithm

When absorption is negligible, thin film theory can be used to predict the relative reflected intensity spectrum produced by a resist coating of thickness d, in the following manner:[227]

$$\text{Relative Reflection} = \frac{A + F}{B + F} \tag{5.10}$$

$$A = \frac{(n_1 n_3 - n_2^2)^2}{(n_2^2 - n_1^2)(n_3^2 - n_2^2)} \tag{5.11}$$

$$B = \frac{(n_1 n_3 + n_2^2)^2}{(n_2^2 - n_1^2)(n_3^2 - n_2^2)} \tag{5.12}$$

$$F = \frac{1}{2}(1 + \cos\phi) \tag{5.13}$$

$$\phi = \frac{4\pi n_{2d}}{\lambda} \tag{5.14}$$

where n_1, n_2 and n_3 are the refractive indices of the ambient, the film and the substrate, respectively, at the wavelength of interest, λ. The response of the film at different wavelengths can be determined if the refractive indices of the three materials can be described over the relevant wavelength range. In the range of interest, 525nm to 850nm, the refractive index of both the resist and substrate can be described with reasonable accuracy utilising the Cauchy Equation (5.7) and the values presented in Table 5–1. The relative reflectance spectra produced using Equation 5.10 exhibit a marked envelope function which is not visible on the Monolight results, particularly in the presence of developer. In order to maximise the correlation between the experimentally determined spectra and the theoretically produced versions, it is necessary to remove the envelope by muliplying the result of Equation 5.7 by

$$\frac{B + 1}{A + 1} \tag{5.15}$$

the reciprocal of the envelope function.[227]

The relative reflection spectrum measured by the Monolight system is scaled so that the highest intensity value becomes 1 and the lowest -1. This normalisation process is necessary, as the spectrum amplitude is highly dependant on the thickness of developer on the film surface and whether any optical scattering, or absorption, is present (from aerosol spray particles or red dissolution product etc.). A series of theoretical spectra are generated using Equations 5.10 to 5.15 for thicknesses between zero and some thickness far in excess of the possible value. These spectra also undergo the same normalisation process as the experimental data.

The measured spectrum is then compared to each of the theoretical spectra and the total mean squared error calculated. The Total Squared Mean Error (TSME) is calculated by summing the squared mean error between the two spectra at each wavelength within the wavelength window of interest (525nm - 850nm in this case). The theoretical spectrum that produces the smallest TSME is most similar to the

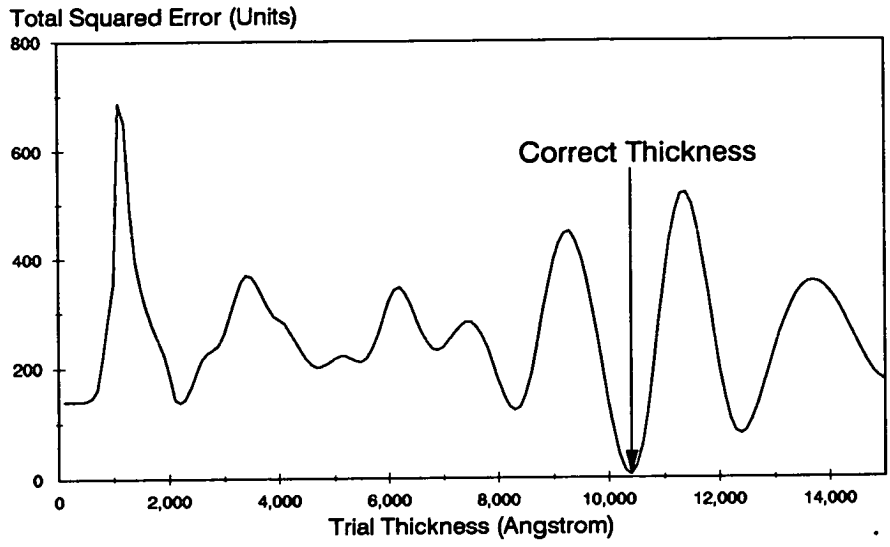

Figure 5–21: *The Total Squared Mean Error (TSME) between the measured spectrum and the theoretical spectra of various thicknesses of resist.*

measured one, so the thickness used to generate that spectrum should be identical to that of the actual film.

Figure 5–21 illustrates the TSME between the 'wet' spectrum of Figure 5–20 and theoretical spectra utilising thicknesses of between 0 and 15000 Angstroms. The lowest TSME occurs for a resist thickness of 10383 Å. This thickness can be chosen unambiguously as the minima values at 8000 and 12000 Å have values of at least 80 TSME units higher. Figure 5–22 illustrates two normalised spectra, the first is the 'wet' measured spectrum of Figure 5–20 and the other is the theoretical spectrum for a 10383 Å resist coating. Good correlation is observed.

5.6.6 TDRM Software

The TDRM software is implemented in two sections, a real time data collection program which stores the measured spectra as the resist develops and an off-line analysis program that uses the previously stored data to determine the film thickness corresponding to each spectrum.

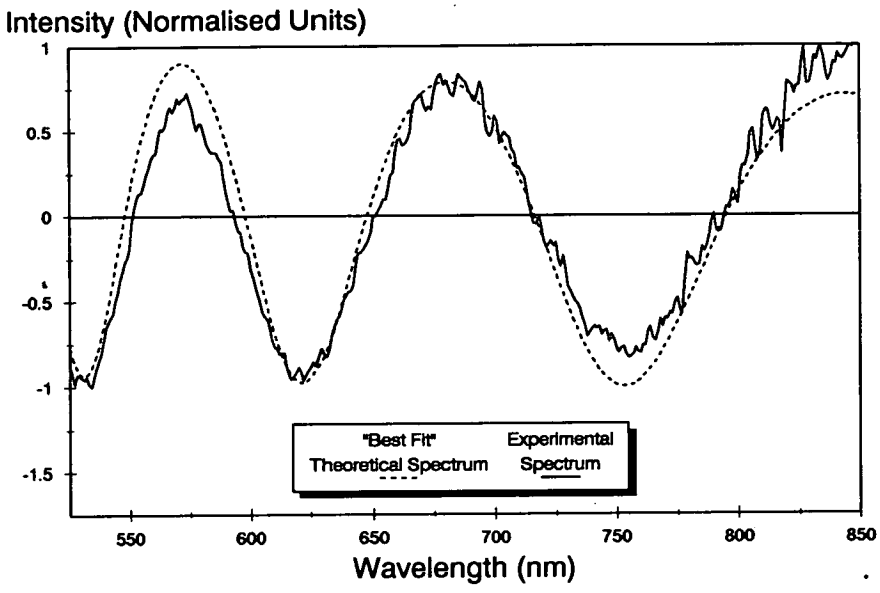

Figure 5–22: *A comparison of a measured spectrum and its 'best fit' theoretical equivalent.*

5.6.6.1 Data Collection Software

Initially, data was collected using the Monolight 6850 Spectral Analysis Software.[235] This standard package will collect spectrum data over a user defined wavelength range, with a specified wavelength step size at regular time intervals. The software will automatically normalise the collected spectrum by a pre-collected reference before storing the data to disk.

If the wavelength range was specified as 525nm to 850nm with a step size of 1nm and the signal was normalised using a bare silicon reference spectrum then reliable thickness measurements can be made.[118]

However, the package has numerous shortcomings. Firstly, the minimum time interval between samples is one second which provides insufficient detail for rapidly developing films. Secondly, each spectrum is saved as an individual file. Whilst this is not a significant problem in itself, the number of files in the data directory affects the hard disk access time. When the number of files in a directory exceeds sixty, the time taken to measure and store a spectrum exceeds the one second collection interval. This introduces in an unknown error in the time interval between samples.

Thirdly, the stored data is in a Monolight proprietary format which must be converted into ASCII format for data analysis. The translation is achieved using a program called 'OSATOASC' provided by Monolight Instruments. Finally, data collection must be started manually, i.e. an operator must press a key as the spray starts or as the jig is submerged. Obviously a small but random time error is introduced into each set of measurements.

A custom spectrum acquisition program, 'TDRM', was written in Microsoft C utilising the Monolight 6860 Control Software C Library.[236] This program controls the spectrum analyser and will automatically collect and store relative reflection spectra during development. The data collected during development is normalised by a bare silicon reference signal which is collected at the beginning of a measurement session. When development is being monitored the relative reflection spectra for each wafer are stored serially in a single continuous file. An explicit collection time is associated with each spectrum in the file. Data is collected using either a fixed interval time (of 1 second or greater) or the free-run mode. In the free-run mode a new spectrum is collected immediately after the prior one has been stored to disk. This results in a collection rate of between 3 and 4 spectra per second. Data collection may be started either manually or by the application of a falling voltage edge on the controller unit BNC trigger. This is achieved using either the track microswitch or the immersion detector, described in Section 5.6.2.

5.6.6.2 Analysis Software

Two essentially identical versions of the C program, 'ANALYSE', were written; one analyses data produced by the Monolight spectral analysis software and the other data generated by the 'TDRM' program. Both programs use the same implementation of the algorithm described in Section 5.6.5.

The first relative reflection spectrum in a given data file is read in and normalised into the -1 to +1 format. The initial resist thickness is calculated by comparing the spectrum to theoretical values for resist thicknesses of between 3000Å and 20000Å. This calculation is done using a three stage approach to im-

prove calculation times. Initially, the correct thickness is found to the nearest 100 Å. The accuracy is then improved by checking a ±100Å region around this value in steps of 10Å. A final value is then obtained by using steps of 1Å in the ±10 Å region around the second value. The thickness corresponding to the observed spectrum is therefore obtained to the nearest 1Å, in a few seconds. An output file is opened and both the collection time (0 in the case of the first measurement) and thickness are recorded.

The process is repeated for each subsequent spectrum in the data file. Calculation time is minimised by using knowledge of the development process to limit the scope of the initial search values. i.e., the next thickness should be equivalent or less than the previous one. Practically, the 100Å step size search is limited to a range of 200Å higher than the last recorded thickness to 1000 Å lower. These values may be altered if the dissolution rate of the film is known to be particularly high, or low. Again, the time of collection and the calculated thickness are stored in an output file.

5.6.7 Measurement Repeatability and Accuracy

The repeatability of measurements using the software above is approximately ±5Å when the film is dry. This degrades to about ±35 Å under continuous spray conditions.[118] The calculated values compare favourably with those obtained from established semiconductor metrology tools. The 10383 Å film discussed in Section 5.6.5 was measured as 10420 Å by a Nanospec AFT. The deviations between the two values can be explained by the Nanospec's use of a different, fixed resist refractive index dispersion.

The Cauchy coefficients used in the 'TDRM' program were those for the unexposed resist, given in Table 5–1. Using the values for the completely exposed resist only increases the measured thickness by around 25 Å, so it was deemed acceptable to use the unexposed values for all exposure levels.

Examination of theoretical spectra generated for the wavelength window, between 525nm and 850nm, shows that intensity extrema are present within the

window until a thickness of 2500Å is reached. As the algorithm above utilises the extrema positions to determine the thickness, it will obviously fail at, and below, this thickness.

Measurements below 2500Å require knowledge of the absolute relative reflection spectrum produced by the film.[226,237] This is not possible in a development situation since an unknown level of attenuation is introduced by various absorption and scattering effects. Absorption is primarily due to the developer but is dependant on the puddle thickness and the amount of dissolution product within it. Scatter is introduced by aerosol developer particles during spray and puddle surface roughness which may be extreme during puddle formation.

5.6.8 Spray Measurements

Figure 5–23 shows output from the 'TDRM' and 'ANALYSE' software for the case of a track-based continuous spray development process. The resist (HiPR6512) received an 80mJ/cm^2 g-line exposure under the standard conditions, as detailed in Chapter 2, Table 2–2 with the omission of the PEB. Inspection of the Figure reveals the 'staircase' effect caused by the standing wave effect during exposure. It is also clear that the thickness algorithm has failed, as expected at around 2500Å.

Figure 5–24 illustrates the system output for a similarly processed resist film which has received the standard 60 second PEB. Again, the algorithm fails at around 2500Å but this time the strong 'staircase' effect has been removed by the diffusion during the bake. Careful inspection of the figure shows that a small residual effect is still present. Numerous examples of TDRM output for continuous spray processes, as well as that for puddle and immersion processes, will be presented in Chapter 6.

5.6.9 Puddle Measurements

Figures 5–25 and 5–26 show TDRM software output for HiPR6512 wafers developed in a stationary puddle process. The first wafer did not receive a PEB whilst

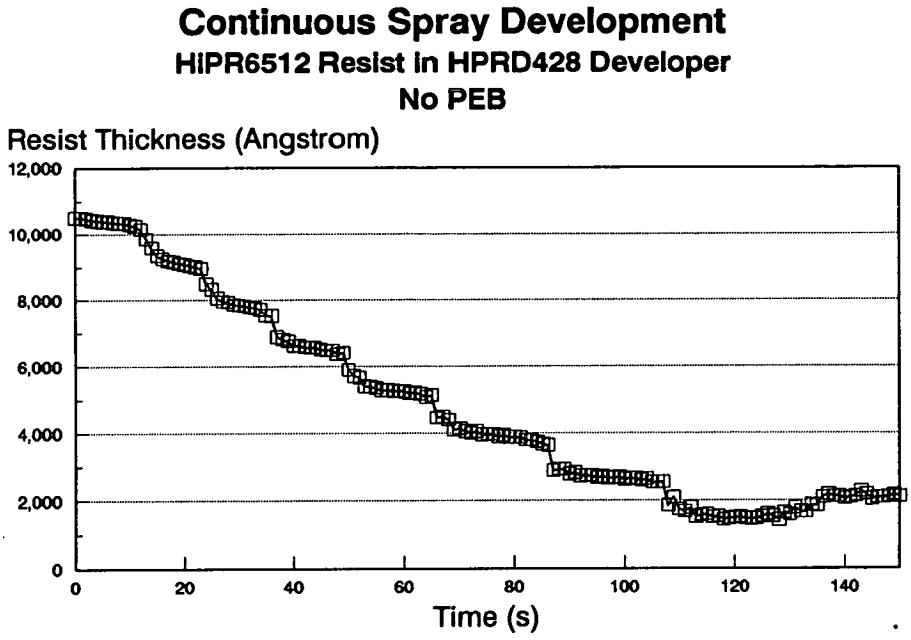

Figure 5–23: *Typical output from the TDRM/ANALYSE programs for a track-based continuous spray development process which omits a PEB.*

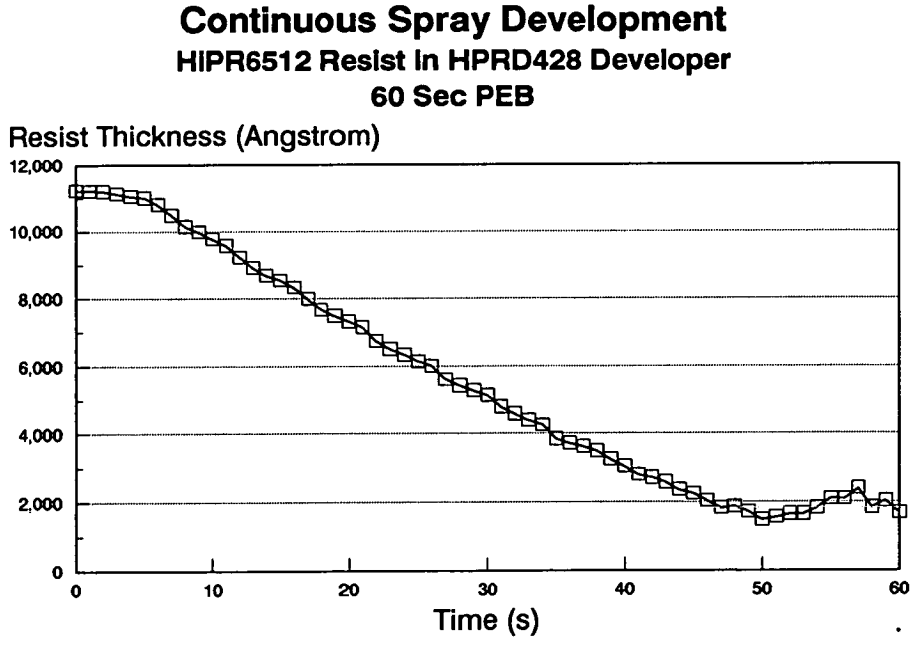

Figure 5–24: *Typical output from the TDRM/ANALYSE programs for a track-based continuous spray development process utilising a PEB.*

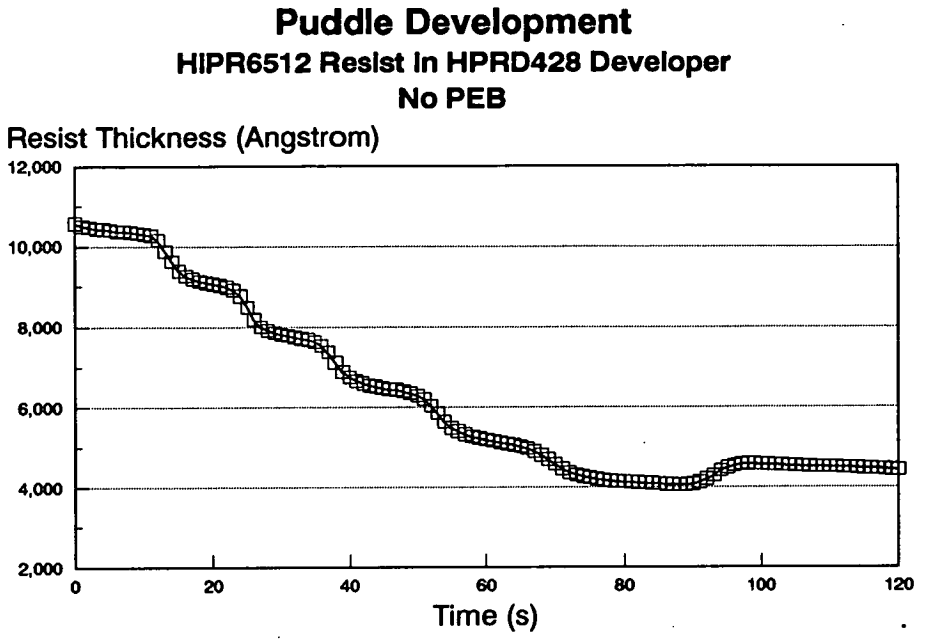

Figure 5–25: *Typical output from the TDRM/ANALYSE programs for a track-based puddle development process which omits a PEB.*

the second did. Again, the standing wave 'staircase' is clearly evident on the wafer which was not baked after exposure. The most striking feature in the figures is the apparent failure of the thickness determination at around 4000 Å. Inspection of wafers developing in a puddle mode revealed a build up of a red dissolution product in the developer above exposed regions. Since the algorithm is effective in a continuous spray situation where the red photoproduct is continually removed by the flow of fresh developer it is reasonable to assume that ths material may be responsible for the premature algorithm failure. Monahan[218] noted that this 'red cloud' effect can seriously impact the effectiveness of end-point detection systems.

5.6.9.1 Analysis of Photoproduct Transmission

In an attempt to understand the premature algorthm failure, the spectral absorption of this red dssolution product was investigated.

An HiPR6512-coated wafer was blanket exposed with the E_0 threshold dose required for a 55 second puddle development. The wafer was allowed to puddle

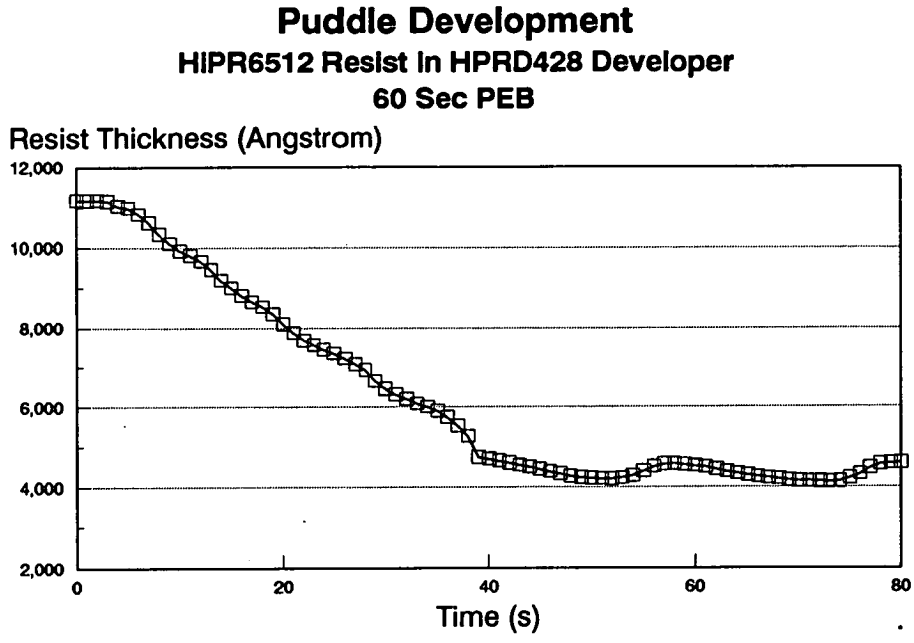

Figure 5–26: *Typical output from the TDRM/ANALYSE programs for a track-based puddle development process utilising a PEB.*

develop for 1 minute to ensure no resist remained on the wafer and any observed attenuation was due purely to dissolution product. A relative reflection spectrum was taken over the range of 350nm to 900nm, referenced to a bare silicon substrate. Further spectra were collected at 20 second intervals. Figure 5–27 illustrates the resulting spectra[238] (the arrows indicate increasing time). Clearly, the material transmits poorly, and non-linearly, in the 500 - 650 nm wavelength range. However, the absorption substantially decreases with time, reaching a stable level after approximately 520 seconds. During this period, there is a slight decrease in the transmission above 700nm, the absorption in this region is relatively linear and substantially lower than at shorter wavelengths.

It is unclear whether the dissolution product is absorbing the light or simply scattering it. However, attempts at measuring the visible absorption spectrum of the puddle after decanting it into a spectrophotometer cell failed to produce any detectable absorption.[238]

This might indicate that the 'red cloud' is a thin concentrated layer close to

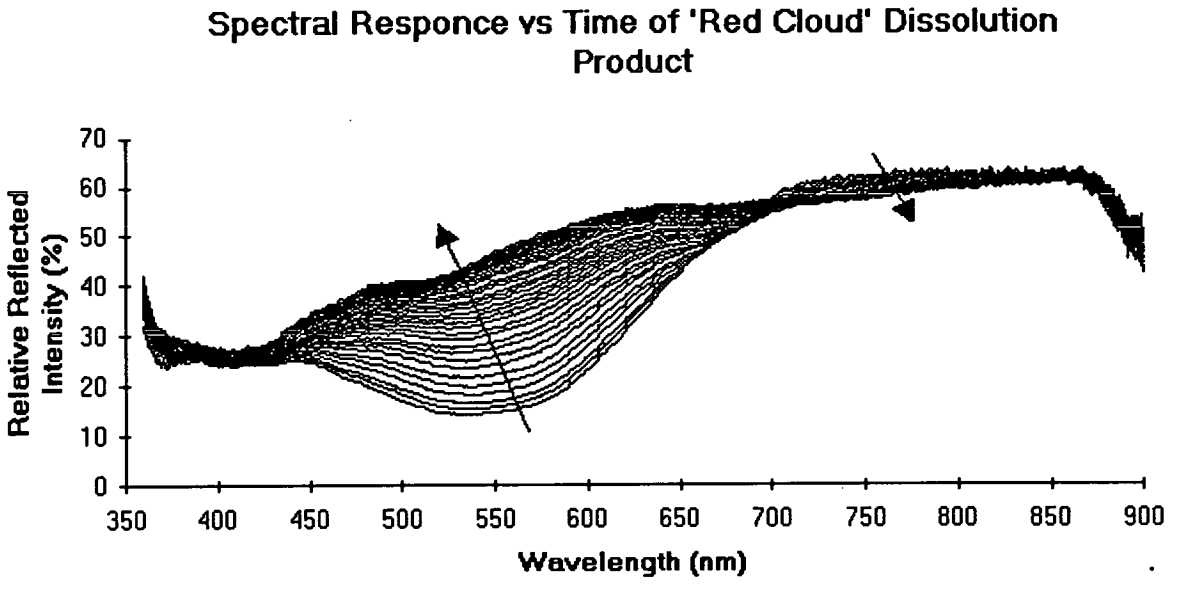

Figure 5–27: *The relatve reflected spectral response of red photoproduct as a function of time. Measurements were made at 20 second intervals. The arrows indicate increasing time.*

the substrate, whose absorption decreases as it disperses by diffusion into the body of the puddle. This follows, if it is considered that the act of decanting the puddle dispenses the dissolution product evenly throughout the collected liquid from which negligible absorption can be detected.

The strong non-linearity in the transmission of the dissolution product results in the failure of the film thickness estimation algorithm at thicknesses around 4100A. Figure 5–28 illustrates the theoretical spectrum for a resist film of that thickness. Although there is a considerable difference between this curve and the absorption curve shown in Figure 5–27 the algorithm only utilises the 525 to 850nm portion of these curves. Within that wavelength window the dominating feature in both plots is the intensity minima close to 550nm. It would appear that as the resist thickness tends towards 4100 Å, the minimum caused by the dissolution product absorption dominates the relative reflection signal from the thin film and the thickness result therefore remains approximately constant as the algorithm latches onto the spurious minimum. The case for this scenario is strong as no

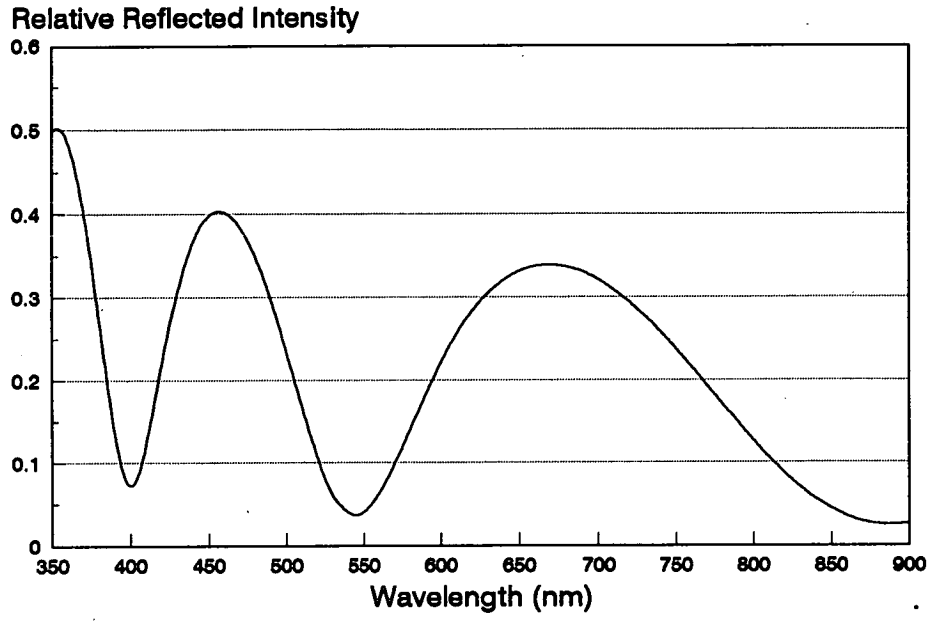

Figure 5–28: *The theoretical spectral response of a 4100 Angstrom resist film.*

such phenomenon occurs during continuous spray dissolution where no dissolution product build up occurs.

It is not possible to compensate for this effect within the algorithm as the amount of dissolution product present depends on how fast the product is generated and dissipates, which is in turn related to resist thickness, exposure dose, developer agitation and probably several other unknown factors.

5.6.10 Immersion Measurements

Figure 5–29 illustrates TDRM output for a wafer developed in a stagnant (non-agitated) immersion mode. The results are similar to those seen during the puddle situation, with premature failure of the algorithm in the region of 4100Å. Again, there is no physical mechanism for removing the red dissolution product produced during development.

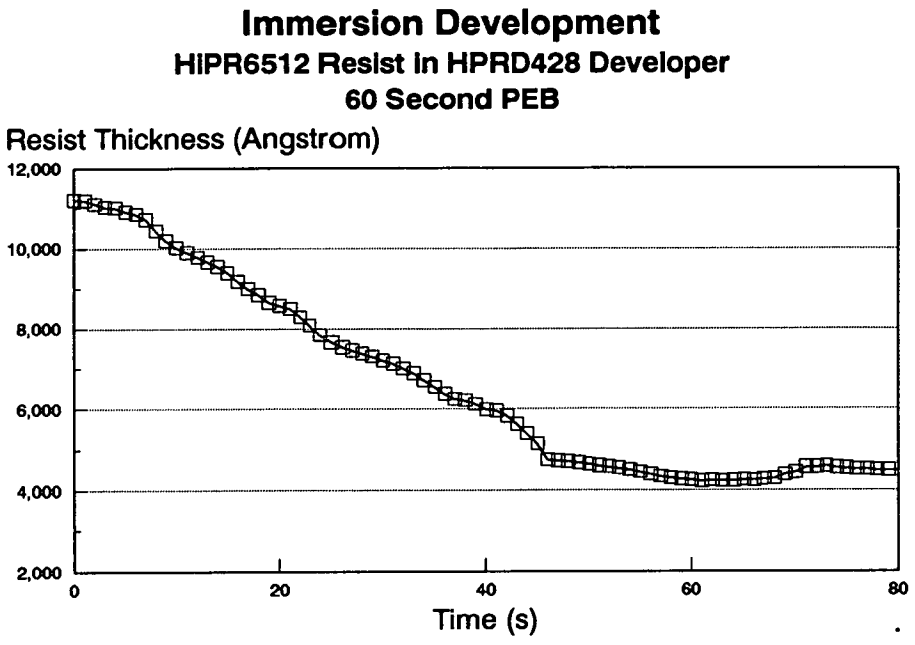

Figure 5–29: *Typical output from the TDRM/ANALYSE programs for a stagnant immersion development process utilising a PEB.*

5.6.11 Advantages and Disadvantages of TDRM System

It can be seen therefore that the TDRM scores over the Perkin-Elmer DRM and the DSM100 in that it can monitor all types of development *in-situ*. Furthermore, the absolute thickness data it provides clearly shows residual standing wave phenomena and surface induction effects.

However, this system, like the DSM100, can only monitor a single exposure dose at one time. If it is considered that the Perkin-Elmer system can study up to 20 different exposure doses simultaneously, the time penalty involved in both wafer preparation and experiment runs can be realised. Additionally, the resist thicknesses which can be studied are limited by photoproduct attenuation and ultimately by the polychromatic measurement algorithm employed.

5.7 Conversion of a Perkin-Elmer DRM 5900 for Puddle Measurements

The greatest deficiency of the TDRM is its inability to monitor more than one exposure zone during development, hence multiple wafers must be run to characterise a given resist/developer process. The Perkin-Elmer DRM, on the other hand, can monitor up to 20 exposure zones simultaneously. In an attempt to allow fast characterisation of puddle processes, a Perkin-elmer DRM was modified to monitor a pseudo-puddle process. A comparison of the obtained data and *in-situ* measurements made using the TDRM allow the accuracy and validity of such a technique to be evaluated. This is discussed in Chapter 6.

The major problem in converting an immersion DRM to monitor puddle processing is that the wafer is normally held vertically. Initial attempts to use a prism or mirror to reflect the DRM interrogating beam from the horizontal to the vertical plane were unsuccessful, primarily due to the fact that the beam's return path to the detector is not parallel to the initial path (see Section 5.4.2.1).

The final, if somewhat inelegant, solution was to stand the DRM on its end. A slight angle of inclination was required to prevent the developer from running off the wafer. The tilt was applied in such a manner that the face plate of the wafer holder assembly was perfectly level.

The wafer under study is located in the normal position on the wafer holder and 15ml of developer is applied directly to substrate surface from a plastic beaker. Extreme care is required during application as the meniscus is easily broken. If this occurs the wafer will rapidly dewet. The wafer locating screws on the wafer holder must be removed to prevent contact with the wafer edge, which once again leads to dewetting. In the absence of the screws, the wafer must be positioned carefully by hand and is held in place by the application of de-ionised water to its reverse side. In all other aspects, the DRM operation is identical to the immersion technique.

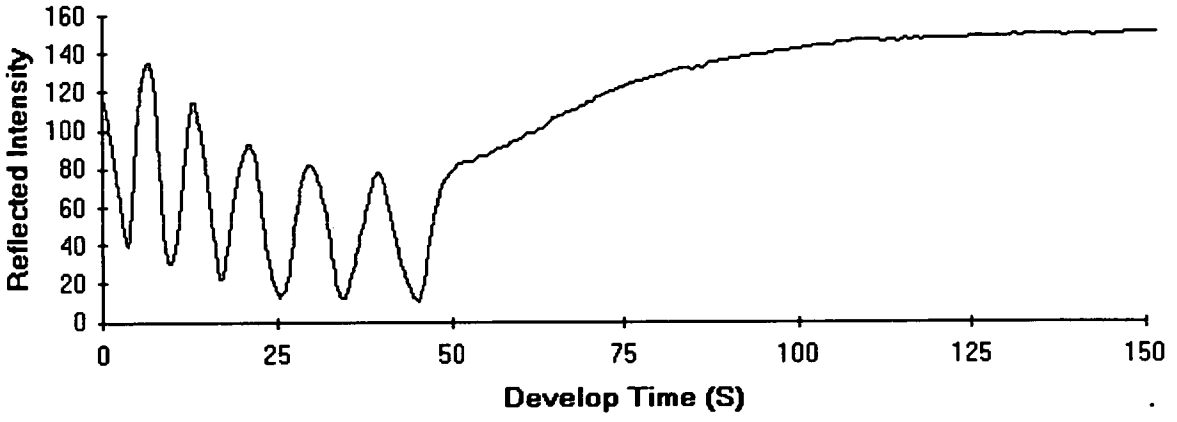

Figure 5–30: *Reflected intensity (632.8nm) versus time for 1.18μm of HiPR6512 developing in HPRD428. 100*mJcm^{-2} *g-line exposure, stagnant immersion development.*

5.7.1 Monochromatic Wavelength Optimisation

The Perkin-Elmer DRM monitors the developing resist film using a wavelength of 632.8nm. Inspection of the absorption curve for the 'red cloud' dissolution product (Figure 5–27) predicts that this should affect the reflected signal significantly. Figure 5–30 shows the reflected DRM signal from a HiPR6512 coated wafer developing in HPRD428 during static immersion (under standard conditions). It can be seen clearly that both the peak and trough intensities are attenuated by the dissolution product build up during development. After developer has 'broken through' the resist film, the reflected intensity gradually rises as the dissolution product dissipates.

Figure 5–31 illustrates identically processed resist developed under the pseudo-puddle conditions. Once again, the maximum and minimum intensities drop as development progresses. In this case the rise in reflected intensity after resist 'break-through' is more gradual, requiring many hundreds of seconds. This difference in post-development reflected signal recovery can be attributed to the wafer orientation. In the immersion situation, the wafer is held vertically, and the red region can be observed 'bleeding' down the wafer, from the exposure zones, under

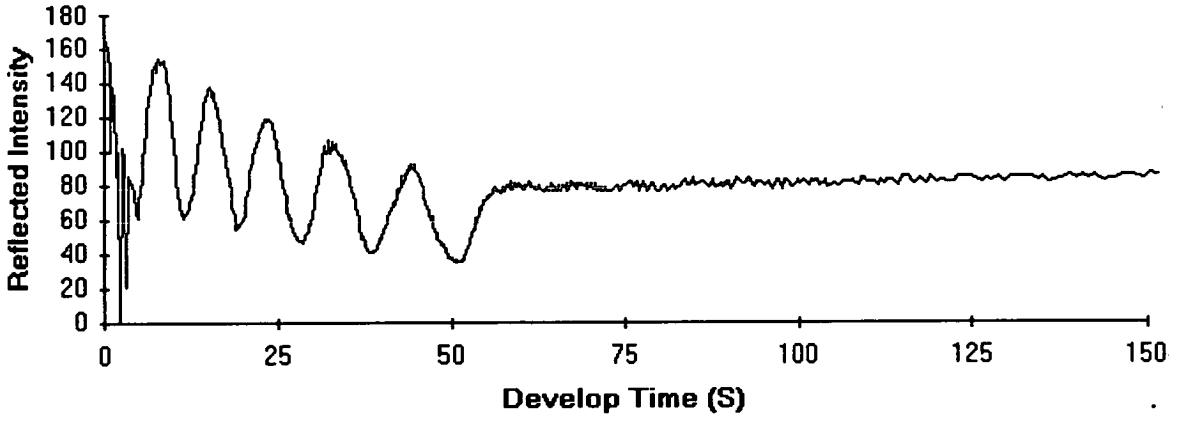

Figure 5–31: *Reflected intensity (632.8nm) versus time for 1.18μm of HiPR6512 developing in HPRD428. 100*mJcm^{-2} *g-line exposure, pseudo-puddle development.*

the force of gravity. In the pseudo-puddle case, the wafer is horizontal hence the dissolution product tends to remain above the exposure zone and the total volume of developer in the puddle is much smaller than in the immersion tank.

Inspection of the dissolution product spectral response (Figure 5–27) indicates that the use of an interrogation wavelength in excess of 700nm should yield a more 'ideal' interferometric signal. In order to verify this hypothesis the DRM's operating wavelength was altered by replacing the 632nm filter with one centred on 700nm. This wavelength was chosen as the anti-reflective coatings in the DRM optics have an operating range of 546nm to 700nm. Figure 5–32 shows the reflection signal for the modified system under stagnant immersion development and is directly comparable with Figure 5–30. While some attenuation is still evident, it is much less severe. More importantly, a very clear end-point is visible and the signal remains stable thereafter; this was true in all cases studied.

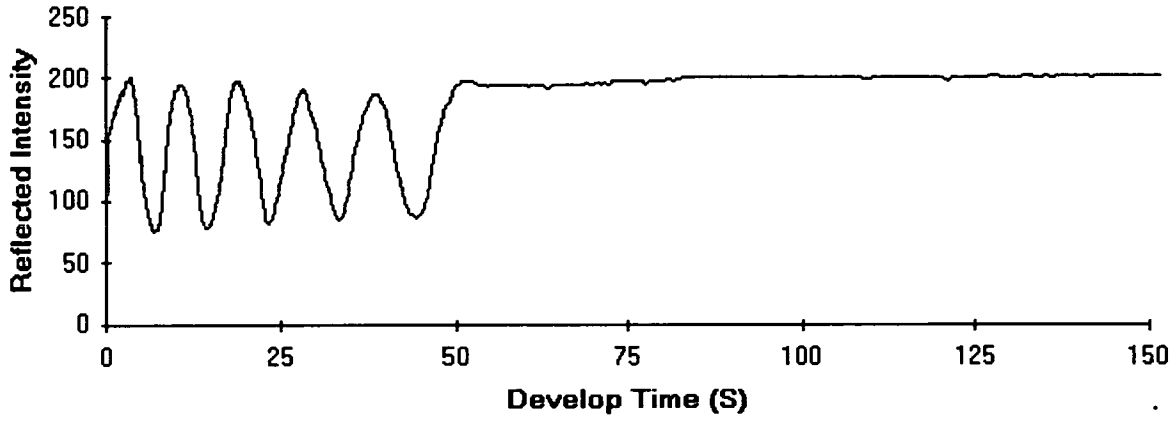

Figure 5–32: *Reflected intensity (700nm) versus time for 1.18μm of HiPR6512 developing in HPRD428. 100*mJcm^{-2} *g-line exposure, stagnant immersion development.*

5.8 Summary

This chapter has discussed the various DRM hardware commonly used, and discussed the theory behind their use.

A novel polychromatic TDRM (Track Development Rate Monitor) has been introduced which is capable of measuring development *in-situ* on real processing equipment, either track or immersion bath. The system outputs a series of absolute thicknesses which clearly show surface induction effects and residual standing waves. Although the TDRM allows characterisation of all types of development process, a separate wafer must be used for each exposure dose.

In an attempt to speed up the characterisation of track processes a commercially available immersion DRM, the Perkin-Elmer 5900, has been modified to study a pseudo-puddle process, since this tool can study up to 20 different exposures on a single wafer.

An analysis of the red photoproduct produced during resist development has shown why polychromatic thickness measurements are corrupted during puddle

and immersion processes and how monochromatic interferometric signals may be improved by the selection of an appropriate observation wavelength.

Chapter 6

Development Rate Parameter Extraction and Model Refinement

6.1 Introduction

This chapter describes how DRM output, in conjunction with knowledge of resist processing and exposure conditions, can be used to generate dissolution rate equation parameters suitable for the simulation techniques described in Chapter 4. The conventional methods for achieving this are explained together with the alternative procedure employed during this study.

A parameter verification process is introduced which identifies some weaknesses in the conventional model of lithography. Model refinements are introduced to address these issues, including the derivation of an alternative surface induction expression. The practical problems of implementing these modifications in standard simulation tools are discussed.

Full process characterisation using the TDRM is presented for HiPR6512 and HPR204 photo resists in HPRD428 developer under three development techniques: continuous spray, static puddle and stagnant immersion. These results are compared to results from a Perkin-Elmer DRM (standard immersion mode and pseudo-puddle mode). These comparisons indicate that Perkin-Elmer DRM processing conditions can be optimised to reflect track-based puddle processing with reasonable accuracy.

6.2 Conventional Parameter Extraction

The creation of a dissolution rate curve requires knowledge of development rate as a function of relative inhibitor concentration, M. If the resist's refractive index and Dill exposure parameters are known then the exposure modelling techniques described in Chapter 4, Section 4.3 can be used to calculate the M value at every point in the resist film. The monitoring of a series of open, blanket exposed areas of varying dose can be used to generate a description of how development rate varies with M. Development may be characterised on either matched or reflecting substrates. Whilst the use of the former is simpler, reflecting substrates produce a superior DRM signal and can give additional insight into the resist process. Sections 6.2.1 and 6.2.2 review the documented application of these two approaches.

6.2.1 Parameter Extraction on Matched Substrates

A matched substrate reflects a minimal amount of the exposing wavelength at the resist/substrate interface. This can be achieved by choosing a glass substrate which has refractive index very close to that of the resist film, at the exposing wavelength.[163,187] Provided the refractive index match is poorer at the DRM monitoring wavelength, a reflected interferometric signal can be obtained. Alternatively, substrate reflection at the exposing wavelength can be minimised by applying a film stack to bare silicon substrates. Zee *et al.*[117] showed that a tri-level stack of 45nm of silicon nitride on 80nm of silicon dioxide on 160nm of nitride on a silicon substrate produces under 5% reflection at g-line. However, the substrate reflectance is around 60% at the 632nm wavelength used by the Perkin-Elmer DRM.

The use of a matched substrate simplifies resist characterisation since no, or negligible, standing waves are formed during exposure. In this case, the relative inhibitor concentration (M) is relatively uniform within the film, increasing slightly with depth as absorption attenuates the incident exposing radiation. Similarly,

dissolution rates change slowly during the development as the inhibitor level increases.

Dill[163] and Kim,[187] both used this matched approach to characterise resist development. Multiple matched substrates are coated with a resist film of a given thickness and exposed with a wide range of exposures. A DRM is then used to map resist thickness against time for the developing wafers. The resulting output is used to calculate the instantaneous development rate of the resist at a variety of resist thicknesses ranging from almost zero to full film thickness. An exposure simulation program such as SAMPLE is then used to calculate the instantaneous relative inhibitor concentration at each relevant thickness. The instantaneous development rate is then plotted against the instantaneous M value. A plot of this type, reproduced from work by Zee *et al.*,[117] is shown in Figure 6–1. Separate bulk and surface phenomena can be observed in the plot. The main cluster of points represents the bulk behaviour but a second less numerous set of points is also observed. These points originate near the film surface where induction effects result in much lower dissolution rates at equivalent inhibitor concentrations. Appropriate bulk dissolution rate equation parameters can be obtained by fitting the desired rate equation to the data points exhibiting bulk behaviour. In Figure 6–1, the line labelled 'bulk' is the best fit of the standard Kim equation to bulk data. Once the bulk behaviour has been described, surface induction behaviour may be characterised. The surface to bulk ratio function, f(0,M), described in Chapter 4, Section 4.6.3.2 is varied until it best matches the lowest points on the plot. The line labelled 'surface' in Figure 6–1 is the 'best fit' to the data of the predetermined bulk equation multiplied by f(0,M).

Software suites such as PARMEX[239] have been developed to perform the above operations automatically with the minimum of user intervention.

Although matched substrates allow easy inhibitor concentration calculations, there are several drawbacks. In the case of matched glass substrates the reflections from the substrate during development are weak and can be easily swamped by noise, say in the case of spray development. Additionally, equipment employing

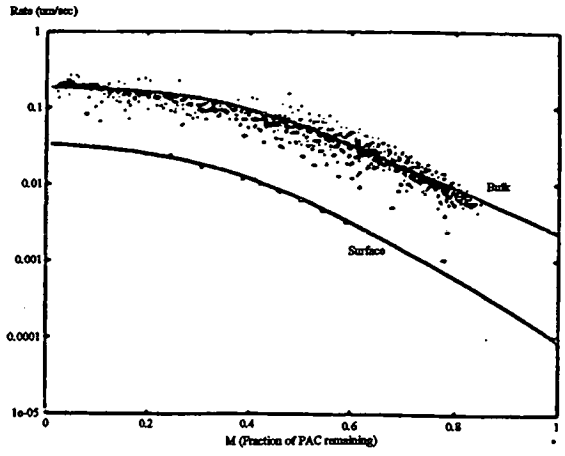

Figure 6–1: *Instantaneous dissolution rate versus instantaneous relative inhibitor concentration (M) for Shipley S1400-31 Photo Resist in MF319 Developer.*

optical wafer sensors, e.g., the SVG86 Series tracks, fail to detect transparent substrates resulting in misprocessed or damaged substrates.

The problems with matched film stack substrates are a little different. The reflectivity of the stack is highly wavelength dependant; whilst this is acceptable for monochromatic DRMs (assuming reflectivity is high at the interrogating wavelength), it can be problematic for polychromatic systems if regions of particularly low reflectivity occur within the system wavelength window, as is the case with Zee's stack scheme.

6.2.2 Parameter Extraction on Reflecting Substrates

The derivation of dissolution rate equation parameters on reflecting substrates is similar to the method described in the previous section but is complicated by the standing waves during exposure. Again, instantaneous dissolution rates are taken from DRM output plotted against instantaneous inhibitor concentrations calculated using simulations.

The presence of the standing waves results in local exposure variations within the resist, of as much as a factor of 8 over a 650Å distance. Consequently dissolution rates also change by large factors over these short distances during

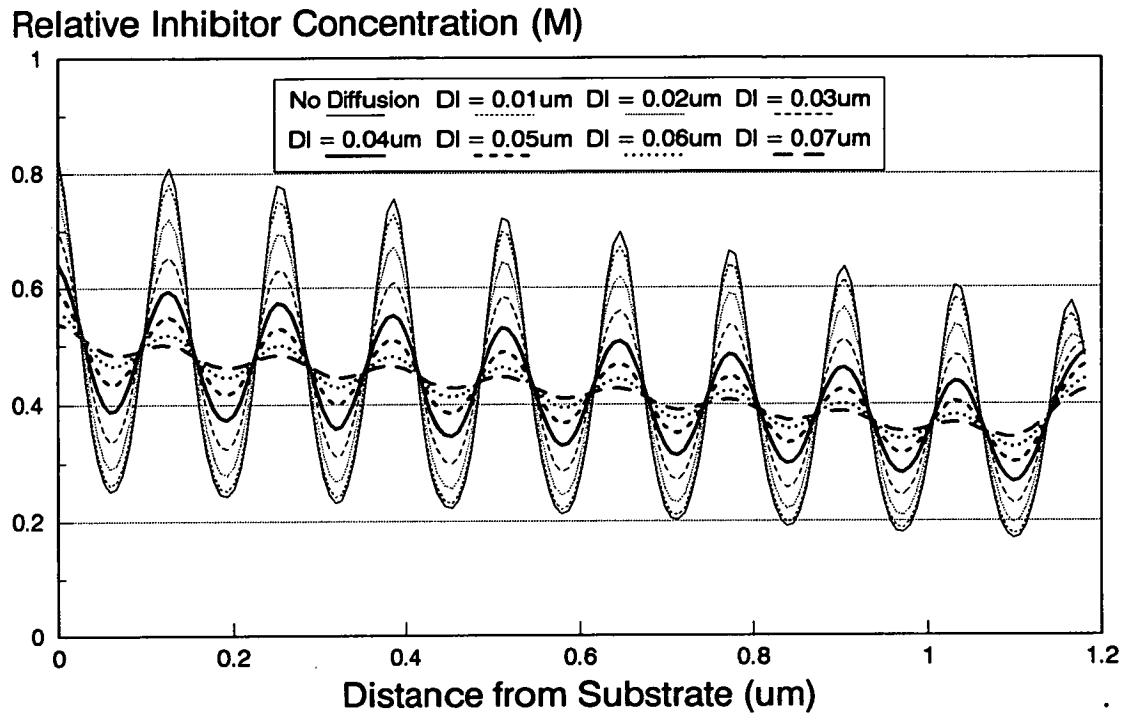

Figure 6–2: *Modelled normalised PAC distribution for a g-line exposed HiPR6512 resist film as a function of characteristic diffusion length,* D_l.

development.[240] A slight mismatch between calculated and actual depths can have a substantial effect on the final rate equation fit, as incorrect M values are matched to the experimental dissolution rates.[240]

The situation is futher complicated when a PEB is used. During the bake, the resist undergoes two changes. Firstly, the inhibitor undergoes diffusion, as described in Chapter 4, Section 4.5. The level of diffusion is dependant on the resist chemistry, PEB temperature, the PEB time and softbake conditions. In the model, the degree of diffusion is determined by a characteristic diffusion length (D_l). Figure 6–2 shows how sensitive the relative inhibitor distribution is to this value. The illustrated distributions are for a 1.18μm film of HiPR6512 under g-line exposure on a silicon substrate. An accurate estimation of the correct diffusion length for a given arbritrary process is nearly impossible, resulting in a high probability of inaccurate mapping between dissolution rate and M.

Additionally , the resist undergoes densification during the PEB. This reduces

the total physical thickness of the film, often by several percent. It must be assumed that the distance between inhibitor maxima and minima also reduces.

It can be seen that although the mapping procedure is still straightforward, the use of a reflecting substrate introduces several potential sources of major inaccuracy. Section 6.3 presents an alternative approach to characterising resists on reflecting substrates which is less sensitive to the effects of the PEB and local exposure variations.

6.3 An Averaged Approach to Parameter Extraction

An alternative method of analysing DRM data to produce a description of dissolution rate versus relative inhibitor concentration can be used, provided the process contains a PEB.

The average dissolution rate within the bulk of the resist is determined for a given exposure from DRM data. The rate is calculated over a given thickness range which excludes regions near the resist surface and the substrate where induction effects may be present. Typically, limits would be 20% and 85% of the pre-development thickness. Obviously, in the case of some TDRM monitored wafers the lower bound must be raised to reflect the the limit of accurate measurements.

It should be noted that an average dissolution rate cannot be truly measured for a process that does not contain a PEB. Unbaked films develop in strata with the low dissolution rate regions dominating. The average dissolution rate over the bulk region is therefore underestimated.

The single dissolution rate value obtained from the above process is plotted against the average relative inhibitor concentration within the region used to generate the rate value. Again, an exposure simulator such as SAMPLE is used to generate this value.

Diffusion Length (μm)	Average M (0 - 100% Full Thickness)	Average M (20 - 85% Full Thickness)
0.00	0.424	0.418
0.01	0.424	0.418
0.02	0.424	0.418
0.03	0.424	0.418
0.04	0.424	0.418
0.05	0.425	0.418
0.06	0.425	0.417
0.07	0.425	0.417
0.08	0.425	0.417

Table 6–1: *The average relative inhibitor level within an 1.18μm HiPR6512 film as a function of characteristic diffusion length, for a nominal 100*mJcm^{-2} *g-line exposure.*

Although this approach is relatively intuitive, and has been used previously by Hansen,[212] careful consideration of the calculation details reveal that it has substantial advantages over the instantaneous mapping technique discussed in Section 6.2 when reflecting substrates are used.

Simulations reveal that the average inhibitor concentration value over a fixed region in the resist is virtually independant of diffusion length. This is illustrated in Table 6–1 which details the average relative inhibitor concentration within a 1.18μm coating of HiPR6512, flood exposed with 100mJ/cm^2 of g-line exposure, as predicted by SAMPLE, as a function of PEB characteristic diffusion length. The average value in the entire film is compared with the average value over the 20% to 85% region.

The results clearly show that the average inhibitor level in the film is independent of diffusion length, when rounding errors are ignored. This should not be unexpected as the diffusion algorithm merely redistributes the inhibitor. This contrasts with reality where elevated temperature during the bake thermally de-

composes some inhibitor. This is compensated for in the simulation by setting the maximum inhibitor level (1) to be the level of undestroyed PAC in an unexposed coating which has undergone both the standard softbake and PEB processes, i.e., characterisation is only valid for one set of bake conditions.

Inspection of the average relative inhibitor concentration in any arbitrary region in the bulk of the film shows that the level is also independent of the diffusion length. Typically, the average values calculated during the following work employed a diffusion length of 0.06μm.

The PAC distribution after exposure is calculated using the resist thickness at the time of exposure followed by a diffusion. The modelled resist thickness remains unchanged, however in reality the film thickness reduces. This can be approximated by a uniform scaling of the simulation output such that the new model 'resist surface' is the measured post-PEB thickness. This approximation will be discussed further in Section 6.6.3. Any minor errors incurred by this assumption are minimised by the averaging process.

If multiple wafers are analysed, using exposure doses that provide average M values spanning the 0 to 1 range then a bulk dissolution rate equation can be fitted to the points. Moreover, the 'best fit' values to that equation are independent of the characteristic diffusion length used in the latent image calculation.

6.4 Parameter Extraction Software

6.4.1 Perkin-Elmer derived Dissolution Data

Chapter 5, Section 5.4.2.3 described how OCG proprietary programs processed raw Perkin-Elmer DRM data on a IBM compatible PC to produce a series of data sets representing resist thickness versus time for different exposures. Further programs, also written by S.Hansen (OCG Microelectronic Materials), process this data further to produce rate equation parameters.

The 'DRM3' program[212] calculates the average dissolution rate in the region between 20% and 80% of the full thickness from the thickness versus time pairs produced by 'DRM2'. The average value is the gradient of the 'best fit' straight line through the relevant points as determined by linear regression. The calculated rates are stored with the original data for subsequent processing.

The following program, 'DRM4', calculates the PAC distribution associated with each zone, assuming a uniform resist film on a silicon substrate. Mack's standing wave equation and Dill's bleaching model are used. The results give good agreement with SAMPLE.[212] A diffusion using Fick's law is performed using a fixed characteristic diffusion length of 0.08μm. The program calculates the average inhibitor concentration in the 20 - 80% thickness region and stores this with the average rate data.

The final program in the software suite, 'DRM5', fits dissolution rate equations to inhibitor versus rate data. The program can analyse the data produced by the other 'DRM' programs or may be used in a 'stand alone' mode analysing x,y (M,rate) pairs entered by hand. The program will fit any of the equations discussed in Chapter 4, Section 4.6.1. The SIMPLEX algorithm[241] is used to find the 'best fit' of the chosen rate equation to the data. The program allows the user to constrain or float any of the rate equation parameters. An option exists to fit the data to the logarithm of the dissolution rate rather than the straight rate; this is useful as it weights low dissolution rates (< 10Ås^{-1}) more favourably against the higher ones (> 800Ås^{-1}).

6.4.2 TDRM Derived Dissolution Data

The average dissolution rates for the TDRM data were calculated using an upper limit of 85% (1.00μm for a 1.18μm film) and a lower limit of 47% (0.55μm) or 34% (0.40μm) depending the available TDRM data. The lower values were chosen to be well in excess of the known measurement failure level to ensure no spurious data was included. Again, linear regression was used to find the best fit straight line.

No automated software was created to calculate the inhibitor concentration. Appropriate values were generated using SAMPLE and knowledge of the resist thickness and exposure settings. The 'DRM5' program was then used to analyse the resulting data and provide dissolution rate equation parameters.

6.5 Experimental Bulk Rate Results for HiPR6512 and HPR204

6.5.1 Results from the TDRM

The TDRM was used in conjunction with the above techniques to characterise HiPR6512 and HPR204 resists in HPRD428 under three development processes: stagnant immersion, continuous spray and stationary puddle. The resists were processed as detailed in Chapter 2, Table 2–2 and exposed with g-line radiation.

Exposure was modelled using the Dill parameters detailed in Chapter 4, Table 4–1. It was determined that the exposure doses detailed in Table 6–2 would provide average M values of an appropriate range. The values are based on multiples of the resist's clearing energy in a 60 second continuous spray development process.

During continuous spray experiments, wafers were rotated at 500 rpm and the developer applied at a rate of $1.6 mls^{-1}$ using a fan nozzle. A reduced spin speed of 100 rpm was used for developer application during puddle processing. Developer application lasted 1.5 seconds and was made at the same dispense rate. The wafers remain stationary for the remainder of the experiment. Chapter 7, Section 7.5.1 details the reasoning behind the rotation speeds used during puddle formation and continuous spray.

Immersion processing utilised a standard immersion bath but without agitation (circulation). Several blanket exposed wafers were developed in the bath before experiments commenced to ensure a degree of novolak loading, as would be typical in a production immersion environment. The developer in the bath was replaced after all twelve wafers in one run of exposures were processed. The solution was

Multiple of 60Sec Immersion E_0	HiPR6512 Exposure $mJcm^{-2}$	HPR204 Exposure $mJcm^{-2}$
0.2	15.9	12.5
0.3	23.9	18.8
0.4	31.9	25.0
0.5	39.8	31.3
0.6	47.8	37.6
0.8	63.7	50.1
1.0	79.6	62.6
1.5	119.5	93.9
2.0	159.3	125.2
3.0	238.9	187.8
4.0	318.6	250.4
8.0	637.2	500.8

Table 6–2: *The exposure doses used to characterise HiPR6512 and HPR204 photoresists in HPRD428 developer.*

Resist	Process	R_1 (Å/s)	R_1 (Å/s)	R_s	a	b
HiPR6512	Spray	1266	0.354	16.2219	3.0946	0.98562
	Puddle	988	1.376	11.6596	1.30580	0.97426
	Immersion	907	1.028	8.2376	-0.67788	0.99574
HPR204	Spray	1638	5.120	13.9458	3.74389	0.89981
	Puddle	1438	2.656	14.2669	1.83481	0.96781
	Immersion	1105	1.624	8.4409	-1.26437	0.99747

Table 6–3: *The 'best fit' 5 parameter Kim rate equation parameters for the experimental data as determined by the 'DRM5' software from TDRM output.*

not altered between wafers. Again, this reflects a production immersion process. In all the experiments the developer temperature was kept at 21°C.

Two, or three, repeats of each exposure dose were monitored for each combination of resist and develop process. Long develop times were required for many of the low exposure doses, often over 15 minutes. It should be noted that in the case of continuous spray development it was necessary to restrict develop times to prevent excessive developer consumption. In such instances average develop rates and inhibitor concentrations had to be calculated over more restricted ranges, reflecting the available data.

Figures 6–3 to 6–8 show the data sets generated for each process. In each case the 'best fit' of the 5 parameter Kim rate equation is also shown. The fits were determined using the 'DRM5' program with the log weighting system. The rate equation parameter values are detailed in Table 6–3.

Inspection of the plots reveals that the spread of the experimental points is greatest for the immersion development process. The variability in the track-based processes is markedly less and approximately equal. This illustrates the superior reproducibility of track processing over traditional immersion techniques even when relatively few wafers are developed and bath lifetimes are short.

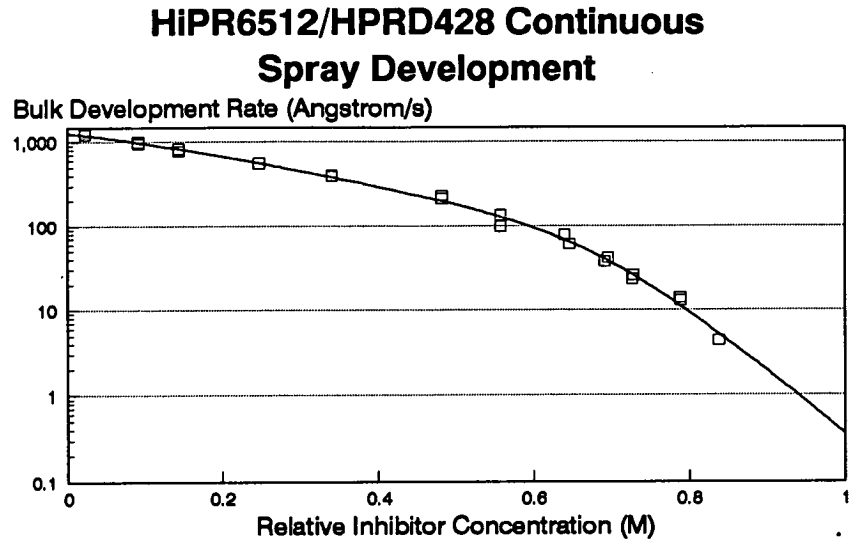

Figure 6–3: *Dissolution rate versus relative inhibitor concentration for the continuous spray development of HiPR6512 resist in HPRD428 developer under g-line exposure, as determined from TDRM data. Solid line indicates the 'best fit' of the 5 parameter modified Kim dissolution rate equation.*

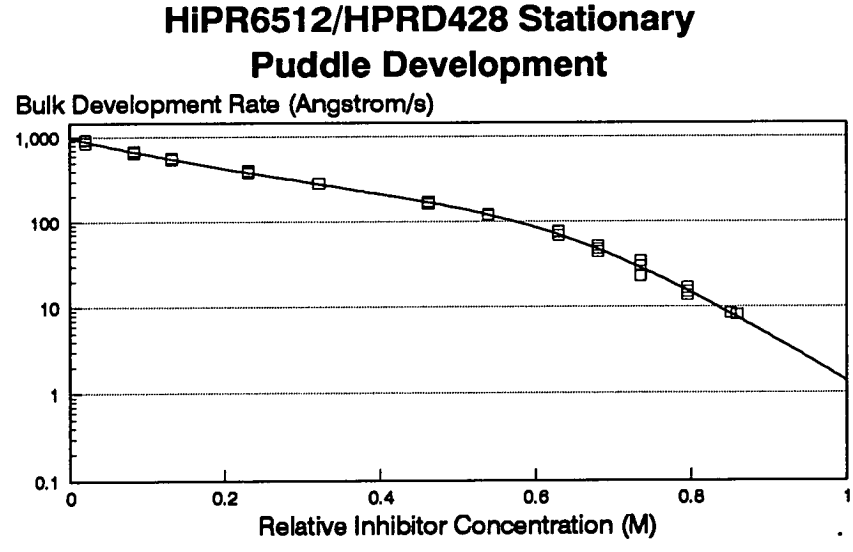

Figure 6–4: *Dissolution rate versus relative inhibitor concentration for the static puddle development of HiPR6512 resist in HPRD428 developer under g-line exposure, as determined from TDRM data. Solid line indicates the 'best fit' of the 5 parameter modified Kim dissolution rate equation.*

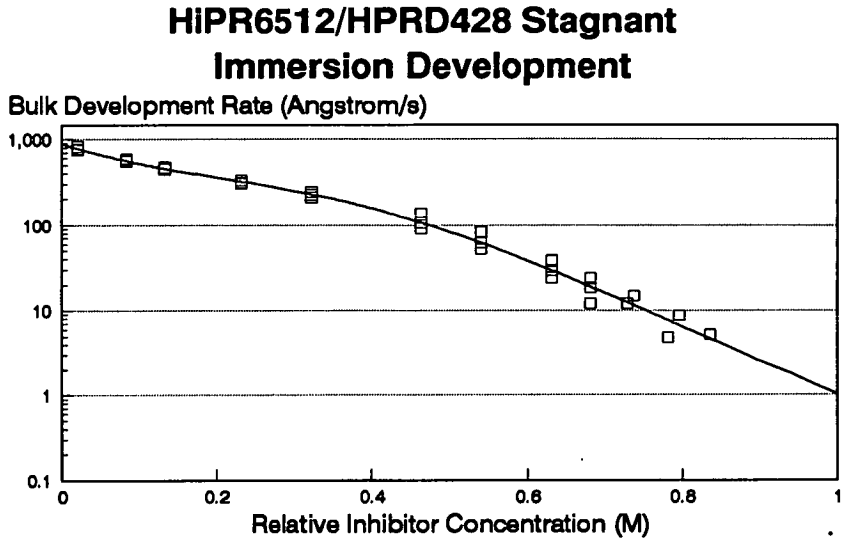

Figure 6–5: *Dissolution rate versus relative inhibitor concentration for the stagnant immersion development of HiPR6512 resist in HPRD428 developer under g-line exposure, as determined from TDRM data. Solid line indicates the 'best fit' of the 5 parameter modified Kim dissolution rate equation.*

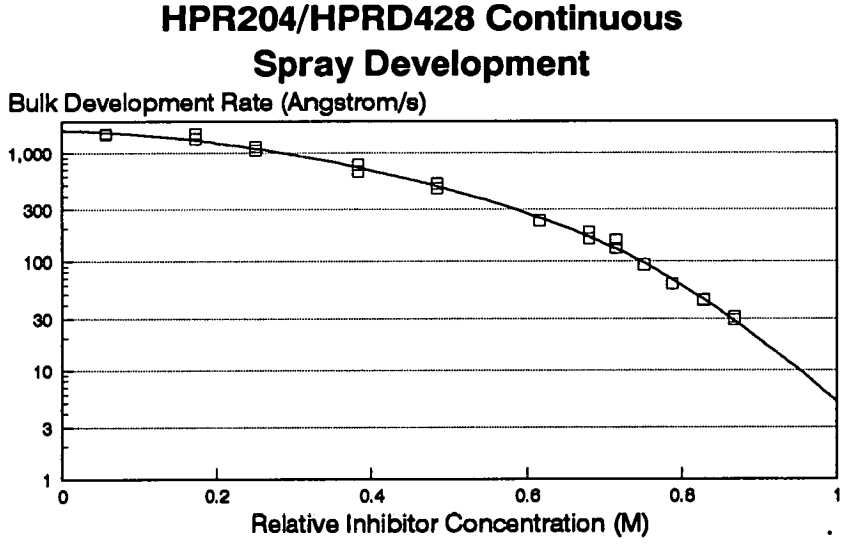

Figure 6–6: *Dissolution rate versus relative inhibitor concentration for the continuous spray development of HPR204 resist in HPRD428 developer under g-line exposure, as determined from TDRM data. Solid line indicates the 'best fit' of the 5 parameter modified Kim dissolution rate equation.*

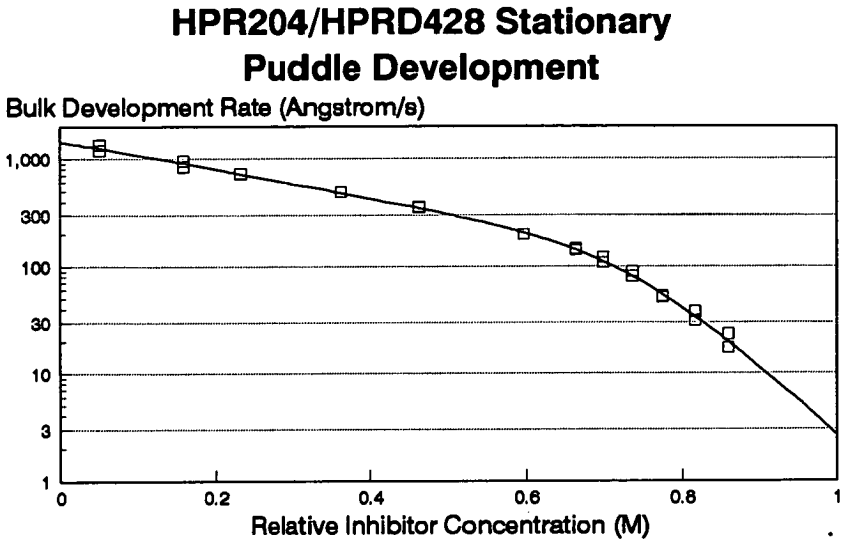

Figure 6–7: *Dissolution rate versus relative inhibitor concentration for the static puddle development of HPR204 resist in HPRD428 developer under g-line exposure, as determined from TDRM data. Solid line indicates the 'best fit' of the 5 parameter modified Kim dissolution rate equation.*

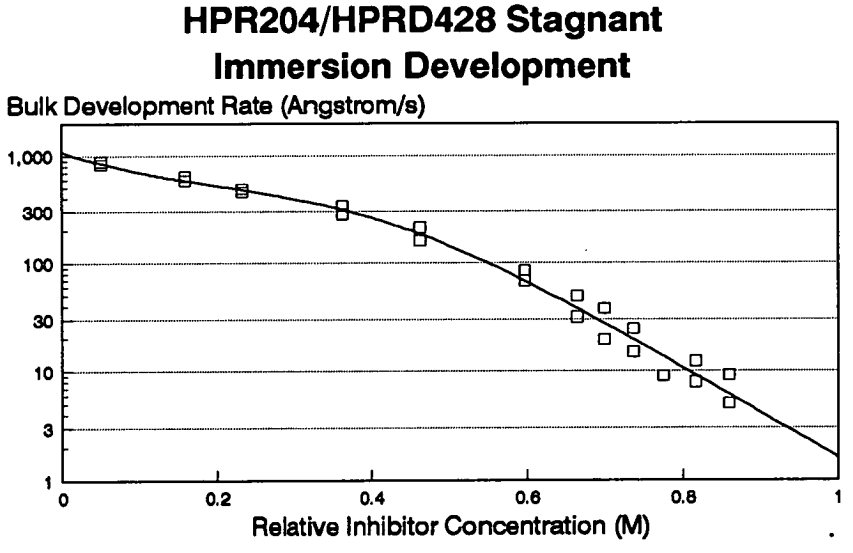

Figure 6–8: *Dissolution rate versus relative inhibitor concentration for the stagnant immersion development of HPR204 resist in HPRD428 developer under g-line exposure, as determined from TDRM data. Solid line indicates the 'best fit' of the 5 parameter modified Kim dissolution rate equation.*

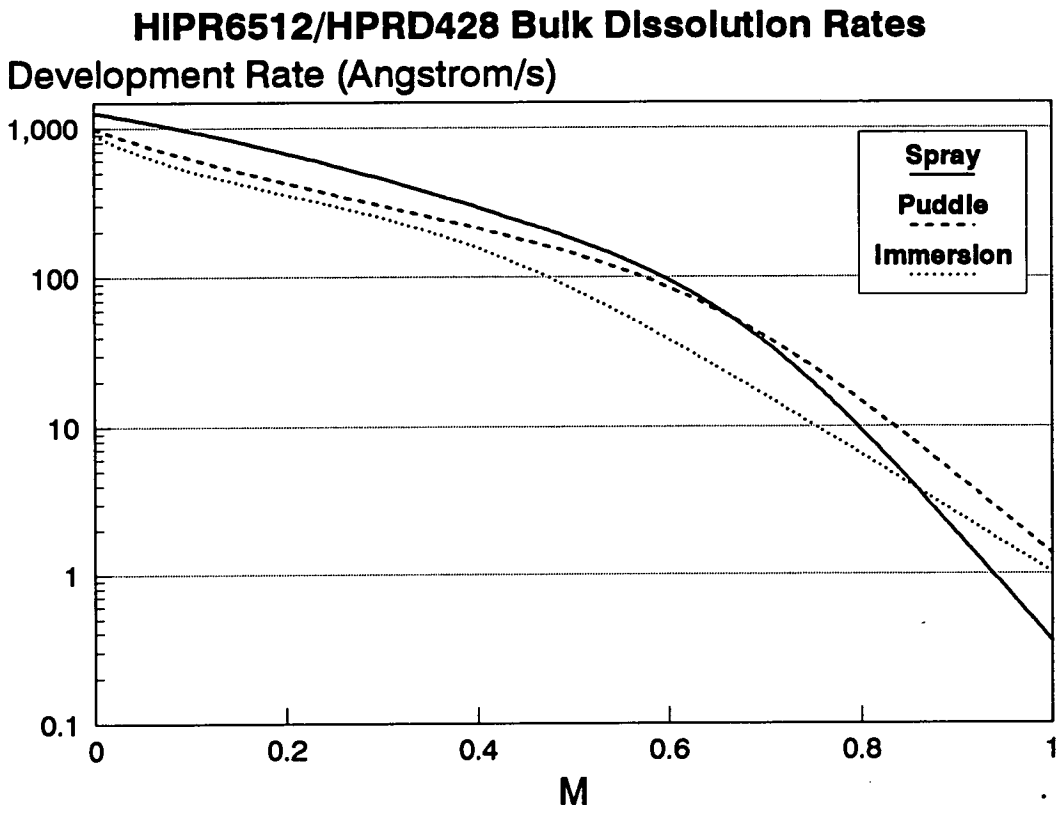

Figure 6–9: *Comparison of stagnant immersion, continuous spray and static puddle 'best fit' rate equations for HiPR6512 resist in HPRD428 developer.*

6.5.2 Discussion of the TDRM-derived rate equation parameters

Figures 6–9 and 6–10 compare the three modified Kim dissolution rate equation curves determined for the two resist/developer combinations. The most obvious feature of the graphs is the rate order of the three development processes. Continuous spray is faster than puddle which is in turn faster than stagnant immersion.

The only striking anomaly observed occurs in the low PAC conversion region of the HiPR6512 spray curve, where the predicted dissolution rates appear very low. This may be explained by the limited amount of experimental data used to characterise this region of the plot. During continuous spray processing a maximum develop time of 400 seconds per wafer was used (0.64 litre), in an effort to conserve developer. The rate estimation was therefore made over a reduced

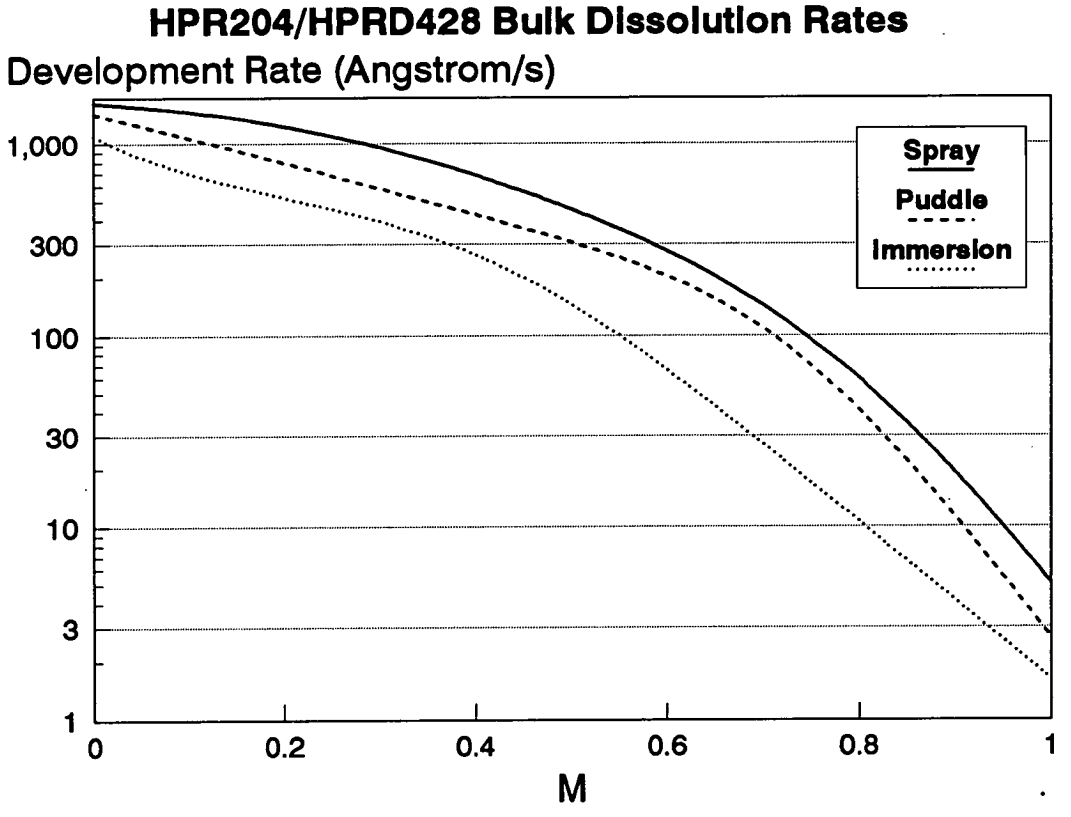

Figure 6–10: *Comparison of stagnant immersion, continuous spray and static puddle 'best fit' rate equations for HPR204 resist in HPRD428 developer.*

DRM Equipment	R_1 (Å/s)	R_2 (Å/s)	R_s	a	b
TDRM	907	1.028	8.2376	-0.67788	0.99574
Perkin-Elmer	1003	0.710	8.9515	-1.66190	0.99840

Table 6–4: *Modified Kim rate equation parameters as derived by the TDRM and Perkin-Elmer DRM systems for the stagnant immersion development of HiPR6512 resist in HPRD428 developer.*

portion of the bulk region (as little as 10% of the total thickness). This adds a degree of uncertainty into the average development rate fit and may have led to artificially low values. Further evidence presented in Section 6.7.2.4 supports the theory that the rates in this portion of the curve should be greater.

Examination of the respective curves and the exponential rate equation parameters, R_3, a and b (documented in Table 6–3), reveals a good correlation between the general shape of the curves for each development process. This suggests that each development process has, to some extent, a characteristic shape, at least in the case of the HPRD428.

6.5.3 Results from the Perkin Elmer DRM

6.5.3.1 Comparison with TDRM Immersion Results

Dissolution rates for the immersion development of HiPR6512 in HPRD428, under standard conditions were made by Hansen during early collaborative work.[118] Figure 6–11 illustrates the data points and 'best fit' 5 parameter Kim rate equation. Table 6–4 details the parameter values for this fit and compares them with the TDRM derived values. The TDRM fit is also included in Figure 6–11 to allow a visual comparison of the two rate equations. Excellent correlation is observed. This shows TDRM results are equivalent to those produced by 'accepted' commercial equipment, validating the equipment and measurement algorithms.

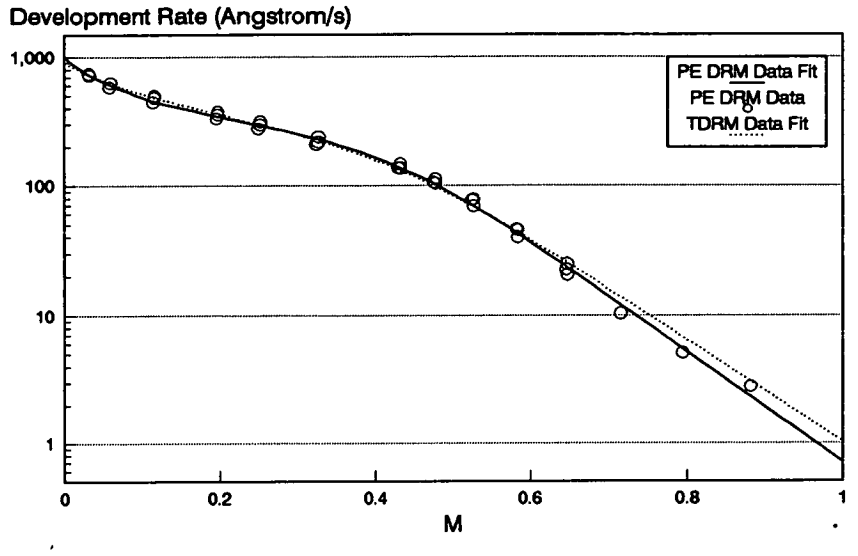

Figure 6–11: *The experimental dissolution rate versus relative inhibitor data points for HiPR6512 stagnant immersion development in HPRD428, as determined by a Perkin-Elmer DRM. The 'best fit' 5 parameter Kim rate equation is shown as is the TDRM-derived rate equation fit.*

A similar comparison was carried out for the HPR204/HPRD428 combination. Table 6–5 compares the 'best fit' dissolution rate equation parameters and Figure 6–12 compares the fits graphically with the Perkin-Elmer DRM data. Inspection of Figure 6–12 reveals that the development rate observed by the Perkin-Elmer DRM at low PAC conversions is considerably higher than that seen during the TDRM observations.

DRM Equipment	R_1 (Å/s)	R_2 (Å/s)	R_s	a	b
TDRM	1105	1.624	8.4409	-1.26437	0.99747
Perkin-Elmer	1097	4.529	5.6842	-5.43088	0.99990

Table 6–5: *Modified Kim Rate equation parameters as derived by the TDRM and Perkin-Elmer DRM systems for the stagant immersion development of HPR204 resist in HPRD428 developer.*

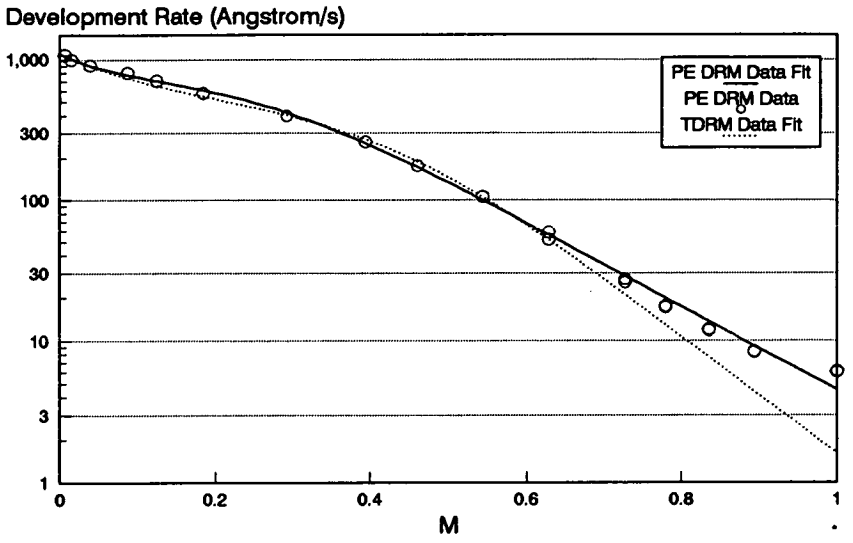

Figure 6–12: *The experimental dissolution rate versus relative inhibitor data points for HPR204 stagnant immersion development in HPRD428, as determined by a Perkin-Elmer DRM. The 'best fit' 5 parameter Kim rate equation is shown as is the TDRM-derived fit.*

The HPR204 Perkin-Elmer DRM experiments were carried out at the OCG Research Centre, East Providence utilising a GCA stepper. Investigation showed that the shutter control of this exposure tool was not sufficiently accurate to control the low exposure doses required in the HPR204 experiment. The lack of control resulted in higher than desired exposure doses. This problem was avoided in the TDRM experiments as the EMF's Optimetrix steppers have a 'POWER' command allowing the energy output of the lamp to be reduced. This increases the exposure time required for a given dose, reducing the effect of any shutter error.

Errors at low exposure doses were prevented during further Perkin-Elmer work by utilising a different exposure system. A filtered 'Oriel' UV lamp was used to expose the wafers through an 'Optoline' mask. This mask has 16 regions of different, known g-line transmission ranging from 2% to 96%. This configuration allowed superior low dose control during further Perkin-Elmer DRM experimentation.

DRM Equipment	R_1 (Å/s)	R_2 (Å/s)	R_s	a	b
Perkin-Elmer	764	1.469	10.9808	1.14984	0.97780
TDRM	988	1.376	11.6596	1.30580	0.97426

Table 6–6: *Modified Kim Rate equation parameters as derived by the TDRM and Perkin-Elmer DRM systems for puddle development and pseudo-puddle development, respectively, of HiPR6512 resist in HPRD428 developer.*

6.5.3.2 Pseudo-Puddle results

Table 6–6 details the rate equation parameters derived by the Perkin-Elmer DRM in pseudo-puddle mode for HiPR6512 with HPRD428. The TDRM puddle values are shown for comparison. Figure 6–13 shows the data points obtained and the 'best fit' rate equation. Again, the full TRDM puddle fit is shown for comparison. Neglecting the small divergence between the two fits at low M values, the agreement between the TDRM and Perkin-Elmer fits is excellent. This result would suggest that the pseudo-puddle process reflects the genuine SVG puddle process with reasonable accuracy.

6.5.3.3 'Fresh' Developer Immersion Results

The Perkin-Elmer DRM was run in standard stagnant immersion mode utilising fresh developer. Fresh developer from an unopened bottle was placed in the developer tank for each wafer. The developer was not preloaded with exposed resist and the wafer under study was inserted immediately after the developer was decanted. It was hoped that in each case little or no carbon dioxide neutralisation had occured and no loading effects were present. As there was no agitation, this scenario should be as close to the static puddle situation as possible, using immersion development.

Table 6–7 details the 'best fit' rate equation parameters to the data obtained and compares them with the values obtained for the standard DRM immersion

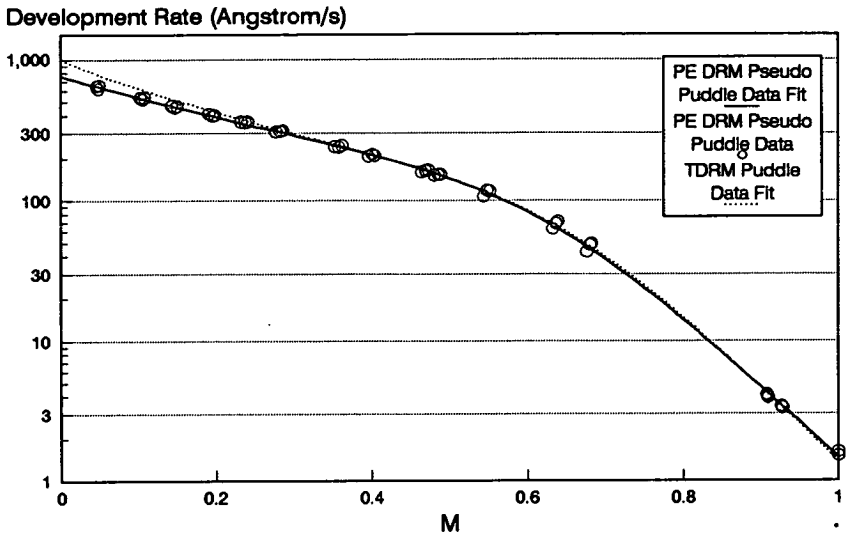

Figure 6–13: *The experimental dissolution rate versus relative inhibitor data points for HiPR6512 pseudo-puddle development in HPRD428, as determined by a modified Perkin-Elmer DRM. The 'best fit' 5 parameter Kim rate equation is shown as is the TDRM-derived fit.*

process, the pseudo-puddle process and the TDRM true puddle process. Figure 6–14 shows the data points and the 'best fit' rate equation. Figure 6–15 compares the data points with the standard immersion procedure results, highlighting the obvious discrepancy between these two data sets. Figure 6–16 shows the data set once again, this time comparing it to the pseudo-puddle rate equation and the TDRM puddle rate equation. It can be clearly seen that the 'fresh developer' stagnant immersion scenario is a fair approximation of a static puddle process and is quite different from the standard production type immersion process.

DRM Equipment	R_1 (Å/s)	R_2 (Å/s)	R_s	a	b
Perkin-Elmer 'fresh developer'	772	2.355	8.3932	0.15124	0.98520
Perkin-Elmer Standard immersion	1003	0.710	8.9515	-1.66190	0.99840
Perkin-Elmer Pseudo-puddle	764	1.469	10.9808	1.14984	0.97780
TDRM Puddle	988	1.376	11.6596	1.30580	0.97426

Table 6–7: *Modified Kim Rate equation parameters as derived by the Perkin-Elmer DRM and TDRM systems for 'fresh developer' immersion development, standard immersion development, pseudo puddle development and true puddle development of HiPR6512 resist in HPRD428 developer.*

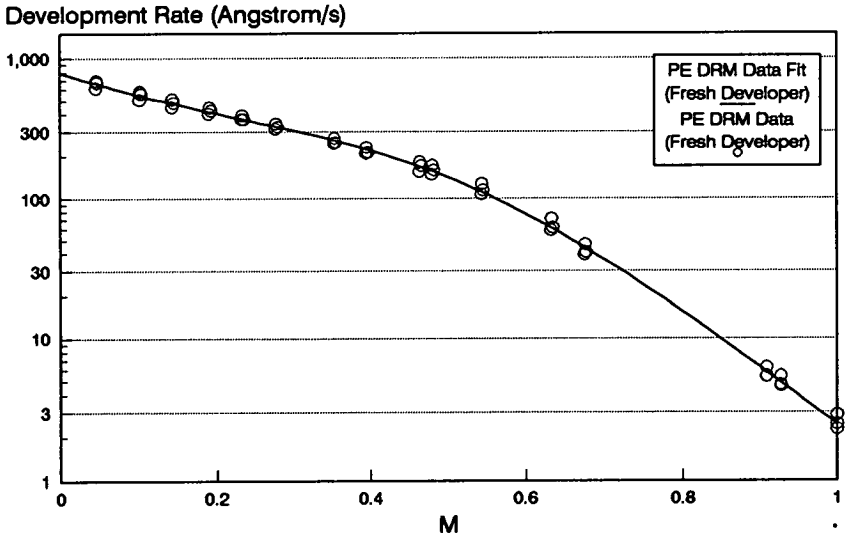

Figure 6–14: *The experimental dissolution rate versus relative inhibitor data points for HiPR6512 'fresh developer' stagnant immersion development in HPRD428, as determined by a Perkin-Elmer DRM. The 'best fit' 5 parameter Kim rate equation is illustrated.*

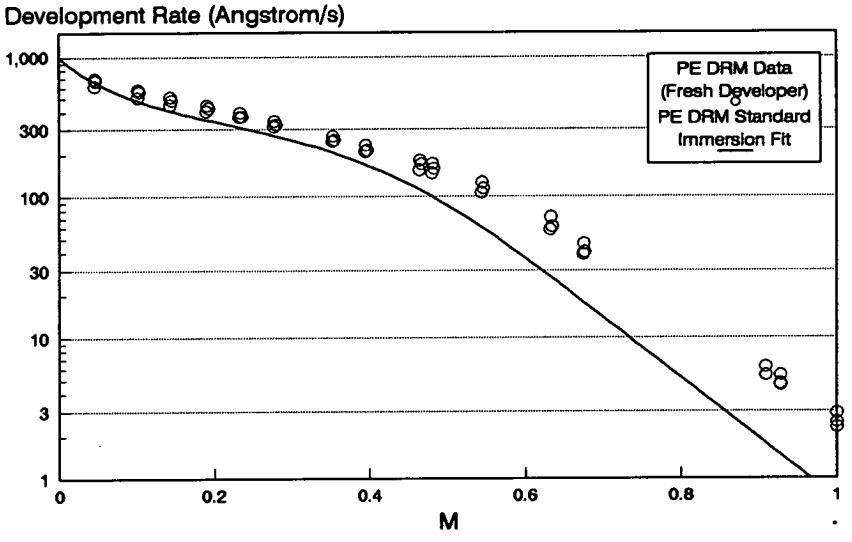

Figure 6–15: *The experimental dissolution rate versus relative inhibitor data points for HiPR6512 'fresh developer' stagnant immersion development in H-PRD428, as determined by a Perkin-Elmer DRM. The 5 parameter Kim rate equation for the standard Perkin-Elmer stagnant immersion process is overlaid for comparison.*

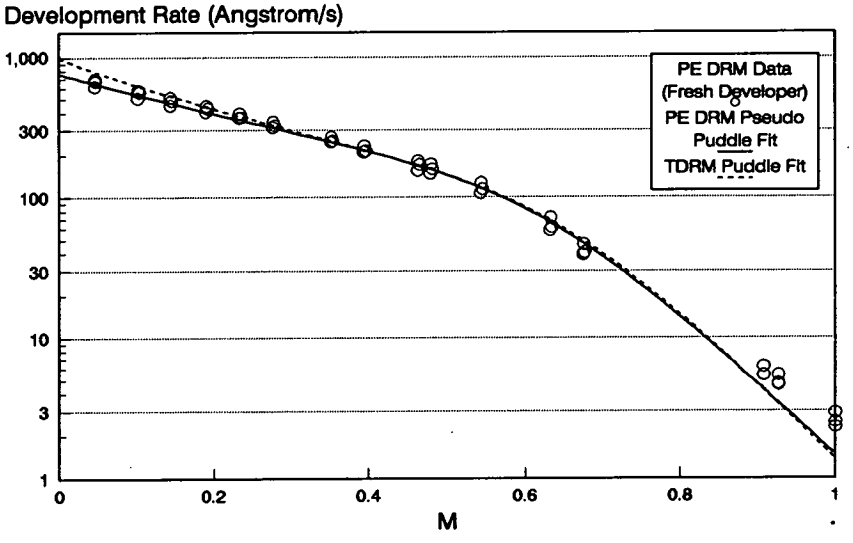

Figure 6–16: *The experimental dissolution rate versus relative inhibitor data points for HiPR6512 'fresh developer' stagnant immersion development in H-PRD428, as determined by a Perkin-Elmer DRM. The 5 parameter Kim rate equations for the Perkin-Elmer pseudo-puddle process and the TDRM true puddle process are overlaid for comparison.*

DRM Wavelength	R_1 (Å/s)	R_2 (Å/s)	R_s	a	b
700 nm	907	2.274	8.5764	0.52296	0.98415
632 nm	772	2.355	8.3932	0.15124	0.98520

Table 6–8: *Modified Kim Rate equation parameters as derived by the Perkin-Elmer DRM for 'fresh developer' immersion development of HiPR6512 resist in HPRD428 developer at operating wavelengths of 632nm and 700nm.*

6.5.3.4 Results from Modified (700nm) DRM

Only a single experiment was run with the Perkin-Elmer system modified to operate at 700nm, due to the tardy arrival of the filter. The process examined a 'fresh developer' process for HiPR6512. Table 6–8 shows the 'best' fit parameters for the derived data and compares them with those generated by the equipment when the standard 632nm filter was utilised. Figure 6–17 illustrates the data points graphically and the two rate equation fits. It can be seen that there is good agreement between the two data sets, as would be expected.

6.6 Parameter Confirmation

Since most dissolution data used for lithography simulation is derived from DRM output, it follows that an ability to replicate the original DRM output accurately using the simulation packages would be verification of the models and parameters used. The introduction of such a 'parameter confirmation' scheme allows the accuracy of modelling concepts and actual parameter values to be evaluated independently, and ensures that other simulation results are as realistic as possible.

None of the simulation packages detailed in Chapter 4, Section 4.7 can produce resist thickness versus development time output directly, so additional software was required to implement the 'parameters confirmation' technique.

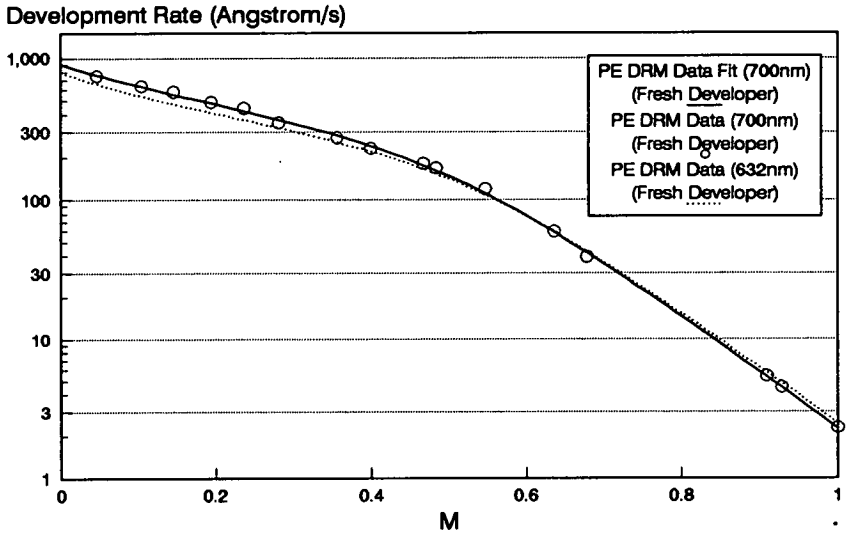

Figure 6–17: *The experimental dissolution rate versus relative inhibitor data points for HiPR6512 'fresh developer' stagnant immersion development in H-PRD428, as determined by a Perkin-Elmer DRM modified to operate at 700nm. The 5 parameter Kim rate equations for the standard (632.8nm) Perkin-Elmer case is overlaid for comparison.*

6.6.1 One Dimensional Lithography Simulation

Two programs, 'FILMLOSS' and '1D', both based around SAMPLE were written to generate the one dimensional, resist thickness versus time, plots necessary to simulate DRM output.

The '1D' program uses SAMPLE to calculate the PAC distribution following exposure and PEB in the central region of an open frame. This distribution, along with the calculated dissolution rate parameters, is used to calculate the development front's 'trajectory' to the substrate.

The second program, 'FILMLOSS', is similar to '1D', but uses complete SAMPLE calculations to generate the development front's progress to the substrate. Although this is considerably slower, it allowed verification of surface inhibition modelling as it is coded into SAMPLE.

6.6.2 Initial Results

Preliminary simulation work was based on recommendations by S.G.Hansen (OCG Microelectronic Materials).[118] The calculated dissolution rate equation parameters were used in conjunction with an assumed diffusion length of 0.08μm. Surface induction modelling was ignored, as the HiPR6512/HPRD428 combination was known to exhibit negligible surface induction.

The results obtained were very promising in that simulations of the three different development techniques gave distinct results which correlated with experimental lithographic results.[118]

However, when the 'FILMLOSS' program was used to compare the simulated and actual development front trajectories, significant differences were observed. Figure 6–18 shows a typical example. The figure illustrates the TDRM output for the puddle development of HiPR6512 after a 47.8mJcm^{-2} g-line exposure and the reconstruction of that output using the derived rate equation parameters (a standard SAMPLE simulation without surface induction using an assumed diffusion length of 0.08μm). Several inaccuracies can clearly be observed. Firstly, the

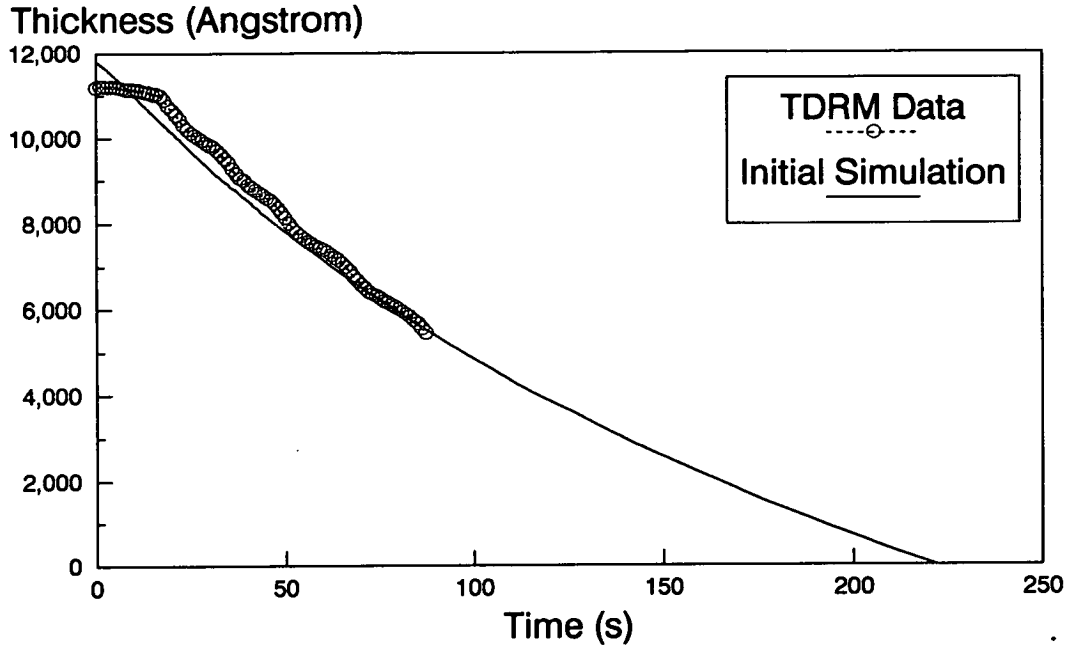

Figure 6–18: *A comparison between experimental dissolution measurements made by the TDRM and the simulated approximation of an identical situation.*

initial film thickness in the simulation is too great. Secondly, the experimental data shows much more evidence of residual standing wave activity, indicating that the simulation characteristic diffusion length is excessive. Finally, when compared to the simulation, it is obvious that the experimental data is exhibiting a signficant amount of induction during the initial stages of development. Derivation of appropriate surface induction parameters and a correct diffusion length coupled with a model refinement reflecting the densification during PEB should allow more relevant simulations to be made.

6.6.3 Film Shrinkage During PEB

The TDRM was used in a 'dry' mode to compare resist thickness before and after PEB processing. This indicated that significant film shrinkage, or densification, occurs during the PEB. An unexposed film the HiPR6512 lost around 5% of its

post-softbake thickness, whilst unexposed HPR204 lost around 2%, under the conditions described in Chapter2, Table 2–2.

Further investigation into the cause of the shrinkage attributed it to two separate effects. The first effect is solvent drive off at elevated temperature, with higher temperatures resulting in greater densification. The difference in the observed shrinkage between the two resists can therefore be attributed to the different solvent systems and the fact that the HiPR6512 process PEB temperature is some 10°C higher than that of the HPR204 process.

The second cause of PEB densification appears to be related to PAC breakdown during exposure. Physical measurement of a patterned resist coating after PEB, but prior to development, with a Sloan Dektak IIA reveals an aproximate 100Å delta between the exposed and unexposed regions.[242,243] The exact degree of shrinkage appears to be linked to the level of energy coupled into the film during exposure. This effect, though significant, is second order when compared to the solvent loss effect.

A possible explanation for this behaviour is that the photoproducts created by the breakdown of the inhibitor are smaller than the original PAC molecules and are able to rearrange themselves more compactly than the unconverted inhibitor molecules during the bake.

The '1D' program was modified to incorporate a simple PEB shrinkage model which assumes an isotropic compression of the PAC distribution. The 'FILMLOSS' program was also modified to incorporate this model. Unfortunately, the model could not be extended to full two dimensional SAMPLE simulations because of the complex nature of the simulation grid structure.

The model only incorporated the solvent loss aspect of resist densification and reduced the film thickness after PEB to a fixed percentage of the pre-exposure thickness. These percentages were experimentally determined as 94.7% of the initial thickness for HPR6512 and 97.8% for HPR204.

Failure to include the shrinkage effect means that additional quantities of re-

sist must be removed during the simulated development. This means that the predicted resist features are too large.

6.6.4 Diffusion Length (D_l) Estimation

Although the bulk averaged technique of generating rate equation parameters, described in Section 6.3, is independant of characteristic diffusion length, a few quick simulations reveal that the choice of D_l strongly influences a simulated thickness versus time graph.

Figure 6–19 illustrates the effect of the diffusion length on the ampltude of the standing wave effects and the dose-to-clear when all other variables are held constant. Two extreme cases are shown, firstly where no diffusion has occurred (i.e. $D_l = 0.00\mu m$) and secondly where all trace of the standing waves has been baked out ($D_l = 0.08\mu m$). A third midpoint ($D_l = 0.04\mu m$) is also included to indicate the non-linearity in the response of E_0 and the standing wave damping.

Figure 6–20 indicates the significant impact on the thickness versus time curve of even modest changes in diffusion length. A 15% change in E_0 is apparent in the example shown. The three traces are typical of moderate PEB processes where some evidence of standing wave behaviour is still visible.

The '1D' program was used to simulate TDRM output, utilising the shrinkage model described in Section 6.6.3. The diffusion length was varied until traces parallel to the experimental data were obtained. The parallel nature indicates that bulk behaviour is well modelled. The offset between the TDRM data and the simulation is due to surface induction effects.

It was found that a D_l value of $0.05\mu m$ yielded the best simulated dissolution curves for both resist systems. Figure 6–21 shows the simulated dissolution front trajectory for the exposure dose used in Figures 6–19 and 6–20 using a diffusion length of $0.05\mu m$ and experimental TDRM data. Excellent correlation is observed.

As the diffusion length should only be dependent on the resist type and thermal processing, verification of the correct value is confirmed by the good agreement

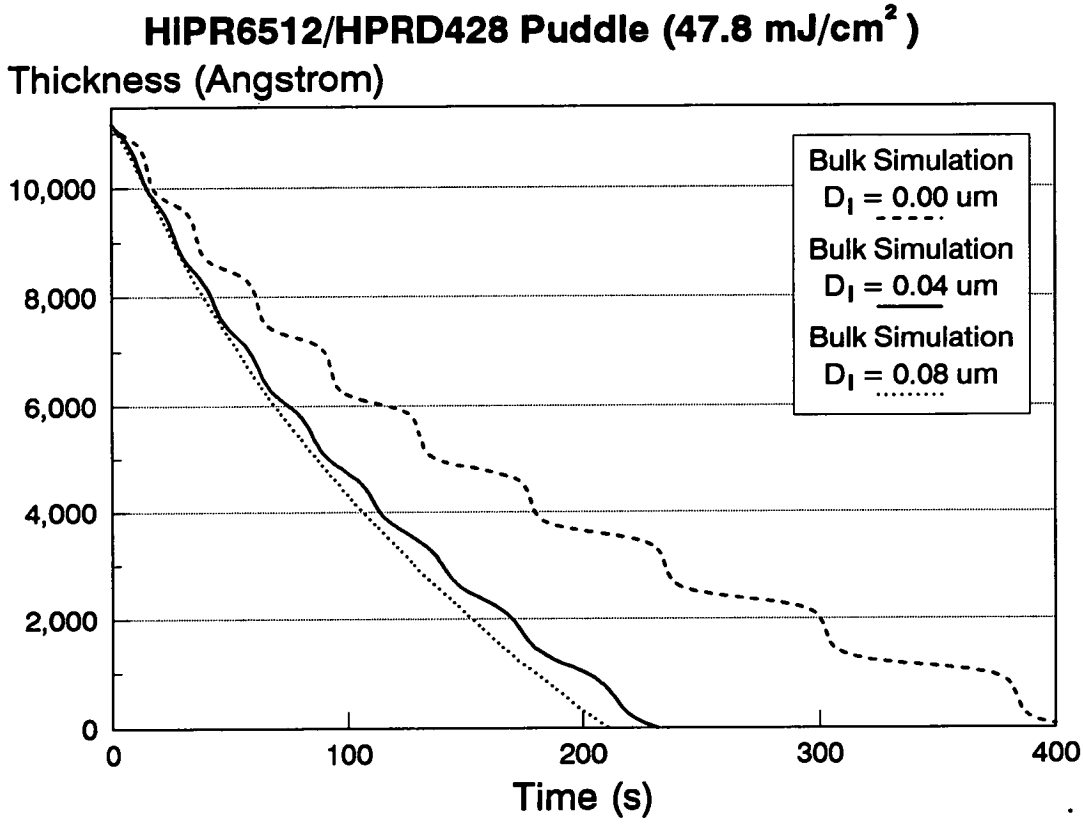

Figure 6–19: *Simulated DRM output utilising characteristic diffusion lengths (labelled* D_l*) of 0.00* μm*, 0.04* μm *and 0.08* μm.

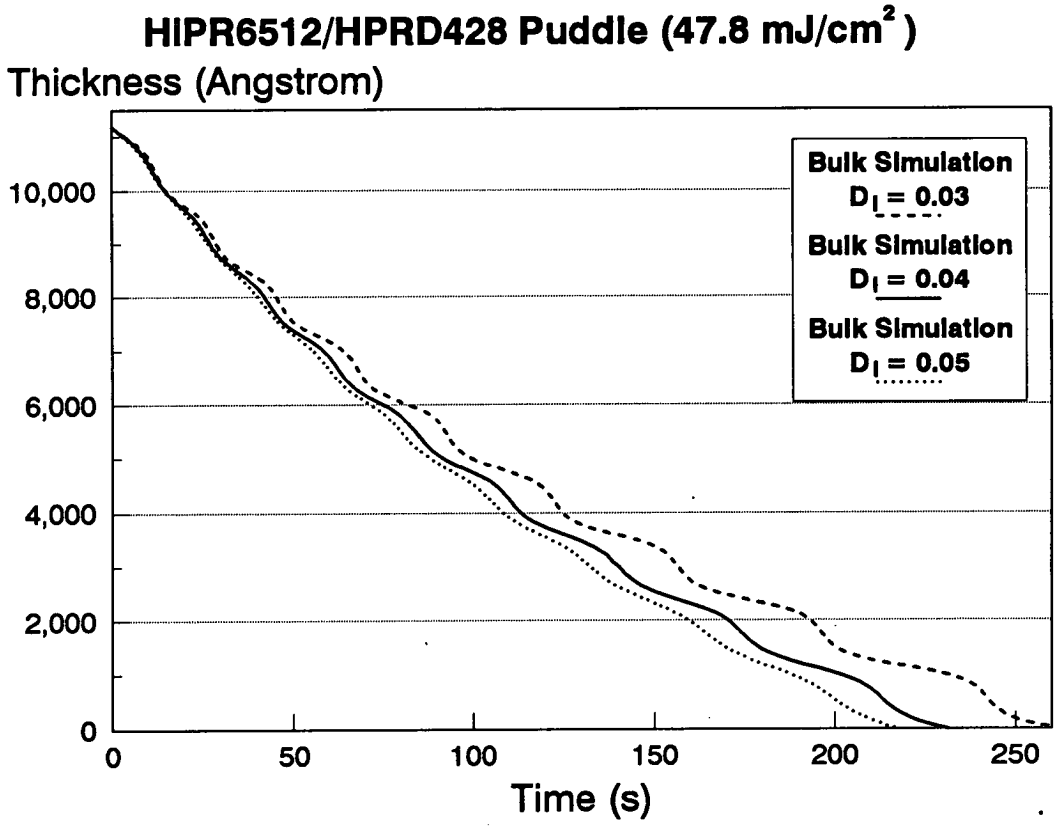

Figure 6–20: *Simulated DRM output utilising characteristic diffusion lengths (labelled* D_l*) of 0.03* μm*, 0.04* μm *and 0.05* μm.

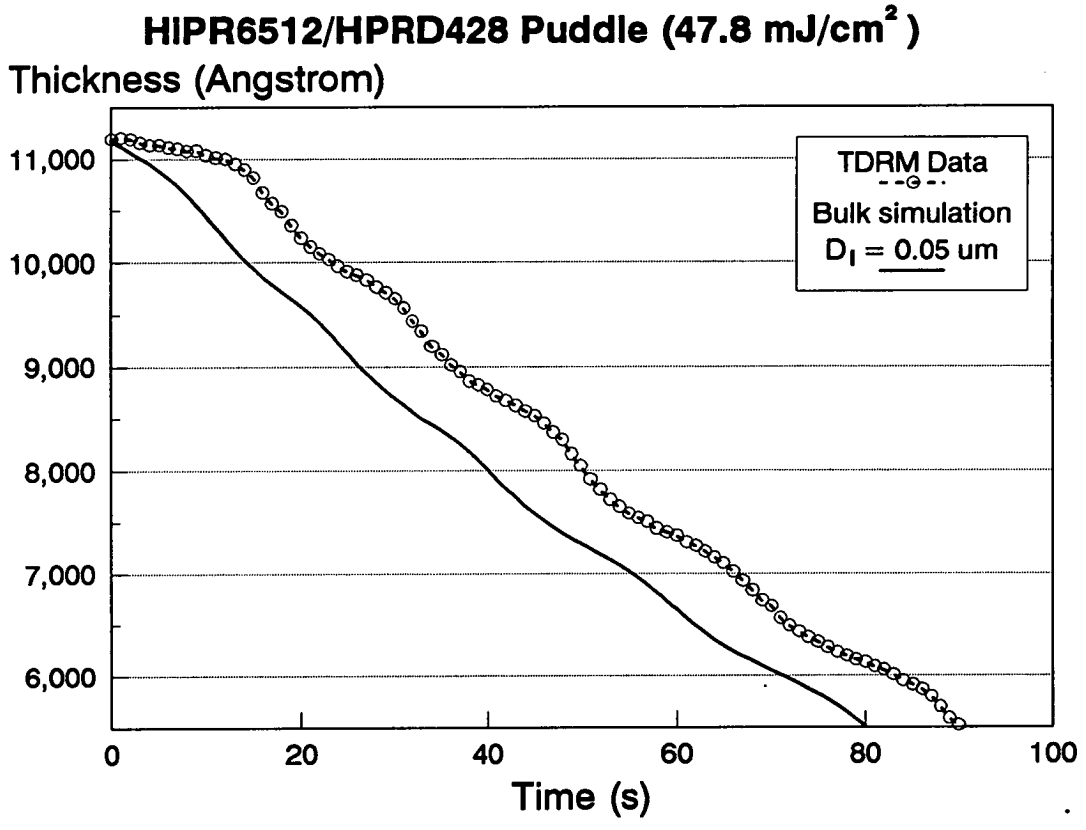

Figure 6–21: *A comparson of TDRM dissolution data and a bulk simulation utilising a characteristic diffusion length of 0.05μm for the puddle development of HiPR6512 in HPRD428.*

between the simulations and the experimental data for all three development techniques. Figure 6–22 illustrates how the bulk behaviour of the puddle dissolution of HPR204 in HPRD428 is well described over a wide range of exposures using a diffusion length of 0.05μm and the bulk rate parameters detailed in Table 6–3. Again, the figures show that surface induction modelling is necessary for accurate simulation of dissolution behaviour, even with these resists which reportedly exhibit negligible inhibition effects.

Inspection of Figures 6–21 and 6–22 shows that the level of residual standing wave activity visible in the simulations and experimental data is comparable.

6.7 Surface Induction Modelling

Careful inspection of the complete TDRM output for both resist/developer combinations shows that the depth at which full bulk behaviour is exhibited is independent of both exposure and development process. This indicates that the exponentially increasing model proposed by Kim[187] should be appropriate.

6.7.1 The Kim Model

As detailed in Chapter 4, Section 4.6.3.2, Kim proposed that a multiplier function can be used in conjunction with the bulk rate equation to describe surface induction. The development rate at a given depth, z, is given by

$$\mathrm{Rate(z,M)} = \mathrm{f(z,M)R_{bulk}(M)} \tag{6.1}$$

The induction multiplier function, f(z,M), can be split into separate functions of z and M, since the inhibition depth is independent of exposure. An increasing exponential was chosen as the z function yielding an induction multiplier of the form

$$\mathrm{f(z,M)} = 1 - (1 - \mathrm{f(0,M)})e^{-\frac{z}{R_L}} \tag{6.2}$$

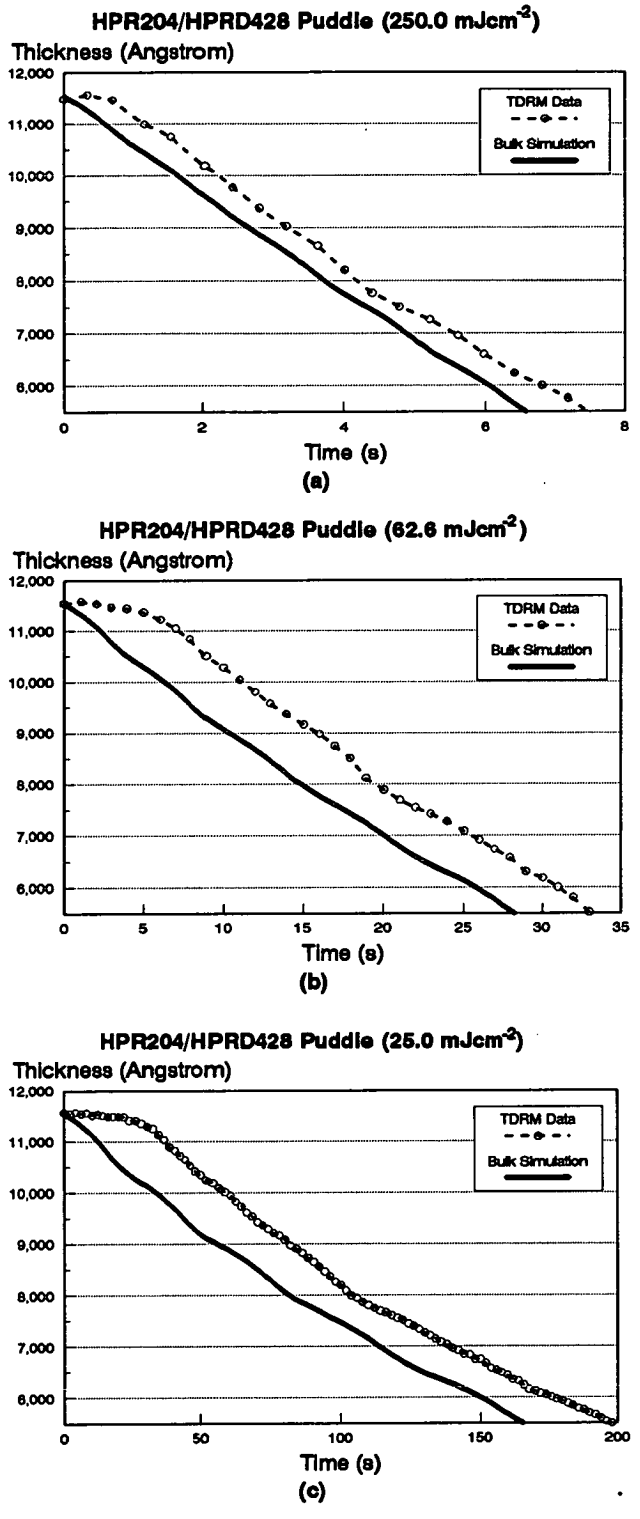

Figure 6–22: *Experimental data and equivalent simulations for the puddle development of HPR204 in HPRD428 at three different exposure energies.*

where f(0,M) is a function describing the ratio of surface to bulk dissolution rates and R_L is a characteristic induction length.

Attempts to fit this function to the experimental data were successful, in that the exponential z function fitted all the data well with a constant R_L value for each resist. Unfortunately, the f(0,M) values required seemed very erratic and did not fit the linear function proposed by Kim or the single value proposed by Mack.

6.7.2 A New Surface Induction Model

Careful consideration of the Kim multiplier function (Equation 6.2), the TDRM output and one dimensional bulk parameter simulations allow a new multiplier function to be derived using the general form proposed by Kim but with a novel f(0,M) function.

6.7.2.1 Derivation of f(0,M)

Dill stated that in a uniformly exposed film, with fraction M of the inhibitor remaining, the time taken to reach a given depth, d, could be calculated by the integral[162]

$$t(M,d) = \int_0^d \frac{dz}{R(M)} \tag{6.3}$$

In the case of a bulk rate simulation this can be evaluated quite simply:

$$t(M,d) = \int_0^d \frac{1}{R_{bulk}(M)} dz \tag{6.4}$$

$$= \frac{1}{R_{bulk}(M)} \int_0^d 1 dz \tag{6.5}$$

$$= \frac{1}{R_{bulk}(M)} [z]_0^d \tag{6.6}$$

$$= \frac{d}{R_{bulk}(M)} \tag{6.7}$$

The induction layer can be thought of as a 'skin' of thickness 's', where 's' is the depth from the initial resist surface at which full bulk dissolution behaviour is first exhibited. The value of this depth can be determined from experimental data (see Section 6.7.2.2).

The function t(M,s) will be defined as the time taken to reach depth 's' in a film with a uniform inhibitor distribution of M. A second function, $t_a(M,s)$, can be defined as the time a *bulk rate simulation* takes to reach depth 's' assuming a uniform inhibitor distribution and is given by

$$t_a(M,s) = \frac{s}{R_{bulk}(M)} \tag{6.8}$$

Addition of the Kim surface inhibition multiplier makes the solution to Equation 6.3 more complex

$$t(M,d) = \int_0^d \frac{1}{R(M,z)} dz \tag{6.9}$$

$$= \frac{1}{R_{bulk}(M)} \int_0^d \frac{1}{1 - [1 - f(0,M)]\, e^{-\frac{z}{R_L}}} dz \tag{6.10}$$

$$= \frac{\left[R_L.\log_e[e^{\frac{z}{R_L}} + f(0,M) - 1] + C\right]_0^d}{R_{bulk}(M)} \tag{6.11}$$

$$= \frac{R_L \left[\log_e[e^{\frac{d}{R_L}} + f(0,M) - 1] - \log_e[f(0,M)]\right]}{R_{bulk}(M)} \tag{6.12}$$

If a further function, $t_b(M,s)$, is defined as the time taken to reach depth 's', for a *simulation using full Kim inhibition modelling*, again assuming a uniform inhibitor distribution, then is value is given by

$$t_b(M,s) = \frac{R_L\left[\log_e[e^{\frac{s}{R_L}} + f(0,M) - 1] - \log_e[f(0,M)]\right]}{R_{bulk}(M)} \tag{6.13}$$

The TDRM plots indicate that the surface induction is very strong over a thin region near the resist surface and decays rapidly with depth. It is therefore possible to assume that there is very little change in the PAC concentration over the inhibition region. As the effects of the formula derived from Equations 6.3 to 6.13 will only affect the thin surface region, the condition of uniform M can be considered true.

An accurate estimation of t_a(M,s) and t_b(M,s) can be made from examination of the *TDRM data* and *equivalent bulk dissolution simulation*, respectively. The time taken to reach depth 's' in an exact simulation must be identical to that in the experimental data, i.e., t(M,s) equals $t_a(M,s)$.

The time taken to reach depth 's' can be plotted against the surface M level, as determined by SAMPLE. Figure 6–23 plots the time HPRD428 takes to remove 800Å of HPR204 in a puddle process against surface M, as determined (a) from *experimental TDRM data* and (b) from *bulk parameter '1D' simulations.* It was found that these data sets could be approximated by the function

$$t(M,s) = A(1-M)^{-B} \tag{6.14}$$

Unfortunately, this function is discontinuous when M equals one. Substituting (1.0001 - M) into the equation, has neglegible effect on the accuracy of the output value but renders it valid for all possible M values. The times, t_a(M,s) and t_b(M,s), can now be described as

$$t_a(M,s) = R_a(1.0001 - M)^{-R_b} \tag{6.15}$$

and

$$t_b(M,s) = R_c(1.0001 - M)^{-R_d} \tag{6.16}$$

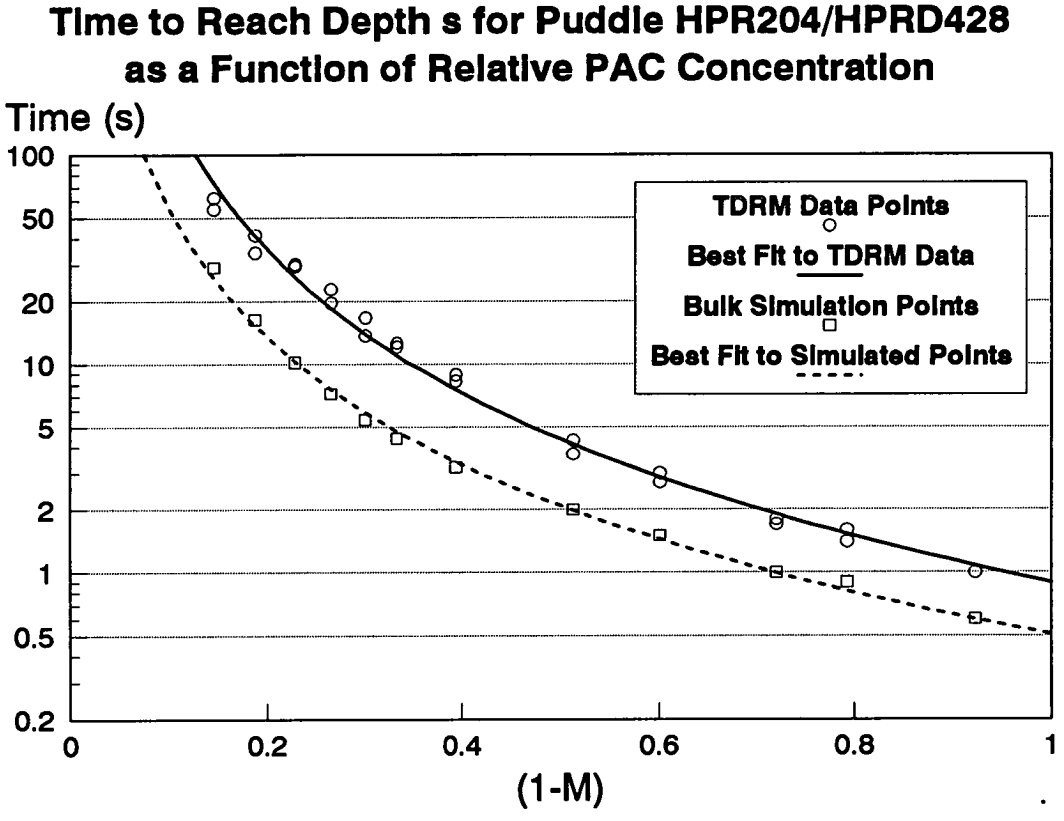

Figure 6–23: *Example of fitting the function* $A(1 - M)^{-B}$ *to TDRM and bulk simulation data.*

Although $t_a(M,s)$ can be calculated directly by dividing 's' by the bulk rate equation, it was found that estimating it in the manner above led to a less complex description of f(0,M), which in turn considerably reduces the time required for development simulation.

If u(M) is defined as the ratio of $t_a(M,s)$ to $t_b(M,s)$ then equations 6.15 and 6.16 can be divided to obtain

$$u(M) = \frac{t_a(M,s)}{t_b(M,s)} = \frac{R_a(1.0001 - M)^{-R_b}}{R_c(1.0001 - M)^{-R_d}} \tag{6.17}$$

$$= \frac{R_a}{R_c}(1.0001 - M)^{(R_d - R_b)} \tag{6.18}$$

From Equation 6.18 it is obvious that u(M) can be described using only two parameters. These two values shall be defined as R_A and R_B and are equal to $\left(\frac{R_a}{R_c}\right)$ and $(R_d - R_b)$, respectively. u(M) now simplifies to

$$u(M) = R_A(1.0001 - M)^{R_B} \tag{6.19}$$

An alternative expression for u(M) can also be obtained by dividing Equation 6.8 by Equation 6.13

$$u(M) = \frac{\left(\frac{S}{R_{bulk}(M)}\right)}{\left(\frac{R_L.\left[\log_e[e^{\frac{S}{R_L}} + f(0,M) - 1] - \log_e[f(0,M)]\right]}{R_{bulk}(M)}\right)} \tag{6.20}$$

This expression can be manipulated to give the surface to bulk ratio function, f(0,M), in terms of u(M).

$$u(M) = \frac{S}{R_L.\left[\log_e[e^{\frac{S}{R_L}} + f(0,M) - 1] - \log_e[f(0,M)\right]} \tag{6.21}$$

$$\Rightarrow \frac{S}{u(M)R_L} = \log_e[e^{\frac{S}{R_L}} + f(0,M) - 1] - \log_e[f(0,M)] \tag{6.22}$$

$$=> e^{\left(\frac{s}{u(M)R_L}\right)} = \frac{e^{\frac{s}{R_L}} + f(0,M) - 1}{f(0,M)} \tag{6.23}$$

$$=> f(0,M) = \frac{e^{\left(\frac{s}{R_L}\right)} - 1}{e^{\left(\frac{s}{u(M)R_L}\right)} - 1} \tag{6.24}$$

f(0,M) can now be defined using Equations 6.19 and 6.24. Surface induction can be fully described once values for 's' and R_L are determined.

6.7.2.2 Derivation of S and R_L

The depth 's' at which full bulk dissolution behaviour is observed in the experimental data can be estimated by comparing the TDRM data with the bulk parameter simulations, such as the case shown in Figures 6–21 and 6–22.

Inspection of Equation 6.2 reveals that f(s,M) should equal one, if true bulk behaviour is to be exhibited. However, to meet this condition R_L would have to tend to zero, unless f(0,M) is equal to one, It was decided that the exponential term, $e^{-\frac{z}{R_L}}$, should be 0.01 at 'z' equals 's'. This guarantees that the dissolution rate at this depth must be in excess of 99% of the bulk rate and also allows the determination of R_L.

$$e^{-\frac{s}{R_L}} = 0.01 \tag{6.25}$$

$$=> -\frac{s}{R_L} = \log_e(0.01) = -4.60517 \tag{6.26}$$

$$=> R_L = \frac{s}{4.60517} \tag{6.27}$$

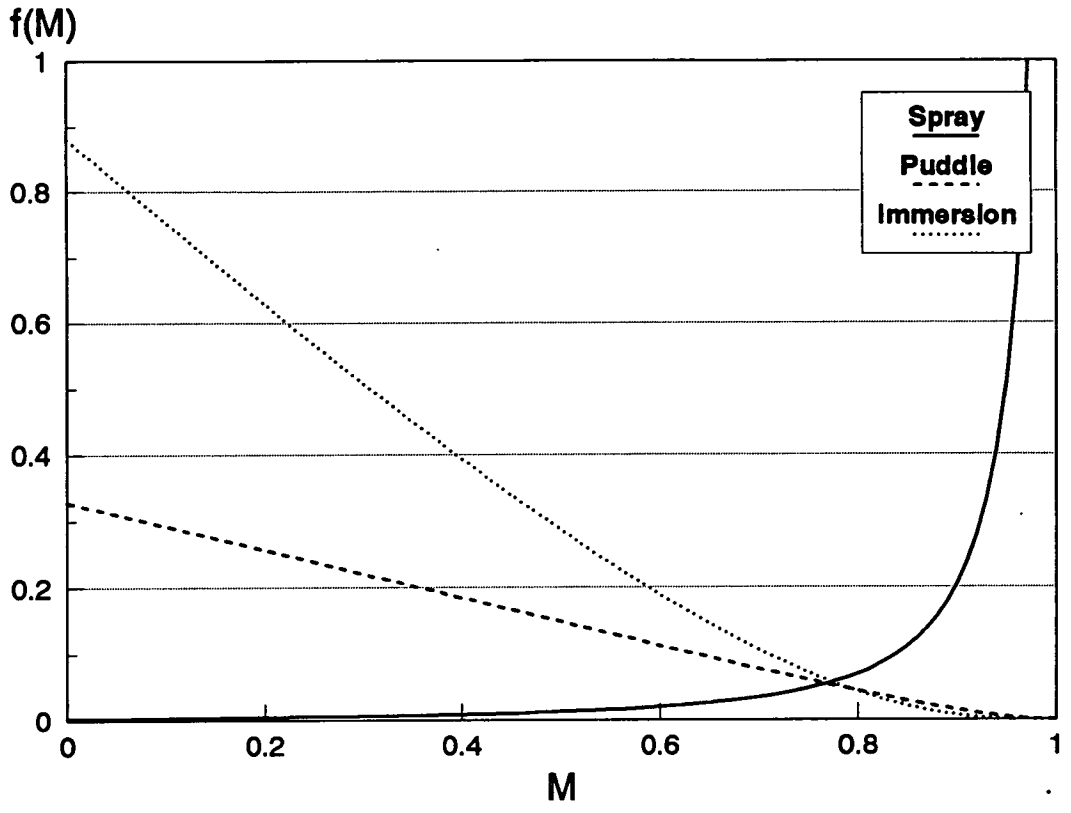

Figure 6–24: *Plots of f(0,M) for HiPR6512 in HPRD428.*

6.7.2.3 Results from Actual TDRM data

Surface induction can therefore be completely described using equations 6.2, 6.19, 6.24 and 6.27, with the parameters R_A, R_B and 's' being taken from a comparison of actual TDRM data and bulk rate simulations of that data.

R_A, R_B and 's' were determined for each of the six processes investigated with the TDRM and are detailed in Table 6–9. The characteristic induction length, R_L inferred from 's' is also tabulated. Figures 6–24 and 6–25 graphically illustrate the function f(0,M) for each process over the full PAC conversion range.

6.7.2.4 Discussion of the Surface Inhibition Parameters

Inspection of Table 6–9 and Figures 6–24 and 6–25 reveals that once again the behaviour of the HiPR6512 spray process differs from the that of the five other

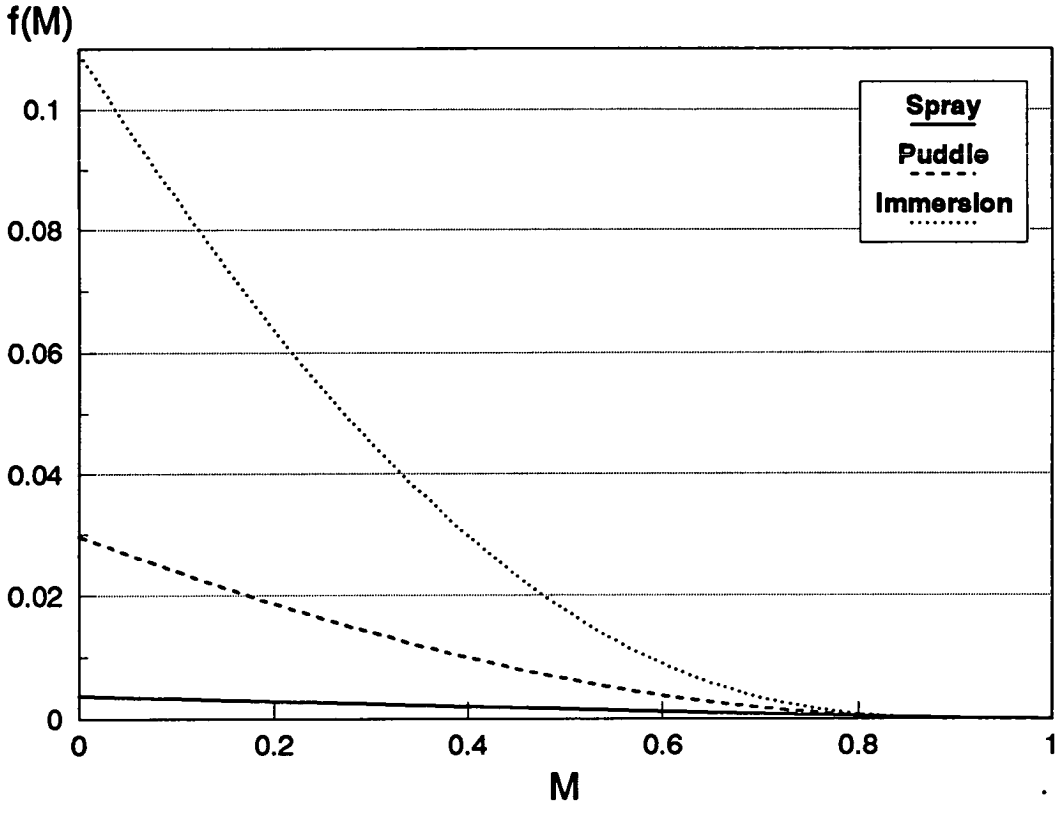

Figure 6–25: *Plots of f(0,M) for HPR204 in HPRD428.*

Resist	Process	s (Å)	R_L (Å)	R_A	R_B
HiPR6512	Spray	1100	238.9	0.438069	-0.230262
	Puddle	1100	238.9	0.806009	0.186852
	Immersion	1100	238.9	0.973364	0.306139
HPR204	Spray	800	173.7	0.451895	0.119075
	Puddle	800	173.7	0.567486	0.247592
	Immersion	800	173.7	0.676361	0.342558

Table 6–9: *Experimentally determined surface inhibition parameters*

processes. The fact that the f(0,M) function produces values greater than one at high M values shows that the predicted bulk dissolution rates require surface enhancement to allow the development front to reach depth 's' in the expected time. This adds further weight to the argument that the rate equation for the HiPR6512 spray process is in error at low PAC conversions.

Despite this apparent error, Figures 6–24 and 6–25 clearly illustrate a trend in the relative inhibition of the three development techniques. In the case of both resists, the immersion process is the one which exhibits the least retardation (i.e. f(0,M) closest to one) and the spray the most.

Several of the results also suggest that the straight line function originally proposed by Kim would be adequate to describe them.

It is worth noting that the induction lengths obtained during this study are an order of magnitude less than those presented by Kim. While this may be due to differences in resist chemistry and processing, the TDRM output indicates that the inhibition region is much thinner than was previously believed and that the initial level of inhibition is high but decays very quickly.

6.7.2.5 Implementation of the Model in SAMPLE

The IBM PC version of SAMPLE v1.7a was modified so that f(0,M) could be specified using the new function. Initial results from the 'FILMLOSS' program showed that the level of surface inhibition present in SAMPLE simulations was much greater than expected.

As previously discussed in Chapter 4, Section 4.7.1 SAMPLE simulates development using small development time increments. The program assumes that the development rate remains constant for the duration of each time step. In a bulk rate simulation this approximation is valid, but when surface inhibition is introduced the instantaneous rate demonstrates a very strong depth dependence. The exponential rise of the inhibition expression f(z,M) requires constant recalculation until it approaches unity. While SAMPLE has been designed to simulate surface

inhibition using the induction lengths observed by Kim, the time increments used are not sufficiently short for the induction lengths observed during this work.

A simple example can illustrate that the apparent excess surface inhibition is caused by insufficient recalculation of the inhibition modifier.

Figure 6–26 illustrates three separate simulations of an HPR204/HPRD428 spray development process, assuming a g-line exposure of 50.1 $mJcm^{-2}$, and actual TDRM data for this exposure. In each simulation the dissolution rate has been recalculated after a fixed depth of resist has been removed. The trace exhibiting the most inhibition was recalculated every 14.6Å and is quite clearly wrong. The second curve has twice as many recalculations (every 7.3Å) and is still incorrect but a definite improvement. The final curve was calculated using a further ten-fold increase in the number of calculations (every 0.73 Å) and is beginning to approach the experimental data. This demonstrates that the recalculation rate of the inhibition expression near the resist surface is critical.

While such a decrease in the iteration step size during development is simple to implement in the '1D' program, a rewrite of the highly complex dissolution module of SAMPLE was beyond the scope of this project. Fortunately, an alternative solution was found.

It was empirically discovered that a compensation factor, χ, could be introduced to the description of f(0,M) in the following manner

$$=> \; f(0,M) \; = \; \frac{e^{\left(\frac{S}{\chi R_L}\right)} \; - \; 1}{e^{\left(\frac{S}{\chi U R_L}\right)} \; - \; 1} \tag{6.28}$$

If χ is set to two, f(0,M) is increased in such a way that the level of surface inhibition exhibited by SAMPLE for all six resist/developer systems is approximately correct for the complete spread of exposure doses investigated. It should be noted that only the f(0,M) term is adjusted, the induction length used remains constant. Figure 6–27 illustrates two output data sets from the 'FILMLOSS' program; the first is without compensation and the other uses a χ factor of 2. The compensated simulation is obviously a better match to the experimental TDRM data.

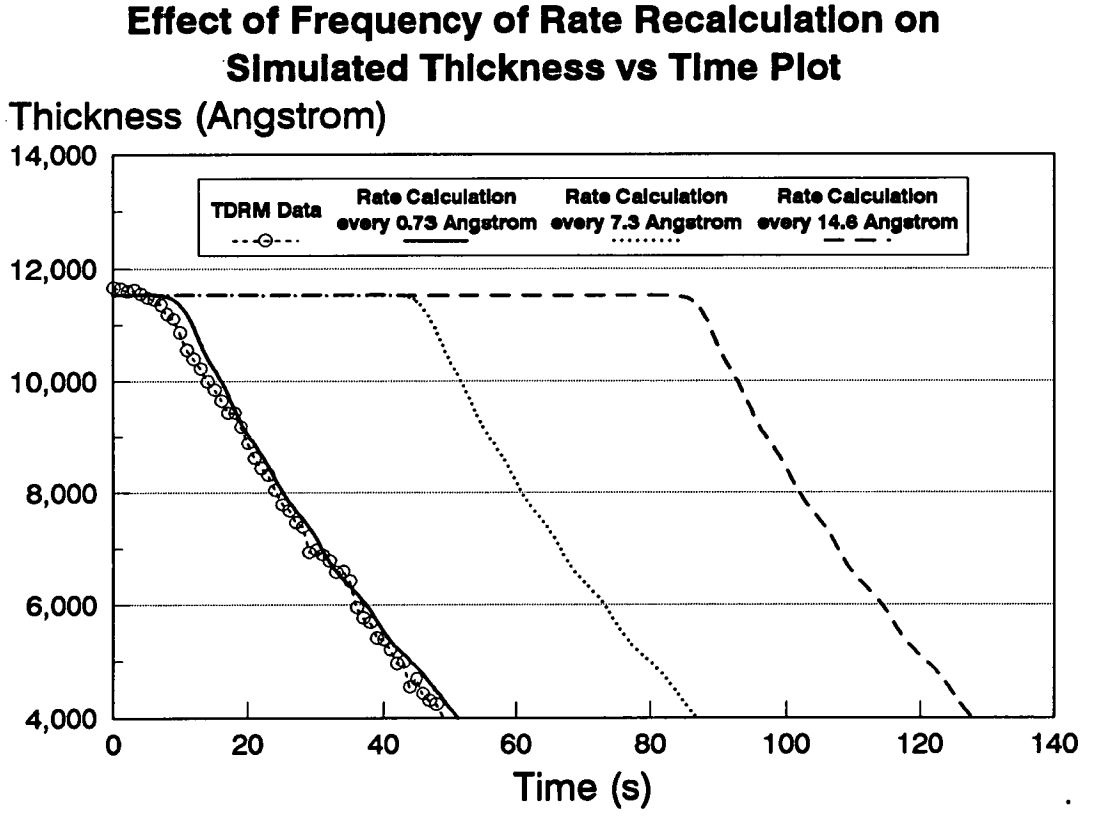

Figure 6–26: *Illustration of the variation in apparent surface inhibition caused by changes in the number of rate recalculations.*

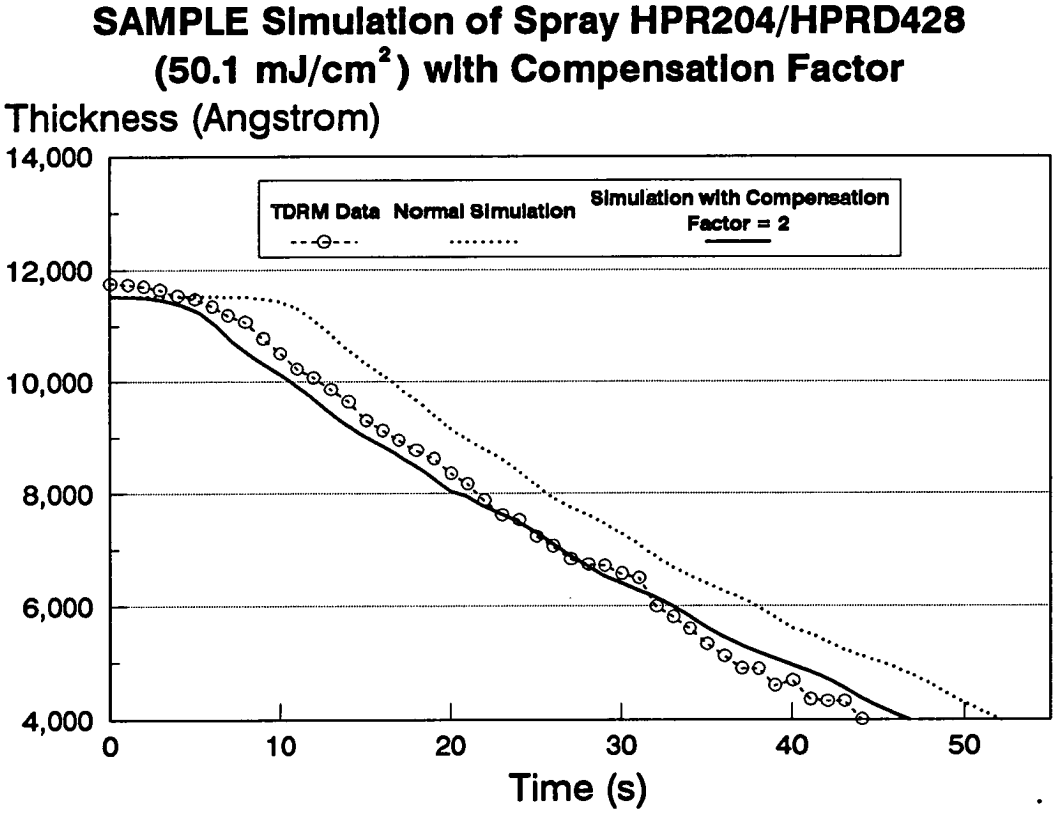

Figure 6–27: *Comparison of experimental TDRM data, a standard SAMPLE simulation and one using a χ value of 2.*

Inspection of how χ alters the value of f(0,M) reveals that a value of 2 is roughly eqivanlent to raising the standard value to the power of $\frac{1}{1.887}$, i.e. a slightly higher than the square root of the true f(0,M) value. The precise value of the reciprocal alters; it is slightly lower at M equals zero and slightly higher at M equals one.

6.7.3 Confirmation of Experimental Results and Model Enhancements

Figures 6–28 and 6–29 compare all the TDRM experimental data for the HiPR6512 puddle process with simulations utilising all the aforementioned modelling. Excellent correlation is seen across the entire range of exposures. Figures 6–30 and 6–31 show results from the HPR204 immersion process and the HiPR6512 spray process which were typical of the others. Again very good correlation is observed between the experimental data and the simulations. The excellent agreement between simulations and experimental data across all six processes investigated suggests that the models used and the parameter values generated are sufficient for accurate quantitive modelling of realistic development processes.

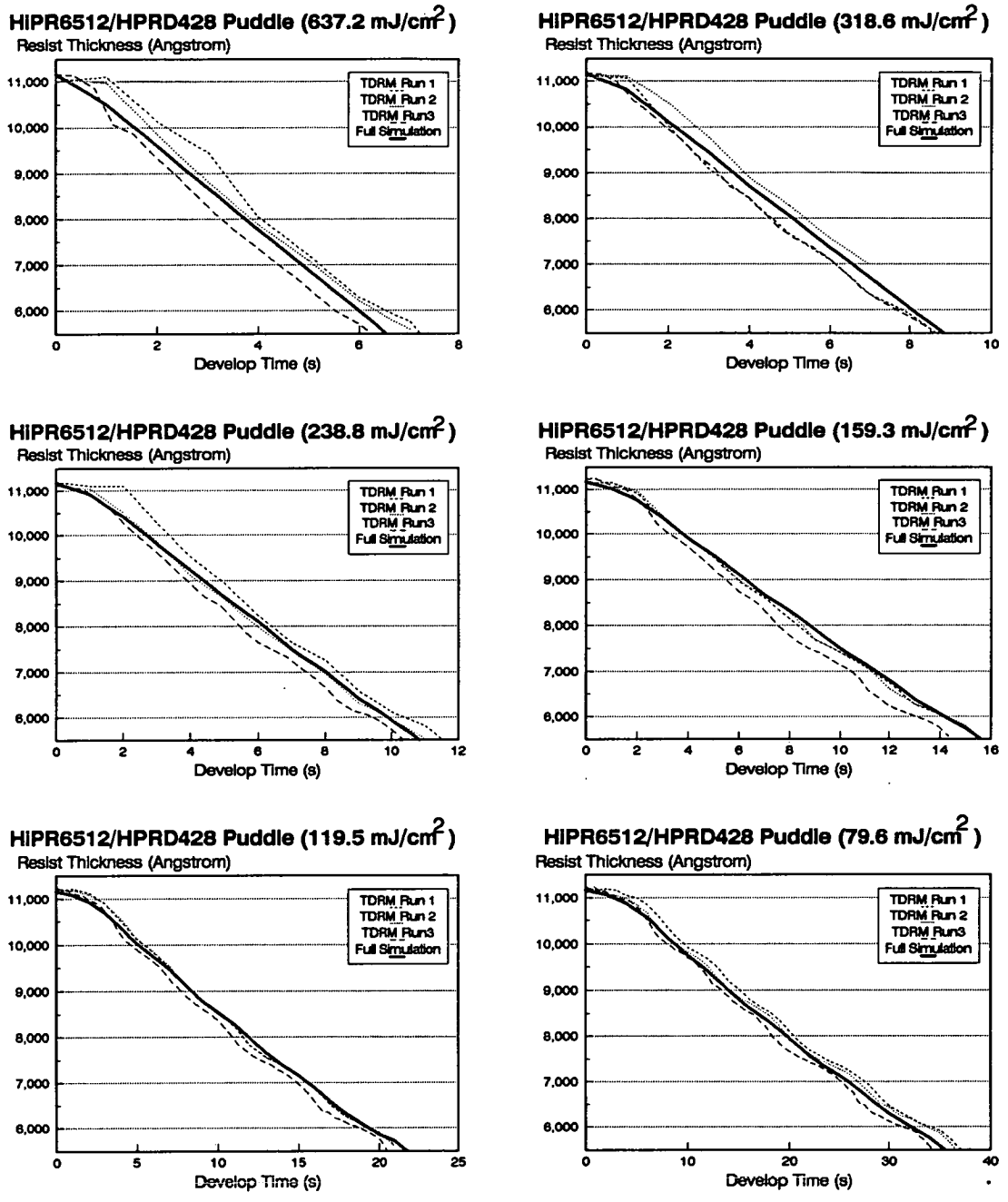

Figure 6–28: *Comparison of experimental data and full model simulations for the puddle development of HiPR6512 in HPRD428 at high exposure doses.*

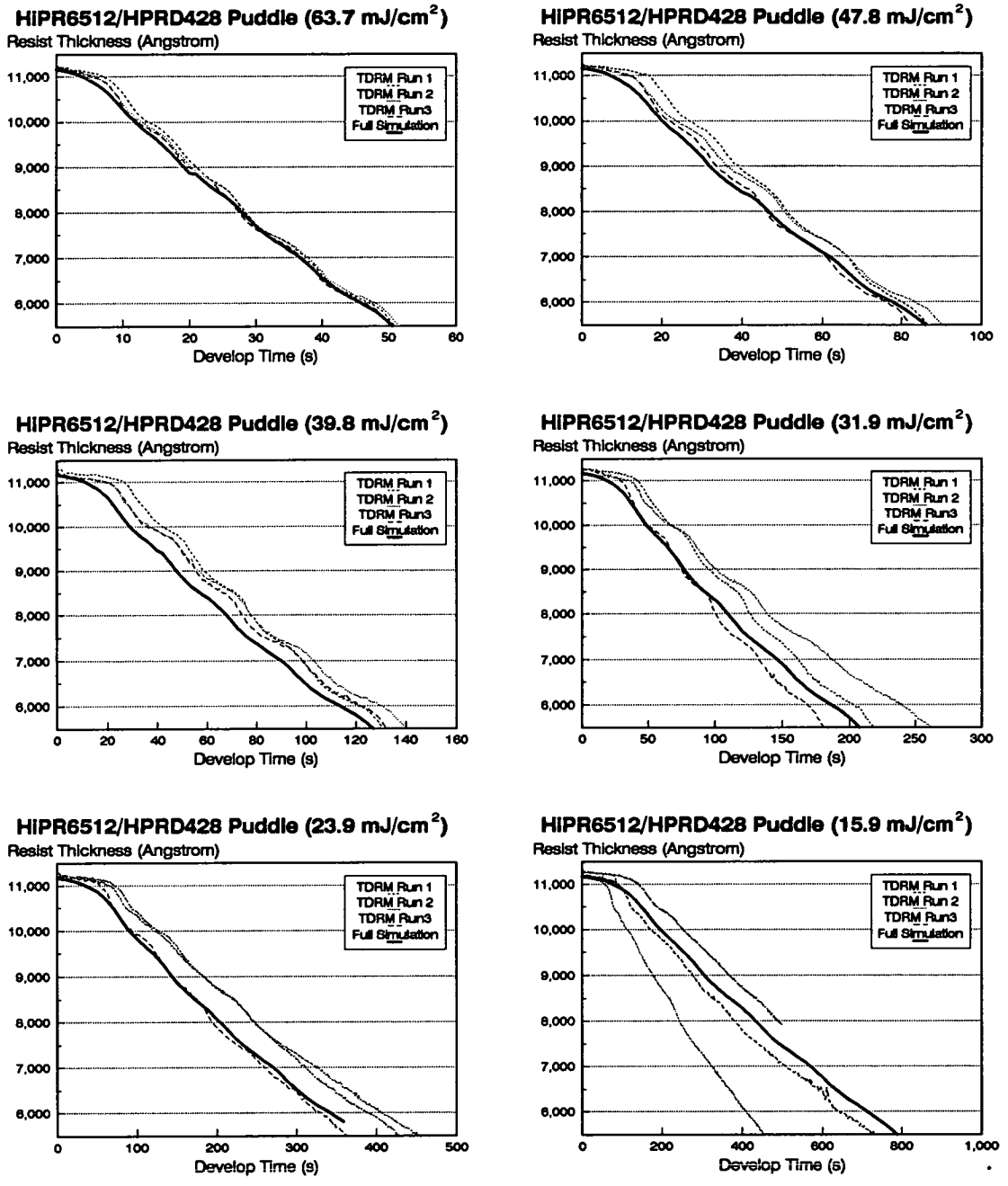

Figure 6–29: *Comparison of experimental data and full model simulations for the puddle development of HiPR6512 in HPRD428 at low exposure doses.*

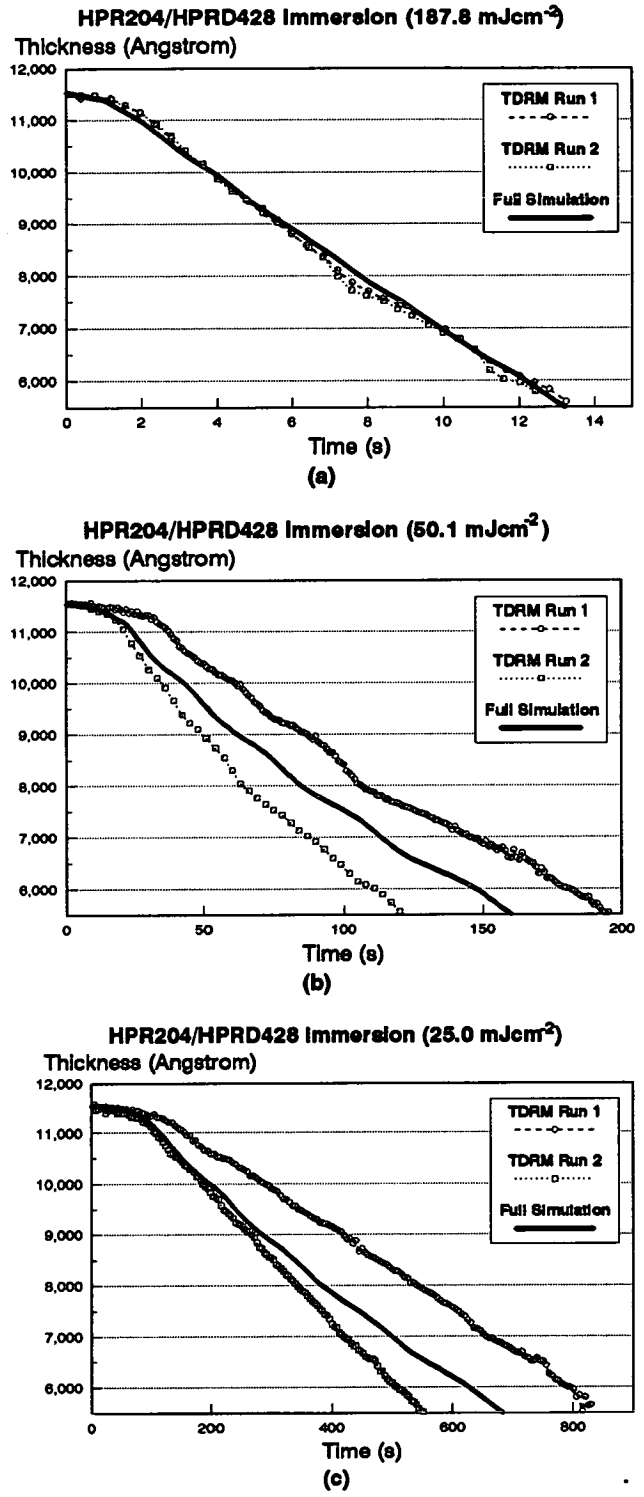

Figure 6–30: *Comparison of experimental data and full model simulations for the stagnant immersion development of HPR204 in HPRD428 at three exposure doses.*

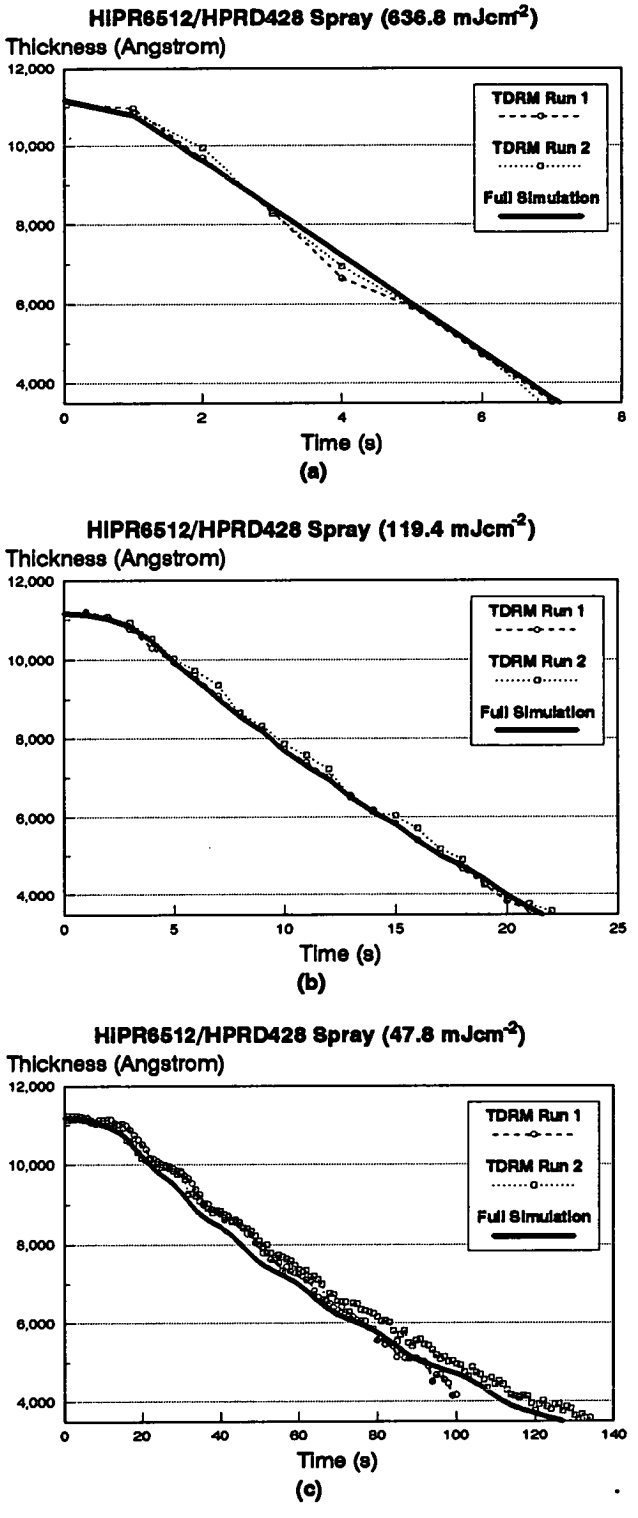

Figure 6–31: *Comparison of experimental data and full model simulations for the contiuous spray development of HiPR6512 in HPRD428 at three exposure doses.*

6.8 Summary

This chapter has introduced the various techniques available to convert DRM output into useful dissolution rate equation parameters. A preferred method for evaluating these parameters on reflecting substrates has been identified. This technique removes much of the uncertainty associated with mapping dissolution rates to relative inhibitor concentrations.

A confirmation procedure was devised which allowed the accuracy of derived parameters to be tested against the original experimental data. The use of this procedure allowed an accurate estimation of the PEB characteristic diffusion length and identified a model weakness in modelling PEB densification. A simple linear compression has been introduced to combat this effect.

The detailed information that the TDRM provides about dissolution near the resist surface has been used to generate a new empirical surface induction model based on the multiplier function devised by Kim. Experimental data indicates that the induction layer is much thinner, but somewhat tougher, than that observed by other researchers.

Finally, comparisons of the experimental data and simulations using all the modelling refinements developed in the chapter, indicate that the models and parameter extraction methods employed produce an excellent reproduction of the observed dissolution.

Chapter 7

Modelling Production Development Processes

7.1 Introduction

Chapters 5 and 6 have described how accurate modelling parameters may be obtained for track-based development processes. The two track-based processes examined so far are, in general, simpler than those used in a genuine manufacturing environment. This chapter examines the modelling accuracy of these simplified cases against experimental lithographic data. It then goes onto describe how these two simple cases may be used to simulate more realistic processes. Again, the accuracy of these results is evaluated by comparison with experimental data. Finally, the processing and physical parameters omitted from the current modelling scheme are reviewed and their impact on absolute accuracy is discussed.

7.2 Modelling Errors

As discussed in Chapter 6 the inclusion of surface induction modelling and PEB densification/shrinkage must be included to yield accurate simulations. Although it was possible to include the new surface induction model in SAMPLE v1.7a, modification of the data structure to simulate PEB shrinkage was not practical in the time available.

In an attempt to understand the error contribution of the two new model refinements, time-to-clear simulation results were prepared for a HiPR6512/HPRD428 puddle process. Simulations were carried out for each of the standard experimental exposure levels. Results were generated for four cases; full modelling, bulk development plus surface induction modelling, bulk development plus densification modelling and standard bulk development modelling. The obtained values are reproduced in Table 7–1, in each case the error between the restricted modelling and the full modelling cases is given.

Inspection of the Table shows that inclusion of surface induction modelling without densification, leads to less accurate results than the use of bulk development modelling alone. This would not be the case for a resist/developer combination exhibiting strong induction effects. However, since the work in this chapter will focus on HiPR6512 processing, it was decided that the use of the surface induction modelling would be omitted in an effort to produce the most 'accurate' quantitative results. The appropriateness of such a decision must be made individually for each resist and will depend on the ratio of densification to induction effect.

It is interesting to note that the bulk plus densification modelling produces more accurate results than either of the two other limited modelling cases.

The effects of densification and surface induction modelling tend to oppose each other, i.e., densification allows development to proceed more quickly whilst surface induction retards it. If the induction effect introduces more delay than the shrinkage removes, it will be 'more accurate' quantitatively to include the induction.

	Full Model	Standard Model		Shrinkage Model		Induction Model	
Exposure Energy $mJcm^{-2}$	Clear Time (s)	Clear Time (s)	Error (%)	Clear Time (s)	Error (%)	Clear Time (s)	Error (%)
637.2	13.07	13.58	+3.9	12.86	-1.6	13.79	+5.5
318.6	18.43	19.09	+3.6	18.08	-1.9	19.45	+5.5
238.9	23.09	23.88	+3.4	22.62	-2.0	24.37	+5.5
159.3	34.47	35.56	+3.2	33.68	-2.3	36.37	+5.5
119.5	48.25	49.68	+3.0	47.05	-2.5	50.91	+5.5
79.6	85.75	88.04	+2.7	83.38	-2.8	90.47	+5.5
63.7	127.87	131.09	+2.5	124.14	-2.9	134.91	+5.5
47.8	233.86	238.43	+2.0	226.46	-3.2	246.71	+5.5
39.8	351.86	358.92	+2.0	339.90	-3.4	371.19	+5.5
31.9	569.27	578.60	+1.6	547.93	-3.7	600.50	+5.5
23.9	1006.08	1015.47	+0.9	961.65	-4.4	1061.11	+5.5
15.9	1932.41	1924.50	-0.4	1822.50	-5.7	2037.59	+5.4
Mean Error			+2.4		-2.0		+5.5

Table 7–1: *HiPR6512/HPRD428 Puddle development time-to-clear simulation results for various exposure levels as determined by the 'FILMLOSS' program. Four modelling cases are shown: full modelling, bulk only modelling, bulk plus surface induction modelling and bulk plus densification modelling. The percent error in time-to-clear versus the full modelling case is detailed for each of the three other restricted model cases.*

7.3 Simulating Pure Spray and Puddle Processes

A simple experiment was performed to compare the accuracy of simulations using the TDRM-derived dissolution rate parameters with the more conventional immersion-derived values for the HiPR6512 resist.[120]

Experimental E_0 swing curves were generated, over the 1.00μm to 1.20μm thickness range, for a 60 Second continuous spray process and a 60 Second stationary puddle process. For consistency with the conditions used to generate the dissolution rate equations, the wafers were spun at 500 r.p.m. during continuous spray processing and puddle formation utilised a 1.5 second application of developer at 100 r.p.m. The 60 second puddle duration was completed by a 58.5 second static puddle.

The wafers were prepared using the standard bake conditions presented in Chapter 2, Table 2–2 and the spin speed during the final spin of coating was altered to obtain the desired resist thicknesses.

The clearing doses were measured using the serpentine exposure run technique described in Chapter 3, Section 3.3.1. The exposure step size utilised was 1.08mJcm^{-2}. The clearing dose was taken to be the lowest exposure dose that completely cleared an entire 2mm by 2mm square open field.

Figure 7–1 compares this experimental data against three SAMPLE simulated E_0 swing curves. Each utilises a 60 second development, but different bulk dissolution parameters; spray, puddle and immersion.[120]

From the figure, it can be clearly seen that the use of appropriate dissolution parameters provides a superior approximation to the actual track process than the use of 'generic' immersion values, which tend to underestimate the photospeed.

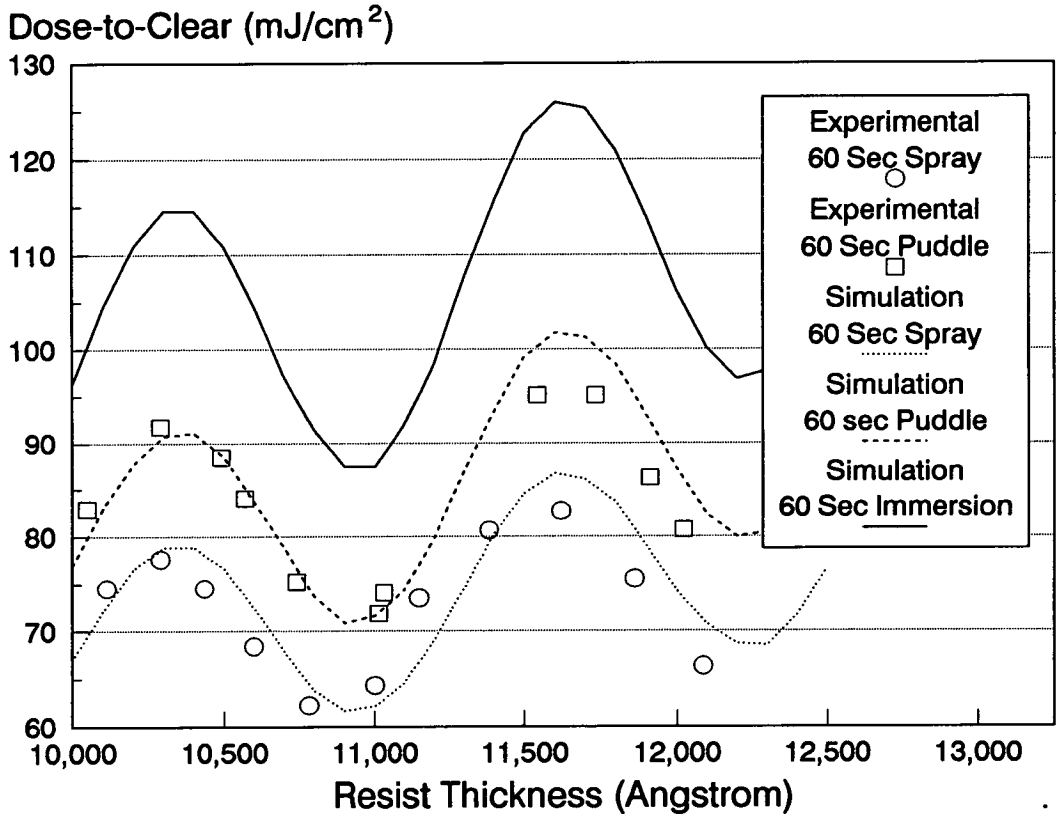

Figure 7–1: *Comparison of experimental and simulated dose-to-clear (E_0) swing curves for HiPR6512 resist in HPRD428 developer.*

7.4 Simulating Practical Spray/Puddle processes

Section 7.3 has illustrated that the use of appropriate dissolution parameters produces accurate quantitative simulation results, however, the two processes described are somewhat artificial. Although continuous spray processes are occasionally used in production environments, spray/puddle or multiple spray/puddle processes are more common. In such processes, a spray period is used to wet the wafer rapidly and form a substantial puddle which is then allowed to stand for a predetermined period. These processes allow a compromise between throughput and developer consumption.

It is well known that process parameters such as E_0, $E_{1:1}$, sidewall angle, CD_{min}, exposure latitude and DOF vary as the spray to puddle time ratio is altered, in a fixed duration process. Obviously, no single set of dissolution rate parameters, of any accuracy, can predict this behaviour.

It is desirable to find a simulation technique which can predict changes in process behaviour, as the spray/puddle ratio is altered. The remainder of this section examines how a single cycle 'spray/puddle' process may be simulated and the degree of correlation between modelled results and actual lithographic observations.

7.4.1 Simulation of Spray/Puddle processes using SAMPLE

As 'accurate' dissolution rate equation parameters are available for both spray and puddle development, a spray/puddle process may be simulated by using spray parameters for the initial spray 'application' period of development and then continuing development with puddle parameters for the remainder of the process duration. SAMPLE v1.7a supports this kind of 'interrupted development' sequence by means of the "contdevel" command.[120]

This approach assumes that the spray and puddle sections of a spray/puddle process can be completely decoupled. Although some sort of transition period must exist, it is hoped that its influence is negligible. In order to test this assumption and confirm the usefulness of the technique, simulations were compared to experimental findings.

7.4.2 Dose-to-Clear (E_0) Values

Dose-to-clear values were measured for seven fixed time (60 Second) HiPR6512/ HPRD428 spray/puddle processes. Seven different spray:puddle time ratios were examined ranging from 'pure puddle' (1.5 second low speed wetting) to full 60 seconds spray using 10 second increments in the spray period.[120] With the exception of the '60 Second puddle' process, spray application was made at 500 R.P.M. and puddle periods were static.

Again E_0 values were determined using the serpentine exposure run technique. Equivalent simulations were made for each spray:puddle ratio using SAMPLE. Figure 7–2 compares the two sets of results. Apart from a systematic error of a couple of $mJcm^{-2}$ in the absolute value of E_0, the simulations track the observed values very well.

7.4.3 Process Latitudes

It was decided to examine how well the simulations would predict HiPR6512/ HPRD428 process latitude as the spray to puddle ratio was altered for a 60 second development process.[120] Spray times of 0 (i.e., 1.5 seconds low speed developer application), 15, 30, 45 and 60 seconds were considered. The nominal resist thickness was 1.18μm and processing conditions were consistent with those described in Chapter 2, Table 2–2. Exposures were made in g-line using the Optimetrix 8605 stepper.

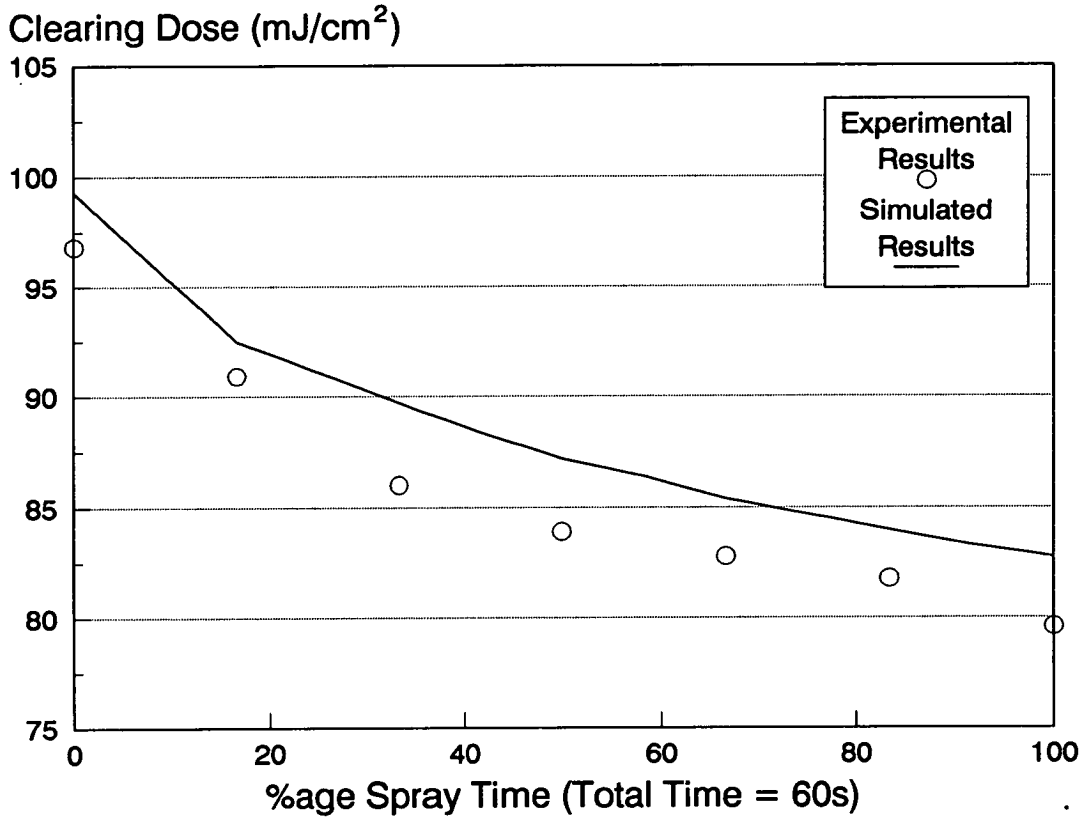

Figure 7–2: *Experimental and simulated dose-to-clear (E_0) values for a 60 second spray/puddle development process as the percentage spray time is increased.*

A 1.2μm line within a 2.4μm pitch periodic pattern was chosen for study, as this represents the specified limit of the stepper for production purposes. No mask bias was present.

Acceptable line profiles were deemed to be those with a 1.2μm $\pm$ 10% base CD with a sidewall angle of 80° or greater.

The process space investigated ranged from 90mJcm^{-2} to 220mJcm^{-2} in 10mJcm^{-2} steps in exposure and from -3.0μm to +3.5μm in 0.5μm steps in defocus. Defocus was referenced to 'best' focus in the experimental case and relative to the resist surface in the case of simulation work.

Mack[130] has shown that 'best' focus occurs when the focused image lies slightly beneath the resist surface; therefore, an offset of up to 0.5μm may exist between the simulated and experimental data sets.

Experimental latitudes were determined using the KLA5015 CPM system, described in Chapter 3, Section 3.2.3.2. The ability of the machine to measure the CD at the top and bottom of the feature separately and give an indication of the feature height means that sidewall angles can be inferred.

Figure 7–3 shows the simulation results for each of the processes of interest: the solid white area illustrates the exposure/focus combinations which meet the acceptance criteria.

Examination of the figure quickly reveals the main drawack of SAMPLE, as discussed in Chapter 4, Section 4.7.2, in that the propagation model treats positive and negative defocus symmetrically. Despite this, definite trends are evident. Firstly, the window increases in the exposure dimension with spray time. Secondly, the window moves to a lower energy range as the puddle time increases. This change opposes the trend in E_0 values (Figure 7–2). It is worth noting that in all cases the $E_{1:1}$ energy is closer to the left edge of the window than the right, indicating greater tolerance to overexposure than to underexposure.

Figure 7–4 shows the experimental results determined by the KLA5015. Many of the low exposure dose features could not be measured, either because the pattern was so underexposed (i.e., large) that the pattern recognition system failed to

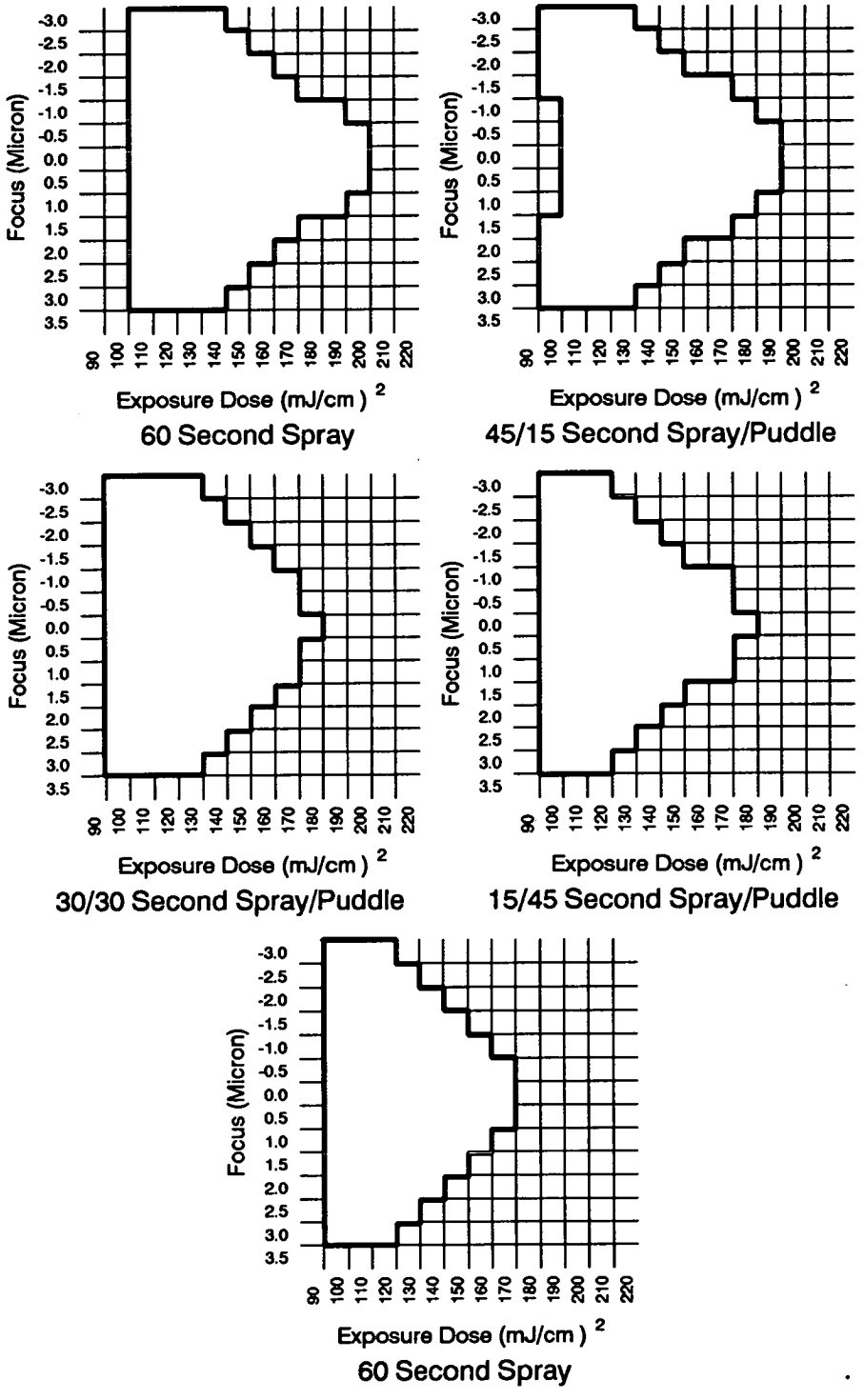

Figure 7–3: *Results from the SAMPLE simulations of the HiPR6512/HPRD428 focus-exposure matrix under the five different spray/puddle processes.*

identify the correct feature or because there was insufficient contrast for edge detection during the measurement.

Inspection of the figure shows similar trends to those observed in the simulation case, with the righthand side of the window moving leftward as the spray time is reduced. Since the position of the lefthand side of the window is not well defined it is impossible to verify that the window size is maximised during the 100% spray process.

It is evident from Figure 7–4 that the experimental window is not symmetrical in the negative and positive defocus regimes. It would appear that the window is larger in negative defocus. Confirmation of the effect would require the implementation of an interrupted develop facility in either PROLITH/2 or DEPICT2.

In order to test the accuracy of the simulations, the predicted results were compared to their experimental equivalents. Figure 7–5 illustrates the overlay of the results for each of the five development processes. Only the positive defocus results are considered. Features correctly predicted as 'in specification' are shaded, those correctly predicted 'out of specification' are left white. Features wrongly predicted in or out of specification are dotted or hatched respectively. Features for which there is no experimental data are also indicated.

It can be seen that, in general, the correlation between the predicted and actual processes is very good and such errors as exist can easily be explained by experimental noise and/or the slight error between 'best' focus and imaging at the resist surface. The good agreement between the simulations and the experimental data validates the assumption that the spray and puddle portions of the development process can be decoupled, at least in the case of this resist/developer combination.

7.4.4 Technique Limitations

Although the application of this modelling technique to a single puddle process appears to have been successful, care should be exercised if extending the theory to multiple spray/puddle processes, where possible inter-puddle induction effects may be occuring. Such induction effects can arise if the first puddle is removed

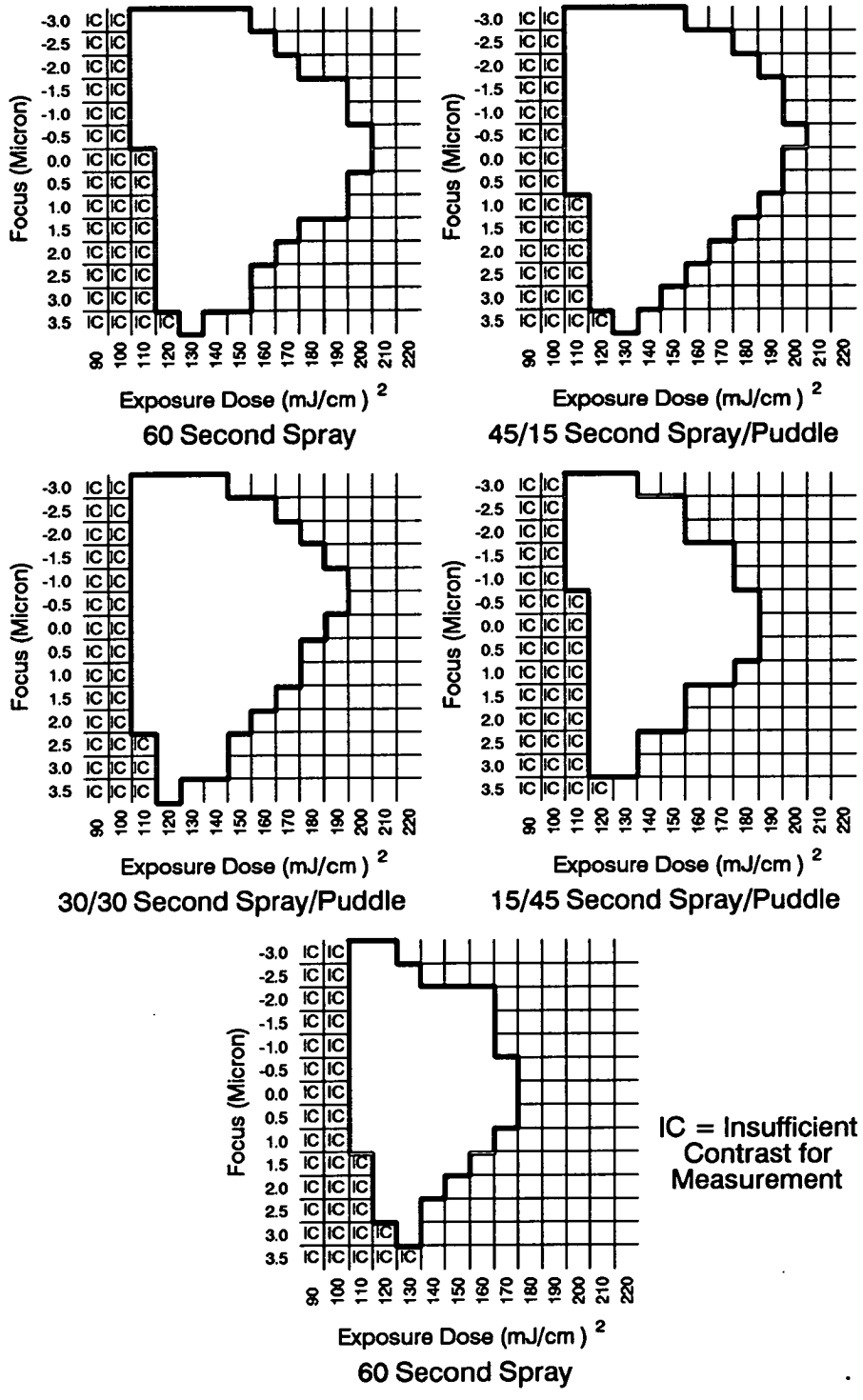

Figure 7–4: *Results from the KLA5015 measurements of the HiPR6512/ HPRD428 focus-exposure matrix under the five different spray/puddle processes.*

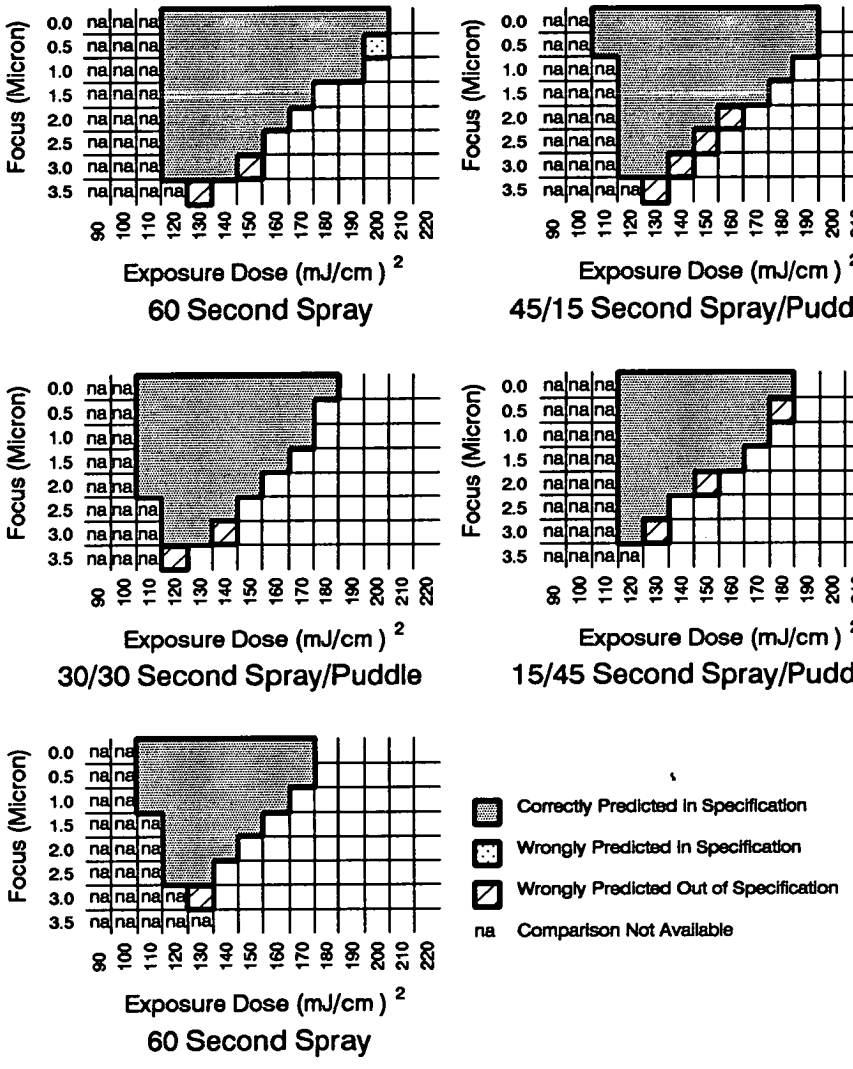

Figure 7–5: *Comparison of the SAMPLE simulations and experimental results for the HiPR6512/HPRD428 focus-exposure matrices under different spray/puddle processes in positive defocus.*

by a short high speed spin before the application of the second puddle or if an interpuddle rinse is used.

7.5 Unaccounted Factors in Current Development Model

Although the above procedure has shown that a single puddle process can be modelled with reasonable success when the process conditions match those used to generate the dissolution rate parameters, most real production processes are even more complex. The following sections explore some issues which are known to affect development rates but are not considered by the current model. Inclusion of these effects is necessary for truly accurate modelling. As these refinements are introduced other less obvious, but important, effects may be identified and included.

7.5.1 Speed of Wafer Rotation

Typically, several spin speeds are used during the spray period of puddle build up. Initially, a high spin speed is used to wet the entire surface (this can be a particular problem with large diameter wafers), the speed is then reduced to build up a thick puddle. This reduction is often done in several stages to help maintain cross-wafer develop uniformity.

When the spin speed is high enough to throw the developer from the wafer, uniformity problems can result. Centripetal force accelerates the developer outward. The consequential greater flow rates near the wafer edge results in more agitation and increased development action. At low spin speeds, developer is not thrown off and only leaves the wafer when the volume exceeds the amount which surface tension will retain in the puddle. At these low spin speeds uniformity problems arise if the spray area remains over one part of the wafer for too long.

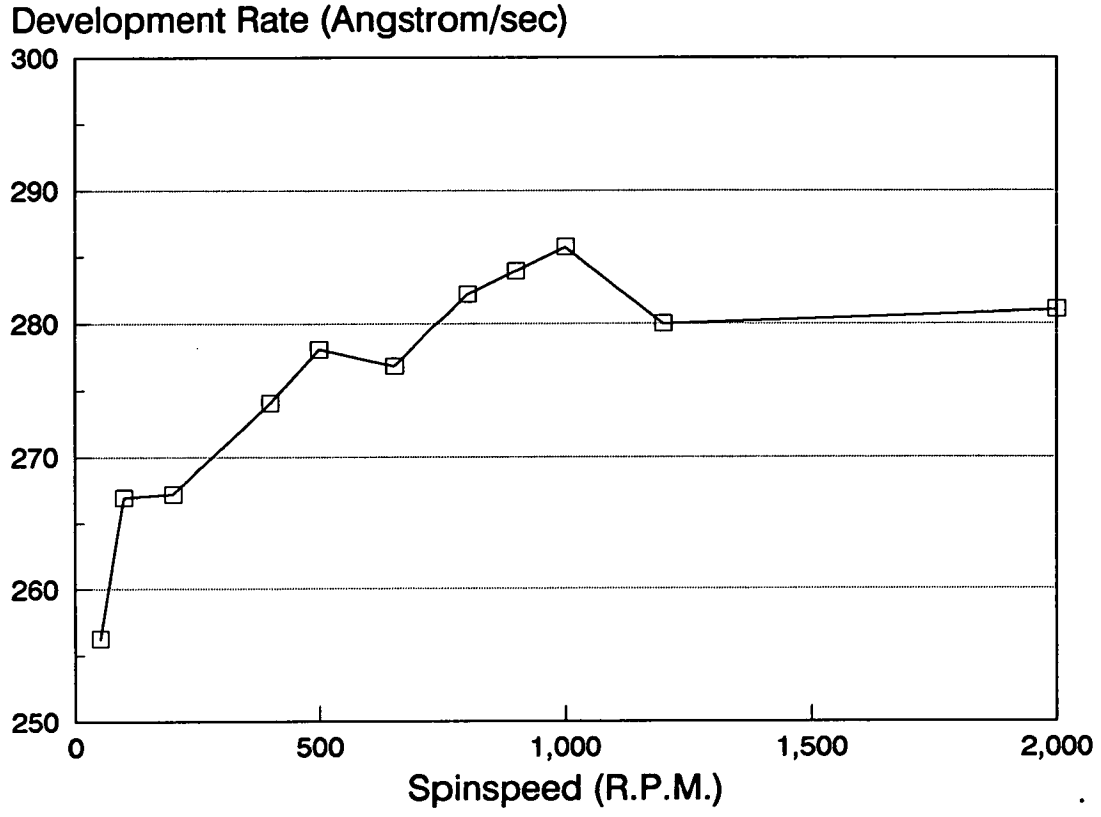

Figure 7–6: *The dissolution rate for a 1.18μm coating of HiPR6512 resist under contiuous spray development in HPRD428 as a function of spin speed after a 79.6*mJcm^{-2} *g-line exposure.*

The precise details of a production program will depend on the track type, the spray nozzle design, the wafer diameter and the developer composition amongst other considerations.

Development rate during a continuous spray process was measured as a function of spin speed for an HiPR6512 coating exposed by 79.6mJcm^{-2} of g-line illumination. The results are plotted in Figure 7–6.

From the figure, it is clear that development rate increases with spin speed, reaching a plateau at around 500 R.P.M. This spin speed was chosen for the continuous spray process during this study, as it was representative of the plateau region but left an adequate puddle on the wafer when abruptly stopped. A lower spin speed of 150 R.P.M. was chosen for puddle formation during the 'pure puddle'

process as it wet the wafer quickly, forming a thick puddle, without introducing the higher development rates observed at greater spin speeds.

Quantitatively accurate modelling of a true production program will therefore require dissolution rate parameters measured at each spin speed used during puddle formation. The simulation would then treat each of these stages in a fully decoupled, sequential manner, similar to the two stage approach described in Section 7.4.1

Similarly, development rate during the puddle portion of the process depends on the spin speed. Although the stationary case considered during this study is very common low spin speeds of between 20 and 50 R.P.M. are sometimes used. This results in some agitation which enhances development rates but can introduce uniformity problems as the centre moves less than the edges. Again, quantitatively accurate simulations will depend on characterisations using the 'correct' puddle spin speed.

7.5.2 Agitation due to Developer Impact

Dissolution rates are also dependant on the way in which the developer impacts the wafer. This depends on the liquid flow rate and the nozzle design. Development rates are considerably higher from fan type nozzles than they are from stream nozzles or low impact nozzles (ultrasonic or E^2), even when flow rates are identical. It is therefore important that the dissolution rate characterisation not only employs the correct process spin speeds, but also utilises production flow rates and the appropriate dispense system.

If the increase in dissolution rate seen during continuous spray is due to the physical impact of the solution on the film, one important question is whether this increase in development rate is isotropic, or biased in the vertical direction. At this time this question is impossible to answer, but must be considered, as it may have serious implications for current modelling validity.

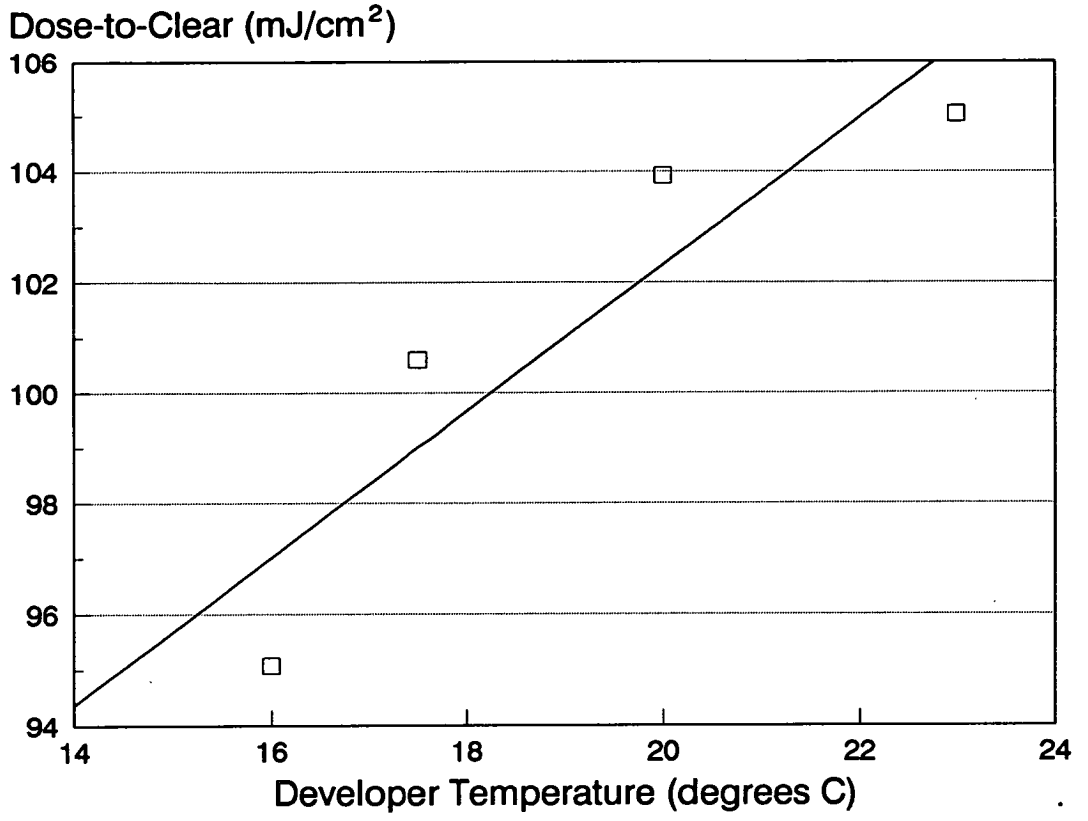

Figure 7–7: *The effect of developer temperature on dose-to-clear for HiPR6512 in HPRD428.*

7.5.3 Temperature profile during Puddle

As discussed in Chapter 2, Section 2.10.3.2 development rate is a function of temperature. Figure 7–7 shows the effect of temperature on the dose-to-clear of HiPR6512 in HPRD428 as determined by Stapleton.[244] A change of around 10% is observed over a 7°C change in temperature.

A wafer-mounted thermocouple was used to investigate developer temperature during track processing. Figure 7–8 shows the temperature at the wafer surface during a continuous spray process. The air temperature in the develop bowl was 19.0°C and the developer temperature prior to spraying was 21.6°C. From the figure it can be seen that the wafer surface cools from the ambient bowl temperature to approximately 18.4°C. This is the developer temperature after the liquid

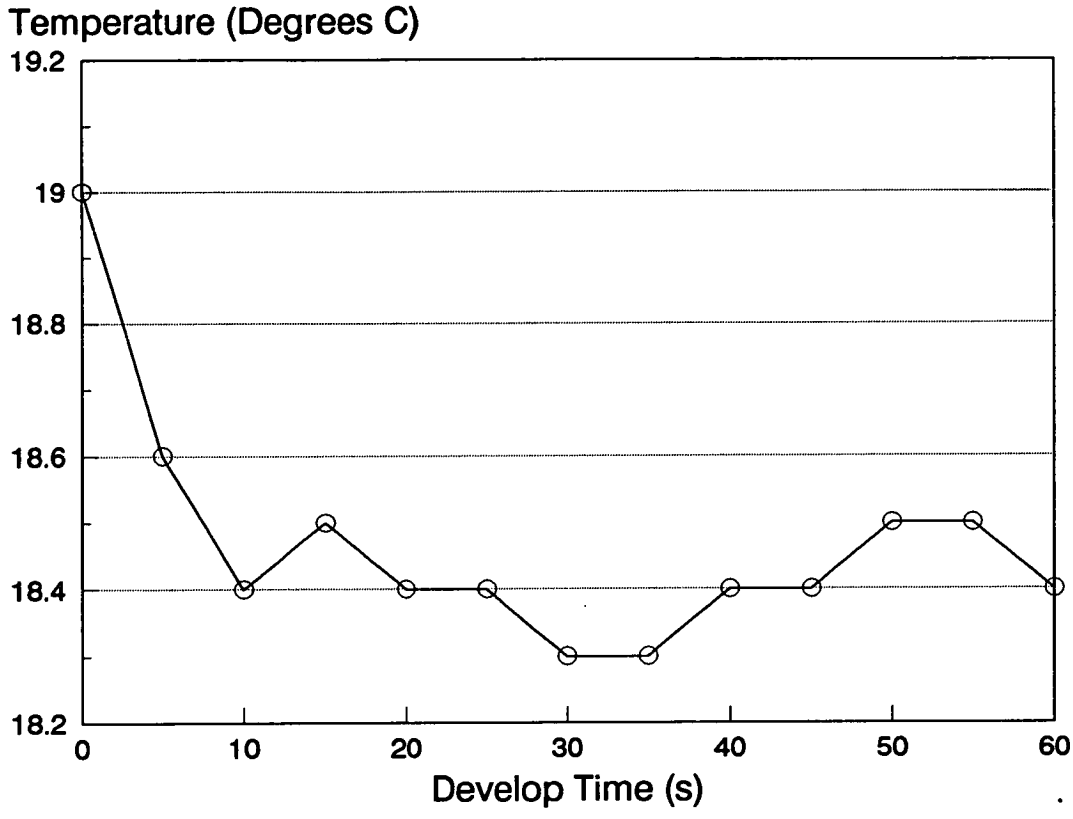

Figure 7–8: *Wafer surface temperature during continuous spray development.*

has undergone expansive cooling in the fan nozzle. The developer temperature appears to remain constant at this level throughout a continuous spray process.

Figure 7–9 shows the wafer surface temperature during a stationary puddle. It can be seen that the temperature falls rapidly (approximately 3°C in the first 60 Seconds) levelling out after around 200 seconds at approximately 13.5°. This evaporative cooling is highly dependant on the bowl exhaust rate. Bearing in mind the effect of temperature on development rate shown in Figure 7–7, the cooling occurring during a typical 60 second puddle could enhance dissolution rates by several percent.

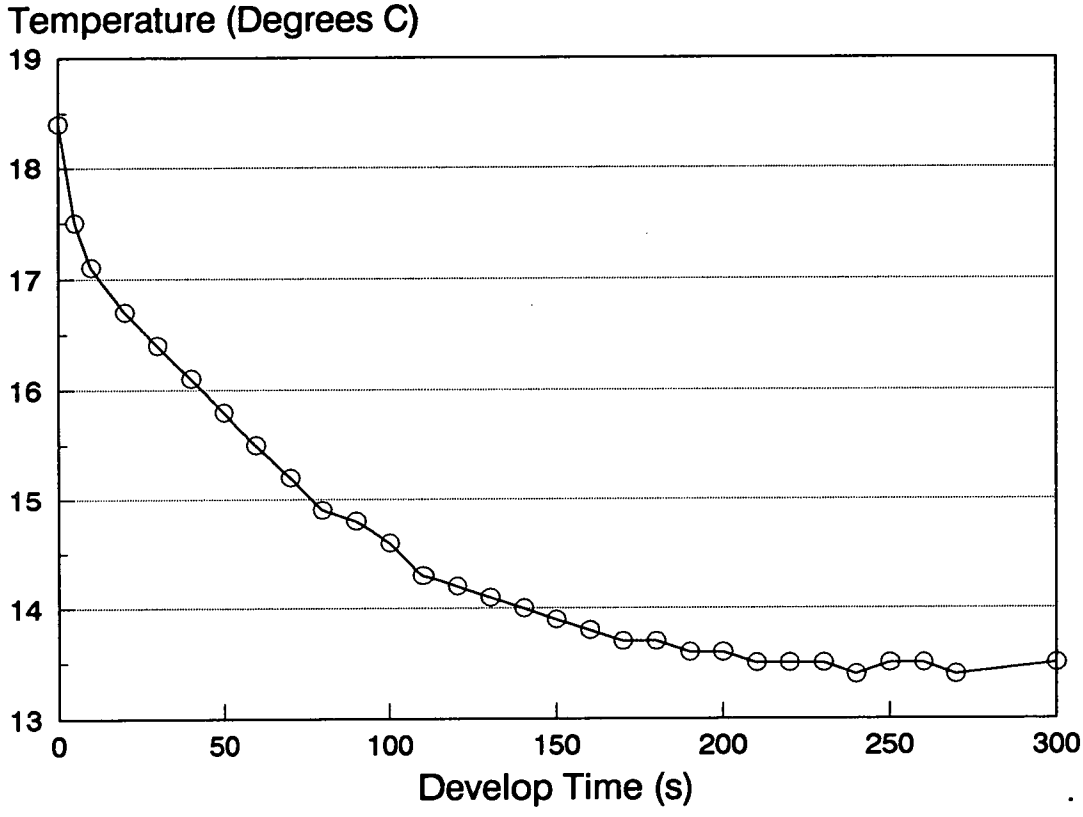

Figure 7–9: *Wafer surface temperature during static puddle development.*

7.6 Summary

Experimental lithographic results have shown that simulations utilising dissolution rate equation parameters generated under a given development process produce quantitatively accurate predictions for that process, which are distinct from those using parameters generated under different development conditions.

This chapter has also demonstrated a new technique for modelling spray/puddle processes. Experimental results have confirmed that this decoupled development model produces realistic values and trends for both E_0 and full process latitude.

The chapter has also addressed some of the additional higher order factors which affect dissolution rates but which are still not considered in current modelling practices.

Chapter 8

Conclusions and Further work

8.1 Thesis Goals

The first chapter identified lithography simulation as a cost-effective characterisation tool for the development of new optical lithography processes and for the screening of new material formulations. However, the utility of simulation in this capacity relies upon the accuracy of both the models employed and the values of the parameters characterising the resist's dissolution properties.

It is known that different development techniques produce lithographic processes with different characteristics. However, although most high resolution production facilities use track development, resist dissolution characterisation is in the main performed in an immersion mode. One of the primary objectives of this project was to develop a DRM tool capable of monitoring resist dissolution under a variety of development processes *in-situ* on actual production equipment with genuine silicon substrates. Such a tool allows discrete parameters to be generated for each development process and differences to be identified.

Having obtained these parameters, simulations can be compared with actual experimental lithographic data. This comparison shows whether the parameter values actually reflect the different development techniques, or whether the dissolution modelling is inadequate. Ideally, the information generated by the DRM could be extrapolated to accurately simulate track-based processes which had not been explicitly studied.

8.2 Thesis Summary

Chapter 2 detailed typical lithographic materials and processing steps, identifying the large number of process parameters which influenced the final lithographic results. Chapter 3 described how these results are analysed to describe the process latitude in a quantifiable manner. The chapter highlighted the large quantity of measurements required to characterise a process. This analysis must be repeated if a process step parameter is altered.

Chapter 4 introduced lithography modelling, describing the models used for resist exposure and development, based on the work of Dill. The particular importance of choosing an appropriate, accurate development rate model was emphasised. The 5 parameter modified Kim rate equation was identified as a suitable model as it fits most dissolution rate data sets well, without introducing an excessive number of characterising parameters.

Chapter 5 reviewed various DRM techniques for determining resist thickness during development. The strengths and weaknesses of the various techniques were identified.

A new Track Development Rate Monitor (TDRM) system was described and the results from the system were presented. The most noteworthy points about the system are as follows:

- The TDRM is a polychromatic measurement tool which yields a series of absolute, unambiguous resist thicknesses. It can monitor resist development *in-situ* on actual semiconductor processing equipment.

- The measurement algorithm appears insensitive to noise introduced by aerosol particles and an unstable puddle surface, allowing a detailed study of development at the resist surfaces.

- TDRM output clearly demonstrates the ability of the system to detect the effects of surface induction eand residual standing waves in the dissolution profile.

Chapter 5 also described modifications to a standard, commercially available Perkin-Elmer 5900 immersion DRM.

- A Perkin-Elmer DRM was modified to utilise a pseudo-puddle process rather than the standard immersion process, allowing resist to be characterised quickly.

- Analysis of the transmission characteristics of dissolved photoproduct led to optimisation of the DRM operating wavelength. Switching from 632nm to 700nm gave a more 'ideal' interferometric signal which simplifies end-point and extrema detection.

Chapter 6 describes how dissolution rate equation parameters can be obtained from DRM data and describes a new technique for verifying the accuracy of the obtained parameters. Finally, a new surface induction model was derived. The parameters for this model can be empirically derived from TDRM output.

The main points worth highlighting from Chapter 6 are as follows:

- A technique has been identified for generating dissolution rate equation parameters from resist films on reflecting substrates which is insensitive to diffusion length values and to mismatches between actual and modelled standing wave periods.

- Rate equation rate parameters were extracted for two resist types in one developer under three different development processes: stagnant immersion, continuous spray and static puddle. For each resist the parameters obtained were distinct for the three processes.

- Excellent correlation was observed between the stagnant immersion parameters generated on the TDRM and those from an industry 'accepted' Perkin-Elmer DRM, validating the TDRM measurements.

- The dissolution data from the Perkin-Elmer DRM in pseudo-puddle mode was in good agreement with that generated by the TDRM monitoring an actual puddle process *in-situ* on track equipment. Similarly, dissolution data generated by the Perkin-Elmer DRM in stagnant immersion mode using freshly decanted developer was also found to be in close agreement with the standard puddle process.

- The concept of 'parameter confirmation' was introduced. This simple technique uses the dissolution rate parameters generated from the analyses of DRM output to reconstruct that experimental data. The technique allows characteristic PEB diffusion length to be estimated and identified a significant modelling error due to PEB densification.

- A simple one dimensional linear compression was introduced to model the PEB densification effect.

- Consideration of the basic Kim surface induction multiplier led to the development of a new surface induction f(0,M) function. The required parameter values can be empirically derived from the analyses of TDRM data and parameter confirmation simulations. The results from the new surface induction model indicate that the surface induction layer is thinner but tougher than that noted by others.

- Parameter confirmation using all the derived parameters and model modifications showed excellent agreement with the TDRM data for all 6 processes investigated, i.e., two resists under each of the three development conditions.

In Chapter 7 simulations using the parameters derived in Chapter 6 are compared with experimental lithographic results to investigate whether appropriately derived parameters lead to more accurate simulations of actual processes. A new technique using spray and puddle rate equations was then introduced in an attempt to model the type of spray/puddle process which is typically used in semiconductor manufacturing plant. Again the predictions of this model were compared to experimental data. The significant outcomes of Chapter 7 were:

- Simulations using appropriately generated derived parameters appear to give better, more quantitatively, correct results than those utilising generic immersion-derived parameters.

- A new 'interrupted development' technique was introduced which appears to approximate a single cycle spray/puddle process with a high degree of accuracy.

8.3 Conclusion

A new tool has been introduced which allows most development processes to be characterised and simulated with reasonable accuracy. A number of model modifications have been proposed which improve simulation accuracy with respect to actual experimental data. A development scheme has been introduced which potentially allows the optimisation of a spray/puddle process using simulation.

Although this work has improved lithography modelling and allowed some processing nuances to be incorporated into simulations, the accuracy of the results is still only in the region of $\pm 5\%$. Whilst this is probably much better than the typical simulation, a very large amount of characterisation work is required. However, this level of accuracy is still insufficient for simulation to be seriously considered as a method for screening new resist formulations. Moreover, collaborative work with Hansen[102] has shown that simulations of resists exhibiting exceptionally high levels of surface induction do not correlate with experimental evidence. The reason for this is thought to be related to PEB diffusion. The solvent content near the resist surface is lower than that in the bulk due to the softbake process, consequently the photoactive compound in this area is less mobile during the PEB diffusion. This and other such issues must be identified and accounted for before simulation can replace experimental work. Additionally, understanding of such mechanisms may identify desirable resist properties which improve lithographic performance.

8.4 Work by Others Based on this Research

Obviously, the TDRM system constructed during this work is capable of monitoring processes other then resist development. Since the completion of the experimental work for this thesis, the TDRM has been used by Porfiris[245] to study the wet stripping action of EKC proprietary products on implanted and dry-etched photoresists.

Secondly, the data this project provided on the developer temperature drop during puddle processing, led to a project on 'The Temperature Control of Developer Solution' by Stapleton.[244] In this work the temperature of the developer puddle was kept constant using an infra-red lamp and a thermocouple feedback system. The TDRM was also used during this work to compare development rates under various temperature regimes. As one might expect from the details in Chapter 2, it was found that maintaining the puddle at ambient temperature actually decreased average dissolution rates.

8.5 Areas of Further Work

Before simulation can be used as a true resist screening tool, lithography modelling must be extended to cover more of the known higher order effects discussed in Chapter 7, Section 7.5. Additionally, interactions between bake conditions and latent image diffusion must be more fully understood and characterised.

A more accurate model of PEB densification would also be appropriate. Characterisation of the effect of partial exposure on the degree of densification is necessary. The TDRM equipment may well prove useful in this investigation if it were mounted *in-situ* above the PEB hotplate.

Finally, a software package should be developed for automated data extraction and parameter confirmation as simulation can only become a valuable screening tool if the technique is fast, reliable and accurate.

Bibliography

[1] SERC School on microfabrication. *Process Architectures and process flow.* Edinburgh Microfabrication Facility, June 1991.

[2] A.S.Oberai. Lithography - challenges of the future. *Solid State Technology*, pages 123 – 128, Sept 1987.

[3] N.M.Donofrio. The real challenge in lithography. In *Kodak Microelectronics Seminar*, pages 4 – 16. Interface'85, 1986.

[4] R.Anderson. Private communication, Nov 1993. Digital Equipment Scotland, South Queensferry.

[5] B.Riester. Private communication, Aug 1994. Texas Instruments Gmbh, Friesing, Germany.

[6] N.Pakdaman. Beyond sub-0.5μm lithography. *Dataquest Perspective - Semiconductor Equipment, Manufacturing and Materials Worldwide*, SEMM-WW-DP-9406, June 1994.

[7] SERC School on microfabrication. *CAM, yield and information management.* Edinburgh Microfabrication Facility, June 1990.

[8] D.W.Johnson and C.A.Mack. I-line, DUV, VUV, or X-ray? In *Optical/Microlithography V.* SPIE Vol. 1674, 1992. Paper no.1674-40.

[9] J.D.Buckley. An advanced h-line stepper. *Solid State Technology*, pages 87 – 91, Jan 1987.

[10] K.Tounai, H.Tanabe, H.Nozue, and K.Kasama. Resolution improvement with annular illumination. In *Optical/Laser Microlithography V.* SPIE Vol. 1674, 1992. Paper no.1674-64.

[11] K.K.H.Toh, G.Dao, H.Gaw, A.R.Neureuther, and L.Fredrickson. Design methodology for dark-field phase-shifted masks. In *Optical/Laser Microlithography IV.* SPIE Vol. 1463, 1991. Paper no. 1463-32.

[12] K.K.H.Toh, G.Dao, R.Singh, and H.Gaw. Optical lithography with chromeless phase-shifted masks. In *Optical/Laser Microlithography IV.* SPIE Vol. 1463, 1991. Paper no. 1463-06.

[13] B.J.Lin. Phase-shifting and other challenges in optical mask technology. *Bacus News*, 7(1): 1 – 11, Feb 1991.

[14] K.Nakagawa, M.Taguchi, and T.Ema. Fabrication of 64M DRAM with i-line phase-shift lithography. *Bacus News*, 7(2): 1 – 4, Mar 1991.

[15] T.Terasawa, N.Hasegawa, H.Lmai, T.Tanaka, and S.Katagiri. Variable phase-shift mask for deep submicron optical lithography. In *Optical/Laser Microlithography IV.* SPIE Vol. 1463, 1991. Paper No. 1463-14.

[16] T.Kokubo. Lithography technology trend. Technical report, Fuji-Hunt, 1992. Presentation at OCG R&D Seminar, Providence, RI.

[17] M.Rothschild, R.B.Goodman, M.A.Hartney, R.R.Kunz, J.H.C.Sedlacek, and D.C.Shaver. Photolithography at 193nm. In *36th International Symposium on Electron, ion, and Photon Beams*, pages 2989 – 2996. American Vacuum Society, 1992.

[18] T.Kokubo, Y.Idemoto, Y.Kawabe, and K.Uenishi. Design of a positive photoresist for submicron imaging assisted by SAMPLE simulation. In *Advances in Resist Technology and Processing V*, pages 355 – 363. SPIE Vol. 920, 1988.

[19] S.G.Hansen. Simulation as a screening tool. Technical report, OCG Microelectronic Materials Inc., 1992. Presentation at OCG R&D Seminar, Providence, RI.

[20] T.Kokubo, S.Sakaguchi, and Y.Kawabe. Resist formulation screening. Technical report, Fuji-Hunt, 1992. Presentation at OCG R&D Seminar, Providence, RI.

[21] J.T.M.Stevenson and A.M.Gundlach. The application of photolithography to the fabrication of microcircuits. *Journal of physics: Scientific Instruments*, 19: 654 – 667, 1986.

[22] Olin Hunt. *Dynamic Training on Waycoat Positive Photoresist*, 1989.

[23] C.A.Mack and J.E.Connors. Fundamental differences between positive and negative tone imaging. In *Optical/Laser Microlithography V.* SPIE Vol. 1674, 1992. Paper no.1674-26.

[24] W.S.Ruska. *Microelectronic Processing*, chapter 4.2: Negative Photoresist, pages 118 – 122. McGraw-Hill, 1987.

[25] B.T.Beauchemin. Private communication, April 1992. OCG Microelectronic Materials, East Providence, RI.

[26] J.S.Petersen. Acid hardening resists for deep UV microlithography: A review of advanced negative resist chemistry and its application. In *SEMICON/Japan*, pages 90 – 101. SEMI, 1990.

[27] J.W.Thackeray, G.W.Orsula, D.Canistro, E.K.Pavelchek, L.E.Bogan, A.K.Berry, and K.A.Graziano. DUV ANR photoresists for 248nm excimer-laser photolithography. In *Advances in Resist Technology and Processing VI.* SPIE Vol. 1086, 1989. Paper No. 1086-34.

[28] C.A.Spence and R.A.Ferguson. Some experimental techniques for characterizing photoresists. In *Advances in Resist Technology and Processing VIII*, pages 324 – 335. SPIE Vol. 1466, 1991.

[29] A.Zampini, P.Turci, G.J.Cernigliaro, H.F.Sandford, and G.J.Swanson. High resolution positive photoresists: Novolak molecular weight and molecular weight distribution effects. In *Advances in Resist Technology and Processing VII*, pages 501 – 512. SPIE Vol.1262, 1990.

[30] C.A.Mack. *Chemistry and kinetics of positive photoresists.* Department of Defence, Fort Meade, MD 20755, 1986.

[31] M.A.Toukhy, T.R.Sarubbi, and D.J.Brzozowy. Technology and chemistry of high temperature positive resist. In *Advances in Resist Technology and Processing VIII.* SPIE Vol. 1466, 1991. Paper no.1466-48.

[32] K.Honda, B.T.Beauchemin, E.A.Fitzgerald, A.T.Jeffries, S.P.Tadros, R.J.Hurditch, A.J.Blakeney, S.Tan, and S.Sakaguchi. Studies of dissolution inhibition mechanism of DNQ-novolak resists, part II, effect of extended ortho-ortho bond in novolak. In *Advances in Resist Technology and Processing VII.* SPIE Vol. 1463, 1991. Paper No. 1463-.

[33] K.Honda, B.T.Beauchemin, R.J.Hurditch, A.J.Blakeney, and T.Kokubo. Studies of dissolution inhibition mechanism of DNQ-novolak resists, part III, secondary inhibition with quanternary ammonium salts in development process. In *Advances in Resist Technology and Processing IX*, pages 297 – 304. SPIE Vol. 1672, 1992.

[34] K.Honda, B.T.Beauchemin, R.J.Hurditch, A.J.Blakeney, Y.Kawabe, and T.Kokubo. Studies of the molecular mechanism of dissolution inhibition of positive photoresist based on novolak-DNQ. In *Advances in Resist Technology and Processing VII.* SPIE Vol. 1262, 1990. Paper no. 1262-22.

[35] K.Honda. Spectroscopic characterization of dissolution behaviour of novolak films. Technical report, OCG Microelectronic Materials Inc., 1992. Report # CEPH-RM-92-2.

[36] H.Nemoto, K.Inomata, T.Ota, Y.Yumoto, T.Miura, and H.Chawana. Structural effects of NQD-PAC and novolak resin on resist performance. In *Ad-*

vances in Resist Technology and Processing IX, pages 305 – 316. SPIE Vol. 1672, 1992.

[37] M.A.Khadin, M.D.Rahman, and D.L.Durham. The nature and degree of substitution patterns in novolaks by carbon-13 NMR spectroscopy. In *Advances in Resist Technology and Processing IX*, pages 347 – 359. SPIE Vol. 1672, 1992.

[38] A.Zampini, R.L.Fischer, and J.B.Wickman. Novolak based thermally resistant positive photoresist: Resin design and performance. In *Advances in Resist Technology and Processing VI*, pages 85 – 96. SPIE Vol. 1086, 1989.

[39] L.Blum, M.E.Perkins, and A.W.McCullough. A study of the dissolution kinetics of a positive photoresist using organic acids to simulate exposed photoactive compounds. In *Advances in Resist Technology and Processing IV*, pages 148 – 153. SPIE Vol.771, 1987.

[40] W.D.Hinsberg, C.G.Willson, and K.K.Kanazawa. Use of a quartz crystal microbalance rate monitor to examine photoproduct effects on resist dissolution. In *Advances in Resist Technology and Processing II*, pages 6 – 13. SPIE Vol.539, 1985.

[41] P.Trefonas, B.K.Daniels, and R.L.Fischer. Photoresist design for submicron optical lithography: Application of polyphotolysis. *Solid State Technology*, pages 131 – 137, Aug 1987.

[42] K.Uenishi, Y.Kawabe, T.Kokubo, S.Slater, and A.Blakeney. Structural effects of DNQ-PAC backbone on resist lithographic properties. In *Advances in Resist Technology and Processing VIII.* SPIE Vol. 1466, 1991. Paper No. 1466-12.

[43] K.Uenishi S.Sakaguchi, Y.Kawabe, T.Kokubo, M.A.Toukhy, A.T.Jeffries, and R.J.Hurditch. Selectively DNQ-esterified PAC for high performance positive photoresists. In *Advances in Resist Technology and Processing IX*, pages 262 – 272. SPIE Vol. 1672, 1992.

[44] S.Tan, S.Sakaguchi, K.Uenishi, Y.Kawabe, T.Kokubo, and R.J.Hurditch. Novel diazonaphthaquinone photoactive compound for g-line/i-line compatible positive photoresist. In *Advances in Resist Technology and Processing VII.* SPIE Vol. 1262, 1990. Paper No. 1262-50.

[45] W.Brunsvold, E.C.Lyons, S.Miura, M.Plat, R.Dammel, O.Evans, M.D.Rahman, D.N.Khanna, S.Jain, P.Lu, and S.Ficner. Novel DNQ PACs for high-resolution i-line lithography. In *Advances in Resist Technology and Processing IX*, pages 273 – 285. SPIE Vol. 1672, 1992.

[46] SERC School on microfabrication. *Lithography.* Edinburgh Microfabrication Facility, June 1991.

[47] L.F.Thompson, C.G.Willson, and M.J.Bowden, editors. *Introduction to Microlithography*, chapter 1: Introduction to lithography. American Chemical Society, 1983. ACS Symposium Series 219.

[48] S.Clifford, B.Hayes, and R.Brade. Results of photolithographic cluster cells in actual production. In *Optical/Laser Microlithography IV*, pages 551 – 557. SPIE Vol.1463, 1991.

[49] A.Englisch and A.Deuter. Automated lithocell. In *Integrated Circuit Metrology, Inspection, and Process Control IV*, pages 272 – 283. SPIE Vol. 1261, 1990.

[50] T.Lauck, M.Nomura, T.Omori, and K.Yoshioka. Effects of wafer cooling characteristics after post exposure bake on critical dimensions. In *Integrated Circuit Metrology, Inspection, and Process Control V*, pages 527 – 538. SPIE Vol. 1464, 1991.

[51] J.Kulp and R.B.Simonton. *CD Shift Resulting from Handling Time Variation in the Track Coat Process.* Eaton Semiconductor Equipment, 1991. Application Note #90.5.

[52] P.Norton. Photoresist process systems. *Electronics Engineering International*, pages 160 – 164.

[53] D.Elliot. *Microlithography: Process technology for IC fabrication*, chapter 2: Wafer production and surface preparation. McGraw-Hill, 1986.

[54] D.Elliot. *Microlithography: Process technology for IC fabrication*, chapter 3: Resist Coating and Softbake. McGraw-Hill, 1986.

[55] J.L.Nistler. A simple technique to analyze conditions that affect submicron photoresist adhesion. Technical report, Advanced Micro Devices, Austin, Texas, 1989.

[56] B.Mohondro. Resist adhesion promoter application. *European Semiconductor*, pages 14 – 15, Nov 1991.

[57] G.MacBeth. *System 6000/6000XL Vapor prime unit (VPU) performance.* Eaton Semiconductor Equipment, 1987. Application Note MS131.

[58] D.J.Elliott. *Integrated Circuit Fabrication Technology*, pages 116 – 123. McGraw-Hill, 1975.

[59] K.L.Mittal. Factors affecting adhesion of lithographic materials. *Solid State Technology*, pages 89 – 100, May 1979.

[60] Yield Engineering Systems Inc. HMDS vacuum vapour prime versus BOX priming.

[61] B.Moffat. Wafer priming: Batch v's track. Yield Engineering Ststems Inc.

[62] D.E.Bornside, C.W.Macosko, and L.E.Scriven. On the modeling of spin coating. *Journal of Imaging Technology*, 13(4): 122 – 129, 1987.

[63] L.M.Peurrung and D.B.Graves. Film thickness profiles over topography in spin coating. *Journal of the Electrochemical Society*, 138(7):2115 – 2124, 1991.

[64] W.J.Daughton and F.L.Givens. An investigation of the thickness variation of spun-on films commonly associated with the semiconductor industry. *Journal of the Electrochemical Society*, 129(1): 173 – 179, 1982.

[65] T.D.Cambria and S.F.Merrow. Process control capability using a diaphragm photochemical dispense system. In *Advances in Resist Technology and Processing VIII*, pages 670 – 675. SPIE Vol.1463, 1991.

[66] J.Kulp. *Optimization of Photoresist Coat Uniformity.* Eaton Semiconductor Equipment, 1990. Application Note #90.1.

[67] D.Goossens. Influence of different exhaust values on coating uniformity of HPR204 and HPR504. Technical report, Olin Hunt, 1988. Report 288-102-02-02.

[68] D.Goossens. Influence of different exhaust values on coating uniformity of HiPR6100 and HiPR6512. Technical report, Olin Hunt, 1988. Report 288-102-02-03.

[69] OCG Microelectronic Materials Inc. *Waycoat HiPR 6500 series g-line/i-line positive photoresists*, 1989.

[70] M.Long and C.Walker. Stress factors in positive photoresist. Technical report, Motorola Semiconductor Group, Phoenix, AZ., 1984.

[71] L.Love. Resist coat uniformity as a function of dispense rate and volume; an evaluation of the cybor resist dispense pump. Technical report, OCG Microelectronic Materials, 1990. MWR Report 90-0623.

[72] M.Towner. Coating uniformity of 1520-107A vs 1520-107B. Technical report, OCG Microelectronic Materials, 1987. Report 187-102-02-03.

[73] P.Kay. Private communication, 1993. Seagate Microelectronics Ltd, Livingston.

[74] M.Thirsk and E.De Meersman. Optimisation of a coating process with HPR-504. Technical report, OCG Microelectronic Materials, 1991. CS Report 291-018.

[75] B.K.Daniels, C.R.Szmanda, M.K.Templeton, and P.Trefonas. Surface tension effects in microlithography– striations. In *Advances in Resist Technology and Processing III*, pages 192 – 201. SPIE Vol. 631, 1986.

[76] E.De Meersman. Defectless coating of ASPR-528. Technical report, OCG Microelectronic Materials n.v., 1990. Report 290-005.

[77] L.D.Pratt. *Photoresist Aerosol Particle during Spin-Coating.* Olin Hunt Speciality Products Inc.

[78] M.Teague. Private communication, 1993. Newport Wafer-Fab Ltd, Newport.

[79] P.Deaken. Private communication, 1992. National Semiconductors Ltd, Fab C, Greenock.

[80] M.Sato and I.Fujii. Spin coating process. United States Patent, Sept 1978. Patent # 4113492.

[81] P.J.Paniez, G.Festes, and J.Chollet. Physical description of lithographic process: Correlation between bake condition and photoresist contrast. In *Advances in Resist Technology and Processing IX*, pages 623 – 637. SPIE Vol. 1672, 1992.

[82] S.Fitzgerald. Private communication, 1994. Shipley Europe Ltd, Coventry.

[83] C.A.Mack and R.T.Carback. Modeling the effects of prebake on positive resist processing. In *Kodak Microelectronics Seminar.* Interface'85, 1985.

[84] M.T.Aronhime, C.Gal, S.Silady, J.J.Grunwald, D.W.Johnson, T.A.Martin, A.C.Spencer, and D.A.Sawoska. Improved thermal stability of high resolution positive photoresists via elevated softbake temperatures. In *Advances*

in Resist Technology and Processing VI, pages 97 – 105. SPIE Vol. 1086, 1989.

[85] L.F.Thompson, C.G.Willson, and M.J.Bowden, editors. *Introduction to Microlithography*, chapter 4: Resist Processing. American Chemical Society, 1983. ACS Symposium Series 219.

[86] W.S.Ruska. *Microelectronic Processing*, chapter 5: Image Creation, pages 118 – 122. McGraw-Hill, 1988.

[87] E.Hecht and A.Zajac. *Optics*, chapter 12: Basics of Coherence Theory, pages 424 – 441. Addison-Wesley, 1974.

[88] S.Wittekoek. Optical lithography for microcircuits. In *Microcircuit Engineering '80*, pages 155 – 170. Delft University, 1980.

[89] M.V.Dusa, T.Perera, and J.Kasahara. Evaluation of a resist-process-stepper combination for three quarter of a micron g-line photolithography. In *Optical/Laser Microlithography IV*. SPIE Vol. 1463, 1991. Paper No. 1463-43.

[90] C.G.M.de Mol P.F.Leuhrman, F.J.van Hout and R.A.George. Improvements in 0.5 micron production wafer steppers. In *Optical/Laser Microlithography IV*. SPIE Vol.1463, 1991. Paper No. 1463-35.

[91] R.Unger and P.D.Sessa. New i-line and deep-UV optical wafer steppers. In *Optical/Laser Microlithography IV*. SPIE Vol. 1463, 1991. Paper No. 1463-63.

[92] R.Chu, J.Greeneich, B.Katz, H.Lin, and D.T.Huang. Advanced lithographic methods for contact patterning on severe topography. In *Electron-Beam, X-ray and Ion Beam Submicrometer Lithographies for Manufacturing*. SPIE Vol. 1465, 1991. Paper No. 1465-32.

[93] B.Katz, J.Greeneich, R.Rogoff, S.Slonaker, S.Wittekoek, P.Luehrmann, M.van den Brink, and D.Ritchie. Evaluation of a high numerical aperture

wide-field stepper for 0.35 micron design rules. In *Optical/Laser Microlithography V.* SPIE Vol. 1674, 1992. Paper no.1674-62.

[94] H.Ohtsuka, T.Taguchi, T.Onodera, and K.Kuwahara. Conjugate twin-shifter mask with multiple focal planes. In *Optical/Laser Microlithography V.* SPIE Vol. 1674, 1992. Paper no.1674-03.

[95] M.A.van den Brink, B.Katz, and S.Wittekoek. New 0.54 aperture i-line wafer stepper with field by field levelling system using global alignment. In *Optical/Laser Microlithography IV.* SPIE Vol.1463, 1991. Paper No. 1463-62.

[96] M.Noguchi, Y.Yoshitake, and Y.Kembo. Resolution enhancement of stepper by complementary conjugated spatial filter. In *Optical/Laser Microlithography V.* SPIE Vol. 1674, 1992. Paper no.1674-69.

[97] N.Shiraish, S.Hirukawa, Y.Takeuchi, and N.Magome. New imaging technique for 64 M-DRAM. In *Optical/Laser Microlithography V.* SPIE Vol. 1674, 1992. Paper no.1674-63.

[98] SVG Lithography Systems Inc. Micrascan II: The ultimate lithography solution for 0.5μm to 0.25μm. Technical Handout, 1993.

[99] p.Burggraaf. Nikon exposes new step-and-scan lithography technology. *Semiconductor International*, page 28, Jan 1995.

[100] C.A.Mack. Analytical expression for the standing wave intensity in photoresist. *Applied Optics*, 25(12):1958 – 1961, 1986.

[101] C.A.Mack. PROLITH: a comprehensive optical model. In *Optical Microlithography IV*, pages 207 – 220. SPIE Vol. 538, 1985.

[102] S.G.Hansen, R.J.Hurditch, D.J.Brzozowy, and S.A.Robertson. Photoresist surface induction and its effect on swing behaviour. In *Advances in Resist Technology and Processing X.* SPIE Vol. 1925, 1993. 626 - 635.

[103] I.B.Binnie. *Critical Dimension Control: Influencing Factors and Measurement.* PhD thesis, University of Edinburgh, 1991.

[104] MICROPOSIT S1800 series photo resists. Shipley Europe Technical Handout, Herald Way, Coventry, 1993.

[105] P.Trefonas, B.K.Daniels, M.J.Eller, and A.Zampini. Examination of the mechanism of the post exposure bake effect. In *Advances in Resist Technology and Processing V*, pages 203 – 211. SPIE Vol. 920, 1988.

[106] M.Daley. Private communication, 1993. Shipley Europe Limited, Coventry.

[107] J.Suydam and S.Butler. Trends in US semiconductor lithography. Presentation at Shipley European Micro Meeting, March 1994. Shipley Company Incorporated, San Jose.

[108] L.D.H.Christensen, K.L.Bell, and N.A.Acuna. Improved CD uniformity as a function of developer chemistry and process parameters derived from a statistically-designed experiment. In *Advances in Resist Technology and Processing VII*, pages 284 – 300. SPIE Vol.1262, 1990.

[109] G.E.Flores, D.H.Norbury, and J.E.Loftus. Lithographic performance and dissolution behaviour of novolak resins for various developer surfactant systems. In *Advances in Resist Technology and Processing IX*, pages 317 – 334. SPIE Vol. 1672, 1992.

[110] C.M.Garza, C.R.Szmanda, and R.L.Fischer. Resist dissolution kinetics and submicron process control. In *Advances in Resist Technology and Processing V*, pages 321 – 338. SPIE Vol. 920, 1988.

[111] W.D.Hinsberg and M.L.Gutierrez. Effect of developer composition on photoresist performance. Report no. 965-IBM-18, IBM Research Labotatories.

[112] R.L.Martin, D.M.Truchon, and M.E.Perkins. TMK-10 MIF developer: Functional evaluation and comparison with MICROPOSIT MF-312 developer. Technical report, Shipley Company Incorporated Newton, April 1981.

[113] A.Ingram. Shipley MP-351 developer tests for Ericsson Components AB. Technical report, Shipley BV, The Netherlands, June 1993.

[114] M.Cooper. The effects of developer temperature on the photospeed and contrast of SPR2-1.3 photoresist. Technical report, Shipley Europe Limited, Coventry, Jan 1991.

[115] M.Clemment. Private communication, 1993. Digital Equipment Scotland, South Queensferry.

[116] P.Johnson. Private communication, 1993. Shipley Europe Ltd, Coventry.

[117] C.Zee, W.R.Bell, and A.R.Neureuther. Effects of developer type and agitation on dissolution of positive photoresist. In *Advances in Resist Technology and Processing V*, pages 154 – 161. SPIE Vol. 920, 1988.

[118] S.A.Robertson, J.T.M.Stevenson, R.J.Holwill, M.Thirsk, I.S.Daraktchiev, and S.G.Hansen. Photoresist dissolution rates: A comparison of puddle, spray and immersion processes. In *Integrated Circuit Metrology, Inspection, and Process Control V*, pages 232 – 244. SPIE Vol. 1464, 1991.

[119] S.A.Robertson, J.T.M.Stevenson, R.J.Holwill, S.G.Hansen, C.E.Ebersole, M.Thirsk, and I.S.Daraktchiev. The modelling of post exposure bake and surface inhibition effects in positive photoresist using absolute thickness data. In *Advances in Resist Technology and Processing IX*. SPIE Vol. 1672, 1992. 540 - 552.

[120] S.A.Robertson, J.T.M.Stevenson, R.J.Holwill, S.G.Hansen, R.J.Hurditch, M.Thirsk, and I.S.Daraktchiev. The simulation of spray/puddle resist development. In *Advances in Resist Technology and Processing X*, pages 178 – 185. SPIE Vol. 1925, 1993.

[121] J.Hutchinson, S.Das, Q.D.Quian, and H.Gaw. Modeling spray/puddle dissolution processes for DUV acid hardening resists. In *Optical/Laser Microlithography V*. SPIE Vol. 1674, 1992. Paper no.1674-31.

[122] D.DeBruin, M.R.Hannifan, M.Ha, and K.Sautter. Linewidth uniformity: a critical evaluation of spray geometry and process interactions in ultrasonic nozzles. In *Advances in Resist Technology and Processing IV*, pages 306 – 313. SPIE Vol.771, 1987.

[123] D.F.Ditmer and M.V.Hanson. Stepper exposed critical dimension tolerances using the vapor jet developer nozzle. In *Optical Microlithography III: Technology for the Next Decade*, pages 203 – 209. SPIE Vol. 470, 1984.

[124] G.MacBeth. *Positive Resist Developing with the System 6000.* Eaton Microlithography Systems Division, 1986. Application Note MS119.

[125] T.Perera. Characteristics of a developer for spray puddle develop processes. In *Advances in Resist Technology and Processing VI*, pages 470 – 483. SPIE Vol. 1086, 1989.

[126] K.J.Orvek and M.L.Dennis. Deep UV and thermal hardening of novolak resists. In *Advances in Resist Technology and Processing IV*, pages 281 – 288. SPIE Vol.771, 1987.

[127] N.Porfiris. Private communication, March 1994. EKC Technology Ltd /Edinburgh Mcrofabrication Facility, University of Edinburgh.

[128] N.Porfiris. Overview of photoresist stripping: Methods, systems and associated problems. Technical report, Edinburgh Microfabrication Facility, 1992.

[129] R.J.Hurditch and I.Daraktchiev. Positive photoresist solvents. In *Proceedings of SEMICON Europe*, April 1994.

[130] C.A.Mack. Understanding focus effects in submicrometer optical lithography. *Optical Engineering*, 27(12): 1093 – 1100, 1988.

[131] S.A.Robertson. SHIPLEY MEGAPOSIT SPR-2FX 1.8JM and SPR518M-A photo resists under g and i-line exposure. Technical report, Shipley Europe Ltd, Coventry, 1994. for Newport Wafer Fab, Newport, Wales.

[132] A.Hayward and M.Shaw. Evaluation of Shipley MF322CD29 with HPR204 and HiPR6517. Technical report, Shipley Europe Ltd, Coventry, 1993. for Siemens, Villach, Austria.

[133] C.A.Mack. Lithographic process optimization. Course Notes, April 1991.

[134] M.A.Toukhy. Development induction mechanism in novolak based resist systems for submicron optical lithography. In *Advances in Resist Technology and Processing IV*, pages 264 – 272. SPIE Vol.771, 1987.

[135] D.Nyyssonen. Linewidth measurement spotlight. *Semiconductor International*, (3): 39 – 56, 1980.

[136] D.Nyyssonen. Optical linewidth measurements on wafers. *Proceedings of SPIE*, 135:115, 1978.

[137] Bio Rad Microscience Division. *Quaestor CD07A Operating Manual*, 1988.

[138] G.Davies and M.Allison. Overlay measurement beyond 16Mbit. *European Semiconductor*, (2): 33 – 34, Feb 1992.

[139] M.Davidson, K.Kaufman, I.Mazzor, and F.Cohen. An application of interference microscopy to integrated circuit inspection and metrology. In *Integrated Circuit Metrology, Inspection and Process Control.* SPIE Vol. 775, 1987.

[140] M.Davidson, K.Kaufman, and I.Mazzor. First results of a product utilizing coherence probe imaging for wafer inspection. In *Integrated Circuit Metrology, Inspection and Process Control II.* SPIE Vol. 921, 1988.

[141] M.T.Postek and D.C.Joy. Microelectronics dimensional metrology in the scanning electron microscope - part 1. *Solid State Technology*, (11): 77 – 85, 1986.

[142] M.T.Postek and D.C.Joy. Microelectronics dimensional metrology in the scanning electron microscope - part 2. *Solid State Technology*, (12): 145 – 150, 1986.

[143] C.A.Mack. Advanced topics in lithography modeling. In *Advances in Resist Technology and Processing III*, pages 276 – 285. SPIE Vol. 631, 1986.

[144] C.A.Mack and P.M.Kaufman. Understanding focus effects in submicron optical lithography, part 2: Photoresist effects. In *Optical/Laser Microlithography II*, pages 304 –323. SPIE Vol.1088, 1989.

[145] S.G.Hansen. Simulating process latitude. *Microlithography World*, 1(2):13 – 15, May/June 1992.

[146] P.Spragg, R.Hurditch, M.Toukhy, J.Helbert, and S.Malhotra. The reliability of contrast and dissolution rate-derived parameters as predictors of photoresist performance. In *Advances in Resist Technology and Processing VIII.* SPIE Vol. 1466, 1991. Paper no. 1466-26.

[147] American Society of Tests and Measurements. *Measurement procedure F1059-87*, 1987.

[148] B.K.Daniels, P.Trefonas, and J.C.Woodbrey. Advanced characterization of positive photoresists. *Solid State Technology*, pages 105 – 110, Sept 1988.

[149] M.C.Flanigan and R.W.Wake. Impact of resist contrast on process latitude: a modeling study. In *Advances in Resist Technology and Processing II*, pages 44 – 51. SPIE Vol. 539, 1985.

[150] S.G.Hansen and R.H.Wang. Using computational experiments and statistics to discover useful predictors of lithographic performance. Technical report, OCG Microelectronic Materials, 1992.

[151] M.Hanabata, A.Furuta, and Y.Uemura. High resolution positive photoresists. In *Advances in Resist Technology and Processing III*, pages 76 – 82. SPIE Vol. 631, 1986.

[152] P.Luehrmann and G.Goodwin. Photoresist process optimization and control using image contrast. Technical report, KTI Chemicals/AMD, 1990. Report 187-102-06-03.

[153] R.W.Wake and M.C.Flanigan. A review of constrast in positive photoresists. In *Advances in Resist Technology and Processing II*, pages 291 – 298. SPIE Vol. 539, 1985.

[154] S.V.Babu and V.Srinivasan. Optical density and contrast of positive photoresists. In *Advances in Resist Technology and Processing II*, pages 36 – 43. SPIE Vol. 539, 1985.

[155] W.G.Waldo and J.N.Helbert. Standing wave interference effects on photoresist contrast. *Journal of the Electrochemical Society*, 137(4):1311 – 1313, 1990.

[156] C.A.Mack. Lithographic optimization using photoresist contrast. *Microelectronics Manufacturing Technology*, (1):36 – 42, 1991.

[157] V.Marriott. High resolution positive resist developers: a technique for functional evaluation and process optimization. In *Optical Microlithography II*, pages 144 – 151. SPIE Vol. 394, 1983.

[158] S.V.Babu and V.Srinivasan. Characterization of positive photoresist performance. *Journal of Imaging Technology*, 11(4):169 – 174, 1985.

[159] Prometrix Corporation. *Automated gamma curve determination*, 1991. Film Thickness Application Note #FT-09.

[160] M.R.Hannifan. Overview of the PACscan 1000 system: A comprehensive photoresist-developer characterization tool. Notes on application capabilities, Site Services, 1992.

[161] S.G.Hansen, G.Dao, H.Gaw, Q.Qian, P.Spragg, and R.J.Hurditch. Study of the relationship between exposure margin and photolithographic process

latitude and mask linearity. In *Optical/Laser Lithography IV.* SPIE Vol. 1463, 1991. Paper no. 1463-16.

[162] F.H.Dill. Optical lithography. *IEEE Transactions on Electron Devices*, ED-22(7): 440 – 444, 1975.

[163] F.H.Dill, W.P.Hornberger, P.S.Hauge, and J.M.Shaw. Characterization of positive photoresist. *IEEE Transactions on Electron Devices*, ED-22(7): 445 – 452, 1975.

[164] K.L.Konnerth and F.H.Dill. In-situ measurement of dielectric thickness during etching or developing processes. *IEEE Transactions on Electron Devices*, ED-22(7): 452 –456, 1975.

[165] F.H.Dill, A.R.Neureuther, J.A.Tuttle, and E.J.Walker. Modeling projection printing of positive photoresists. *IEEE Transactions on Electron Devices*, ED-22(7): 456 – 464, 1975.

[166] C.A.Mack. *Photoresist radiometry for polychromatic exposure systems.* Department of Defence, Fort Meade, MD 20755, 1986.

[167] O.D.Crisalle, S.R.Keifling, D.E.Seborg, and D.A.Mellichamp. A comparison of the optical projection lithography simulators in SAMPLE and PROLITH. Submitted for publication in *IEEE Transactions on Semiconductor Manufacturing*, 1990.

[168] H.J.Levinson and W.H.Arnold. Focus: the critical parameter for submicron lithography. *Journal of Vacuum Science and Technology*, 5:293 – 298, 1987.

[169] H.J.Levinson and W.H.Arnold. Focus: the critical parameter for submicron lithography: Part 2. In *Optical Microlithography VI*, pages 21 – 34. SPIE Vol. 772, 1987.

[170] C.A.Mack. The formation of an aerial image. *Microlithography World*, 2(1):27 – 28, Jan/Feb/Mar 1993.

[171] C.A.Mack. The formation of an aerial image: Part 2. *Microlithography World*, 2(2):25 – 27, Apr/May/Jun 1993.

[172] C.A.Mack. The formation of an aerial image: Part 3. *Microlithography World*, 2(3):23 – 24, Jul/Aug/Sept 1993.

[173] C.A.Mack. The formation of an aerial image: Part 4. *Microlithography World*, 2(4):17 – 18, Oct/Nov/Dec 1993.

[174] C.A.Mack. *Light absorption by a positive photoresist.* Department of Defence, Fort Meade, MD 20755, 1986.

[175] C.A.Mack. Absorption and exposure in positive photoresist. *Applied Optics*, 27(23):4913 – 4919, 1988.

[176] M.S.Yeung. Modeling high numerical aperture optical lithography. In *Optical/Laser Microlithography*, pages 149 – 167. SPIE Vol. 922, 1988.

[177] R.J.Hurditch. *Computer Modelling Update.* OCG Microelectronic Materials, 1989.

[178] C.A.Mack. Private communication, March 1993. FINLE Technologies, Austin, Texas.

[179] C.A.Mack. *Process Specification: Measurement of the positive photoresist parameters A, B and C.* Department of Defence, Fort Meade, MD 20755, 1986.

[180] G.Arthur and B.Martin. Modelling the printability of sub-micron 5x reticle defects at i-line exposure wavelength. In *Optical/Laser Microlithography VII.* SPIE, 1994.

[181] S.G.Hansen. Private communication, Jan 1990. OCG Microelectronic Materials, East Providence, RI.

[182] V.Rao, L.L.Kosbar, C.W.Frank, and R.F.W.Pease. The effects of sensitizer distribution on dissolution inhibition in novolak/diazonapthaquinoneresists. In *Advances in Resist Technology and Processing VIII*, pages 309 – 323. SPIE Vol. 1466, 1991.

[183] V.Rao, W.D.Hinsberg, C.W.Frank, and R.F.W.Pease. The influence of sensitizer spatial distribution on the dissolution mechanism of diazonaphthaquinone resists. In *Advances in Resist Technology and Processing IX*, pages 214 – 230. SPIE Vol. 1672, 1992.

[184] V.Rao, W.D.Hinsberg, C.W.Frank, and R.F.W.Pease. The use of Langmuir-Blodgett deposition to evaluate dissolution behaviour of multicomponent resists. Submitted for publication in *ACS Polymers for Microelectronics Symposium*, 1992.

[185] V.Rao, W.D.Hinsberg, C.W.Frank, and R.F.W.Pease. The influence of residual casting solvent on the dissolution behaviour of diazonaphthaquinone resists. In *Advances in Resist Technology and Processing X*. SPIE Vol. 1925, 1993. Paper No. 1925-54.

[186] C.A.Mack. *A Diffusion Model for Post-Exposure bake.* Department of Defence, Fort Meade, MD 20755, 1986.

[187] D.J.Kim, W.G.Oldham, and A.R.Neureuther. Development of positive photoresist. *IEEE Transactions on Electron Devices*, ED-31(12): 1730 – 1735, 1984.

[188] C.A.Mack. Development of positive photoresists. *Journal of the Electrochemical Society: Solid-state Science and Technology*, 134(1): 148 – 152, 1987.

[189] C.A.Mack. New kinetic model for resist dissolution, 1992.

[190] M.A.Toukhy, S.G.Hansen, R.J.Hurditch, and C.A.Mack. Experimental investigation of a novel dissolution model. In *Advances in Resist Technology and Processing IX*, pages 286 – 298. SPIE Vol. 1672, 1992.

[191] T.Ohfuji, K.Yamanaka, and M.Sakamoto. Characterization and modeling of high resolution positive photoresists. In *Advances in Resist Technology and Processing V*, pages 190 – 197. SPIE Vol. 920, 1988.

[192] R.J.Hurditch. Private communication, May 1992. OCG Microelectronic Materials, East Providence, RI.

[193] Y.Hirai, S.Tomida, K.Ikeda, M.Sasago, M.Endo, S.Hayama, and N.Nomura. Three-dimensional resist process simulator PEACE (Photo and Electron beam lithography Analyzing Computer Engineering system). *IEEE Transactions on Computer-Aided Design*, 10(6):802 – 807, 1991.

[194] K.K.H.Toh and A.R.Neureuther. Three-dimensional simulation of optical lithography. In *Optical/Laser Microlithography IV*, pages 356 – 367. SPIE Vol. 1463, 1991.

[195] E.Barouch, B.Bradie, and S.V.Babu. Three dimensional profile simulation for positive photoresists. In *Advances in Resist Technology and Processing VI*, pages 495 – 501. SPIE Vol. 1086, 1989.

[196] G.Addiego, J.L.Reynolds, K.L.Ng, and M.J.Tilmann. *SAMPLE user guide: simulation and modelling of profiles in lithography and etching.* Department of Electrical Engineering and Computer Sciences, University of California, Berkeley, 1989. Version 1.7a.

[197] S.G.Hansen. *Using SAMPLE on a PC.* OCG Microelectronic Materials, 1990.

[198] C.A.Mack. *PROLITH/2 User's Manual.* FINLE Technologies, Plano, Texas, 1992. Version 2.2 for the PC.

[199] R.J.Visser, H.P.Urbach, A.J.W.Tol, H.Eggink, and E.G.H.M.Kemna. Simulation of latent image manipulation: A versatile simulation program for new photolithographic systems. In *Advances in Resist Technology and Processing VI*, pages 605 – 614. SPIE Vol. 1086, 1989.

[200] D.A.Bernard. Simulation of focus effects in photolithography. *IEEE Transactions on Semiconductor Manufacturing*, 1(3): 85 – 97, 1988.

[201] W.D.Hinsberg, C.G.Willson, and K.K.Kanazawa. Measurement of thin-film dissolution kinetics using a quartz crystal microbalance. *Journal of the Elecrochemical Society*, 133(7):1448 – 1451, July 1986.

[202] W.D.Hinsberg and K.K.Kanazawa. Quartz crystal microbalance thin-film dissolution rate monitor. *Review of Scientific Instruments*, 60(3):489 – 492, March 1989.

[203] W.R.Bell, P.D.Flanner, C.Zee, N.Tam, and A.R.Neureuther. Determination of quantitative resist models from experiment. In *Advances in Resist Technology and Processing V*, pages 382 – 389. SPIE Vol. 920, 1988.

[204] T.A.Carroll and W.F.Ramires. On-line state and model parameter identification of the positive optical photoresist development process. In *Integrated Circuit Metrology, Inspection and Process Control IV*, pages 390 – 401. SPIE Vol. 1261, 1990.

[205] T.A.Carrol and W.F.Ramirez. Optimal control of positive optical photoresist development. In *Integrated Circuit Metrology, Inspection, and Process Control V*, pages 222 – 231. SPIE Vol. 1464, 1991.

[206] A.E.Novembre, W.T.Tang, and P.Hsieh. An in situ interferometric analysis of resist development on photomask substrates. In *Integrated Circuit Metrology, Inspection, and Process Control III*, pages 460 – 468. SPIE Vol. 1087, 1989.

[207] J.S.Petersen, A.Kozlowski, K.Eastwood, M.K.Swan, and M.Stan. Dissolution rate studies of some metal-ion-free developers during various modes of automated spray development. In *Advances in Resist Technology and Processing II*, pages 284 – 290. SPIE Vol.539, 1985.

[208] N.R.Farrar. Resist contrast measurements using a development rate monitor. In *Advances in Resist Technology and Processing IV*, pages 299 – 304. SPIE Vol.771, 1987.

[209] J.F.Bohland, H.F.Sandford, and S.A.Fine. Effects of dye additions on the exposure and development characteristics of positive photoresists. In *Advances in Resist Technology and Processing II*, pages 267 – 274. SPIE Vol. 539, 1985.

[210] Perkin-Elmer Applied Optics Division. *DRM operator's manual for Model 5900 Development rate monitor*, 1987. Revision D.

[211] M.R.Hannifan. Lithacon 808 process analyzer. Notes on application capabilities, Site Services, 1991.

[212] S.G.Hansen. *DRM Data Analysis on a PC.* OCG Microelectronic Materials, 1990.

[213] M.Thomson. In-situ develop end point control to eliminate CD variance. In *Integrated Circuit Metrology, Inspection, and Process Control IV*, pages 512 – 525. SPIE Vol. 1261, 1990.

[214] L.Lauchlan, K.Sautter, T.Batchelder, and J.Irwin. In-line automatic photoresist process control. In *Advances in Resist Technology and Processing II*, pages 227 – 233. SPIE Vol. 539, 1985.

[215] L.J.Uhler. Automatic linewidth control system. In *Integrated Circuit Metrology, Inspection, and Process Control*, pages 2 – 7. SPIE Vol. 775, 1987.

[216] T.Hagi, Y.Okuda, and T.Ohkuma. Critical dimension control using development end point detection for wafers with multilayer structures. In *Integrated Circuit Metrology, Inspection, and Process Control V*, pages 215 – 221. SPIE Vol. 1464, 1991.

[217] C.Nygren, J.Daggett, and J.Grambow. Using develop endpoint detection to eliminate photolithography process variation. *Microelectronics Manufacturing Technology*, 14(3): 24 – 30, 1991.

[218] K.M.Monahan. Endpoint detection of photoresist development using multiple wavelengths and polarized light. In *Integrated Circuit Metrology, Inspection, and Process Control III*, pages 332 – 331. SPIE Vol. 1087, 1989.

[219] A.G.Reid and K.M.Sautter. Develop end-point detection - a manufacturer's perspective. In *Integrated Circuit Metrology, Inspection and Process Control.* SPIE Vol. 1673, 1992. Paper No. 1673-21.

[220] Site Services Inc. Process control through develop endpoint control. Technical Handout, August 1990.

[221] R.B.Ananthakrishnan and J.A.Tuttle. Algorithm for computing thin-film thicknesses. *IBM Technical Disclosure Bulletin*, 18(11): 3618 – 3620, 1976.

[222] A.Kaiser. Semiconductor thin film optical constant determination and thin film thickness measurement equipment correlation. In *Integrated Circuit Metrology, Inspection, and Process Control V*, pages 386 – 392. SPIE Vol. 1464, 1991.

[223] Pliskin. Refractive index dispersion of dielectric films used in the semiconductor industry. *Journal of the Elecrochemical Society*, 134(11):2819 – 2826, Nov 1987.

[224] Prometrix Corporation. *SpectraMap SM300 Film Thickness Mapping System Users Guide*, April 1991. Appendix A: Measurement Theory.

[225] R.W.Ditchburn. *Light*, chapter 3.17 Dispersion, pages 59 – 60. Dover Publications, 1961.

[226] S.E.Stokowski. Measuring refractive indices of films on semiconductors by micro-reflectometry. In *Integrated Circuit Metrology, Inspection, and Process Control IV*, pages 253 – 263. SPIE Vol. 1261, 1990.

[227] I.Franz and W.Langheinrich. A simple non-destructive method of measuring the thickness of transparent thin films between 10 and 600 nm. *Solid-State Electronics*, 11: 59 – 64, 1968.

[228] P.Matthijs. Determination of the refractive index of HPR204 and HiPR6512. Technical report, Olin Hunt, 1988. Report 288-102-02-02.

[229] C.Beck. Determination of the refractive index of HPR-504 and HiPR-6517 GH. Technical report, Olin Hunt Speciality Products NV, 1990. Report 290-630-01-02.

[230] Monolight Instruments Ltd. Optical spectrum analyser. Technical Handout, 1989.

[231] Monolight Instruments Ltd. *6000 Series Optical spectrum analyser system instruction manual*, 1988. v 1.00.

[232] Monolight Instruments Ltd. *6100 Series Scanning monochromators and detectors*, 1991. Application Note Number 1.0.

[233] Monolight Instruments Ltd. *6800 Series Optical spuctrum analyser Instruction manual*, 1989. v 1.00.

[234] Monolight Instruments Ltd. *Fibre Optic Light Guides*, 1991. Application Note Number 4.0.

[235] Monolight Instruments Ltd. *Spectral Analysis Software model 6850 Instruction Manual*, 1989. v 1.20.

[236] Monolight Instruments Ltd. *Control Software Library for 6801/2 Model 6860 Reference Manual*, 1991. v 1.00.

[237] R.Eandi, W.Hunn, M.Eckhardt, H.Engel, and H.Becker. Optical thick and thin film metrology on various substrates using a high resolution reflection spectrophotometer. In *Integrated Circuit Metrology, Inspection, and Process Control III*, pages 446 – 457. SPIE Vol. 1087, 1989.

[238] S.A.Robertson and S.G.Hansen. Using a Perkin-Elmer DRM for puddle measurements. Technical report, OCG Microelectronic Materials, 1992. Report CEPH-RM-92-6.

[239] A.S.Chiu, R.A.Ferguson, T.Doi, A.Wong, N.Tam, and A.R.Neureuther. Resist parameter extraction (PARMEX) with graphical user interface in X. In *Advances in Resist Technology and Processing VIII*, pages 641 – 652. SPIE Vol.1463, 1991.

[240] J.Hayes, W.R.Bell, R.Ferguson, and A.R.Neureuther. Resist characterization on reflecting substrates. In *Advances in Resist Technology and Processing III*, pages 8 – 13. SPIE Vol.1262, 1986.

[241] M.S.Caceci and W.P.Cacheris. Fitting curves to data: The Simplex algorithm is the answer. *BYTE*, pages 340 – 362, May 1984.

[242] A.Ross and J.T.M.Stevenson. Investigation of latent images in photoresist. Technical report, Edinburgh Microfabrication Facility, 1990. IED Project 2242 Report.

[243] A.Ross and J.T.M.Stevenson. Recognition and measurement of latent images in photoresist. Edinburgh Microfabrication Facility. Laboratory Notes, 1990.

[244] S.A.Stapleton. Temperature control of developer solution, May 1994. B.Eng Hons Project Report HSP1011, University of Edinburgh.

[245] N.Porfiris. Real-time monitoring of resist stripping and diffusion studies. Technical report, EKC Technology Ltd/Edinburgh Microfabrication Facility, 1994.